Universidade de São Paulo

Faculdade de Filosofia, Ciências e Letras de Ribeirão Preto

Departamento de Química

Programa de Pós-Graduação em Química

"Investigação do papel do estrôncio na fisiologia óssea: da perspectiva da biologia molecular para suas aplicabilidades"

"Investigation of the role of strontium on bone physiology: from a molecular biology perspective to applicability"

MSc. Larwsk Hayann Gonçalves da Silva

Tese apresentada à Faculdade de Filosofia, Ciências e Letras de Ribeirão Preto da Universidade de São Paulo, como parte das exigências para a obtenção do título de Doutor em Ciências, Área: **Química**

Ribeirão Preto- SP

2023

Universidade de São Paulo

Faculdade de Filosofia, Ciências e Letras de Ribeirão Preto

Departamento de Química

Programa de Pós-Graduação em Química

"Investigação do papel do estrôncio na fisiologia óssea: da perspectiva da biologia molecular para suas aplicabilidades"

"Investigation of the role of strontium on bone physiology: from a molecular biology perspective of applicability"

MSc. Larwsk Hayann Gonçalves da Silva

Orientadora: Profa. Dra. Ana Paula Ramos

Versão corrigida

Tese apresentada à Faculdade de Filosofia, Ciências e Letras de Ribeirão Preto da Universidade de São Paulo, como parte das exigências para a obtenção do título de Doutor em Ciências, Área: **Química**

Ribeirão Preto- SP

2023

FICHA CATALOGRÁFICA

HAYANN, Larwsk

Investigação do papel do estrôncio na fisiologia óssea: da perspectiva da biologia molecular para suas aplicabilidades. Ribeirão Preto, 2023

X pag,184: i1; 30cm

Tese de Doutorado, apresentada à Faculdade de Filosofia, Ciências e Letras de Ribeirão Preto da Universidade de São Paulo –

Área de concentração: Química

Orientadora: RAMOS, Ana Paula.

1. Osso. 2. Biomateriais. 3. Biomineralização. 4. Vesículas de matriz

“Do not go gentle into that good night,

Old age should burn and rave at close of day,

Rage, rage against the dying of the light

Though wise men at their end know dark is right,
Because their words had forked no lightning, they
Do not go gentle into that good night.”

Dylan Thomas

A minha mãe, hoje e sempre,
Serei eternamente grato.

Agradecimentos

A deus e a minha orientadora espiritual por me fornecer força contínua e por nunca me deixar desistir

À minha família. Em especial a minha mãe que me educou e me forneceu valores para a vida, sem a senhora nada disso seria possível. Ao meu padrasto Rui Miguel, que sempre me tratou com gentileza, muito obrigado por todo o suporte que me foi dado, obrigado por ter me acolhido em Portugal e por ter me proporcionado educação. Agradeço também a minha Avó a qual eu tenho como uma segunda mãe; os meus tios (Junior e sua esposa Claudiana, Raurissom e Rômulo e sua esposa Eva, e Auderício); as tias (Haldjany e Rascquejany) por todo o suporte fornecido durante toda uma vida. Aos meus primos (Lucas, João Marcelo, Amanda, Alciano e recentemente a Thalita), que apesar da distância os tenho como irmãos. Agradeço a todos vocês pelo suporte, e compreensão diante da distância e dos inúmeros eventos pelo qual não pude estar presente. Amo vocês.

À minha orientadora Prof. Ana Paula que me abriu as portas do doutorado, que me educou e me deus valores para a vida, que sempre foi uma amiga, que me proporcionou a dádiva da educação. A senhora serei eternamente grato.

Ao meu co-orientador Prof. Pietro Ciancaglini, que me abriu as portas do seu laboratório, que me acolheu como seu aluno, que me ensinou valores e princípios. Obrigado pelo cafezinho de todo o dia, e obrigado por tudo.

A todos os membros atuais e que já passarem pelo laboratório da Prof. Ana Paula, em especial a Maryanne, Lucas e Bianca. Obrigado pelos ensinamentos, e por todo o suporte.

Aos membros do laboratório do Prof. Pietro, em especial ao Luís, Juçara e Heitor. Obrigado por todos os momentos de alegria, de descontração, de discussão científica e suporte. Vocês fizeram cada dia desse doutorado mais leve. Não poderia deixar de agradecer a menina Juçara por toda a comida que nos foi fornecida diariamente, incluindo pão de queijo, bolo, torta, docinho, salgadinho, e a lista continua.

Aos amigos que fiz na USP no decorrer desses quatro anos, em especial a Greicy, Leonardo, Adriano e Mariana. Meus mais sinceros agradecimentos.

A pessoa mais especial da minha vida, Marina, minha namorada, a qual está presente em todos os momentos da minha vida. Muito obrigado por estar sempre ao meu lado me apoiando, me dando coragem, me incentivando a ser uma pessoa melhor. Você foi o maior e melhor presente que a USP e o Brasil me deram. Eu te amo.

A segunda família que Deus me deu, serei também eternamente grato por tudo, em especial minha sogra (Márcia), meu sogro (João), minha cunhada (Marisa) e seu esposo Leonardo, a Tia Marli, ao Tio Valter, ao Victor. É claro que não poderia deixar de agradecer a Dory (minha preferida), a Pandora, recentemente a Kiara, ao Luke e a Vitória, cachorrinhos lindos enviados por Deus para nos alegrar a vida.

Aos meus amigos de infância em especial o Luan, Nicárcio, Thales, Caike, Cadu, Cardoso e Estêvão. Obrigado por todo o suporte e compreensão quanto a distância. Obrigado pela amizade de uma vida. Obrigado por todos os momentos de alegria, de bebedeira e de brincadeira. Amo todos vocês. Não poderia esquecer, desculpa aí ter nascido.

Um agradecimento especial aos meus amigos de Faculdade, Fernando e Bárbara. Obrigado pela compreensão, por todo o suporte, por todas as noites de estudo e por toda a alegria. Me deem um sobrinho.

Á Universidade de São Paulo, que me forneceu toda a estrutura e suporte para a execução do doutorado.

Á CNPq e CAPES por terem me fornecido todo o apoio financeiro e concessão da bolsa de doutorado e da bolsa CAPES PRINT para o exterior

Os meus mais sinceros agradecimentos,

Larwsk Hayann

Acknowledgments

I would like to express my gratitude to Prof. Dobrawa Napierala for accepting me during the internship period. Undisputedly, you educated me on how to be a better scientist and a person. With you, I had the best scientific meetings and conversations ever, it will never be forgotten.

I could not wait to thank my friends Kaoru, Mairobys, Esther, Paulina, Esther, Juliane and Carlos. Thank you, my friends, for all the support and friendship that you provided me during my stay in Pittsburgh. I will never forget our happy moments, our laughs, jokes, and of course our time in Mario´s. I miss you every day.

I would like to thank the University of Pittsburgh and the NIH for providing me with all the structure to develop my research.

My endless gratitude,

Larwsk Hayann

“Remember to look up at the stars and not down to your feet Try to make sense of what you see and wonder about what makes the universe exist. Be curious. And however difficult life may seem, there is always something you can do and succeed at. It matters that you don´t just give up.”

Stephen Hawking

Abstract

The development of biocompatible materials able to trigger specific cellular responses at the molecular level is the focus of tissue engineering. This challenging task involves the activation of specific molecular pathways by bioactive compounds added to the composition of biomaterials to enhance the biological response. In the special case of bone tissue, nanoparticles composed of hydroxyapatite (HA) have proven to be an excellent alternative to activate osteoblasts, the cells responsible for the formation of the bone extracellular matrix. This effect is assigned to the similarities between the mineral portion of the bone and the composition of HA.

Calcium ions can be replaced by other divalent cation in the structure of HA. Among them, the substitution by strontium has been studied due to the ability of these ions to regulate the activity of osteoclasts, cells responsible for bone resorption. For instance, strontium ranelate was used in the past to treat osteoporosis. However, the need of using high doses of the compound in order to have pharmacological responses was also cause of pathological mineralization and the use of the drug was discontinued. Since then, other compounds able to control osteoblasts and osteoclasts activity using low strontium concentration have been focus of attention. However, the action of strontium upon mineralization competent cells at a molecular is still not fully understood.

In this thesis, we synthesized a class of special nanoparticles enriched with strontium. The nanoparticles mimic the structure and composition of biological apatite, the mineral portion of the bone. We divided the text into two fundamental parts. First, we sought to understand whether the nanoparticles containing strontium would be capable of modulating osteocompetent cells in vitro. Hence, we investigated their role in promoting biomineralization. We synthesized apatite containing different percentage of calcium replacement by strontium: (1) hydroxyapatite-based nanoparticles in the absence of strontium, named NanoSr 0%, (2) HAp-based NanoSr 10%, where 10% of calcium was replaced by strontium, and (3) HAp-based NanoSr 90%. We observed that NanoSr 90% was the most effective nanoparticle in inducing mineral deposition in the extracellular matrix by osteoblasts. Moreover, NanoSr 90% upregulated markers of osteoblast differentiation and maturation, as well as was linked to high alkaline phosphatase activity. After that, we studied the NPs´ effect on osteoclast survival and differentiation. We observed that all the NPs had the ability to inhibit osteoclast differentiation without affecting their viability.

Afterward, we analyzed whether NanoSr 90% associated with a worldwide used porous polymethylmethacrylate cement (pPMMA) would effectively bring benefits to the biomaterial as an agent of strontium delivery in vivo using rabbits as animal models. We noticed that NanoSr90% modulated OCN and BMP2 gene expression levels, which are markers of osteoblast turnover. Additionally, we observed osteoblast migration towards the pPMMA cement area, as well as collagen type I deposition, which are indicative of bone formation. These outcomes advocate that NanoSr 90% is a strong candidate to be further tested as an active biomaterial.

In the second part of the thesis, we focused on understanding how strontium regulates biomineralization at the molecular level. Here, we opted to use strontium ranelate as the main source of strontium instead of the nanoparticles due to the following reason, the cell line chosen for this characterization (odontoblast, 17IIA11) is already committed to a mineralizing phenotype, hence they do not require a differentiation step. For this reason, the extracellular matrix (ECM) full mineralization occurs in approximately 6 days. The NPs

requires at least 14 days to have its maximum delivery of strontium into the media, which is not viable to be tested for this cell line. Additionally, as a comparison, we also studied the effect of Ca^{2+} in the form of $CaCl_2$ and inorganic phosphate (Pi), which are the two most well-known ions involved with bone physiology. Herein, we hypothesized that strontium affects mineralization on two different levels, (1) by regulating osteogenic markers and cell commitment, and (2) by regulating the secretion and function of matrix vesicles (MVs). The results revealed that Sr^{2+} regulated Erk1/2 and CREB signaling pathways, as well as modulated osteogenic-related genes. The effect of Sr^{2+} on osteocompetent cells is dose-dependent, which means that high doses of Sr^{2+} abolished mineralization, while low doses promoted it.

Further, we treated the cells with the ions and isolated the matrix vesicles trapped in the extracellular matrix. A curious and yet not fully understood behavior was perceived. Here, we found that strontium diminished MVs' release, but enhanced their ability to mineralize the ECM. The morphology of the vesicles was characterized by atomic force (AFM) and transmission electron (TEM) microscopy. The results revealed changes in the viscoelastic properties of MVs derived from cells treated with Pi, $CaCl_2$, and strontium. Finally, we determined the MV´s lipid content using lipidomic analysis, which showed that the lipid composition entirely changes depending on the treatment. MVs derived from cells stimulated with strontium were enriched in ceramide (Cer) and sphingomyelin (SM) lipids, which are required for MV turnover.

In conclusion, the findings presented in this thesis attested for the potential use of strontium-based nanoparticles for bone repair. Additionally, this thesis added one more brick to the overall and ever-growing knowledge regarding the strontium basic mechanisms of action on osteocompetent cells. Finally, for the first time in the literature we have demonstrated that strontium affects the MVs lipid content profile, which in turn increased the matrix vesicle function.

Keywords: bone, biomaterials, biomineralization, matrix vesicles and strontium

Resumo

O desenvolvimento de materiais biocompatíveis capazes de desencadear respostas celulares específicas em nível molecular é o foco da engenharia de tecidos. Esta tarefa desafiadora envolve a ativação de vias moleculares específicas por compostos bioativos adicionados à composição dos biomateriais para potencializar a resposta biológica. No caso especial do tecido ósseo, as nanopartículas compostas por hidroxiapatita (HA) têm se mostrado uma excelente alternativa para ativar os osteoblastos, células responsáveis pela formação da matriz extracelular óssea, e inibir os osteoclastos, células envolvidas com a reabsorção óssea. Este efeito é atribuído às semelhanças entre a porção mineral do osso e a composição do AH.

Em adição, os íons cálcio pode ser substituídos por outros cátions divalentes na estrutura da HA. Dentre eles, a substituição por estrôncio tem sido estudada devido à capacidade desses íons em regular a atividade dos osteoblastos e osteoclastos. Por exemplo, o ranelato de estrôncio foi usado no passado para tratar osteoporose. Porém, a necessidade do uso de altas doses do composto para obter respostas farmacológicas desejáveis também foi causa de mineralização patológica, e com isto o uso do medicamento foi descontinuado. Desde então, outros compostos capazes de controlar a atividade de osteoblastos e osteoclastos utilizando baixas concentrações de estrôncio têm sido foco de atenção. No entanto, a ação do estrôncio na mineralização de células competentes em nível molecular ainda não é totalmente compreendida.

Nesta tese, sintetizamos uma classe especial de nanopartículas enriquecidas com estrôncio. As nanopartículas mimetizam a composição e estrutura da apatita biológica, constituinte que compõe a porção mineral do osso. Dividimos o texto em duas partes fundamentais. Primeiramente, buscamos entender se as nanopartículas (NPs) contendo estrôncio seriam capazes de modular células osteocompetentes (osteoclastos e osteoblastos) *in vitro*. Portanto, investigamos seu papel na promoção da biomineralização. Sintetizamos apatita contendo diferentes percentuais de substituição de cálcio por estrôncio: (1) nanopartículas à base de hidroxiapatita na ausência de estrôncio, foram denominadas NanoSr 0%, (2) NanoSr 10%, onde 10% do cálcio foi substituído por estrôncio, e (3) NanoSr 90%, onde 90% do cálcio foi substituído por estrôncio. Observamos que a nanopartícula, NanoSr 90, foi mais eficiente na indução da deposição mineral na matriz extracelular pelos osteoblastos. Além disso, o NanoSr 90% regulou positivamente os marcadores de diferenciação e maturação dos osteoblastos, bem como foi ligado à alta atividade da fosfatase alcalina. Depois disso, estudamos o efeito das NPs na sobrevivência e diferenciação dos osteoclastos. Observamos que todos os NPs tiveram a capacidade de inibir a diferenciação dos osteoclastos sem afetar sua viabilidade.

Em seguida, analisamos se o NanoSr 90% associado a um cimento poroso de polimetilmetacrilato (pPMMA) traria efetivamente benefícios ao biomaterial como agente de entrega de estrôncio *in vivo*, para isto foi utilizado coelhos como modelo animal deste estudo. Observamos que NanoSr 90% modularam os níveis de expressão dos genes *Ocn e Bmp2*, que são marcadores de diferenciação e ativação de osteoblastos. Além disso, observamos migração de osteoblastos em direção à área do cimento pPMMA, bem como deposição de colágeno tipo I, indicando a formação de matrix óssea. Estes resultados defendem que o NanoSr 90% é um forte candidato para ser testado como um biomaterial ativo.

Na segunda parte da tese, buscámos compreender como o estrôncio regula a biomineralização de células osteocompetentes a nível molecular. Aqui, optamos por

utilizar o ranelato de estrôncio como principal fonte de estrôncio ao invés das nanopartículas pelo seguinte motivo, a linhagem celular escolhida para esta caracterização (odontoblasto, 17IIA11) já apresenta um fenótipo mineralizante, portanto não necessita de uma etapa de diferenciação. Por este motivo, a mineralização completa da matriz extracelular (MEC) ocorre em aproximadamente 6 dias. As NPs necessitam de pelo menos 14 dias para terem sua entrega máxima de estrôncio no meio, o torna inviável o seu uso nesta linhagem celular. Além disso, como comparação, também estudamos o efeito do Ca^{2+} na forma de $CaCl_2$ e fosfato inorgânico (Pi), que são os dois íons mais conhecidos envolvidos na fisiologia óssea. Aqui, levantamos a hipótese de que o estrôncio afeta a mineralização em dois níveis diferentes, (1) regulando marcadores osteogênicos e atua no comprometimento celular, e (2) regulando a secreção e função das vesículas da matriz (VMs). Os resultados aqui observados revelaram que Sr^{2+} regulou as vias de sinalização Erk1/2 e CREB, bem como modulou genes relacionados à osteogênese. Em adição, foi observado que o efeito do Sr^{2+} nas células osteocompetentes é dependente da dose, o que significa que altas doses de Sr^{2+} inibiram a mineralização, enquanto doses baixas a promoveram.

Além disso, tratamos as células com os íons e isolamos as vesículas da matriz presas na matriz extracelular (MEC). Observamos um comportamento curioso, mas ainda não totalmente compreendido. Aqui, foi mostrado que o estrôncio diminuiu a liberação das VMs, mas aumentou sua capacidade de mineralizar a MEC. Em seguida, estudamos a morfologia das vesículas por microscopia de força atômica (MFA) e eletrônica de transmissão (MET). Os resultados revelaram alterações nas propriedades viscoelásticas das VMs derivadas de células tratadas com Pi, $CaCl_2$ e estrôncio. Por fim, determinamos o conteúdo lipídico das VMs por meio de análise lipidômica, que mostrou que a composição lipídica sofre alteração a depender do estímulo fornecido para as células. Por exemplo, as VMs derivadas de células estimuladas com estrôncio foram enriquecidas em lipídeos ceramida (Cer) e esfingomielina (SM), dois lipídios ligados ao desenvolvimento ósseo.

Em conclusão, os resultados apresentados nesta tese atestam o potencial uso de nanopartículas à base de estrôncio para reparo ósseo. Além disso, esta tese acrescentou mais um tijolo ao conhecimento geral e cada vez maior sobre os mecanismos básicos de ação do estrôncio nas células osteocompetentes. Finalmente, pela primeira vez na literatura demonstramos que o estrôncio afeta o conteúdo lipídico dos VMs, o que por sua vez foi associada com alta atividade das VMs.

Palavras-chave: osso, biomateriais, biomineralização, vesículas de matrix e estrôncio

LIST OF FIGURES

LIST OF TABLES

CONTENTS

I

General aspects of bone tissue

II

Biomaterials- concepts and applications

III

Aims and motivations

IV

A nontoxic strontium nanoparticle capable of modulating osteocompetent cells

V

Strontium regulates biomineralization at the molecular level

VI

General discussion & Final conclusions

Chapter I

General aspects of bone tissue

1. General aspects of bone tissue

Bone is a connective tissue characterized by a mineralized extracellular matrix. Like other connective tissues, the bone consists of cells and extracellular matrix. The primary characteristic that differentiates bone from other connective tissues is the mineralization of its matrix, which confers support and protection to soft tissues. The inorganic phase of the bone is majority formed by biological apatite, a calcium phosphate that shares similarities with hydroxyapatite (HA) [$Ca_{10}(PO_4)_6(OH)_2$]. However, in biological apatite, Ca^{2+} and PO_4^{3-} ions can be replaced by other cations, like Mg^{2+}, Zn^{2+} $Sr^{2+,}$ and CO_3^{2-}, respectively. The chemical composition of biological apatite has been suggested here [1]. Due to its mineral content, bone also serves as a storage site for Ca^{2+}, Pi, and other important ions[2]. Thus, in addition to the support and protection function, bone provides homeostatic regulation of blood calcium levels.

Bone also contains an organic matrix composed mainly of type I collagen and non-collagenous molecules. Though the major structural component of bone matrix is type I collagen, other types of collagen as type III, XI, XIII, and can also be found [3]. Altogether, they correspond to about 90% of the total weight of the bone organic matrix. The organic matrix also contains non-collagenous molecules (~ 10%) that constitute the ground substance of bone. They play an important role in bone development, remodeling, and repair. These compounds can be divided into four groups:

- Proteoglycans: The major components found in this group are the glycosaminoglycans (keratan sulfate, chondroitin sulfate, and hyaluronan). They contribute to the strength of the bone, to binding growth factors and to regulate mineralization[3] .
- Multiadhesive glycoproteins: they are responsible for binding collagen fibers and bone cells to the mineralized ground matrix. The most studied proteins in this group are osteonectin and sialoproteins (e.g., osteopontin, sialoprotein I and II). Osteonectin organizes the growth of apatite minerals throughout the collagen fiber[4]. On the other hand, osteopontin helps the attachment of cells to the bone matrix.
- Vitamin K-dependent proteins: osteocalcin is the main example of this class, which is mainly involved in the systemic control of calcium level and osteoclast activity;

- Growth factors and cytokines: Insulin-like growth factors (IGFs), TNF-α, TGF-β, bone morphogenic proteins (BMPs), and interleukins.

  From this brief description, it is clear that the bone is a example of a tissue with complex function and composition.

1.1 The general structure of the bone tissue

The bone tissue is fundamentally composed by cells (osteoblasts, chondrocytes, osteoclasts, osteocytes), an inorganic matrix, an organic matrix, and other connective tissues, like hematopoietic tissue (blood-forming progenitors and non-blooding forming cells), fat tissue, blood vessels, and nerves[5]. Anatomically, the adult human skeleton comprises 213 bones. Two distinct structural arrangements can be recognized in the bone structure **(Figure 1.1)**, (1) Cortical bone formed by a dense layer exposed to outside of the bone with a porosity of 5 to 10 %. It provides maximum resistance to torsion and bending, and (2) Trabecular bone, a spongelike meshwork consisting of trabeculae which forms the interior of the cancellous bone (spongy), with a porosity of 50 to 90%. The inner spaces within the meshwork are continuous and are occupied by marrow and blood vessels[3].

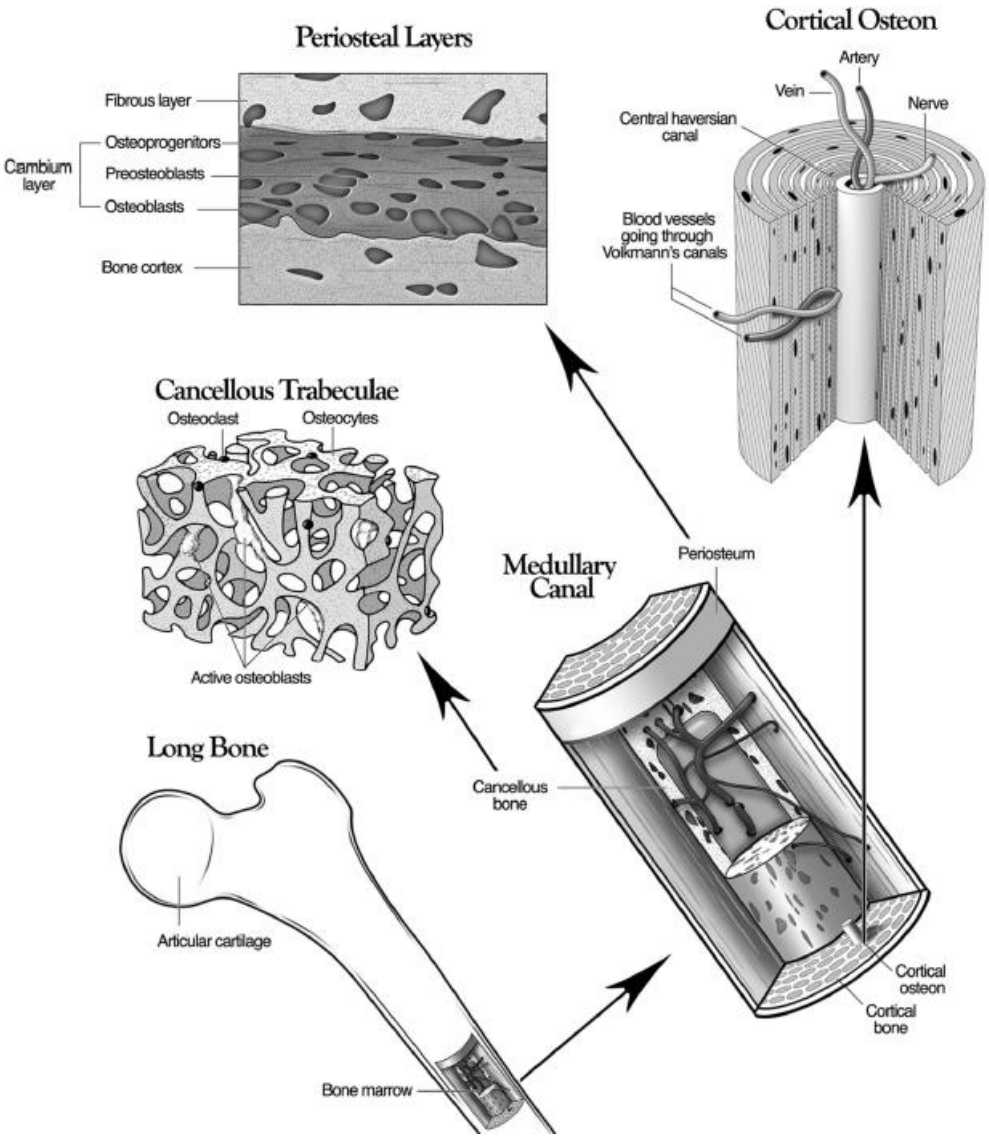

FIGURE 1. 1. BONE STRUCTURE WITH ITS COMPONENTS.

Bones can be classified into hard cortical-made components or spongy-like components (cancellous or trabecular components). Cortical bone provides the strength, and its major component is the osteon. Spongy-like or cancellous areas are responsible to maximize nutrient diffusion and facilitate the transport of cytokines and hormones important in bone and mineral homeostasis. Periosteal layers (or periosteum) cover the external surface of cortical bone, which facilitates an attachment site for ligaments, an additional vascular supply, and osteoprogenitor cells involved with bone repair/remodeling. Adapted with permission from reference[5].

They can also be classified according to their location, shape, consistency, and size [6,7]. Here, by means of simplification, we will divide them into the two most common descriptors used in the literature: flat bones and tubular (long) bones. However, there is a third classification that encompasses those bones in which their shape does not fit into any one of the two other groups, that is the case of the irregular bones (e.g., vertebra and ethmoid bone).

- Tubular bones: long bones of the extremities, the clavicles, and short tubular bones of the hands, femur, and feet.
- Flat bones: bones of the craniofacial skeleton and scapulae, sternum, and ribs.

The biggest portion (body) of the long bone is called diaphysis with two expanded ends (epiphysis) **Figure 1.2**, in-between one can find the metaphysis. The articular surface of the epiphysis is covered with hyaline cartilage and is responsible for epiphysis protection. The inner portion of the bone is filled with a liquid tissue, called marrow.

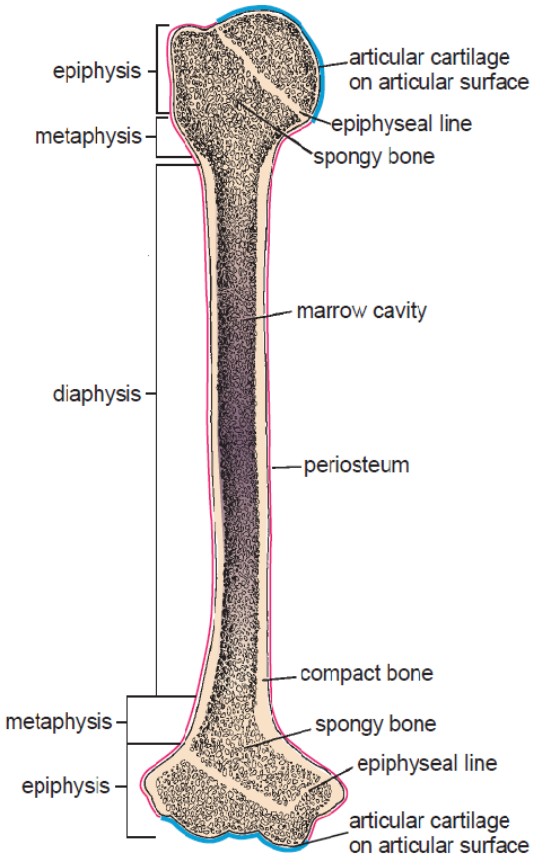

FIGURE 1. 2. LONG BONE STRUCTURE

A typical long bone presents a large marrow cavity surrounded by compact bone, called diaphysis. The two extremities (proximal and distal ends) are called epiphyses, and they are majority formed by spongy (cancellous) bone with a thin outer layer of compact bone. Metaphysis corresponds to the area between the epiphysis and diaphysis. Articular cartilage (blue) is covered by hyaline cartilage and avoids bone depletion. The outer surface (pink) of the bone is covered by a fibrous layer of connective tissue containing osteoprogenitor cells, called periosteum. Adapted with permission from reference[3].

Mature compact bone is formed by cylindrical structures called osteons, which consist of concentric *lamellae* **Figure 1.3.** In the center, one can find a central canal (Osteonal or Haversian canal) which contains the vascular and nerve supply of the osteon. Also, osteocytes can be found in the canaliculi. The canaliculi system is an intertwined net of small channels responsible for the passage of substances/nutrients

between the osteocytes and blood vessels. The blood that supplies the bone tissue comes from the marrow cavity into and through the bone tissue via periosteal veins (Volkmann´s canals and Haversian canals)[3].

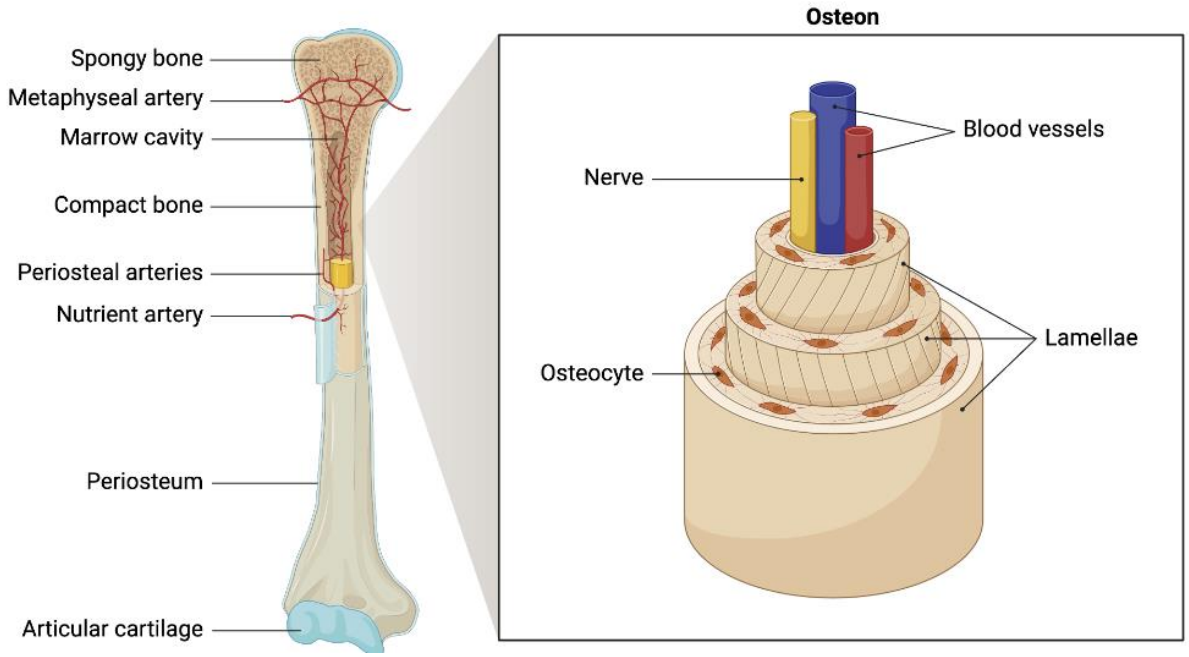

FIGURE 1. 3. STRUCTURE OF MATURE OSSEOUS TISSUE

Mature compact bone tissue is formed by cylindrical structures called osteons. Osteon consists of a central canal called the osteonic canal (haversian canal), which is surrounded by concentric rings of an osteogenic matrix (*lamellae).* Osteocytes cells can be found between the rings of the matrix, and they are responsible for nutrient exchange. Source: author archive. This image was assembled using dynamic BioRender assets.

Immature bone is defined as any bone initially formed in the skeleton of a developing fetus. The major differences between immature and mature bone are listed below and can be histologically visualized in the **Figure 1.4**:

- They lack organized lamellated appearance;
- Greater cell number per unit area;
- The cells found in immature bone are randomly arranged, whereas mature bone is highly organized, and the cells are usually arranged with their axes pointing in the same direction as the lamellae;

- Immature bone matrix has more ground substance, and it usually stains more intensely with hematoxylin;
- Immature bone collagen fiber is usually referred to as (woven bone or bundle bone) due to its interlacing arrangement of the collagen fibers.

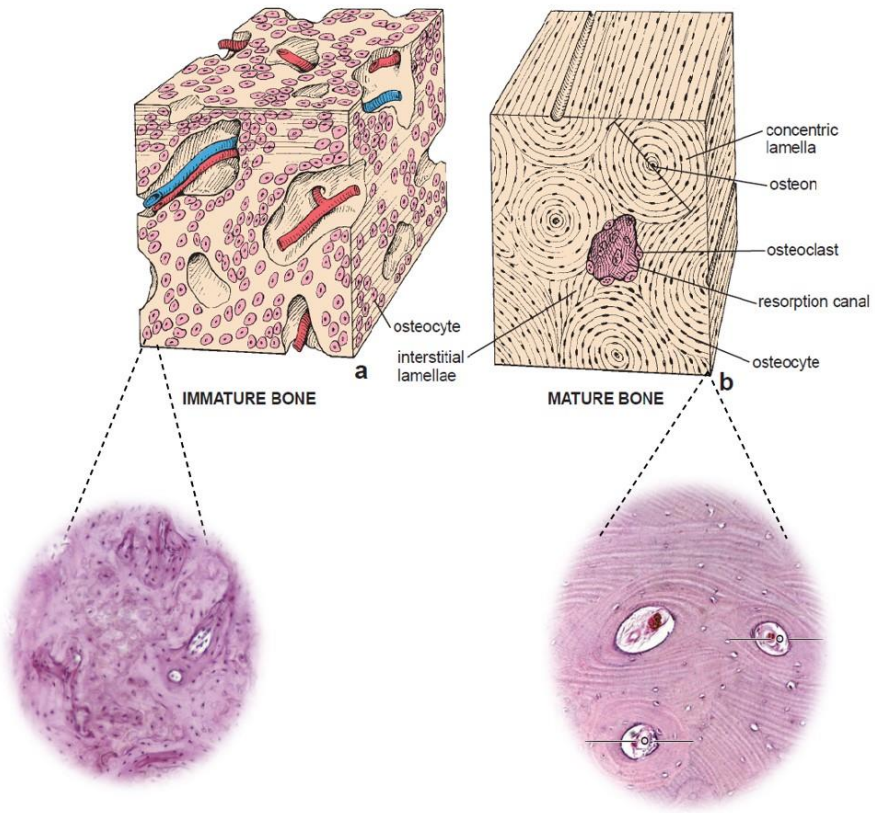

FIGURE 1. 4. IMMATURE AND MATURE BONE STRUCTURE VISUALIZATION

Immature and mature bone structure visualization. **Up:** The major difference between mature and immature bone is the lack of organized lamellae of the latter, due to the interlacing arrangement of the collagen fibers. Moreover, the cells are randomly arranged in the immature bone, whereas in mature bone they assume a circular fashion that reflects the lamellar structure of the Haversian system. Resorption canals in mature bone follow Haversian direction. **Down**: Histology (H&E staining), primary bone (woven or immature bone) presents more cells in comparison to mature bone (secondary or lamellar bone). Mature bone presents various structures called osteons (o) with concentric lamellae. Haversian canals (mature bone) contain blood vessels and connective tissue. Adapted with permission from reference[3].

In addition, immature bone is not heavily mineralized when it is formed, even though its mineralization process happens quicker than mature bone. Interestingly, immature bone is also present in adults, especially where there is a remodeling process going on. They can be found more commonly in the alveolar sockets (oral cavity) and inserted tendons area[3].

1.2. Cells of bone tissue

Bone cells correspond to almost 10% of the total organic bone volume. They can be distinguished according to their origin. Osteoprogenitor cells derived from mesenchymal stem cell (MSC) lineage differentiate into osteoblasts and osteocytes. Bone marrow hematopoietic stem cells (HSC) produce osteoclasts **(Figure 1.5)**. In the case of osteoprogenitor cells derived from MSC, each cell undergoes a transformation from a less mature form to a more mature one. On the other hand, osteoclasts originate from a different cell line. Osteoprogenitor cells can be found in different regions of the bone, like bone channels, periosteum, marrow, and endosteum.

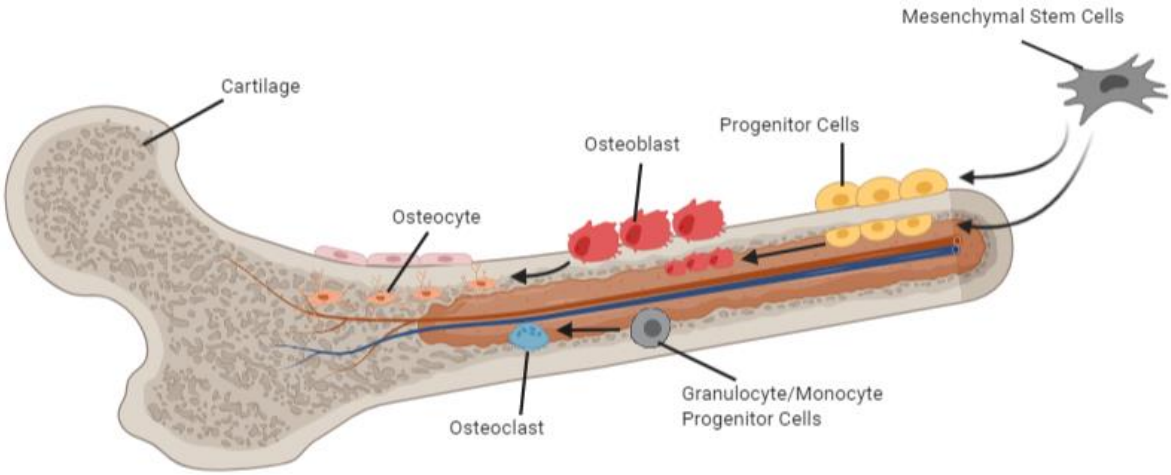

FIGURE 1. 5. SCHEMATIC REPRESENTATION OF THE MAIN CELLS FOUND IN BONE.

Schematic representation of the main cells found in bone. The differentiation of mesenchymal stem cells (MSC) leads to the osteochondrogenic lineage, meanwhile, the osteoclasts are derived from hematopoietic precursors.

As it will be discussed later in this chapter, the osteoprogenitor cells remain undifferentiated. Upon specific molecular signals, cells migrate, proliferate, and differentiate into osteoblasts and other cell lines **(Table 1.1).**

TABLE 1.1. THE DIFFERENTIATION OF PROGENITOR CELLS INTO SPECIALIZED CELL LINES REQUIRES A SOPHISTICATED AND ORGANIZED SIGNALING PROCESS

Cell line	Signals	Refs
Osteoblasts	BMPs family, TGF-β, WNT/β-catenin, IF	8–10
Osteocytes	Wnt/β-catenin, PTG, sclerostin	11,12
Osteoclasts	M-CSF, TNF, ILs, RANKL, IL-1, IL-6	3,13–15
Chondrocytes	FGFs, BMPs family, TNF-α, EGF	16,17

Osteoblasts are the main bone-forming cells. They are specialized in the synthesis and secretion of organic bone matrix, also responsible for the mineralization of the ECM. Upon activation, osteoblast assumes one of the three fates: remain as quiescent osteoblasts (which is marked by high alkaline phosphatase activity), dedifferentiate to the osteoprogenitor cell line, or differentiate to osteocytes[6,18]. Osteoblasts control osteoclastogenesis by synthesizing and secreting RANKL and M-CSF and inhibit osteoclastogenesis upon secretion of osteoprotegerin (OPG), a natural inhibitor of RANKL[9].

Nonetheless, bone also contains osteoclasts which are derived from bone marrow HSC. Osteoclasts are specialized, multinucleated cells found at sites of bone remodeling (resorption), and they can be found in shallow depressions of bone surface called Howship lacunae[19]. They are derived from the fusion of mononuclear hemopoietic cells (macrophage progenitor cells). Upon cytokine stimulation, cells committed to become osteoclasts express two important transcription factors, (c-fos and NFκB), followed by the expression of the receptor activator of nuclear factor κ B(RANK) on its membrane surface. The interaction with the RANK ligand molecule (RANKL) is essential for osteoclast differentiation, maturation, and survival in normal bone tissue.

The RANK/RANKL/OPG system was discovered in the 90s and plays a fundamental role in bone homeostasis. The interaction in this system demonstrates that the osteoblasts control osteoclasts (maturation and activity) through the secretion of either RANKL (pro-osteoclastogenesis) or OPG (anti-osteoclastogenesis). OPG protects bone from excessive resorption by competing with the RANKL for this receptor (RANK). It can be concluded that RANKL-OPG concentration determines bone mass and strength [20]. However, RANKL can be also secreted by activated T lymphocytes, thus inflammation is a strong osteoclastogenesis driver[21–23].

Activated osteoclasts adhere to the bone surface and develop brush borders. Next, they secret hydrochloric acid to dissolve the inorganic matrix and many collagenases, thus breaking down the organic matrix. In addition, osteoclasts can only resorb mineralized bone. The major cytokines that regulate osteoclast formation and activity are as follows: NF-κB ligand, OPG, IL-1, PTH, calcitonin, and vitamin D [5,24,25].

Further, osteocytes account for 90-95% of all bone cells in the adult skeleton. They are found throughout the bone matrix in spaces called vacuoles or lacunae. By definition, osteocytes are osteoblasts that surround themselves with secreted organic matrix[26]. The interplay between osteocyte, osteoclast, and osteoblast has been described, for example the death of osteocytes through trauma, cell senescence, or apoptosis results in osteoclast activation and consequently bone resorption, followed by repair via osteoblast activity[6]. This bystander activity helps to maintain calcium homeostasis [25,27].

So far, we have discussed the most common cells responsible for bone homeostasis, however, many other cells can be found in the bone, like the bone-lining cells [28,29]. Cells found outward the bone surfaces are called periosteal, meanwhile, those found lining inside the bone surfaces are called endosteal cells. These cells are derived from osteoblasts, and they are thought to act as a nutritional support for osteocytes. Yet, they facilitate and regulate the movement of calcium and phosphate into and out of the bone[30,31].

1.3. Osteogenesis

Bone development is traditionally classified as intramembranous and endochondral[13]. A third class called ectopic calcification has been suggested, however, it is related to inappropriate (pathological) mineralization of soft tissues [32]. The difference between the previous two classification (intramembranous and endochondral) relies on either the presence a cartilage model as bone precursor, intramembranous ossification. On the contrary, if there is hyaline cartilage serving as the precursor bone model, it is called endochondral ossification. Here we will briefly discuss both the events.

1.3.1. Intramembranous ossification

This process involves the differentiation and migration of MSCs to form osteoblasts. Osteoblasts gather themselves into clusters and form an ossification center.

From a cellular biology perspective, the cytoplasm of these osteoprogenitor cells changes and a dense Golgi area becomes evident, thus signalizing the differentiation into osteoblast, which then starts secreting collagen (mostly type I), bone sialoproteins, osteocalcin, and other osteogenic markers [33]. Calcium deposition to the osteoid matrix results in the hardening of the matrix and embroilment of osteoblasts, then resulting in the differentiation of osteoblasts into osteocytes. As the process continues the newly organized tissue becomes more vascularized and overpopulated of MSCs. This process leads to the formation of trabecular/cancellous bone, the vessels will generate the bone marrow, and MSCs attached to the new bone surface will form the periosteum. Cells found in the inner layer of the periosteum differentiate into osteoblasts and start secreting osteoid matrix parallel to the existing matrix, thus forming layers. Later, these layers will be known as cortical bone. Intramembranous ossification is responsible for the formation of the flat bones (skull and face) the mandible and the clavicle[34].

1.3.2. Endochondral ossification

Similar to intramembranous ossification, endochondral ossification starts with the proliferation, migration, and aggregation of MSCs to the unmineralized area. Under the influence of different cytokines (Table 1), the MSCs start expressing and secreting collagen type II and X and differentiate into chondrocytes, which are responsible for the production of an extracellular matrix (cartilage) that will serve as a template for bone growth [16,17,33]. The cartilage is a glass-like (hyaline) structure and it can be found in many joint surfaces, for example, ribs, nose, larynx, and trachea. During extracellular matrix calcification, the nutrients stop reaching the chondrocytes leading them to apoptosis. With the death of the chondrocytes, voids, and lacunae are created in the cartilage, which allows the migration of MSCs and blood vessels. Further, this will become the marrow cavity. The transport of osteoblast into the cartilage triggers the transformation of the perichondrium to the periosteum. The primary ossification center occurs when osteoblasts start mineralizing the diaphyseal region of the periosteum (periosteal collar). With the establishment of the periosteal bony collar, the chondrocytes in the midregion of the cartilage model become hypertrophic. As the chondrocytes enlarge, their surrounding cartilage matrix is resorbed, forming a thin irregular cartilage plate between the hypertrophic cells. The synthesis of alkaline phosphate by the chondrocytes results in the mineralization of the organic matrix. Concomitantly, osteoblasts are mineralizing the diaphysis, as the extremities of the bone cartilage continues to proliferate and grow, this

event is responsible for the longitudinal bone growth. This entire process repeats itself (secondary ossification) after birth when mineralization of the epiphyseal ends occurs[3,35]. Endochondral ossification is responsible for the growth of long bones.

1.4. Molecular aspects of bone mineralization

As aforementioned, bone growth and maintenance are carried through many biological events involving cellular and physiological stimuli. Here, we will focus on the molecular aspects involved in osteoblast turnover and bone mineralization, thus even though we shall discuss bone resorption eventually, we shall not dig further into its mechanisms.

1.4.1. MSCs Differentiation into osteoblasts

The osteoblasts synthesis route relies on the migration, proliferation, and differentiation of MSCs, which reside in the bone marrow [9,36]. MSC has the potential to differentiate into many cell lines (**Figure 1.6**), it includes adipocytes, myoblast, chondrocytes, fibroblasts, and osteoblasts, to cite only a few [8]. This process is highly controlled by cytokines (Table 1), growth factors, and mechanic stimuli, which culminate in the transcription of osteogenic-related genes, leading to the differentiation and specialization of different cell lines. For example, the transcription of Runx2 and Osterix (Osx) are both necessary for osteoblasts differentiation; SOX5/ 6/ 9 is necessary for chondrocyte differentiation; myoblasts are regulated by the expression of MyoD, and so on [8].

Many other genes (especially transcription factors) are highly involved in osteoblast turnover, like the AP-1 family, Atf4, and WNT/β-catenin signaling [37]. For example, Atf4 is known to control the expression of collagen type I and osteocalcin [38,39];

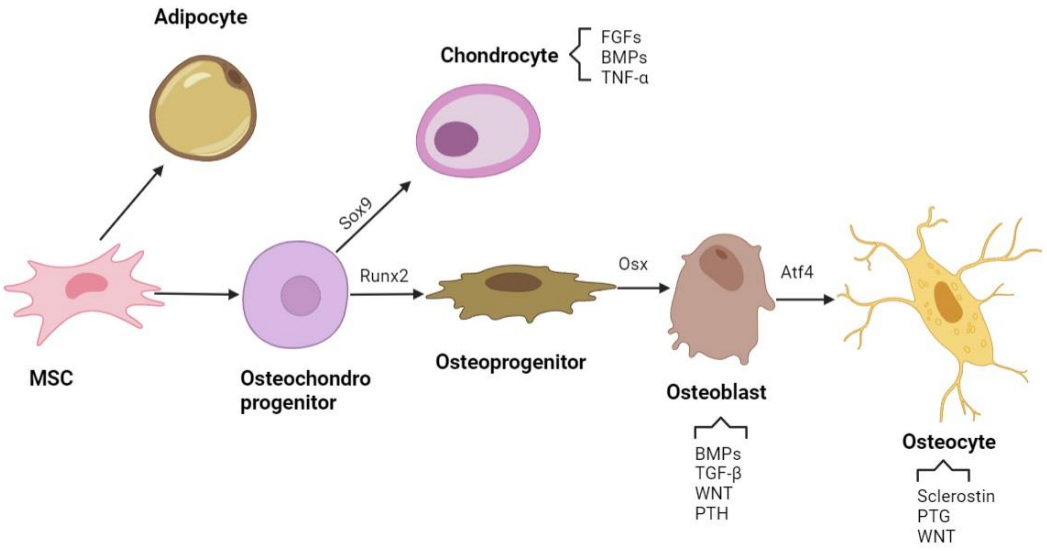

FIGURE 1. 6. SCHEMATIC REPRESENTATION OF MSC DIFFERENTIATION INTO DIFFERENT CELL LINES.

In addition, MSC maturation into different cell lines, as osteoblasts, demands a highly organized process that some authors [9,40] distinguish into at least five steps:

- MSC commitment to osteo-chondroprogenitors cell line (these cells are enriched in Runx2 and collagen 2α expression);
- Commitment to the osteoprogenitor cell line (Osx expression);
- Osteoprogenitor proliferation followed by osteoblast maturation (start to express osteocalcin and collagen type I);
- And finally, osteoblast apoptosis

A compelling review regarding cell line stage and gene expression profile can be found elsewhere [41–43].

1.4.2. Molecular pathways governing osteoblast turnover and activity

Signaling pathways controlling osteoblast activity and turnover are frightfully complex and they may be activated by hormones, growth factors, cytokines, and mechanical stimuli. They are activated during bone development (osteogenesis) as well as bone remodeling (homeostasis). It is important to point out that these pathways are not isolated, and they communicate and stimulate each other. Here, we will outline some of the most studied pathways responsible for controlling osteoblast activity. **Figure 1.7** displays some signaling pathways responsible for osteoblast homeostasis.

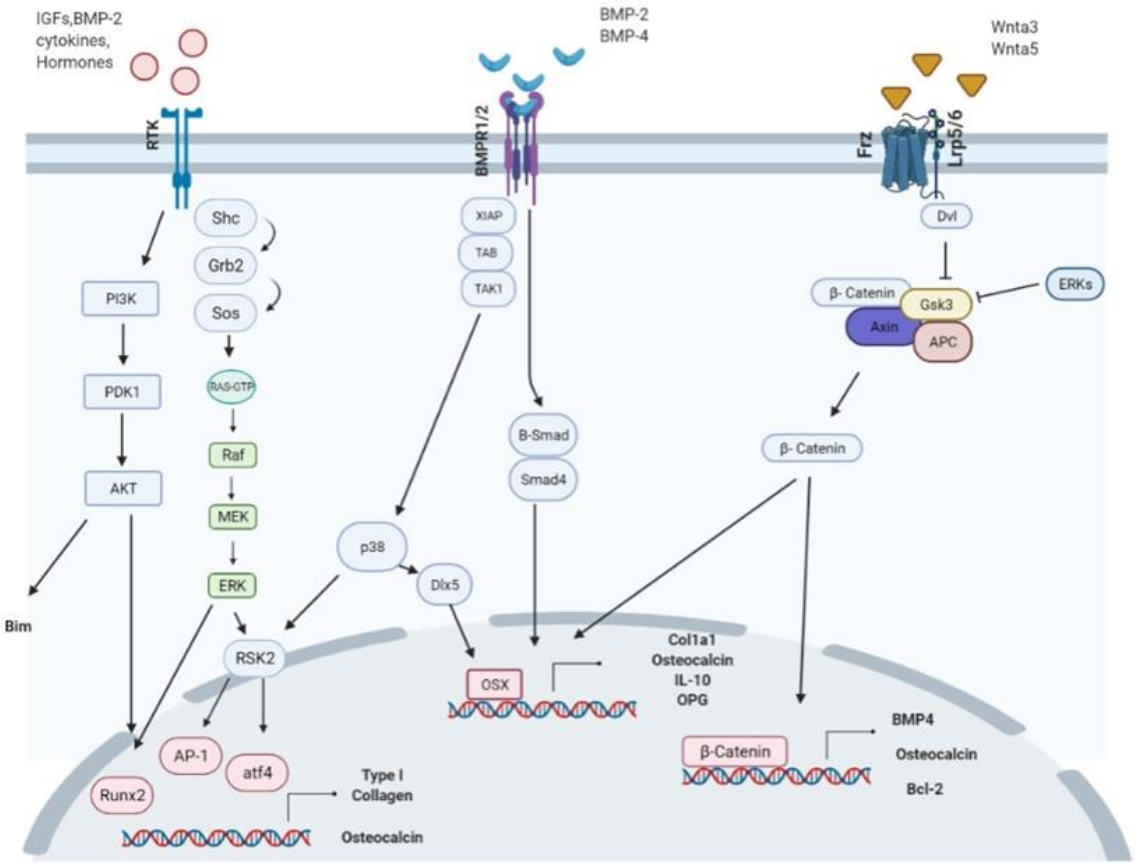

FIGURE 1. 7. SIMPLIFIED REPRESENTATION OF THE MAJOR SIGNALING PATHWAYS THAT GOVERN OSTEOBLAST TURNOVER

BMPs pathway

One of the most well-studied pathways involved in osteoblast homeostasis is the Bone Morphogenic Protein (BMP) pathway. In 1988, it was discovered the first BMP (BMP-2) member of this huge family (~12 BMPs have been identified), as a potent inducer of bone and cartilage formation[44]. BMPs constitute the largest subdivision of the TGF-β superfamily [45]. Unlike TGF-β members that use Smad2/3 as signal transducers, BMPs use Smad 1/5/8 [46]. In addition, BMPs can either sensibilize the canonical pathway BMPR-Smad or the non-canonical MAPK, PI-3K-Akt pathways[47].

Further, two receptors (BMP receptor type I and II, Ser/Thr kinase) are found on the osteoblast´s cell surface. BMPs first activate BMP receptor type II which leads to phosphorylation of the type I receptor. Once activated, the type I receptor phosphorylates Smad 1/5/8 and activates the downstream cascade leading to the Smad accumulation in

the nucleus. Smad complex (B-Smad and Smad4) regulates transcription factors of BMP target genes (Figure 1.7). Though it will not be discussed here, BMP signaling is tightly regulated and for each step of the cascade, there are several BMP antagonists in the extracellular matrix that are responsible for the negative control of the pathway [8,48,49]. For example, at the receptor level, Smad 6 and 7 behave like a decoy ligand by competing with BMP 2 and 4 for the BMP receptor 1 binding site [8]. Also, B-Smads can be degraded by the ubiquitin-proteosome system[50].

The BMP-Smad pathway regulates almost every stage of the osteoblast turnover, which includes the osteoblast differentiation from MSC, the expression of OCN, collagen, several transcription factors, etc. by these cells, and osteoclast-osteoblast communication[51–53]. In 1955, it was reported that the deletion of BMP2 and BMP4 resulted in mice with impaired bone development and osteoblast function[54], which was later linked to the reduced expression of Runx2 and Osx [55]. A wealth review regarding BMP signaling can be found here[44,56].

Wnt/β-Catenin pathway

The Wnt signaling pathway regulates several cellular processes (growth, differentiation, function, and apoptosis) and plays a crucial role in the development and maintenance of many tissues. However, the canonical pathway Wnt/β-catenin is particularly important in bone development [10].

Wnt family has at least 19 members and plays an important role in embryogenesis, postnatal development, and tumorigenesis[57]. The activation of this pathway requires the binding of the Wnt protein to its receptor, frizzled receptor, and the low-density lipoprotein receptor-related protein 5 and 6 (Lrp5/6) coreceptors. The parathyroid hormone receptor (PTH) can also activate these receptors, but it will not be discussed here [58,59]. However, in case of Wnt proteins are not expressed or if their binding to their receptor is blocked, degradation of β-catenin happens via interaction with the APC-Gsk3-Axin complex [10,60]. Under resting conditions, APC-Axin is a scaffold protein to Gsk3, which allows the Gsk3 kinase to phosphorylate β-catenin, targeting it for degradation by the β-TrCP-mediated ubiquitin/proteasome pathway. On the other hand, upon Wnt stimulation, the cascade downstream is activated through the complex Disheveled, Axin, and Frat-, which hampers the complex APC-Axin-Gsk3 by targeting and inhibiting Gsk3, thus causing the hyperphosphorylation of β-catenin. Consequently, stabilized β-catenin accumulates in the

cytosol and migrates toward the nucleus. Once in the nucleus, β-catenin interacts with the T cell factor lymphoid enhancer-binding factor (TCF/LEF) transcription factor and regulates many osteogenic-related genes, such as Myc, cyclin D, c-Jun, BMP4, Runx2, OCN, and so on [8,10] (Figure 1.7).

Wnt signaling is tightly regulated by several antagonists. For example, extracellular proteins (e.g., Sost and DKK) can bind LRP5/6 and inhibit the activation of the Wnt pathway [61–63]. Wnt signaling controls bone development and homeostasis in many ways, including cell commitment of MSCs, osteoblast proliferation, apoptosis, and osteoblast-osteoclast communication [10,64,65]. Loss-of-function mutation of LRP5 in patients is linked to severe osteoporosis [66], meanwhile, a mutation in the N terminus of human LRP5 reduces the affinity between LRP5 for Dkk1 (receptor antagonist) resulting in high bone mass [67–69].

Furthermore, it was found that the Wnt/β-catenin pathway stimulated the expression of Runx2 and OCN, and also downregulated the expression of C/EBP alpha, PPAR gamma, and Sox9. These results point toward the conclusion that the Wnt/β-catenin pathway favors osteoblast differentiation and inhibits chondrocyte differentiation [70,71]. Later, Rodda and McMahon (2006) confirmed the previous result by showing that β-catenin deletion in MSC hampered osteogenesis but enhanced chondrogenesis [40]. Wnt was also associated with osteoblast proliferation and survival [8,72–75]. Finally, Wnt/β-catenin signaling communicates with the BMP signaling, since Wnt1 and Wnt3a are induced by BMP-2[76].

MAPK pathway

The mitogen-activated protein kinase (MAPK) signaling is one of the most studied pathways in cellular biology. This pathway uses a cascade of at least three protein kinases to transduce an extracellular signal into an intracellular signal leading to gene transcription[77]. Generally, MAPK is activated by mitogenic signals (insulin, growth factors, cytokines, hormones, etc.)[78,79]. The sequential phosphorylation cascade starts with the activation of the receptor. The best-studied MAPK signaling activators in bone are the fibroblast growth factor (FGFs) and the insulin-like growth factor (IGFs), which stimulate the Receptor Tyrosine Kinase (RTK) leading to its dimerization and activation. Once activated, RTK can regulate itself by autophosphorylation as well as phosphorylate adaptor proteins, like Shc and Grb2, thus forming a complex. Once activated by

phosphorylation, Grb2 is recognized by Sos, which recruits Ras to the proximity of the plasma membrane, culminating in Ras activation. Finally, Ras can stimulate MAPKKK, which phosphorylates MAPKK. The later phosphorylate Erk1/2 (MAPK). This process is often called the “three protein kinases cascade” [80]. Erk1/2 phosphorylate transcription factors (e.g., c-Jun and c-Fos), which regulate gene transcription (Figure 1.7).

Nonetheless, MAPK is a promiscuous pathway that regulates many other signaling cascades (e.g., RSKs, MKs) [81]. It was previously shown that IGF-1 could induce the expression of Sp7 by activating the MAPK pathway[82]. However, the function of IGF in bone growth is not fully accepted, since some papers show that IGF inhibits osteoblasts differentiation, but facilitates osteochondrogenesis by upregulating the Sox2 gene [83]. The role of Erk on osteoblast turnover is still contradictory and not fully understood. One possible mechanism is that Erk positively controls Runx2 phosphorylation, thus increasing Runx2 activity[84]. Therefore, MAPK might indirectly regulate osteoblast differentiation through the activation of other downstream pathways [55,85,86].

Mechanical stress signaling

The last signaling process that we will discuss here is mechanical-related stress signaling. Though this thesis does not directly approach this type of signaling, it is important to keep in mind the importance of such stimuli. It is known that mechanical loading as well as gravity plays a crucial role in bone homeostasis. In addition, osteoblasts contain mechanoreceptors on their surface that respond to mechanical stress [87]. Also, the lack of mechanical stimuli negatively regulates osteoblast turnover, for example, due to long-term immobilization or low gravity, which were linked to osteoporosis[88–91]. Many signaling pathways are modulated by mechanical stress, such as Wnt/β-catenin, PKA, MAPKs, and Ca^{2+}, resulting in the control of osteogenic-linked genes[92], for example, Runx2 e other transcriptional factors[93].

Another important point in bone mineralization and the cellular pathways that drive this process is the release of extracellular vesicles by mineral competent cells. The vesicles able to bind to collagen fibers and to mineralize the ECM are named matrix vesicles.

1.4.3. Extracellular matrix mineralization by matrix vesicles

Origins

The mineralization of the extracellular matrix is a highly organized process (cell-regulated event) that occurs in bone, cementum, dentin, and enamel teeth. Mineralization-competent cells (osteoblasts, chondrocytes, odontoblasts) release a special class of extracellular vesicles, referred to as matrix vesicles (MVs), that play a pivotal role in ECM mineralization[94]. Pi and Ca^{2+} ions signaling participate in the biogenesis of MVs as was demonstrated using ion homeostasis and mineralization disorders studies in humans[95–99]. At the molecular level, Pi, and Ca^{2+} support the osteo/chondrogenic differentiation of progenitor cells, thus stimulating the release and function of MVs[95].

High-resolution microscopic imaging analysis shed light on the cellular mechanisms involved in MV´s biogenesis and their release by mineralizing-competent cells[100–103]. The analysis revealed that skeletal and dental cells are enriched in microvesicles containing minerals released from their plasma membrane [104–107]. It has been suggested that MVs are released through a mechanism involving microvilli budding from the plasma membrane[94]. Furthermore, comparative MVs´ proteomics and lipidomic data shared similarities in molecular composition with the cell membrane microvilli [108,109]. Among the similarities, we can quote cytoskeleton proteins (e.g., tubulin and actin), transporters (annexins, Na^+/K^+ ATPase), tissue non-specific alkaline phosphatase (TNAP)[109]. Also, the lipid content of matrix vesicles is similar to those found in lipid rafts, like sphingomyelin, ceramide, phosphatidylinositol, fatty acids, to cite a few [110–112]. Altogether, this evidence strongly suggests that MVs originate directly from the lipid raft domains of osteocompetent cells. Whether this mechanism is solely responsible for the release of MV is still under debate [113], and some authors [114,115] suggest that the MVs are formed inside the cells.

Matrix vesicle structure, protein, and lipid content

Matrix vesicles are spherical bilayered microstructures ranging from 100-300 nm in diameter able to bind to extracellular collagen and function as nanoreactors ready to nucleate calcium phosphates and conduct mineral growth and propagation onto the collagen fiber. Curiously, MVs are the only extracellular vesicles able to bind to collagen [94].

Regarding the lipid composition, MVs are enriched in lipids with a high affinity for Ca^{2+}, for example, sphingomyelin and cholesterol. Moreover, proteomics data indicate

that MVs are rich in proteins involved with the extracellular transport of P_i (PiT-1) and Ca^{2+} (annexins A2, A5, and A6)[94,109,116,117]. Also, the membrane of MVs contains specialized enzymes, such as tissue non-specific alkaline phosphatase, nucleotide pyrophosphatase phosphodiesterase 1 (NPP1), and phosphoethanolamine/phosphocholine phosphatase 1 (PHOSPHO1)[118–121] **Figure 1.8**.

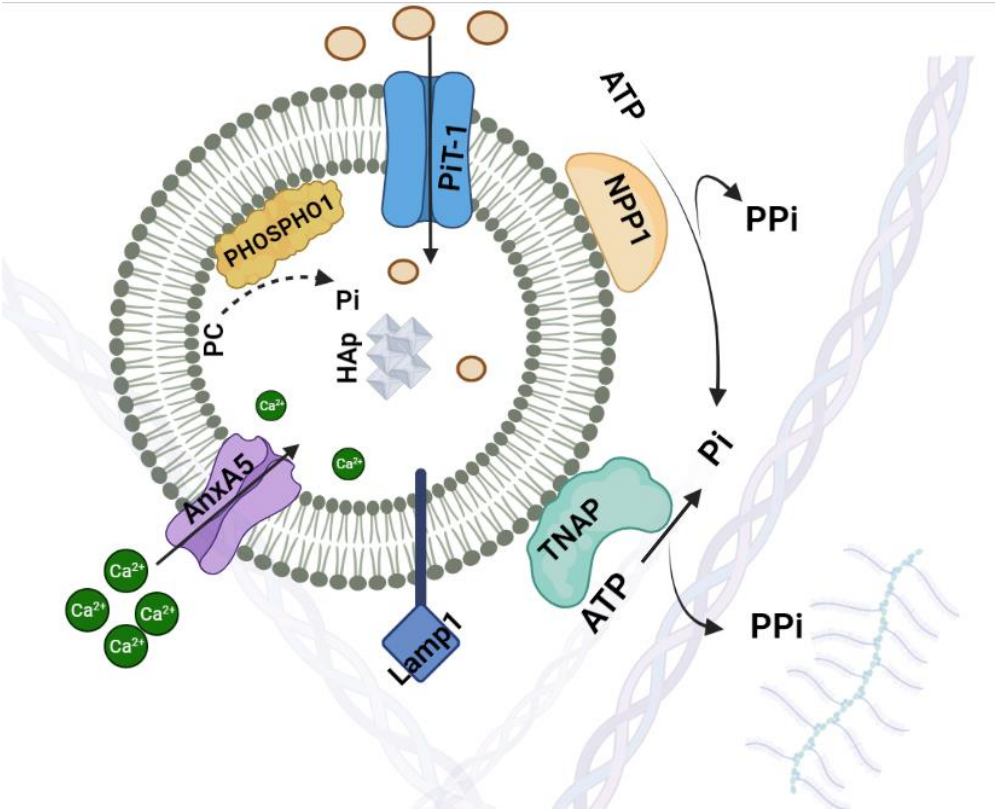

FIGURE 1. 8. SCHEMATIC REPRESENTATION OF THE CURRENT KNOWLEDGE OF THE BIOCHEMICAL PATHWAYS INVOLVED IN MV MINERALIZATION.

Here, we represented the Pi turnover as well as the Ca^{2+} uptake altogether. For simplification, one can separate both events. Pi turnover pathways involved the action of phosphatase (PHOSPHO1, NPP1, and TNAP) as well as the action of Pi transporters (PiT-1). PHOSPHO1 generates Pi in the MV lumen by the hydrolysis of phosphocholine (PC) derived from sphingomyelin (SM) by the action of SMPD3 (not represented). On the extracellular level, the propagation of apatite throughout the collagen matrix is mediated by the action of both phosphatases, TNAP and NPP1. TNAP hydrolyses ATP (adenosin triphosphate) and PPi (pyrophosphate) to obtain Pi and PPi. TNAP is responsible for increasing the Pi concentration but also restricts PPi availability. Since PPi is a strong mineralization inhibitor, TNAP regulates the balance of Pi/PPi ratio, hence controlling biomineralization. Nonetheless, NPP1 produces PPi and Pi from ATP and also is involved with the PPi/Pi balance. TNAP and PHOSPHO1 deficiency was related to hypomineralization, while NPP1 ablation was linked to hypercalcification (20684022). This exemplifies that the cooperation between PHOSPHO1, TNAP, and NPP1 provides an additional level of metabolic control over biomineralization. Moreover, Ca^{2+} transporters (AnxA family) and other unidentified calcium carriers (UCC) (not represented) are responsible for the uptake and early accumulation of Ca^{2+} inside the vesicles.

Each phosphatase and transporter are specialized in the uptake and storage of Ca^{2+} and P_i inside the MV lumen. For example, TNAP and NPP1 hydrolyze ATP to release respectively Pi and PPi extraluminally, which is then transported towards the MVs lumen by the transporter P_iT-1. It is important to point out that the balance between the production of P_i (by TNAP) and PP_i (by NPP1) levels will affect the MV capacity in nucleating apatite[94] since the PPi is a potent mineralization inhibitor and it is linked to pathological mineralization [122].

Additionally, the importance of TNAP to mineralization and P_i extraluminal balance has previously been described[123,124]. Here, I would like to highlight the importance of TNAP for health biomineralization. As mentioned previously, TNAP is attached to the outer leaflet of osteoblast´s cell membrane and it is primarily involved with the ATP hydrolysis to form Pi and PPi[125]. Millán and coworkers initially showed that the inactivation of the TNAP gene was linked to reduced longitudinal growth, hypo-mineralized areas in bone, as well as reduced survival in mice. Years later, TNAP deficiency was associated with hypophosphatasia[96,123] and osteopenia [126]. On the contrary, overexpression of TNAP was linked to vascular calcification[127,128] and stimulates vascular smooth muscle cell trans-differentiation into chondrocytes[129]. Moreover, intraluminal PHOSPHO1 releases Pi from the precursors' phosphocholine (PC) and phosphoethanolamine derived from the membrane phospholipids[130,131].

Nucleation and growth of mineral crystals

Biomineralization involves a sequential change in the structure and composition of the mineral, rather than a single-step pathway. The pathways of crystallization under chemical constraints can be found elsewhere [132]. Also, the Ca/P molar ratio changes are linked to age and degree of mineralization[132]. It also varies on other species [133]. Briefly, apatite synthesis is favored by the nucleation process within a supersaturated solution of Ca^{2+} and phosphate ions ($H_2PO_4^-$ and HPO_4^{2}), and the whereby of this process has been debated here[134]. There are two reliable mechanisms to describe biological mineralization accepted by the international scientific community, they are, (1) heterogenous nucleation and (2) physical-chemical or not-dependent of MVs nucleation processes. The first mechanism relies on organic and inorganic precursor seeds to direct the formation of apatite from soluble inorganic ion. In this case, investigators propose that the matrix vesicles are the site of initial or primary nucleation[134]. The transport, entrapment and

confinement of Ca^{2+} and Pi, together with the presence of other molecules and particles, provided by MVs favor the increase in the local supersaturation of the ions, which results in the lowering of the Gibbs free energy barrier to form the mineral first nuclei [135–137]. Moreover, the second mechanism proposes that the nucleation of apatite direct starts and are facilitate by matrix macromolecules, especially collagen, phosphoproteins, phospholipids and proteolipids[138–140]. Despite we recognize that either hypothesis for the initiation of mineralization is feasible, here we will focus our attention in the mechanism mediated by MVs.

The term nucleation refers to the phase transition from a state of high free energy (solvated state of the ionic precursors) to a state of lower free energy (synthesis of the biomineral crystal lattice). Once the mineral nuclei are formed inside the vesicles, the accumulation of additional ions leads to the growth of the particles (spontaneous process driven by free energy), followed by the disruption of the vesicle membrane, and propagation of the minerals onto the collagen fibers[141,142].

Nature has found a way to overcome chemical constraints (nucleation barrier) during biomineralization by compartmentalizing and controlling the chemical environment, regulating the pH, and synthesizing inhibitors, catalysts, and intermediates, thus decreasing the energy barrier. Besides collagen itself, many biomolecules contribute to this process, for example, the class of small integrin-biding ligand N-linked glycoprotein family(SIBLING), bone sialoprotein, and osteopontin, among others[143–148]The detailed physical-chemical laws that govern such a process are out of the scope of this thesis, however, they can be revised here[108,132]. How the apatite organizes itself along the collagen lattice will be discussed in the next section.

Biological apatite deposition onto the extracellular matrix

The most predominant component of the extracellular matrix present in the bone, tendon, dentin, and cementum is the type I collagen, which serves as a natural scaffold for biomineralization. Type I collagen is a helical polypeptide consisting of three individual chains (two α_1-helices and one α2-helices). Type I collagen organization is crucial for mineral deposition, supporting the structure versus function relationship described to all the proteins[149–152]. The extracellular collagen helices (~300 nm length) assemble themselves in such a way creating holes and overlap zones of approximately 40 and 27nm respectively. This architecture has a periodicity of ~67 nm, which gives rise to a

higher-ordered fiber **Figure 1.9.** Mineral aggregation inside the collagen fibrils is denominates *intrafibrillar mineralization*. Hence, the microarchitecture created by the collagen 3D disposition provides the perfect platform for nucleation and mineral growth in between the fibrils as first proposed by[151,153]. Further, other models [152,154] have been proposed where mineral deposition occurs outside (interfibrillar) the collagen matrix through distinct events.

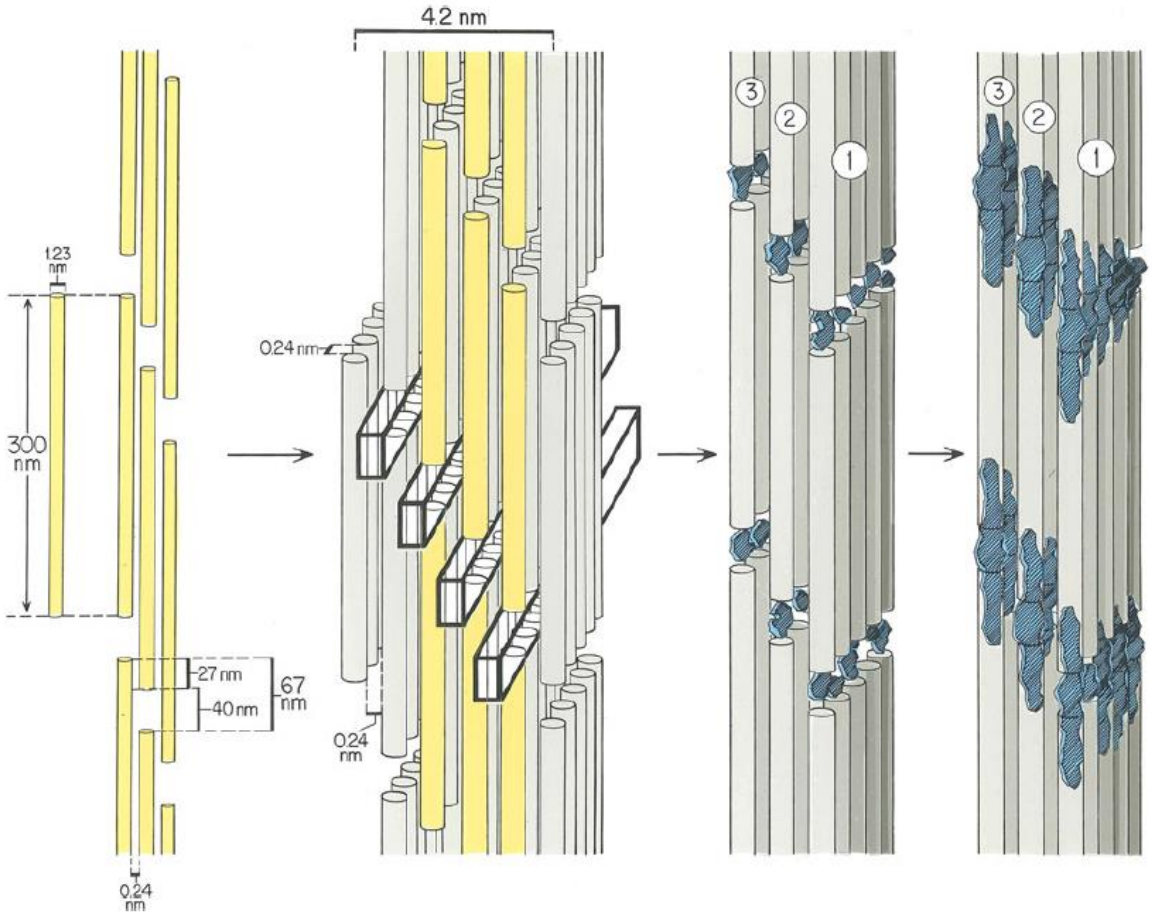

FIGURE 1. 9. 2D AND 3D MODEL OF INTRAFIBRILLAR AND INTERFIBRILLAR COLLAGEN WITH MINERAL GROWTH ASSEMBLY PREVIOUSLY STUDIED BY [151,153,155].

A single collagen molecule (left side) is 1.23 mm in diameter and 300 nm in length. The 2D aggregation of the fibrils forms an array with characteristic holes (40 nm) and overlap zones (27 nm). 2D architecture transition into 3D assemblages creates channels throughout the model. Adapted with permission from reference[156].

Independently of the type of bone being synthesized, the secretion of ECM by either osteoblast or chondrocytes, precedes the mineral deposition by the matrix vesicles. Under transmission electron microscopy (TEM), an initial stage of mineral deposition can be found **(Figure 1.10**), often referred to as *calcification nodules* (CN). Calcification nodules are found in the collagen fibrils (Co) interfibrillar spaces, and they may vary in size. The appearance of these calcification nodules is intimately related to different components, such as collagen type I charged amino acids, proteoglycans, non-collagenous proteins and membrane vesicles[151,154,157].

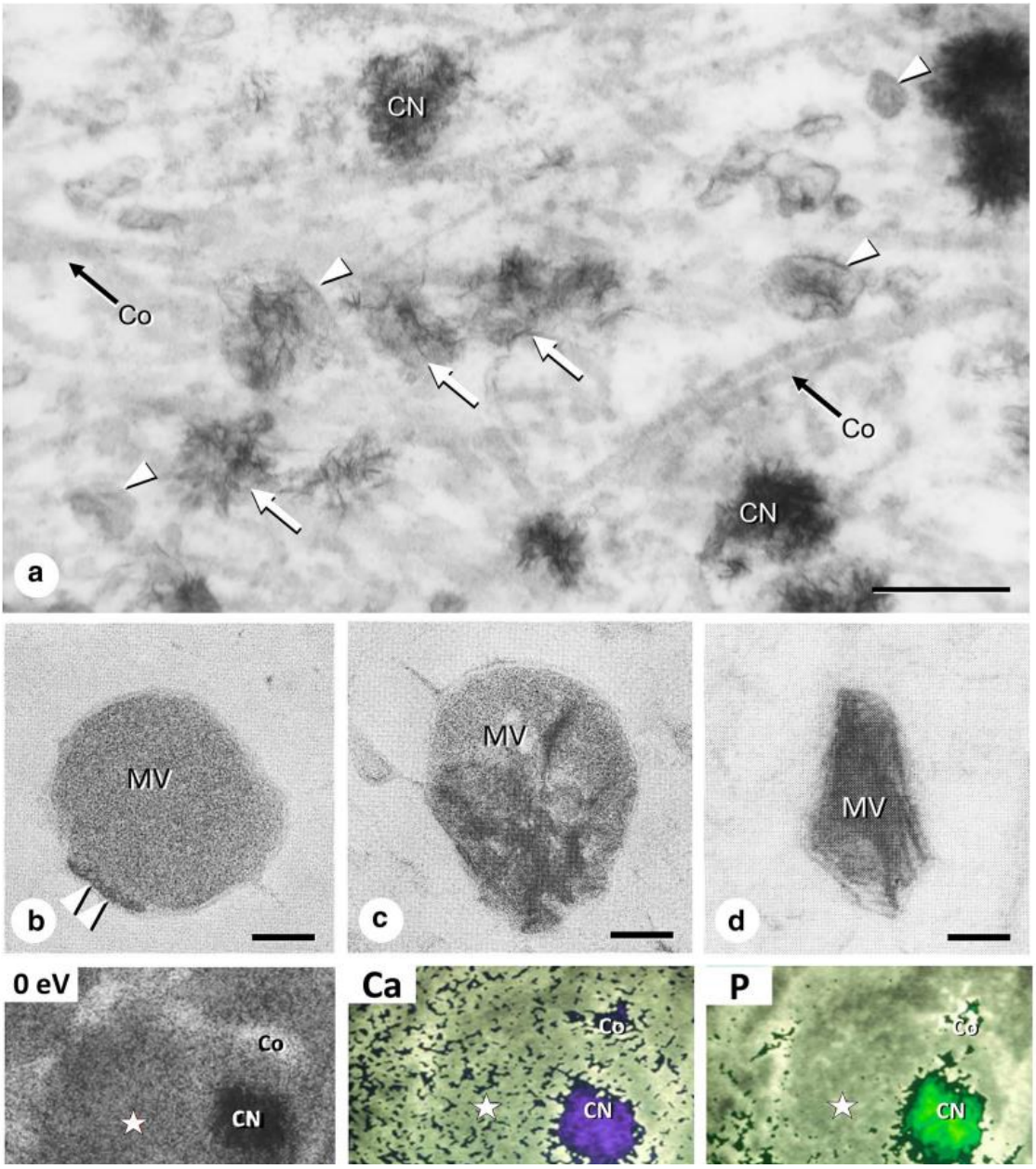

FIGURE 1. 10. TEM OBSERVATION OF MATRIX VESICLES AND CALCIFYING NODULES IN OSTEOID.

Panel **(A)** a high magnification of osteoid reveals the presence of matrix vesicles (white arrowheads), calcifying nodules (CN) and collagen fibrils (Co). Panel **(B)** rapid freezing technique demonstrates electron dense materials (white arrow heads) along the MV plasma membrane at the early stage of mineralization. Panel **(C)** MV are enriched in needle-like mineral crystal structures. Panel **(D)** MV inner crystal aggregates penetrate the MV membrane and are delivered into the ECM. Panels **(E-G)** elemental mapping analysis performed by energy-filtering transmission electron microscopy on calcifying nodules. Panel **(E)** TEM image reveals calcifying nodules (Co) and collagen fibrils (Co). Asterisk indicates the area among the calcifying nodule and collagen fibrils. Panel **(F)** Ca^{2+} is found in the proximity of CN, while Pi is attached to collagen fibrils and far from CN. Image adapted with permission from reference[158].

Early mineralization steps coincide with the appearance of many MVs **(Figure 1.10a)** and early crystal formation can be observed**.** Curiously, these crystals appear to be associated in and out the membrane of MVs **(Figure 1.10 b-d).** Elemental mapping analysis performed by electron energy loss spectroscopy (EELS) has demonstrated that the distribution of Ca^{2+} and phosphate varied according to the constituent nature, e.g., calcium was primarily associated with the proteoglycan-rich peripheral region of the matrix vesicle presented in the osteoid, while phosphate was predominantly found in organic materials, such as collagen fibrils [159] **(Figure 1.10e-g)**. The implication of this find, suggests that Ca^{2+} is abundant in the close proximity of the MV, while phosphorus somehow remains distant from the MV and calcifying nodules [160].

In poorly mineralized areas of osteoid, the extracellular meshwork of organic substances may limit the production of hydroxyapatite and inhibit the precipitation of mineralized crystals by controlling the spatial distribution of Ca^{2+} and phosphate, even if the extracellular fluid is supersaturated with both elements, as some believe[160]. One possible mechanism that nature found to overcome this constraint is through the creation of matrix vesicles-associated ions transporters as discussed previously **(section: Matrix vesicle structure, protein, and lipid content)**. Since phosphate is not abundant in the MV periphery, other form of phosphate uptake is required, for example through the action of the Pi transporters (PiT-1), or the phosphohydrolase activity of PHOSPHO1, to cite a few.

Mineralization of the collagen matrix **mediated** *by matrix vesicles*

Despite the attempt to delineate the molecular mechanism by which the MVs operate, much remains to be understood. Early transmission electron microscopy studies reported that mineral crystallites of bone were closely related to the structural disposition of type I collagen matrix[152,161]. Hence, it was evident that these two components were intimately related in bone. In 1957, it was hypothesized that type I collagen was the

nucleator of hydroxyapatite during boning formation[162]. The discovery of a membrane-bound vesicles embedded with the collagenous matrix in 1967, shed light on the biological mineralization process event[163,164]. These vesicles were later named matrix vesicles (MVs) and they were reported to be the sites of *de novo* apatite mineralization during growth plate development[163,164]. Later studies demonstrated that the MVs also bind type II and X collagen presented in growth plate cartilage (95,525 paper2). These studies revealed that the biding between collagen type II and MVs are facilitate by a protein, AnxA5, find in the MV membrane[165,166]. Despite these studies focused solely in growth plate cartilage, other studies involving the mineral deposition in sites where the type I collagen is a dominant structural protein, also demonstrated that AnxA5 bind to the collagen matrix and enhances mineral deposition[167].

There are two theories that explain collagen mineralization: (i) the hole zone theory, and (ii) the mineralization takes place along the superhelix of collagen fibrils. The hole zone theory postulates that during the non-mineralizing phase, the gaps found within the collagen fibrils are filled with small proteoglycans (decorin and biglycan)[160]. Upon removal of these proteins, extracellular Ca^{2+} and phosphate fill in the gap to generate calcium phosphate, hence mineralizing the collagen fibrils from the inside. This theory advocate that the initial mineralization starts in the collagen fibrils holes. On the other hand, transmission electron microscopy observations, revealed that the mineralization spread out from the contact point of calcifying nodules towards the periphery of collagen fibrils **(Figure 1.11a-c)**[168]. This finding suggests that collagen mineralization is associated with calcifying nodules[168,169]. Additionally, high TEM high magnification demonstrates that the spicules of calcium phosphate crystals are found in the fibrillar structures identical to the superhelix of collagen fibrils, which suggests that mineral crystals are deposited on the superhelix, which serves as scaffold[160] **(Figure 1.11b-e).** In contrast to the hole zone theory, panel C and D **(Figure 1.11)** reveals no spontaneous mineral deposition inside collagen fibrils, indicating that collagen mineralization is intrinsically related to the deposition of CN performed by the MVs, rather than spontaneous mineral deposition.

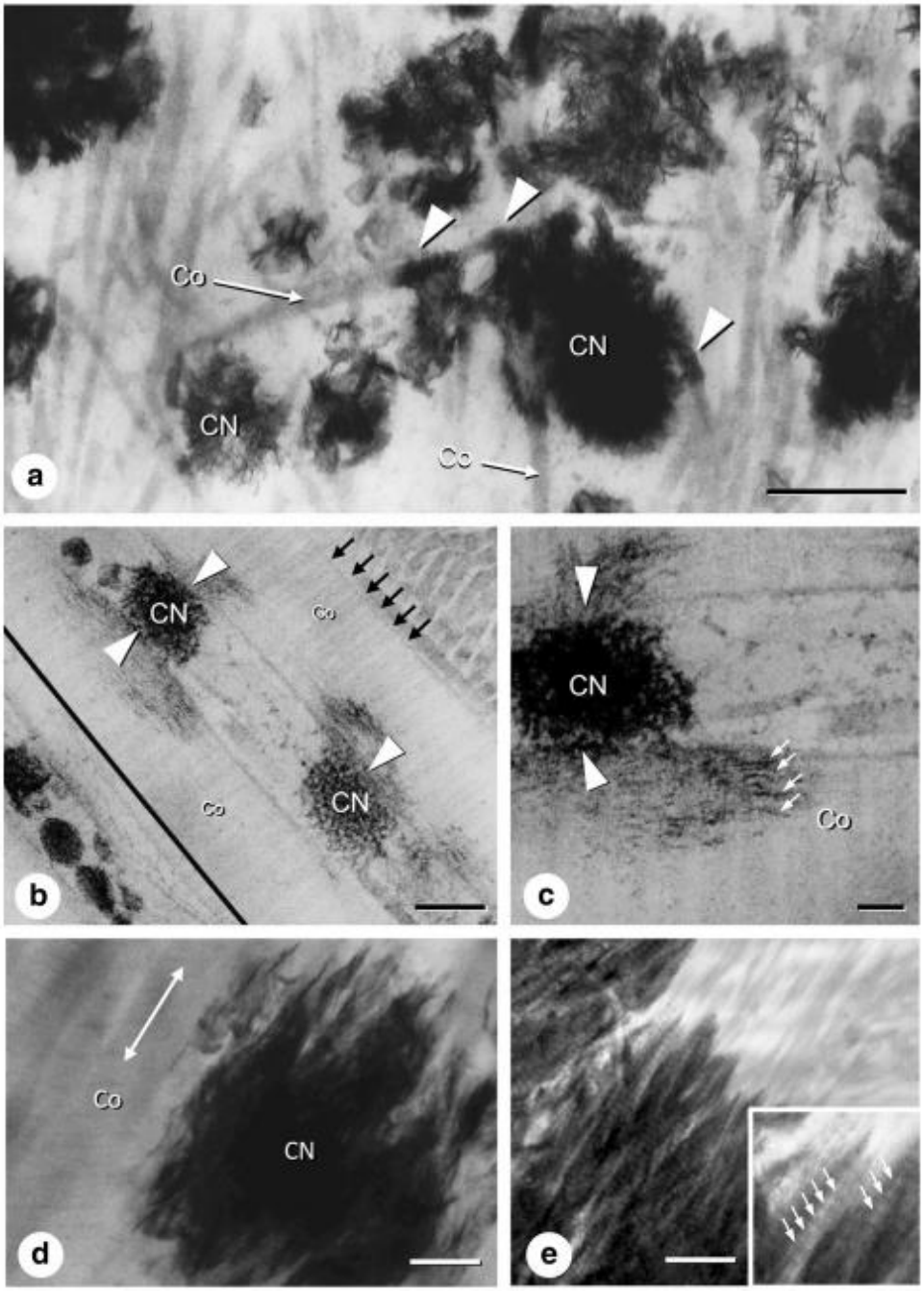

FIGURE 1. 11. TRANSMISSION ELECTRON MICROSCOPY ANALYSIS OF COLLAGEN MINERALIZATION.

Panel **(A)** several calcifying nodules (CN) can be visualized throughout the osteoid matrix making contact with the collagen fibrils (Co). Panel **(B)** Mineral crystal is localized on the collagen fibrils at the contact points of calcifying nodules and the collagen fibrils Higher magnification demonstrates that calcifying nodules spread out their mineral crystals (white arrowheads) onto the surfaces of marginal collagens fibrils (black arrows). Panel **(C)** the distribution of mineral crystals extends from the calcifying nodules through the collagen fiber (white arrows). Panel **(D)** A higher magnification of panel C showing the spread of mineral crystals. Panel **(E)** mineral crystals tips growth follows the longitudinal axis of collagen fibrils (white arrows). Image adapted with permission from reference[160].

References

1. Robin, M. *et al.* The Concentration of Bone-Related Organic Additives Drives the Pathway of Apatite Formation. *Cryst. Growth Des.* **21**, 3994–4004 (2021).

2. Grabowski, P. Physiology of bone. *Endocr. Dev.* **16**, 32–48 (2009).

3. Ross, M. H., & Pawlina, W. *Histology: A text and atlas: With correlated cell and molecular biology*. (2010).

4. Komori, T. What is the function of osteocalcin? *J. oral Biosci.* **62**, 223–227 (2020).

5. Buck, D. W. & Dumanian, G. A. Bone biology and physiology: Part I. The fundamentals. *Plast. Reconstr. Surg.* **129**, 1314–1320 (2012).

6. Clarke, B. Normal bone anatomy and physiology. *Clin. J. Am. Soc. Nephrol.* **3 Suppl 3**, S131-9 (2008).

7. Buckwalter, J. A., Glimcher, M. J., Cooper, R. R. & Recker, R. Bone biology. II: Formation, form, modeling, remodeling, and regulation of cell function. *Instr. Course Lect.* **45**, 387–99 (1996).

8. Chau, J. F. L., Leong, W. F. & Li, B. Signaling pathways governing osteoblast proliferation, differentiation and function. *Histol. Histopathol.* **24**, 1593–606 (2009).

9. Harada, S. & Rodan, G. A. Control of osteoblast function and regulation of bone mass. *Nature* **423**, 349–55 (2003).

10. Krishnan, V., Bryant, H. U. & Macdougald, O. A. Regulation of bone mass by Wnt signaling. *J. Clin. Invest.* **116**, 1202–9 (2006).

11. Schaffler, M. B. & Kennedy, O. D. Osteocyte signaling in bone. *Curr. Osteoporos. Rep.* **10**, 118–25 (2012).

12. Goldring, S. R. The osteocyte: key player in regulating bone turnover. *RMD open* **1**, e000049 (2015).

13. Marx, R. E. Bone and bone graft healing. *Oral Maxillofac. Surg. Clin. North Am.* **19**, 455–66, v (2007).

14. Xing, L., Schwarz, E. M. & Boyce, B. F. Osteoclast precursors, RANKL/RANK, and immunology. *Immunol. Rev.* **208**, 19–29 (2005).

15. Feng, X. RANKing intracellular signaling in osteoclasts. *IUBMB Life* **57**, 389–95 (2005).

16. Hoffman, L. M., Weston, A. D. & Underhill, T. M. Molecular mechanisms regulating chondroblast differentiation. *J. Bone Joint Surg. Am.* **85-A Suppl**, 124–32 (2003).

17. Li, J. & Dong, S. The Signaling Pathways Involved in Chondrocyte Differentiation and Hypertrophic Differentiation. *Stem Cells Int.* **2016**, 2470351 (2016).

18. Buckwalter, J. A., Glimcher, M. J., Cooper, R. R. & Recker, R. Bone biology. I: Structure, blood supply, cells, matrix, and mineralization. *Instr. Course Lect.* **45**, 371–86 (1996).

19. Everts, V. *et al.* The bone lining cell: its role in cleaning Howship's lacunae and initiating bone formation. *J. Bone Miner. Res.* **17**, 77–90 (2002).

20. Boyce, B. F. & Xing, L. Functions of RANKL/RANK/OPG in bone modeling and remodeling. *Arch. Biochem. Biophys.* **473**, 139–46 (2008).

21. Walsh, M. C. & Choi, Y. Regulation of T cell-associated tissues and T cell activation by RANKL-RANK-OPG. *J. Bone Miner. Metab.* **39**, 54–63 (2021).

22. Okamoto, K. & Takayanagi, H. Osteoimmunology. *Cold Spring Harb. Perspect. Med.* **9**, (2019).

23. Hienz, S. A., Paliwal, S. & Ivanovski, S. Mechanisms of Bone Resorption in Periodontitis. *J. Immunol. Res.* **2015**, 615486 (2015).

24. Boyle, W. J., Simonet, W. S. & Lacey, D. L. Osteoclast differentiation and activation. *Nature* **423**, 337–42 (2003).

25. Blair, H. C. & Athanasou, N. A. Recent advances in osteoclast biology and pathological bone resorption. *Histol. Histopathol.* **19**, 189–99 (2004).

26. Bonewald, L. F. & Johnson, M. L. Osteocytes, mechanosensing and Wnt signaling. *Bone* **42**, 606–15 (2008).

27. Rupp, M. *et al.* Osteocytes. *Z. Orthop. Unfall.* **157**, 154–163 (2019).

28. Lee, J. Y., Yang, J.-Y. & Kim, S. W. Bone Lining Cells Could Be Sources of Bone Marrow Adipocytes. *Front. Endocrinol. (Lausanne).* **12**, 766254 (2021).

29. Eriksen, E. F. Cellular mechanisms of bone remodeling. *Rev. Endocr. Metab. Disord.* **11**, 219–27 (2010).

30. Miller, S. C., de Saint-Georges, L., Bowman, B. M. & Jee, W. S. Bone lining cells: structure and function. *Scanning Microsc.* **3**, 953–60; discussion 960-1 (1989).

31. Matic, I. *et al.* Quiescent Bone Lining Cells Are a Major Source of Osteoblasts During

Adulthood. *Stem Cells* **34**, 2930–2942 (2016).

32. Przybylski, A. Discharge pattern of single neuronal units in cortical projection area of vagus nerve during successive episodes of hypoxia. *Acta Physiol. Pol.* **27**, 413–24 (1976).

33. Breeland, G., Sinkler, M. A. & Menezes, R. G. *Embryology, Bone Ossification*. *StatPearls* (2023).

34. Percival, C. J. & Richtsmeier, J. T. Angiogenesis and intramembranous osteogenesis. *Dev. Dyn.* **242**, 909–22 (2013).

35. Ortega, N., Behonick, D. J. & Werb, Z. Matrix remodeling during endochondral ossification. *Trends Cell Biol.* **14**, 86–93 (2004).

36. Yang, X. & Karsenty, G. Transcription factors in bone: developmental and pathological aspects. *Trends Mol. Med.* **8**, 340–5 (2002).

37. Karsenty, G. Transcriptional control of skeletogenesis. *Annu. Rev. Genomics Hum. Genet.* **9**, 183–96 (2008).

38. Yang, X. *et al.* ATF4 is a substrate of RSK2 and an essential regulator of osteoblast biology; implication for Coffin-Lowry Syndrome. *Cell* **117**, 387–98 (2004).

39. Zhang, K. *et al.* The PERK-EIF2α-ATF4 signaling branch regulates osteoblast differentiation and proliferation by PTH. *Am. J. Physiol. Endocrinol. Metab.* **316**, E590–E604 (2019).

40. Rodda, S. J. & McMahon, A. P. Distinct roles for Hedgehog and canonical Wnt signaling in specification, differentiation and maintenance of osteoblast progenitors. *Development* **133**, 3231–44 (2006).

41. Koo, K.-T. *et al.* Time-dependent expression of osteoblast marker genes in human primary cells cultured on microgrooved titanium substrata. *Clin. Oral Implants Res.* **25**, 714–22 (2014).

42. Qi, H. *et al.* Identification of genes responsible for osteoblast differentiation from human mesodermal progenitor cells. *Proc. Natl. Acad. Sci. U. S. A.* **100**, 3305–10 (2003).

43. Kulterer, B. *et al.* Gene expression profiling of human mesenchymal stem cells derived from bone marrow during expansion and osteoblast differentiation. *BMC Genomics* **8**, 70 (2007).

44. Salazar, V. S., Gamer, L. W. & Rosen, V. BMP signalling in skeletal development, disease and repair. *Nat. Rev. Endocrinol.* **12**, 203–21 (2016).

45. Derynck, R. & Budi, E. H. Specificity, versatility, and control of TGF-β family signaling. *Sci. Signal.* **12**, (2019).

46. Benitez, M. A. *et al.* Mother-fetus transference of lead and cadmium in rats: involvement of metallothionein. *Histol. Histopathol.* **24**, 1523–30 (2009).

47. ten Dijke, P. & Hill, C. S. New insights into TGF-beta-Smad signalling. *Trends Biochem. Sci.* **29**, 265–73 (2004).

48. Itoh, S. & ten Dijke, P. Negative regulation of TGF-beta receptor/Smad signal transduction. *Curr. Opin. Cell Biol.* **19**, 176–84 (2007).

49. Lee, P. S. W., Chang, C., Liu, D. & Derynck, R. Sumoylation of Smad4, the common Smad mediator of transforming growth factor-beta family signaling. *J. Biol. Chem.* **278**, 27853–63 (2003).

50. Dupont, S. *et al.* Germ-layer specification and control of cell growth by Ectodermin, a Smad4 ubiquitin ligase. *Cell* **121**, 87–99 (2005).

51. Cao, X. & Chen, D. The BMP signaling and in vivo bone formation. *Gene* **357**, 1–8 (2005).

52. Miyazono, K., Maeda, S. & Imamura, T. BMP receptor signaling: transcriptional targets, regulation of signals, and signaling cross-talk. *Cytokine Growth Factor Rev.* **16**, 251–63 (2005).

53. Lowery, J. W. & Rosen, V. The BMP Pathway and Its Inhibitors in the Skeleton. *Physiol. Rev.* **98**, 2431–2452 (2018).

54. Winnier, G., Blessing, M., Labosky, P. A. & Hogan, B. L. Bone morphogenetic protein-4 is required for mesoderm formation and patterning in the mouse. *Genes Dev.* **9**, 2105–16 (1995).

55. Wang, X., Goh, C. H. & Li, B. p38 mitogen-activated protein kinase regulates osteoblast differentiation through osterix. *Endocrinology* **148**, 1629–37 (2007).

56. Li, X. & Cao, X. BMP signaling and skeletogenesis. *Ann. N. Y. Acad. Sci.* **1068**, 26–40 (2006).

57. Moon, R. T., Kohn, A. D., De Ferrari, G. V & Kaykas, A. WNT and beta-catenin signalling: diseases and therapies. *Nat. Rev. Genet.* **5**, 691–701 (2004).

58. Chen, T., Wang, Y., Hao, Z., Hu, Y. & Li, J. Parathyroid hormone and its related peptides in bone metabolism. *Biochem. Pharmacol.* **192**, 114669 (2021).

59. Carrillo-López, N. *et al.* Role of the RANK/RANKL/OPG and Wnt/β-Catenin Systems in

CKD Bone and Cardiovascular Disorders. *Calcif. Tissue Int.* **108**, 439–451 (2021).

60. Hay, E. *et al.* Interaction between LRP5 and Frat1 mediates the activation of the Wnt canonical pathway. *J. Biol. Chem.* **280**, 13616–23 (2005).

61. He, X., Semenov, M., Tamai, K. & Zeng, X. LDL receptor-related proteins 5 and 6 in Wnt/beta-catenin signaling: arrows point the way. *Development* **131**, 1663–77 (2004).

62. Hecker, E. *et al.* International symposium: skin carcinogenesis in man and in experimental models. Heidelberg, Federal Republic of Germany, 29-31 October 1991. *J. Cancer Res. Clin. Oncol.* **118**, 321–8 (1992).

63. Mao, B. *et al.* Kremen proteins are Dickkopf receptors that regulate Wnt/beta-catenin signalling. *Nature* **417**, 664–7 (2002).

64. Glass, D. A. & Karsenty, G. In vivo analysis of Wnt signaling in bone. *Endocrinology* **148**, 2630–4 (2007).

65. Robling, A. G. & Bonewald, L. F. The Osteocyte: New Insights. *Annu. Rev. Physiol.* **82**, 485–506 (2020).

66. Gong, Y. *et al.* LDL receptor-related protein 5 (LRP5) affects bone accrual and eye development. *Cell* **107**, 513–23 (2001).

67. Ai, M., Holmen, S. L., Van Hul, W., Williams, B. O. & Warman, M. L. Reduced affinity to and inhibition by DKK1 form a common mechanism by which high bone mass-associated missense mutations in LRP5 affect canonical Wnt signaling. *Mol. Cell. Biol.* **25**, 4946–55 (2005).

68. Boyden, L. M. *et al.* High bone density due to a mutation in LDL-receptor-related protein 5. *N. Engl. J. Med.* **346**, 1513–21 (2002).

69. Van Wesenbeeck, L. *et al.* Six novel missense mutations in the LDL receptor-related protein 5 (LRP5) gene in different conditions with an increased bone density. *Am. J. Hum. Genet.* **72**, 763–71 (2003).

70. Day, T. F., Guo, X., Garrett-Beal, L. & Yang, Y. Wnt/beta-catenin signaling in mesenchymal progenitors controls osteoblast and chondrocyte differentiation during vertebrate skeletogenesis. *Dev. Cell* **8**, 739–50 (2005).

71. Hill, T. P., Später, D., Taketo, M. M., Birchmeier, W. & Hartmann, C. Canonical Wnt/beta-catenin signaling prevents osteoblasts from differentiating into chondrocytes. *Dev. Cell* **8**, 727–38 (2005).

72. Bodine, P. V. N. *et al.* The Wnt antagonist secreted frizzled-related protein-1 is a negative regulator of trabecular bone formation in adult mice. *Mol. Endocrinol.* **18**, 1222–37 (2004).

73. Babij, P. *et al.* High bone mass in mice expressing a mutant LRP5 gene. *J. Bone Miner. Res.* **18**, 960–74 (2003).

74. Bodine, P. V. N. *et al.* The Wnt antagonist secreted frizzled-related protein-1 controls osteoblast and osteocyte apoptosis. *J. Cell. Biochem.* **96**, 1212–30 (2005).

75. Almeida, M., Han, L., Bellido, T., Manolagas, S. C. & Kousteni, S. Wnt proteins prevent apoptosis of both uncommitted osteoblast progenitors and differentiated osteoblasts by beta-catenin-dependent and -independent signaling cascades involving Src/ERK and phosphatidylinositol 3-kinase/AKT. *J. Biol. Chem.* **280**, 41342–51 (2005).

76. Rawadi, G., Vayssière, B., Dunn, F., Baron, R. & Roman-Roman, S. BMP-2 controls alkaline phosphatase expression and osteoblast mineralization by a Wnt autocrine loop. *J. Bone Miner. Res.* **18**, 1842–53 (2003).

77. Gerhard, K. *Biochemistry of signal transduction and regulation*. (2014).

78. Murphy, L. O. & Blenis, J. MAPK signal specificity: the right place at the right time. *Trends Biochem. Sci.* **31**, 268–75 (2006).

79. Kolch, W. Coordinating ERK/MAPK signalling through scaffolds and inhibitors. *Nat. Rev. Mol. Cell Biol.* **6**, 827–37 (2005).

80. McKay, M. M. & Morrison, D. K. Integrating signals from RTKs to ERK/MAPK. *Oncogene* **26**, 3113–21 (2007).

81. Anjum, R. & Blenis, J. The RSK family of kinases: emerging roles in cellular signalling. *Nat. Rev. Mol. Cell Biol.* **9**, 747–58 (2008).

82. Celil, A. B. & Campbell, P. G. BMP-2 and insulin-like growth factor-I mediate Osterix (Osx) expression in human mesenchymal stem cells via the MAPK and protein kinase D signaling pathways. *J. Biol. Chem.* **280**, 31353–9 (2005).

83. Mansukhani, A., Ambrosetti, D., Holmes, G., Cornivelli, L. & Basilico, C. Sox2 induction by FGF and FGFR2 activating mutations inhibits Wnt signaling and osteoblast differentiation. *J. Cell Biol.* **168**, 1065–76 (2005).

84. Ge, C., Xiao, G., Jiang, D. & Franceschi, R. T. Critical role of the extracellular signal-regulated kinase-MAPK pathway in osteoblast differentiation and skeletal development. *J. Cell Biol.* **176**, 709–18 (2007).

85. Ulsamer, A. *et al.* BMP-2 induces Osterix expression through up-regulation of Dlx5 and its phosphorylation by p38. *J. Biol. Chem.* **283**, 3816–26 (2008).

86. Akiyama, H. *et al.* Interactions between Sox9 and beta-catenin control chondrocyte differentiation. *Genes Dev.* **18**, 1072–87 (2004).

87. Robling, A. G., Castillo, A. B. & Turner, C. H. Biomechanical and molecular regulation of bone remodeling. *Annu. Rev. Biomed. Eng.* **8**, 455–98 (2006).

88. Inoue, D. [Musculoskeletal rehabilitation and bone. Mechanical stress on the skeletal system]. *Clin. Calcium* **20**, 503–11 (2010).

89. Zhang, L., Zheng, Y.-L., Wang, R., Wang, X.-Q. & Zhang, H. Exercise for osteoporosis: A literature review of pathology and mechanism. *Front. Immunol.* **13**, 1005665 (2022).

90. Herrmann, M. *et al.* Interactions between Muscle and Bone-Where Physics Meets Biology. *Biomolecules* **10**, (2020).

91. Takahashi, K. *et al.* Gravity sensing in plant and animal cells. *NPJ microgravity* **7**, 2 (2021).

92. Akhter, M. P. *et al.* Bone biomechanical properties in LRP5 mutant mice. *Bone* **35**, 162–9 (2004).

93. Hughes-Fulford, M. Signal transduction and mechanical stress. *Sci. STKE* **2004**, RE12 (2004).

94. Bottini, M. *et al.* Matrix vesicles from chondrocytes and osteoblasts: Their biogenesis, properties, functions and biomimetic models. *Biochim. Biophys. acta. Gen. Subj.* **1862**, 532–546 (2018).

95. Chaudhary, S. C. *et al.* Phosphate induces formation of matrix vesicles during odontoblast-initiated mineralization in vitro. *Matrix Biol.* **52–54**, 284–300 (2016).

96. Orimo, H. The mechanism of mineralization and the role of alkaline phosphatase in health and disease. *J. Nippon Med. Sch.* **77**, 4–12 (2010).

97. Bielesz, B., Klaushofer, K. & Oberbauer, R. Renal phosphate loss in hereditary and acquired disorders of bone mineralization. *Bone* **35**, 1229–39 (2004).

98. Marini, F., Giusti, F., Iantomasi, T. & Brandi, M. L. Congenital Metabolic Bone Disorders as a Cause of Bone Fragility. *Int. J. Mol. Sci.* **22**, (2021).

99. Reznikov, N. *et al.* Biological stenciling of mineralization in the skeleton: Local enzymatic removal of inhibitors in the extracellular matrix. *Bone* **138**, 115447 (2020).

100. Hale, J. E. & Wuthier, R. E. The mechanism of matrix vesicle formation. Studies on the composition of chondrocyte microvilli and on the effects of microfilament-perturbing agents on cellular vesiculation. *J. Biol. Chem.* **262**, 1916–25 (1987).

101. Rabinovitch, A. L. & Anderson, H. C. Biogenesis of matrix vesicles in cartilage growth plates. *Fed. Proc.* **35**, 112–6 (1976).

102. Borg, T. K., Runyan, R. & Wuthier, R. E. A freeze-fracture study of avian epiphyseal cartilage differentiation. *Anat. Rec.* **199**, 449–57 (1981).

103. Akisaka, T. & Shigenaga, Y. Ultrastructure of growing epiphyseal cartilage processed by rapid freezing and freeze-substitution. *J. Electron Microsc. (Tokyo).* **32**, 305–20 (1983).

104. Anderson, H. C., Garimella, R. & Tague, S. E. The role of matrix vesicles in growth plate development and biomineralization. *Front. Biosci.* **10**, 822–37 (2005).

105. Magne, D. *et al.* Phosphate is a specific signal for ATDC5 chondrocyte maturation and apoptosis-associated mineralization: possible implication of apoptosis in the regulation of endochondral ossification. *J. Bone Miner. Res.* **18**, 1430–42 (2003).

106. Garcés-Ortíz, M., Ledesma-Montes, C. & Reyes-Gasga, J. Presence of matrix vesicles in the body of odontoblasts and in the inner third of dentinal tissue: a scanning electron microscopic study. *Med. Oral Patol. Oral Cir. Bucal* **18**, e537-41 (2013).

107. Rilla, K. *et al.* Hyaluronan production enhances shedding of plasma membrane-derived microvesicles. *Exp. Cell Res.* **319**, 2006–2018 (2013).

108. Abdallah, D. *et al.* Fatty acid composition in matrix vesicles and in microvilli from femurs of chicken embryos revealed selective recruitment of fatty acids. *Biochem. Biophys. Res. Commun.* **446**, 1161–4 (2014).

109. Balcerzak, M. *et al.* Proteome analysis of matrix vesicles isolated from femurs of chicken embryo. *Proteomics* **8**, 192–205 (2008).

110. Lorent, J. H. & Levental, I. Structural determinants of protein partitioning into ordered membrane domains and lipid rafts. *Chem. Phys. Lipids* **192**, 23–32 (2015).

111. Róg, T. & Vattulainen, I. Cholesterol, sphingolipids, and glycolipids: what do we know about their role in raft-like membranes? *Chem. Phys. Lipids* **184**, 82–104 (2014).

112. Balcerzak, M. *et al.* A comparative analysis of strategies for isolation of matrix vesicles. *Anal. Biochem.* **361**, 176–82 (2007).

113. Ghossoub, R. *et al.* Syntenin-ALIX exosome biogenesis and budding into multivesicular

bodies are controlled by ARF6 and PLD2. *Nat. Commun.* **5**, 3477 (2014).

114. Mahamid, J. *et al.* Bone mineralization proceeds through intracellular calcium phosphate loaded vesicles: a cryo-electron microscopy study. *J. Struct. Biol.* **174**, 527–35 (2011).

115. Boonrungsiman, S. *et al.* The role of intracellular calcium phosphate in osteoblast-mediated bone apatite formation. *Proc. Natl. Acad. Sci. U. S. A.* **109**, 14170–14175 (2012).

116. Thouverey, C. *et al.* Proteomic characterization of biogenesis and functions of matrix vesicles released from mineralizing human osteoblast-like cells. *J. Proteomics* **74**, 1123–34 (2011).

117. Cornely, R., Rentero, C., Enrich, C., Grewal, T. & Gaus, K. Annexin A6 is an organizer of membrane microdomains to regulate receptor localization and signalling. *IUBMB Life* **63**, 1009–17 (2011).

118. Yadav, M. C. *et al.* Skeletal Mineralization Deficits and Impaired Biogenesis and Function of Chondrocyte-Derived Matrix Vesicles in Phospho1(-/-) and Phospho1/Pi t1 Double-Knockout Mice. *J. Bone Miner. Res.* **31**, 1275–86 (2016).

119. Andrilli, L. H. S. *et al.* NPP1 and TNAP hydrolyze ATP synergistically during biomineralization. *Purinergic Signal.* (2022) doi:10.1007/s11302-022-09882-2.

120. Kirsch, T. *et al.* Annexin V-mediated calcium flux across membranes is dependent on the lipid composition: implications for cartilage mineralization. *Biochemistry* **36**, 3359–67 (1997).

121. Chavkin, N. W., Chia, J. J., Crouthamel, M. H. & Giachelli, C. M. Phosphate uptake-independent signaling functions of the type III sodium-dependent phosphate transporter, PiT-1, in vascular smooth muscle cells. *Exp. Cell Res.* **333**, 39–48 (2015).

122. Garimella, R., Bi, X., Anderson, H. C. & Camacho, N. P. Nature of phosphate substrate as a major determinant of mineral type formed in matrix vesicle-mediated in vitro mineralization: An FTIR imaging study. *Bone* **38**, 811–7 (2006).

123. Millán, J. L. & Whyte, M. P. Alkaline Phosphatase and Hypophosphatasia. *Calcif. Tissue Int.* **98**, 398–416 (2016).

124. Millán, J. L. Alkaline Phosphatases : Structure, substrate specificity and functional relatedness to other members of a large superfamily of enzymes. *Purinergic Signal.* **2**, 335–41 (2006).

125. Bolean, M. *et al.* Biophysical aspects of biomineralization. *Biophys. Rev.* **9**, 747–760 (2017).

126. Zhang, H. *et al.* Promotion effect of FGF23 on osteopenia in congenital scoliosis through FGFr3/TNAP/OPN pathway. *Chin. Med. J. (Engl).* **136**, 1468–1477 (2023).

127. Savinov, A. Y. *et al.* Transgenic Overexpression of Tissue-Nonspecific Alkaline Phosphatase (TNAP) in Vascular Endothelium Results in Generalized Arterial Calcification. *J. Am. Heart Assoc.* **4**, (2015).

128. Sebastián-Serrano, Á. *et al.* TNAP upregulation is a critical factor in Tauopathies and its blockade ameliorates neurotoxicity and increases life-expectancy. *Neurobiol. Dis.* **165**, 105632 (2022).

129. Fakhry, M. *et al.* TNAP stimulates vascular smooth muscle cell trans-differentiation into chondrocytes through calcium deposition and BMP-2 activation: Possible implication in atherosclerotic plaque stability. *Biochim. Biophys. acta. Mol. basis Dis.* **1863**, 643–653 (2017).

130. Dillon, S., Staines, K. A., Millán, J. L. & Farquharson, C. How To Build a Bone: PHOSPHO1, Biomineralization, and Beyond. *JBMR plus* **3**, e10202 (2019).

131. Ciancaglini, P. *et al.* Kinetic analysis of substrate utilization by native and TNAP-, NPP1-, or PHOSPHO1-deficient matrix vesicles. *J. Bone Miner. Res.* **25**, 716–723 (2010).

132. Habraken, W. J. E. M. *et al.* Ion-association complexes unite classical and non-classical theories for the biomimetic nucleation of calcium phosphate. *Nat. Commun.* **4**, 1507 (2013).

133. Akiva, A. *et al.* Mineral Formation in the Larval Zebrafish Tail Bone Occurs via an Acidic Disordered Calcium Phosphate Phase. *J. Am. Chem. Soc.* **138**, 14481–14487 (2016).

134. Golub, E. E. Biomineralization and matrix vesicles in biology and pathology. *Semin. Immunopathol.* **33**, 409–17 (2011).

135. STRATES, B. & NEUMAN, W. F. On the mechanisms of calcification. *Proc. Soc. Exp. Biol. Med.* **97**, 688–91 (1958).

136. FLEISH, H. & NEUMAN, W. F. Mechanisms of calcification: role of collagen, polyphosphates, and phosphatase. *Am. J. Physiol.* **200**, 1296–300 (1961).

137. Sikirić, M. D. & Füredi-Milhofer, H. The influence of surface active molecules on the crystallization of biominerals in solution. *Adv. Colloid Interface Sci.* **128**–**130**, 135–58 (2006).

138. He, G., Dahl, T., Veis, A. & George, A. Nucleation of apatite crystals in vitro by self-assembled dentin matrix protein 1. *Nat. Mater.* **2**, 552–8 (2003).

139. He, G. *et al.* Phosphorylation of phosphophoryn is crucial for its function as a mediator of biomineralization. *J. Biol. Chem.* **280**, 33109–14 (2005).

140. Gajjeraman, S., He, G., Narayanan, K. & George, A. Biological assemblies provide novel templates for the synthesis of hierarchical structures and facilitate cell adhesion. *Adv. Funct. Mater.* **18**, 3972–3980 (2008).

141. Favarin, B. Z. *et al.* Lipid composition modulates ATP hydrolysis and calcium phosphate mineral propagation by TNAP-harboring proteoliposomes. *Arch. Biochem. Biophys.* **691**, 108482 (2020).

142. Xu, Y. *et al.* Intermolecular channels direct crystal orientation in mineralized collagen. *Nat. Commun.* **11**, 5068 (2020).

143. Fisher, L. W., Torchia, D. A., Fohr, B., Young, M. F. & Fedarko, N. S. Flexible structures of SIBLING proteins, bone sialoprotein, and osteopontin. *Biochem. Biophys. Res. Commun.* **280**, 460–5 (2001).

144. Fisher, L. W. & Fedarko, N. S. Six genes expressed in bones and teeth encode the current members of the SIBLING family of proteins. *Connect. Tissue Res.* **44 Suppl 1**, 33–40 (2003).

145. Chen, Y., Bal, B. S. & Gorski, J. P. Calcium and collagen binding properties of osteopontin, bone sialoprotein, and bone acidic glycoprotein-75 from bone. *J. Biol. Chem.* **267**, 24871–8 (1992).

146. George, A. & Veis, A. Phosphorylated proteins and control over apatite nucleation, crystal growth, and inhibition. *Chem. Rev.* **108**, 4670–93 (2008).

147. Sodek, J., Ganss, B. & McKee, M. D. Osteopontin. *Crit. Rev. Oral Biol. Med.* **11**, 279–303 (2000).

148. George, A. *et al.* The carboxyl-terminal domain of phosphophoryn contains unique extended triplet amino acid repeat sequences forming ordered carboxyl-phosphate interaction ridges that may be essential in the biomineralization process. *J. Biol. Chem.* **271**, 32869–73 (1996).

149. ROBINSON, R. A. An electron-microscopic study of the crystalline inorganic component of bone and its relationship to the organic matrix. *J. Bone Joint Surg. Am.* **34-A**, 389–435; passim (1952).

150. ROBINSON, R. A. & WATSON, M. L. Collagen-crystal relationships in bone as seen in the electron microscope. *Anat. Rec.* **114**, 383–409 (1952).

151. Silver, F. H. & Landis, W. J. Deposition of apatite in mineralizing vertebrate extracellular matrices: A model of possible nucleation sites on type I collagen. *Connect. Tissue Res.* **52**, 242–54 (2011).

152. Glimcher, M. J. The nature of the mineral component of bone and the mechanism of calcification. *Instr. Course Lect.* **36**, 49–69 (1987).

153. Lees, S. Considerations regarding the structure of the mammalian mineralized osteoid from viewpoint of the generalized packing model. *Connect. Tissue Res.* **16**, 281–303 (1987).

154. Landis, W. J. *et al.* Mineralization of collagen may occur on fibril surfaces: evidence from conventional and high-voltage electron microscopy and three-dimensional imaging. *J. Struct. Biol.* **117**, 24–35 (1996).

155. Landis, W. J., Song, M. J., Leith, A., McEwen, L. & McEwen, B. F. Mineral and organic matrix interaction in normally calcifying tendon visualized in three dimensions by high-voltage electron microscopic tomography and graphic image reconstruction. *J. Struct. Biol.* **110**, 39–54 (1993).

156. Landis, W. J. & Jacquet, R. Association of calcium and phosphate ions with collagen in the mineralization of vertebrate tissues. *Calcif. Tissue Int.* **93**, 329–37 (2013).

157. Jiang, C., Zurick, K., Qin, C. & Bernards, M. T. Probing the influence of SIBLING proteins on collagen-I fibrillogenesis and denaturation. *Connect. Tissue Res.* **59**, 274–286 (2018).

158. Hasegawa, T. Ultrastructure and biological function of matrix vesicles in bone mineralization. *Histochem. Cell Biol.* **149**, 289–304 (2018).

159. Hoshi, K., Ejiri, S. & Ozawa, H. Localizational alterations of calcium, phosphorus, and calcification-related organics such as proteoglycans and alkaline phosphatase during bone calcification. *J. Bone Miner. Res.* **16**, 289–98 (2001).

160. Hasegawa, T. *et al.* Ultrastructural and biochemical aspects of matrix vesicle-mediated mineralization. *Jpn. Dent. Sci. Rev.* **53**, 34–45 (2017).

161. Landis, W. J., Hodgens, K. J., Arena, J., Song, M. J. & McEwen, B. F. Structural relations between collagen and mineral in bone as determined by high voltage electron microscopic tomography. *Microsc. Res. Tech.* **33**, 192–202 (1996).

162. Glimcher, M. J., Hodge, A. J. & Schmitt, F. O. MACROMOLECULAR AGGREGATION STATES IN RELATION TO MINERALIZATION: THE COLLAGEN-HYDROXYAPATITE SYSTEM AS STUDIED IN VITRO. *Proc. Natl. Acad. Sci. U. S. A.* **43**, 860–7 (1957).

163. Bonucci, E. Fine structure of early cartilage calcification. *J. Ultrastruct. Res.* **20**, 33–50

(1967).

164. Anderson, H. C. Electron microscopic studies of induced cartilage development and calcification. *J. Cell Biol.* **35**, 81–101 (1967).

165. Wu, L. N., Genge, B. R., Lloyd, G. C. & Wuthier, R. E. Collagen-binding proteins in collagenase-released matrix vesicles from cartilage. Interaction between matrix vesicle proteins and different types of collagen. *J. Biol. Chem.* **266**, 1195–203 (1991).

166. Poole, A. R., Matsui, Y., Hinek, A. & Lee, E. R. Cartilage macromolecules and the calcification of cartilage matrix. *Anat. Rec.* **224**, 167–79 (1989).

167. Chen, N. X., O'Neill, K. D., Chen, X. & Moe, S. M. Annexin-mediated matrix vesicle calcification in vascular smooth muscle cells. *J. Bone Miner. Res.* **23**, 1798–1805 (2008).

168. Ozawa, H., Hoshi, K. & Amizuka, N. Current Concepts of Bone Biomineralization. *J. Oral Biosci.* **50**, 1–14 (2008).

169. Amizuka, N. *et al.* Vitamin K2, a gamma-carboxylating factor of gla-proteins, normalizes the bone crystal nucleation impaired by Mg-insufficiency. *Histol. Histopathol.* **23**, 1353–66 (2008).

Chapter II

Biomaterials: concepts and applications

1. Biomaterials- concepts and applications

The use of biomaterials in medicine is described before Christ. The oldest register of prostheses dates back to 1065 B.C. when Egyptians used wooden-based materials to replace amputated fingers. Since this period, **(Figure 2.1),** human beings never stopped creating new and advanced forms of biomaterials aiming at life quality as well as aesthetics [1,2].

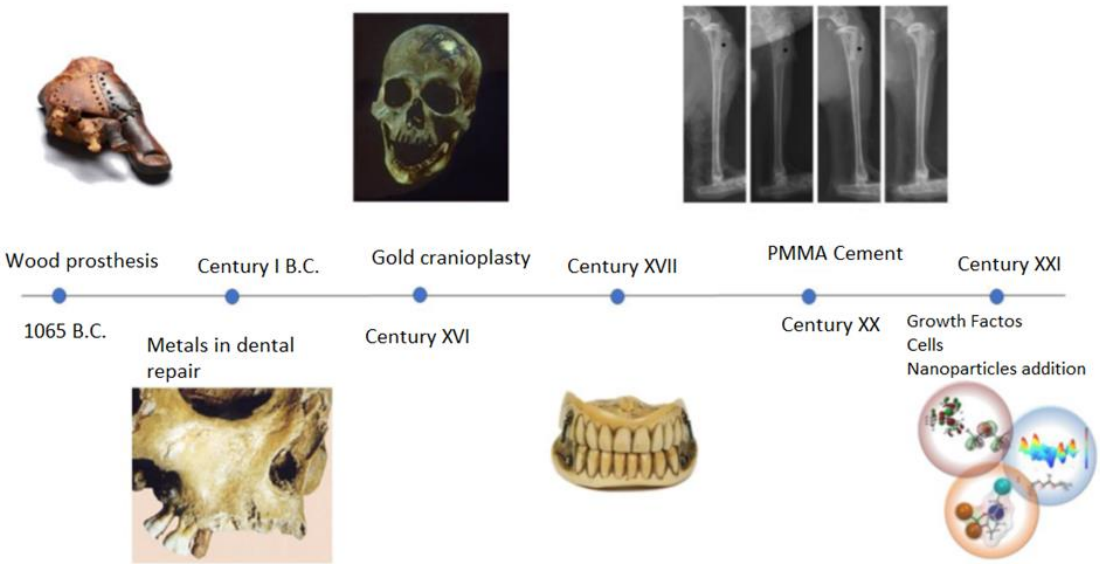

FIGURE 2. 1. SCHEMATIC REPRESENTATION DEMONSTRATING THE BIOMATERIAL EVOLUTION THROUGHOUT HISTORY

Also, the definition of biomaterial as well as their purpose changed over the centuries. Nowadays, biomaterials can be classified into two categories, according to their chemical structure (metal, ceramic, polymer, and so on), and their degree of interaction with the biological environment (inert, bioactive, and bioresorbable).

The biomaterials field has its border being pushed due to the ever-advance knowledge of molecular biology, biochemistry, and engineering. In this regard, since the '60s, millions of patients have had their life quality improved through the use of biomaterials and well as biomedical devices. In this chapter, I aim at discussing the evolution of biomaterials throughout history and how one can take advantage of molecular biology and chemistry to develop biomaterials with high bioactivity.

1.1. Evolution of biomaterials

The engineering knowledge needed to develop and improve biomaterials´ performance follows the concepts of molecular biology and biochemistry aiming at increasing the bioactivity. The evolution of biomaterials can be classified into three generations (1st, 2nd, and 3rd generation), according to their chemical structure (metal, ceramic, polymer, and composites), and according to their degree of interaction with the host (inert, bioactive and bioresorbable) **(Figure 2.2)** [2–5].

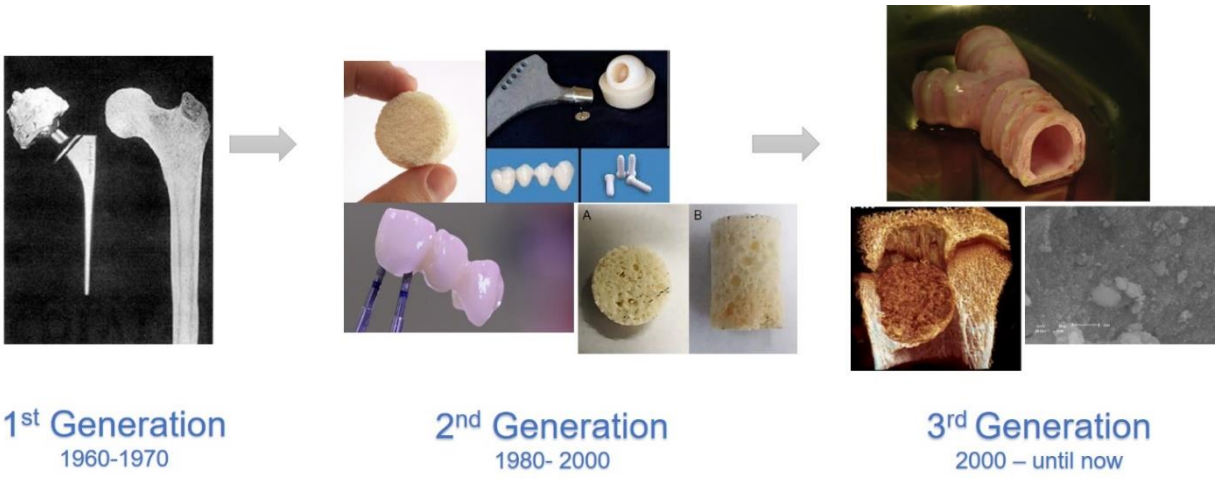

FIGURE 2. 2. SCHEMATIC REPRESENTATION OF THE BIOMATERIAL´S EVOLUTION IN THE LAST DECADES

One can separate the biomaterials into three generations. The 1st generation of the modern era mainly focused on inertness and the implanted material (prostheses) should have similar physical property of the replaced tissue; the 2nd generation aimed at bioactivity and lower toxicity; finally, the 3rd generation of biomaterials took advantage of the modern knowledge of molecular biology, chemistry, and engineering to develop a new class of biomaterials able to stimulate cellular responses at the molecular level.

Biomaterials: 1st generation

The first generation of biomaterials was developed between 1960 and 1970. At that time, the knowledge of the immune system was not as deep as it is nowadays. So, the major goal of the 1st generation of biomaterials was to archive a suitable combination of physical properties to match those of the replaced tissue with a minimal toxicity response in the host [3], in other words, the biomaterial should be inert (i.e., bioinert).

Biomaterials: 2nd generation

Presumably, the second generation of biomaterials aimed at the development of materials with increased bioactivity with reduced toxicity [6,7]. In this sense, we can quote bioactive glasses, ceramics, glass ceramics, polymers, and many other biomaterials (**Figure 2.2)**. Even though, a certain level of bioactivity was reached in this type of biomaterials, approximately one-third to half of the prostheses likely will fail within the first 10 years, thus requiring a reparative surgery [8,9]. It leads us to the main 21st-century challenge.

Biomaterials: 3rd generation

The increased knowledge about the complex biology systems allowed scientists and engineers to work together and develop a new class of biomaterials that were able to stimulate specific cellular responses at the molecular level [5,10]. The third-generation search for the development of biomaterials with specific cellular response to targe molecular pathways related to tissue repair. The two most common ways to approach this could be, (a) to use progenitor and/or differentiated cells associated with resorbable scaffolds, followed by the implantation in the damaged area; and (ii) to use biomaterials based on powders, solutions, and nanoparticles to stimulate local or systemic delivery of controlled bioactive molecules (e.g., growth factors, hormones, ions, drugs, and so forth). The chemical nature and the biological function of molecules must be known and previously tested. Once implanted, these materials shall drive specific molecular routes related to the activation of genes involved with the tissue-repairing system [5,10]. For example, the use of BMP-2 in association with 3D-printing and/or hydrogels-based scaffolds has been extensively used aiming at bone repair [11–15], since BMP-2 is a strong osteoinductive factor.

The definition of biomaterials has changed in the last decades. In 1967, Dr. Jonathan Cohen stated the following, “There is no current agreement on what distinguishes biomaterials from others. For the purpose of this article, I [Dr. Jonathan Cohen] will include all the materials, except drugs and sutures, which are used as implants”[16]. Note that the controlled release of drugs using scaffolds, or biomimetic systems, has emerged as the primary carrier for treating diseases [17–25].

Moreover, in 1987, Prof. David Franklyn Williams proposed a new and refined way to define biomaterials, as follows: "… a substance that has been engineered to take a form which, alone or as part of a complex system, is used to direct, by control of interactions with components of living systems, the course of any therapeutic or diagnostic procedure". And then he added up, "A biomaterial is a non-viable material used in a medical device, intended to interact with biological systems" [26]. And most recently, a group of world experts in the biomaterial field suggested an even more refined definition, as follow: "a material designed to take a form which can direct, through interactions with living systems, the course of any therapeutic or diagnostic procedure (National Institute of Standards and Technology, NIST).

In the last few pages of this chapter, we shall focus our discussion on the 2nd generation of biomaterial based on polymethylmethacrylate cement. Then, we will discuss how one can take advantage of its bone-like structure and mechanical properties to carry nanoparticles able to release osteo-inductor ions capable of modulating osteoblast activity. This will be the main subject of this chapter.

2. Polymethylmethacrylate cement: a 2nd generation biomaterial that carries bone-like properties

Acrylic acid and its derivatives have been explored since 1890, however, only in 1901 with the availability of solid (transparent polymer) material, that acrylic acid started to be further used in industry. Acrylic monomers, methyl, and ethyl acrylate, derivatives produced perfect clear solid, resistant and aesthetically acceptable polymers. Due to this characteristic, many dentists leaned toward this type of material[27].

Only in 1931, the commercial production of the harder polymethyl methacrylate (PMMA) occurred, with the introduction of Plexiglas® [28]. This material was extensively used to produce biomedical protection items, such as masks that protect against microorganisms. In 1937, PMMA was sold in the form of granules and powders [29], which provides handling advantages. As a curious historical fact, during World War II, neurosurgeons started using PMMA for cranioplasties, likely due to its strength and its light weight [30]. A few years later, almost 95% of the dental market consumed any product based on PMMA [29]. However, only in the ´50s with the advancing medical research, the use of PMMA aimed at orthopedic prostheses came true [30]. Another hallmark was that at

the time the so-called “room-temperature polymerization” form of PMMA was available for purchase, which provided an easy-handling characteristic for this material [31].

Nowadays, PMMA is used in several areas of medicine, for example, bone cement, screw fixation in bone, lens, orthodontics, filler for bone cavities, to fixate prostheses, and so forth [32]. Here we will focus on PMMA-cement aiming at long-bone repair.

Further, bone substitutes (bone fillers) are mostly used to fill small fractures, avoid misalignments of the prostheses with the host surrounding bone, afford early weight bearing due to its resistance, and so on. Based on this, the ideal bone substitutes should have the following characteristics, (1) they should be biocompatible (2) they should not evoke any adverse inflammatory response, (3) they should be easily manipulated into the bone defect, (4) they should be osteoinductive, osteoconductive, and resorbable, (5) it should be easily traceable, and finally (6) it should be sterilizable and cheap [33]. PMMA holds some of those characteristics, for example, PMMA displays early mechanical resistance, unlimited disposability, biocompatibility, low toxic effect, is easy to handle, shows plasticity, and overall, it is cheap compared to other forms of biomaterials.

The use of PMMA in orthopedics started in 1960 with Dr. Charnley and Smith [29,30]. Since then, it has been widely used in joint replacement surgery[34,35], hip implant [36], reconstruction and stabilizing spine surgery [37], reconstruction of cranial defects [38], and filling of small (non-critical, <10mm) fractures [39]. However, the use of solid PMMA cement brings some limitations and troublesome outcomes. For instance, PMMA loosening is a common downside of using this type of material, and it is frequently observed in radiographs [40,41]. It likely happens due to the formation of blood clots, ischemic necrosis leading to the loosening of the block (implant), and a fibrosis layer around it [42]. Thus, one way to overcome such problems is by creating porous in the PMMA cement [43].

In this regard, porosity allows the free movement of fluids as well as vascular invasion, which reduces the odds of necrosis [40]. Also, an interconnected net of porous facilitates osteointegration[44], since osteoblasts can migrate and secrete extracellular matrix inside, in between, and on the cement surface. Another interesting characteristic is that the porous cement increases the compatibility between the scaffold and the trabecular bone, as described elsewhere[45,46]. Finally, one of the overlooked features displayed by creating porous in the cement is that it decreases the maximum temperature reached during cement preparation[47].

Moreover, due to PMMA cement's inability to guide specific cellular responses, this material is still considered a 2nd generation biomaterial. Researchers is always searching for new approaches to improve the integration of implants into the bone through the addition of bioactive additives. The use of PMMA cement as the primary carrier (scaffold) of osteogenic inductors has been described [48–54].

In the last few years, our group has developed and characterized biomaterials capable of inducing osteoblast turnover and activity[55–57]. In special, Tomazela et al. (2022) have shown that the addition of Sr^{2+} -substituted hydroxyapatite nanoparticles (NPs) to the porogenic PMMA cement increased its bioactivity by stimulating osteoblast migration, differentiation, and activity. The NPs' structure and biological bone apatite are very much alike, also the NPs allow the controlled local delivery of Sr^{2+}, which is an interesting characteristic if one thinks of inducing the local action of osteoblasts. In the next topic, we shall discuss why strontium is a compelling ion to be used as a bioactive biomaterial. Yet, the addition of NPs to polymeric matrices may also improve the mechanical properties of the final biomaterial[5,10,58].

The biological role of strontium

The physiological applicability of strontium (Sr^{2+}) dates back to the ´70s. Papillon observed that Sr^{2+} could be incorporated into the bones of animals fed with small amounts of this ion. However, the first use of Sr^{2+} as a therapeutic drug was reported more than a century later with the observation of early mineralization in osteoporotic patients treated with Sr^{2+}-lactate[59,60]. In the last few years, an approved form of strontium, strontium ranelate (SR), has been widely used to treat postmenopausal osteoporosis, being also linked to the reduction of fractures in the femoral colon[61–63].

What makes strontium a unique element is its chemical similarity with Ca^{2+} and the so-called characteristic dual effect, which means that Sr^{2+} decreases bone resorption through the inhibition of osteoclasts and stimulates bone formation by increasing osteoblast differentiation, and activity[64–67]. However, the molecular events related to these processes are not fully comprehended.

Studies have shown that Sr^{2+} acts upon frizzled/Lpr5/6 receptors as well as calcium-sensing receptors (CaSR)[68,69]. Both processes are involved with the regulation of osteogenic-related genes (e.g., *Runx2, Ocn, Bmp2, Collagen type I, and Sp7*) [70–72]. In

the literature, the most studied interaction leading to osteoblast activation happens between Sr^{2+} and CaSR.

CaSR receptor was first discovered in the ´90s, and since then its role in bone modeling has been revealed. Moreover, CaSR participates in Ca^{2+} homeostasis by allowing cells in the parathyroid gland as well as renal tubules to sense extracellular levels of Ca^{2+} thus regulating the release of parathyroid hormone (PTH)[73]. Recently, it was found that bone cells can also sense and regulate Ca^{2+} levels. Curiously, the CaSR homologous receptor was also found in osteoclast precursors, mature osteoclasts, and osteoblasts[74]. Its role varies among the cells, they participate in almost every stage of cell homeostasis, for example, cell growth, differentiation, and apoptosis.[74]

The CaSR is a g-protein-coupled receptor (GPCR) that upon stimulation displays a series of intracellular pathways leading to gene expression. At the molecular level, when stimulated by calcium, g-protein activates the subunits Gα1 and Gαq/11, which in turn activate cellular effectors such as protein kinase A (PKA), phospholipases C, and protein kinase C (PKC)[75]. Also, extracellular Ca^{2+} is known to activate Erk1/2 and Akt signaling and Wnt expression[65,75]. Either pathway is related to replication, differentiation, and osteoblast survival[76,77].

In the literature, much of the knowledge regarding CaSR activation by Sr^{2+} as well as osteoblast turnover comes from Ca^{2+}- related pathways, since Sr^{2+} and Ca^{2+} are chemically similar. In this sense, scientists have consistently tried to extrapolate their knowledge about Ca^{2+} biological properties to explain the biological effect of Sr^{2+}. How the CaSR receptor modulates osteoblast-osteoclast function and communication is still unclear. However, one possible mechanism involved in Sr^{2+} -osteoblast-osteoclast interaction has been proposed[63].

Initially, the activation of osteoblasts by Sr^{2+} occurs in two distinct ways, first increasing the differentiation of MSC into osteoblasts, and second by inducing osteoblast function through the activation of osteogenic-related genes (phosphatases, collagen secretion, transcription factors, and so on)[63,78]. Once activated, osteoblasts secret the

ECM, and OPG. OPG, as described previously, negatively regulates osteoclast differentiation by competing with the RANK receptor, RANKL, **Figure 2.3**.

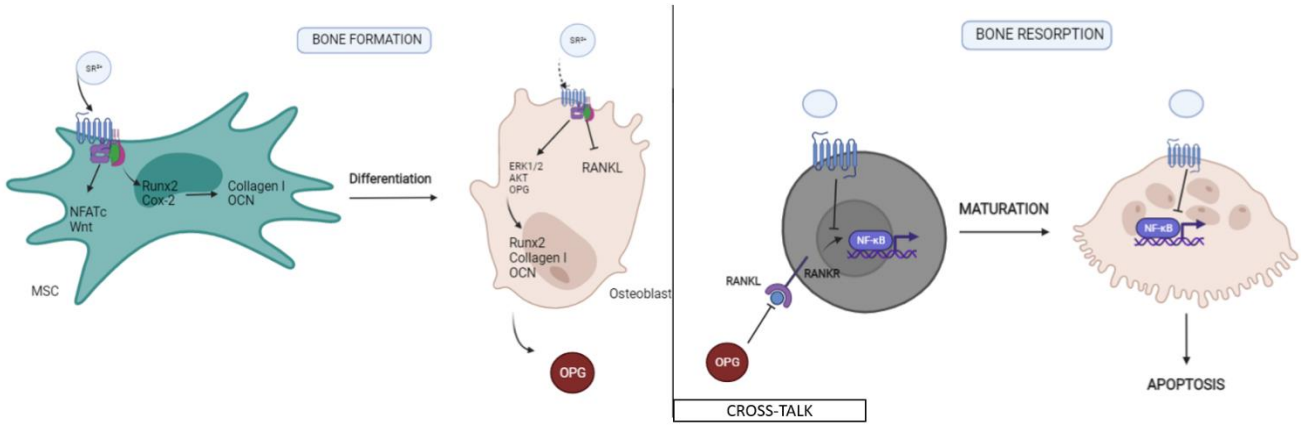

FIGURE 2. 3. SCHEMATIC MECHANISM OF SR2+ ACTION UPON BONE FORMATION AND BONE RESORPTION.

Adapted with permission from reference[63].

The differentiation of bone marrow stromal cells (BMSC) into mature osteoclasts involves the regulation of nuclear factor-kappa B (NF-κB) signaling, which is activated by RANKL[78]. Curiously, Ca^{2+} stimulates CaSR promoting the nuclear translocation of NF-κB resulting in the differentiation of BMSC into osteoclasts. Contrary to what was observed for calcium, Sr^{2+} displays an inhibitory effect on osteoclasts[64,79]. Upon treatment with Sr^{2+}, reduced formation of osteoclasts was associated with the inhibitory translocation of NF-κB to the nucleus[80], **Figure 2.3**. Also, it was observed that Sr^{2+} changes the osteoclasts' actin cytoskeleton and the sealing zone, which hampers the formation of ruffled-like border formation and reduces osteoclast activity[81]

2.1 Overall conclusion

The first chapter of this manuscript describes the fundamental aspects of bone biology. Throughout the chapter, it explained the most actual knowledge regarding bone tissue organization, development, and maintenance. The molecular mechanisms governing bone-related cell homeostasis were also highlighted through the

characterization of signaling pathways associated with bone development. Then, we described the interaction between the organic collagen matrix and the possible mechanisms involved with mineral deposition organization, and how proteins can coordinate this process. Finally, we detailed the role of matrix vesicles in ECM mineralization. In the second chapter, we focus on the history, classification, and function of biomaterials. We presented the porous PMMA-based cement, and how it helped to increase the life quality of thousands of millions of people worldwide. However, the use of porous PMMA cement brings some limitations, mainly due to its lack of bioactivity. Our group overcame this problem by synthesizing and adding a new class of nanoparticles-containing strontium that resembles biological apatite structures. The role of Sr^{2+} in bone development and maintenance is still under debate, though many studies have proposed that Sr^{2+} affects osteoblasts, and osteoclasts via CaSR.

References

1. Huebsch, N. & Mooney, D. J. Inspiration and application in the evolution of biomaterials. *Nature* **462**, 426–32 (2009).

2. Marin, E., Boschetto, F. & Pezzotti, G. Biomaterials and biocompatibility: An historical overview. *J. Biomed. Mater. Res. A* **108**, 1617–1633 (2020).

3. Hench, L. L. Biomaterials. *Science* **208**, 826–31 (1980).

4. Bonfield, W., Grynpas, M. D., Tully, A. E., Bowman, J. & Abram, J. Hydroxyapatite reinforced polyethylene--a mechanically compatible implant material for bone replacement. *Biomaterials* **2**, 185–6 (1981).

5. Hench, L. L. & Polak, J. M. Third-generation biomedical materials. *Science* **295**, 1014–7 (2002).

6. Hench, L. L. & Wilson, J. Surface-active biomaterials. *Science* **226**, 630–6 (1984).

7. Hench, L. L., Polak, J. M., Xynos, I. D. & Buttery, L. D. K. Bioactive materials to control cell cycle. *Mater. Res. Innov.* **3**, 313–323 (2000).

8. Schoen, F. J., Levy, R. J. & Piehler, H. R. Pathological considerations in replacement cardiac valves. *Cardiovasc. Pathol.* **1**, 29–52 (1992).

9. L.L.hench, Wilson, J. W. Clinical perfomance of skeletal prostheses. *Chapman Hall* (1996).

10. Hench, L. L. & Thompson, I. Twenty-first century challenges for biomaterials. *J. R. Soc. Interface* **7 Suppl 4**, S379-91 (2010).

11. Fitzpatrick, V. *et al.* Functionalized 3D-printed silk-hydroxyapatite scaffolds for enhanced bone regeneration with innervation and vascularization. *Biomaterials* **276**, 120995 (2021).

12. Zhang, X. *et al.* Enhanced bone regeneration via PHA scaffolds coated with polydopamine-captured BMP2. *J. Mater. Chem. B* **10**, 6214–6227 (2022).

13. Ding, T., Kang, W., Li, J., Yu, L. & Ge, S. An in situ tissue engineering scaffold with growth factors combining angiogenesis and osteoimmunomodulatory functions for advanced periodontal bone regeneration. *J. Nanobiotechnology* **19**, 247 (2021).

14. Chen, X. *et al.* Enhanced bone regeneration via spatiotemporal and controlled delivery of a genetically engineered BMP-2 in a composite Hydrogel. *Biomaterials* **277**, 121117 (2021).

15. Sun, T. *et al.* Guided osteoporotic bone regeneration with composite scaffolds of mineralized ECM/heparin membrane loaded with BMP2-related peptide. *Int. J. Nanomedicine* **13**, 791–804 (2018).

16. Cohen, J. Biomaterials in orthopedic surgery. *Am. J. Surg.* **114**, 31–41 (1967).

17. Berillo, D., Yeskendir, A., Zharkinbekov, Z., Raziyeva, K. & Saparov, A. Peptide-Based Drug Delivery Systems. *Medicina (Kaunas).* **57**, (2021).

18. Ma, J. *et al.* Biodegradable fibre scaffolds incorporating water-soluble drugs and proteins. *J. Mater. Sci. Mater. Med.* **26**, 205 (2015).

19. Yang, Y. & El Haj, A. J. Biodegradable scaffolds--delivery systems for cell therapies. *Expert Opin. Biol. Ther.* **6**, 485–98 (2006).

20. Kannigadu, C. & N'Da, D. D. Recent Advances in the Synthesis and Development of Nitroaromatics as Anti-Infective Drugs. *Curr. Pharm. Des.* **26**, 4658–4674 (2020).

21. Liu, Y. *et al.* 3D-bioprinted BMSC-laden biomimetic multiphasic scaffolds for efficient repair of osteochondral defects in an osteoarthritic rat model. *Biomaterials* **279**, 121216 (2021).

22. Huang, Q. *et al.* Hydrogel scaffolds for differentiation of adipose-derived stem cells. *Chem. Soc. Rev.* **46**, 6255–6275 (2017).

23. Hao, L. *et al.* Biofabrication of cell-free dual drug-releasing biomimetic scaffolds for meniscal regeneration. *Biofabrication* **14**, (2021).

24. Yao, Z. *et al.* Biomimetic multilayer polycaprolactone/sodium alginate hydrogel scaffolds loaded with melatonin facilitate tendon regeneration. *Carbohydr. Polym.* **277**, 118865 (2022).

25. Ribeiro, V. P., Pina, S., Oliveira, J. M. & Reis, R. L. Silk Fibroin-Based Hydrogels and Scaffolds for Osteochondral Repair and Regeneration. *Adv. Exp. Med. Biol.* **1058**, 305–325 (2018).

26. Williams, D. . *Definitions in biomaterials: proceedings of a consensus conference of the European Society for Biomaterials*. (Elsevier Science, 1987).

27. Price, C. A. A history of dental polymers. *Aust. Prosthodont. J.* **8**, 47–54 (1994).

28. Rueggeberg, F. A. From vulcanite to vinyl, a history of resins in restorative dentistry. *J. Prosthet. Dent.* **87**, 364–79 (2002).

29. Peyton, F. A. History of resins in dentistry. *Dent. Clin. North Am.* **19**, 211–22 (1975).

30. DiMaio, F. R. The science of bone cement: a historical review. *Orthopedics* **25**, 1399–407; quiz 1408–9 (2002).

31. Kraft, J. Polymethylmethacrylate--a review. *J. Foot Surg.* **16**, 66–8 (1977).

32. Frazer, R. Q., Byron, R. T., Osborne, P. B. & West, K. P. PMMA: an essential material in medicine and dentistry. *J. Long. Term. Eff. Med. Implants* **15**, 629–39 (2005).

33. Pryor, L. S. *et al.* Review of bone substitutes. *Craniomaxillofac. Trauma Reconstr.* **2**, 151–60 (2009).

34. Gibon, E. *et al.* The biological response to orthopedic implants for joint replacement. II: Polyethylene, ceramics, PMMA, and the foreign body reaction. *J. Biomed. Mater. Res. B. Appl. Biomater.* **105**, 1685–1691 (2017).

35. Weber, S. C. & Chapman, M. W. Adhesives in orthopaedic surgery. A review of the literature and in vitro bonding strengths of bone-bonding agents. *Clin. Orthop. Relat. Res*. 249–61 (1984).

36. Miron, R. J. & Zhang, Y. F. Osteoinduction: a review of old concepts with new standards. *J. Dent. Res.* **91**, 736–44 (2012).

37. Baumhauer, J., Pinzur, M. S., Donahue, R., Beasley, W. & DiGiovanni, C. Site selection and pain outcome after autologous bone graft harvest. *Foot ankle Int.* **35**, 104–7 (2014).

38. Jensen, S. S. & Terheyden, H. Bone augmentation procedures in localized defects in the alveolar ridge: clinical results with different bone grafts and bone-substitute materials. *Int. J. Oral Maxillofac. Implants* **24 Suppl**, 218–36 (2009).

39. Cimatti, B. *et al.* Safety, osseointegration, and bone ingrowth analysis of <scp>PMMA</scp> -based porous cement on animal metaphyseal bone defect model. *J. Biomed. Mater. Res. Part B Appl. Biomater.* **106**, 649–658 (2018).

40. Lewis, G. Properties of acrylic bone cement: state of the art review. *J. Biomed. Mater. Res*. **38**, 155–82 (1997).

41. Ries, M. D. *et al.* In vivo behavior of acrylic bone cement in total hip arthroplasty. *Biomaterials* **27**, 256–61 (2006).

42. Cimatti, B. *et al.* Safety, osseointegration, and bone ingrowth analysis of PMMA-based porous cement on animal metaphyseal bone defect model. *J. Biomed. Mater. Res. B. Appl. Biomater.* **106**, 649–658 (2018).

43. De Wijn, J. R. Poly(methyl methacrylate)--aqueous phase blends: in situ curing porous

materials. *J. Biomed. Mater. Res.* **10**, 625–35 (1976).

44. Miño-Fariña, N. *et al.* Quantitative analysis of the resorption and osteoconduction of a macroporous calcium phosphate bone cement for the repair of a critical size defect in the femoral condyle. *Vet. J.* **179**, 264–72 (2009).

45. Kundu, Z. S., Gupta, V., Sangwan, S. S. & Rana, P. Curettage of benign bone tumors and tumor like lesions: A retrospective analysis. *Indian J. Orthop.* **47**, 295–301 (2013).

46. Belkoff, S. M. & Molloy, S. Temperature measurement during polymerization of polymethylmethacrylate cement used for vertebroplasty. *Spine (Phila. Pa. 1976).* **28**, 1555–9 (2003).

47. Webb, J. C. J. & Spencer, R. F. The role of polymethylmethacrylate bone cement in modern orthopaedic surgery. *J. Bone Joint Surg. Br.* **89**, 851–7 (2007).

48. Campana, V. *et al.* Bone substitutes in orthopaedic surgery: from basic science to clinical practice. *J. Mater. Sci. Mater. Med.* **25**, 2445–61 (2014).

49. Darjanki, C. M. *et al.* Expression of VEGF and BMP-2 in Osteoblast cells exposed to a combination of polymethylmethacrylate (PMMA) and hydroxyapatite (HAp). *J. oral Biol. craniofacial Res.* **13**, 243–248 (2023).

50. Liu, Z. *et al.* Synergistic effect of HA and BMP-2 mimicking peptide on the bioactivity of HA/PMMA bone cement. *Colloids Surf. B. Biointerfaces* **131**, 39–46 (2015).

51. DeBaun, M. R. *et al.* A bioactive synthetic membrane improves bone healing in a preclinical nonunion model. *Injury* **53**, 1368–1374 (2022).

52. Sa, Y., Yang, F., Wang, Y., Wolke, J. G. C. & Jansen, J. A. Modifications of Poly(Methyl Methacrylate) Cement for Application in Orthopedic Surgery. *Adv. Exp. Med. Biol.* **1078**, 119–134 (2018).

53. Ricker, A., Liu-Snyder, P. & Webster, T. J. The influence of nano MgO and BaSO4 particle size additives on properties of PMMA bone cement. *Int. J. Nanomedicine* **3**, 125–32 (2008).

54. Lu, C.-Y., Church, D. C., Learn, G. D., Pokorski, J. K. & von Recum, H. A. Modified Cyclodextrin Microparticles to Improve PMMA Drug Delivery Without Mechanical Loss. *Macromol. Biosci.* **21**, e2000328 (2021).

55. Cruz, M. A. E. *et al.* Synthesis of Sr-morin complex and its in vitro response: decrease in osteoclast differentiation while sustaining osteoblast mineralization ability. *J. Mater. Chem. B* **7**, 823–829 (2019).

56. Tomazela, L. *et al.* Fabrication and characterization of a bioactive polymethylmethacrylate-based porous cement loaded with strontium/calcium apatite nanoparticles. *J. Biomed. Mater. Res. A* **110**, 812–826 (2022).

57. Dotta, T. C. *et al.* Strontium Carbonate and Strontium-Substituted Calcium Carbonate Nanoparticles Form Protective Deposits on Dentin Surface and Enhance Human Dental Pulp Stem Cells Mineralization. *J. Funct. Biomater.* **13**, (2022).

58. Anderson, J. M., Rodriguez, A. & Chang, D. T. Foreign body reaction to biomaterials. *Semin. Immunol.* **20**, 86–100 (2008).

59. SHORR, E. & CARTER, A. C. The usefulness of strontium as an adjuvant to calcium in the remineralization of the skeleton in man. *Bull. Hosp. Joint Dis.* **13**, 59–66 (1952).

60. DOW, E. C. & STANBURY, J. B. Strontium and calcium metabolism in metabolic bone diseases. *J. Clin. Invest.* **39**, 885–903 (1960).

61. Meunier, P. J. *et al.* The effects of strontium ranelate on the risk of vertebral fracture in women with postmenopausal osteoporosis. *N. Engl. J. Med.* **350**, 459–68 (2004).

62. Reginster, J. Y. *et al.* Strontium ranelate reduces the risk of nonvertebral fractures in postmenopausal women with osteoporosis: Treatment of Peripheral Osteoporosis (TROPOS) study. *J. Clin. Endocrinol. Metab.* **90**, 2816–22 (2005).

63. Marx, D., Rahimnejad Yazdi, A., Papini, M. & Towler, M. A review of the latest insights into the mechanism of action of strontium in bone. *Bone reports* **12**, 100273 (2020).

64. Bonnelye, E., Chabadel, A., Saltel, F. & Jurdic, P. Dual effect of strontium ranelate: Stimulation of osteoblast differentiation and inhibition of osteoclast formation and resorption in vitro. *Bone* **42**, 129–138 (2008).

65. Fromigué, O. *et al.* Calcium sensing receptor-dependent and receptor-independent activation of osteoblast replication and survival by strontium ranelate. *J. Cell. Mol. Med.* **13**, 2189–2199 (2009).

66. Riggs, B. L. & Parfitt, A. M. Drugs Used to Treat Osteoporosis: The Critical Need for a Uniform Nomenclature Based on Their Action on Bone Remodeling. *J. Bone Miner. Res.* **20**, 177–184 (2004).

67. Ducy, P., Zhang, R., Geoffroy, V., Ridall, A. L. & Karsenty, G. Osf2/Cbfa1: A Transcriptional Activator of Osteoblast Differentiation. *Cell* **89**, 747–754 (1997).

68. Kifor, O. *et al.* Regulation of MAP kinase by calcium-sensing receptor in bovine parathyroid and CaR-transfected HEK293 cells. *Am. J. Physiol. Physiol.* **280**, F291–F302 (2001).

69. Chau, J. F. L., Leong, W. F. & Li, B. Signaling pathways governing osteoblast proliferation, differentiation and function. *Histol. Histopathol.* **24**, 1593–606 (2009).

70. Surgery, M. A comparison of osteogenesis-related gene expression of mesenchymal stem cells during the osteoblastic differentiation induced by Type-I collagen and / or fibronectin Ryotaro Ozawa , 1 YoichiYamada , 2 Tetsuro Nagasaka , 3 and Minoru Ueda collagens (type. **1**, 139–146 (2003).

71. Takaoka, S., Yamaguchi, T., Yano, S., Yamauchi, M. & Sugimoto, T. The Calcium-sensing Receptor (CaR) is involved in strontium ranelate-induced osteoblast differentiation and mineralization. *Horm. Metab. Res.* **42**, 627–31 (2010).

72. Sila-asna, M. & Bunyaratvej, A. Osteoblast Differentiation and Bone Formation Gene Expression in Strontium-inducing Bone Marrow Mesenchymal Stem Cell. **53**, 25–35 (2007).

73. Peacock, J. D., Huk, D. J., Ediriweera, H. N. & Lincoln, J. Sox9 transcriptionally represses Spp1 to prevent matrix mineralization in maturing heart valves and chondrocytes. *PLoS One* **6**, e26769 (2011).

74. Cianferotti, L., Gomes, A. R., Fabbri, S., Tanini, A. & Brandi, M. L. The calcium-sensing receptor in bone metabolism: from bench to bedside and back. *Osteoporos. Int.* **26**, 2055–71 (2015).

75. Saidak, Z. & Marie, P. J. Strontium signaling: Molecular mechanisms and therapeutic implications in osteoporosis. *Pharmacol. Ther.* **136**, 216–226 (2012).

76. Kawamura, N. *et al.* Akt1 in Osteoblasts and Osteoclasts Controls Bone Remodeling. *PLoS One* **2**, e1058 (2007).

77. Almeida, M., Han, L., Bellido, T., Manolagas, S. C. & Kousteni, S. Wnt Proteins Prevent Apoptosis of Both Uncommitted Osteoblast Progenitors and Differentiated Osteoblasts by β-Catenin-dependent and -independent Signaling Cascades Involving Src/ERK and Phosphatidylinositol 3-Kinase/AKT. *J. Biol. Chem.* **280**, 41342–41351 (2005).

78. Boyce, B. F. & Xing, L. Functions of RANKL/RANK/OPG in bone modeling and remodeling. *Arch. Biochem. Biophys.* **473**, 139–46 (2008).

79. Baron, R. & Tsouderos, Y. In vitro effects of S12911-2 on osteoclast function and bone marrow macrophage differentiation. *Eur. J. Pharmacol.* **450**, 11–17 (2002).

80. Caudrillier, A. *et al.* Strontium ranelate decreases receptor activator of nuclear factor-KB ligand-induced osteoclastic differentiation in vitro: involvement of the calcium-sensing

receptor. *Mol. Pharmacol.* **78**, 569–76 (2010).

81. Takahashi, N., Sasaki, T., Tsouderos, Y. & Suda, T. S 12911-2 Inhibits Osteoclastic Bone Resorption In Vitro. *J. Bone Miner. Res.* **18**, 1082–1087 (2003).

Chapter III

Aims and motivations

Motivations

Since its approval by the FDA in the ´70s, PMMA cement has been extensively used in orthopedics and the dental field. Many additives have been added to the PMMA cement aiming at increase its bioactivity. Our group has previously published a complete and outstanding in *vitro* study on porous PMMA-cement containing Sr-substituted nanoparticles. However, the previous characterization lacks an *in vivo* model as well as a deep investigation regarding the nanoparticles function, without the effect of the porous PMMA-cement, upon osteoblast turnover.

MVs is part of the biomineralization processes, however there is a lack of knowledge in the literature on the possible effects (if any) of Sr^{2+} on MVs secretion and function. This topic was also explored during this thesis study.

Hypothesis

Throughout this research development, I have tried to understand the biological role of Sr^{2+} based on the assumptions and knowledge developed and registered in many articles in the past few years. So, we hypothesize that due to its similarity with Ca^{2+} and the previous reports on the preferential location of Sr^{2+} in hard tissues, this ion can enhance the biomineralization process affecting cells by indirectly modeling the expression of osteogenic genes, through the activation of signaling pathways and also by biophysically regulating MVs activity. In this sense, Sr^{2+} is a potential candidate for the development of bioactive materials with outstanding performance in biomineralization.

To test this hypothesis, this thesis aimed at exploring the *in vitro* and *in vivo* role of Sr^{2+} on biological mineralization. Here, we investigated using an *in vivo* model whether the nanoparticles-containing Sr^{2+} associated with porous PMMA cement increases osteointegration. Then, we tried to clarify the role of Sr^{2+} at the molecular level by studying signaling pathways and MV secretion and function using osteoblasts.

Specific Aims

To elucidate whether the nanoparticles containing Sr^{2+} associated with porous PMMA cement would enhance osteointegration. We addressed this by injecting the biomaterial into the femur of sixteen adult New Zealand rabbits.

To describe how Sr^{2+} induces both the expression of osteogenic-related genes at the molecular level and the secretion and function of MVs. To accomplish this, we analyzed molecular pathways and gene expression involved in osteogenic function, then we analyzed MVs´ composition, structure, secretion, and function.

Chapter IV

A nontoxic strontium nanoparticle capable of modulating osteocompetent cells

1. Introduction

The bone tissue is continually remodeled according to physiological circumstances through a process that involves bone formation stimulated by osteoblasts and bone resorption by osteoclasts. During this process, bone density as well as its turnover is maintained through the balance of osteoblast/osteoclast activities in healthy adults [1–3]. Notwithstanding, many causalities can disrupt this process including aging, estrogen deficiency, long-term immobilization, chronic use of glucocorticoids, and many other factors that lead to the loss of bone mass and *de novo* fractures [4]. Moreover, the self-reparation ability of the bone tissue may be hindered by critical-size bone defects caused either by trauma or pathologies, like neoplasia. In these cases, a bone substitute is required to replace the damaged tissue.

An ideal bone substitute should display suitable resistance to support the mechanical functions of the natural tissue, unlimited disposability, and biocompatibility [5]. Solid polymethylmethacrylate (PMMA) is the most widely used biomaterial to replace damaged bones in clinics, but it has recently raised some concerns regarding its use due to a lack of adherence between the cement and the host tissue. In this regard, Lewis (1997) and Ries and collaborators (2006) pointed out that PMMA loosening is a frequent drawback observed in radiography, which may also lead to the formation of a fibrous layer, resulting in arthrosis[6]. Additionally, the increase in the local temperature during the PMMA cement polymerization reaction can also contribute to cement loosing and induce necrosis of the adjacent tissue [6,7].

To overcome these failures, Cimatti et al (2017) presented an alternative approach for the synthesis of PMMA-cements based on the formation of interconnected pores through the effervescent reaction between sodium bicarbonate and citric acid[5]. This porous cement presented mechanical and physical properties similar to trabecular bone and among other benefits, the porosity increased connection between the cement itself and the surrounding tissue while decreasing the maximum temperature reached during polymerization. Both characteristics are associated with the free movement of fluids and the facilitation of vascular invasion into the cement, thus avoiding necrosis and loosening [7]. Reproducing the architecture and composition of native tissue is crucial for triggering biological events upon the PMMA cements. However, the low surface energy of the PMMA-based materials may hinder the bioactivity of the cement. An alternative to

overcome these problems is the addition of bioactive materials to the cement's composition. For instance, the addition of nanoparticles to polymeric matrices may also improve the mechanical properties of the final biomaterial [8–10]

In healthy individuals, bone tissue is primarily composed of collagen and bone mineral. The main substituents found in the biological apatite structure are carbonate, which replaces phosphate and hydroxyl groups, and divalent ions like Mg^{2+}, which replace Ca^{2+}. Studies on orthopedic and dental materials showed that HA holds the potential for repairing hard tissue by inducing matrix mineralization [11]. These substitutions can change the solubility and the reactivity of the bone mineral [12]. Taking that into consideration, the modification of synthetic HA with specific elements may originate biomimetic materials with controllable properties and different functions [13]. Among many divalent cations with well-known pharmaceutical potential, strontium (Sr^{2+}) is by far the most well-known bone-forming inducer [14–17]

The first use of Sr^{2+} as a therapeutic was reported more than a century ago with the observation of early mineralization in osteoporotic patients treated with Sr^{2+} lactate [18,19]. Currently, strontium ranelate (SR) has been used to treat postmenopausal osteoporosis, being also linked to the reduction of fractures in the femoral colon [17,20]. Such choice is based on the dual effect of Sr^{2+} acting upon decreasing bone resorption through the inhibition of osteoclast activity and stimulating bone formation through osteoblast differentiation and proliferation [4,14,21,22].

Many studies have shown that Sr^{2+} sensibilizes cells via Wnt signaling and calcium receptors [23,24]. *In vitro,* studies have suggested that strontium directly promotes osteogenesis by stimulating mRNA expression of osteogenesis-related genes such as Runx2, Osteocalcin (OCN), Bone morphogenic protein 2 (BMP2), Collagen, and Osterix (SP7), among many others[25–27]. Taken together, these studies show that strontium may act as a powerful agonist of osteoblast activity.

Recently, our group synthesized and characterized a series of HA nanoparticles based on the replacement of Ca^{2+} by Sr^{2+} in the HA crystal lattice, thus giving rise to Sr^{2+}-containing nanoparticles [28–30]. Promoting controlled and sustained release of ions from the nanoparticles, could be an interesting approach aiming at the bone healing field. Moreover, the most interesting feature regarding the use of strontium ions is their action as biological Boolean-like gates, i.e., they stimulate osteoblasts and at the same time

inhibit osteoclast differentiation and resorption [14,17,31]. So, unlike other divalent cations that hold solely the potential to either activate osteoblast or inhibit osteoclasts, strontium executes both tasks at once.

Another possibility for delivering Sr^{2+} into bone defects is to conjugate the nanoparticles to the porous PMMA cement. So that, the particles can be confined on the porous outer surface facilitating osteogenic responses with low HA concentrations [28]. In this fashion, loading PMMA cements with Sr^{2+} -substituted HA may trigger the gradual release of Sr^{2+} locally and positively stimulate osteogenesis, thus favoring bone formation and avoiding bone resorption. Furthermore, gradual Sr^{2+} delivery may circumvent strontium ranelate side effects, for example, high doses of strontium ranelate were closely related to pathological mineralization and increased the risk of stroke and ischemic cardiac events [28,32]. So, the creation of biomaterial capable of releasing Sr^{2+} in time-dependent doses is pivotal.

Though our group has already tested the bioactivity properties of the PMMA cement containing Sr^{2+} nanoparticles and described how they affect osteoblast activity *in vitro* [28], here we aimed at evaluating the effect of the particles by themselves on the osteoblasts and osteoclast culture to put apart the effect of the cement and to test the real effect of these nanoparticles on the formation of mineralized matrix. In addition, we used rabbits as an animal model to check whether the nanoparticles can trigger and increase mineral deposition on the porous PMMA cement.

Material and methods

2.1. Synthesis of the Sr^{2+}-apatite nanoparticles and cement preparation

Apatite nanoparticles containing Sr^{2+} were synthesized using a chemical precipitation methodology previously described by our group [13]. Briefly, aqueous solution containing $CaCl_2.6H_2O$ (LabSynth) and $SrCl_2$ (LabSynth) with total concentration of $[Ca^{2+}] + [Sr^{2+}] = 0{,}10$ mol. L^{-1} was mixed. So, to address the different Sr^{2+} concentrations used in this study, we mixed different molar percentages of Sr^{2+} in relation to the total Ca^{2+} (Ca^{2+} + Sr^{2+}). We prepared a serie of nanoparticles containing various Sr^{2+} concentrations, where 0% Sr^{2+} we named NanoSr 0%; ,10% Sr^{2+} we named NanoSr 10%,

and finally 90% Sr^{2+} we named NanoSr 90%. For comparative reasons, we used a secondary source of strontium, strontium ranelate (Protus®).

The PMMA cement preparation was performed according to the manufacturer´s protocol (Johnson & Johnson®, De Puy®, SmartSet ™ MV endurance, England). To create porosity, we added sodium bicarbonate and citric acid as described by [5,28]. Shortly, we mixed 40,0 g of the solid compound (MMA monomer) with 10,5 g of sodium bicarbonate (Synth), and 8,0 g of citric acid (Synth). Then, we added 1% (0,4 g) of NanoSr 90% to the cement. After homogenization of the solids, we added 18,8 g of the polymerizing agent (time 0). After 3 minutes, we added 5 mL of deionized water and homogenized it for 1 minute. Then, we added the porous cement to the femur and tibia of male adult rabbits as described in the animal model section.

2.2. Scanning electron microscopy (SEM)

For SEM analysis, the nanoparticles were dehydrated through successive ethanol baths (v /v 30%, 50%, 70%, 80%, 90%, 95%, and 100%) and fixed in 3,6% glutaraldehyde in PBS (v/v). For supercritical CO_2 drying performed on a BAL-TEC 030. Then, Samples coated with gold (10nm layer) were studied by SEM (Zeiss EVO 50-FFCLRP/USP).

2.3. Cell culture

Mouse osteoblast cell line MC3T3-E1 (American Type Culture Collection-ATCC™) were cultured in growth media α-MEM (Gibco) supplemented with 10 vol% fetal bovine serum and 1 vol% penicillin/streptomycin, at 37 ºC in a humidified atmosphere of 95% air and 5% CO_2. MC3T3-E1 cultured in the presence of ascorbic acid displays a time-dependent and sequential expression of osteoblast characteristics similar to the bone formation process *in vivo*[33]. So, to stimulate cell differentiation, we supplemented α- MEM medium with 50 $\mu g.mL^{-1}$ of ascorbic acid and 6 mM of β-glycerophosphate (osteogenic media) changed every 48 h.

2.4. Transmission electron microscopy (TEM)

The morphology of cells under stimulation with the nanoparticles and strontium ranelate (SR) was examined by TEM (JEOL JEM-100 CXII- FMRP/USP) by drying a drop

of cell on a copper grid covered with a conductive polymer. Then, the sample was treated with phosphotungstic acid (PTA, 1%) for 15 min and then analyzed.

2.5. Cell toxicity analysis: MTT assay

To test the cytotoxicity effect of the strontium nanoparticles, cells were trypsinized, resuspended in α- MEM, seeded on a 24-well plate at the density of 2 x 10^4 cells per well, and incubated at 37 ºC and 5% CO_2. Cells were allowed to adhere to the bottom surface of the plate for 24 hours. After that, cells were treated with nanoparticles (NanoSr 0%, NanoSr 10%, NanoSr 90%, and strontium ranelate). Nanoparticles and the strontium ranelate were solubilized in α-MEM at the same concentration of 10 µg/mL. Cell viability was assessed by MTT assay after 7, and 14 of culture as described by[34]. Cell viability was expressed as the percentage of the average of three experiments compared to the untreated control for each day of the culture.

2.6. Alizarin red staining

For the analysis of matrix mineralization, 2x10^4 MC3T3-E1 cells were seeded into 24 well plates. Following 24h of culture at 37ºC, both the nanoparticles at different strontium concentrations and strontium ranelate were added to the osteogenic medium. The medium was replaced every two days. After 21 days of culture, Alizarin Red S staining was applied. To quantify the formation of mineralized nodules, the contents of the wells were solubilized in acetic acid followed by ammonium hydroxide neutralization. The absorbance at 405 nm was read with a spectrophotometer.

2.7. Alkaline phosphatase (ALP) activity

To determine ALP activity, we harvested the plasma membrane fraction in triplicate from cells after 7 and 14 days of culture according to Simão (2007)[35]. ALP activity was accomplished by the degradation of p-nitrophenylphosphate (pNPP) and its subproduct was analyzed. ALP activity was expressed as U mg^{-1} of total protein content, and one unit of enzyme is defined as the amount of enzyme capable of hydrolyzing 1.0 nmol of substrate per mg of protein at 37 ºC.

2.8. Gene expression by RT-qPCR assay

$2x10^4$ MC3T3-E1 cells were seeded into 24-well plates and treated with both the nanoparticles (NanoSr 0%, NanoSr 10%, NanoSr 90%) and the strontium ranelate during 5 and 14 days. Then, we resuspended the cells in 1 ml of Trizol® reagent (Thermo Fisher Scientific), untreated osteoblast cells were used as controls. Total RNA was isolated according to the manufacturer´s protocol. A total of 1µg of total RNA was transcribed into cDNA using the High-Capacity cDNA Reverse Transcription kit (Applied Biosystem™ Foster City, CA, EUA). Quantitative real-time PCR (qPCR) was carried out on an ABI Prism 7500 Sequence detector (Applied Biosystem™ Foster City, CA, EUA). The list of primers used in this work can be below, table 4.1. *GAPDH* was used as endogenous control (reference genes). The thermal condition was as follows: 95ºC for 15 min, followed by 40 cycles at 95 ºC for 15 sec, 60 ºC for 20 sec, and 72 ºC for 20 sec.

TABLE 4. 1. MC3TE-E1 QRT-PCR PRIMER SETS SEQUENCES

Gene	Primer Forward (5´ → 3´)	Primer Reverse (5´ → 3´)
GAPDH	AAAGGGTCATCATCTCCGCC	AGTGATGGCATGGACTGTGG
RUNX2	CTTCACAAATCCTCCCCAAGTG	GGAATGCGCCCTAAATCACTG
SP7	TTCTGCGGCAAGAGGTTCAC	TTGCTCAAGTGGTCGCTTCT
TNAP	CCAGACACAAGCATTCCCACT	CGAAGGGTCAGTCAGGTTGT
OCN	TTCTGCTCACTCTGCTGACC	GCTTGGACATGAAGGCTTTGT

Sequences used for the analysis of mRNA expression by the RT-qPCR technique for the genes *Gapdh, Runx2, Sp7, TNAP,* and *OCN.*

2.9. Western Blotting Analysis

Whole protein extracts were prepared by cell lysis in RIPA buffer followed by quantification determined by micro-BCA protein assay kit (Thermo Scientific, CA, USA). Subsequently, the protein concentration was determined by the method of Bradford (1976), using a solution of bovine serum albumin (BSA, 0.1 mg/mL) as a standard. Absorbance values were obtained using a spectrophotometer (microplate reader), a wavelength of 595nm, and an iMark Microplate Absorbance Reader (BioRad

Laboratories, Inc, CA, USA). For protein analysis, each fraction (50µg) was subjected to SDS-polyacrylamide gel electrophoresis (LAEMMLI, 1970), using the Mini Protean II Dual Slab Cell system (BioRad Laboratories, Inc, CA, USA). Proteins were transferred to nitrocellulose membranes and subsequently passed through the immunodetection process. For this, the membranes were blocked in 5% skim milk powder (BioRad Laboratories, Inc, CA, USA #170-6404) diluted in 1% TBS-T for 2.5 hours at room temperature. Subsequently, the membranes were incubated overnight in a refrigerator with the primary antibodies of TNAP (Abcam®, ab108337) and Runx2 (Cell Signaling, 8486S) diluted at 1:1000 and 1:10000, respectively, in 5% skim milk. The next day, the membranes were washed 3 times (5 minutes each) with TBS-T and incubated with the appropriate secondary antibody for 1 hour at room temperature, followed by a further wash cycle. A secondary antibody was visualized using the ECLTM Western blotting Analysis System chemiluminescent substrate (Abcam®; Cambridge, MA, USA).

2.10. Osteoclast cultures and TRAP staining

Bone marrow cells were aseptically flushed from the femur and tibia of 5 C57BL/6 mice with α-minimum essential medium (α-MEM) supplemented with 10 vol% fetal bovine serum, 100 units/ml of penicillin and 100 mg/ml of streptomycin (Invitrogen Corporation, Carlsbad, CA, USA) over 3 days. The adhered cells (osteoclast progenitors) were plated in 96-well microtiter plates at 2×10^4 cells/well with M- CSF (30 ng/ml) and RANKL (10 ng/ml; R&D Systems, Minneapolis, MN, USA), and the respective nanoparticle (10 µg/mL) and strontium ranelate (0,3 mM). 48 Hours after the stimulus, we fixed the cells and treated them with TRAP staining as described here[36]. TRAP-positive multinucleated cells (>nuclei) were counted as mature osteoclasts. Then, we obtained the images with 10 x magnification using a Leica DM IRB inverted microscope coupled with a DFC490 camera (Leica, Wetzlar, Germany).

2.11. *In Vivo* experiments setup

In order to analyze the ability of the NPs to promote osteointegration in vivo , here we used sixteen adult New Zealand white male rabbits weighing approx. 2.5 kg each were used in this study. The protocol was approved by the local Ethics Committee of the University of São Paulo, São Paulo, Brazil, and was granted the ethics number 042/2018.

The study was carried out in accordance with the relevant guidelines and regulations of Brazilian law animal research nº. 11794, Oct 2008. A total of sixteen implants (PMMA containing strontium nanoparticles) of 500 mg/puncture were used. The rabbits were obtained from a commercial source (Anilab, São Paulo), judged clinically healthy by a veterinarian, and housed at the animal facility medical school department, University of São Paulo. Regarding animal well-being, all the animals were held under veterinary supervision three times a week, maintained in standardized rabbit cages (one rabbit per cage) with automatic environmental regulation of temperature (21-24.5 ºC), humidity (42-57%), and 12-hourly dark and light cycles.

On the day of surgery, the animals were moved from the animal facility to the surgical operating room. Each animal was anesthetized with intramuscular injections of Ketamine (40mg/kg), Xylazine (2mg/kg) before the surgical procedure, morphine (3mg/kg), and isoflurane 4 vol%. To avoid infection, the animals received intramuscular injections of meloxicam (1mg/kg) and terramycin LA (40mg/kg). The leg´s skin was shaved and disinfected with a 2 vol% chlorhexidine gluconate antiseptic solution. All the surgical procedures conducted from now on were handled by a veterinarian. Briefly, a skin cut with a scalpel was used to expose the bone surface. Then, we used a drill bit of 1mm to access the bone lumen and expanded the hole with a drill bit of 8mm to place the cement. Each animal received four implants (two in each leg- femur and tibia), yet we divided the animals into two groups, eight animals received pure PMMA cement and the remaining eight received PMMA load with the NanoSr 90%. No animal died during the procedure and the post-operative time. In the first two days, we performed intramuscular injections of meloxicam (0,5 mg/kg) and tramadol (5 mg/kg) to avoid pain and infections. Throughout the time of healing, we observed no visible signs of discomfort, pain, or infection. A week after the surgery, the animals were visibly active displaying curiosity-like reactions, eating and drinking well. The animals were sacrificed after 8 weeks by a lethal dose of ketamine and xylazine.

2.12. Gene expression - RT-qPCR assay: mRNA isolation from in vivo samples

Bone tissue containing cement were quickly removed from the rabbits' leg shortly after they were sacrificed. Then, using surgical pliers we extracted the cement fraction

followed by –80 ºC storage. After two weeks the cement fraction was removed from the –80 ºC *freezer* and was immediately placed in a mortar containing liquid nitrogen and ground with a pestle as described by Kim Eun-Cheol et al (2016). Total RNA isolation was performed using Trizol® reagent (Thermo Fisher Scientific) as recommended by the manufacturer´s protocol. A total of 1µg of total RNA was transcribed into cDNA using the High-Capacity cDNA Reverse Transcription kit (Applied Biosystem™ Foster City, CA, EUA). Quantitative real-time PCR (qPCR) was carried out on an ABI Prism 7500 Sequence detector (Applied Biosystem™ Foster City, CA, EUA). The list of primers used in this work can be checked below, table 4.2. *GAPDH* and *ACTB* were used as endogenous controls (reference genes). The thermal condition was as follows: 95ºC for 15 min, followed by 40 cycles at 95 ºC for 15 sec, 60 ºC for 20 sec, and 72 ºC for 20 sec.

TABLE 4. 2. RABBIT PRIMERS SET SEQUENCES.

Sequences used for the analysis of mRNA expression by qPCR.

Gene	Sequence (5´ -> 3´)	Gene	Sequence (5´ -> 3´)
Runx2 *Forward*	CACTATCCAGCCACCTTTACTT	SP7 *Forward*	GCACGAAGAAGCCATACTC
Runx2 *Reverse*	TGGCAGGTAGGTATGGTAGT	SP7 *Reverse*	TGACAGAAGCCCATTGGT
Collagen I *Forward*	CGGTGGTTACGACTTTGGTTA	OPN *Forward*	AGAAGGACAGCCATGATGTAAG
Collagen I *Reverse*	CAGAGTGGCATCGACTTCATAG	OPN *Reverse*	ACTATCGATGCTGTGGGAATG
VEGF *Forward*	GAAGAAGGAGACAATAAACCC	OCN *Forward*	CTTCGTGTCCAAGAGGGAGG
VEGF *Reverse*	ACCAGAGGCACGCAGGAA	OCN *Reverse*	CTCCAGGGGATCCGGGTAA
ALP *Forward*	CCCTCATGTGATGGCTTACG	BMP2 *Forward*	GGAAGAACTGCCAGAAAC
ALP *Reverse*	CTCAGAACAGGACGCTCAGG	BMP2 *Reverse*	GACCTGCTAATCCTCACG

2.13. Histology

The tibia of the rabbits was fixed in paraformaldehyde solution (pH 7.4), decalcified in EDTA solution (8%), and dehydrated in increasing ethanol concentrations (70 – 100%). Using a rotative RM2255 microtome (Leica Biosystems), thin 5µm sections from the interface bone/cement defect were prepared and stained with hematoxylin and eosin (H&E) and Masson´s trichrome staining. An experienced pathologist examined at least 10 sections. The bone new formation, blood infiltration, and inflammatory reaction were examined.

2.14. Computerized Tomography

Image acquisition was performed using a 16-slice multidetector computed tomography system (Aquilion Lightning, Canon Medical Systems, Otawara, Japan), operating at 120 kVp and 160 mA, with an image resolution of 512 x 512 pixels and a slice thickness of 0.5 mm.

2.15. Push-out test

The specimens were submitted to the pull-out test (push-out), in the mechanical tests at the bioengineering laboratory of the medical school of Ribeirão Preto - USP (EMIC DL2000), with the company's load cell, with a load capacity of 2kN. *Teses* software version 3.04, adapted to the machine, plots force x displacement graphs and tables with values of maximum force, deformation at maximum force, and Young's modulus (Mpa).

2.16. Raman

Mineral structure deposition on the porous PMMA cement was determined by RAMAN spectra (n=5) in the range of 170-3000 cm^{-1} using the QE Pro RAMAN High-performance Spectrometer (Ocean Insight, Orlando, FL-USA) loaded with a 785-nm laser. The laser power was set at 50%, with a 30-s integration time.

2.17. Statistical analysis

In vitro and in vivo results were evaluated by ANOVA test, and all experiments were conducted at least three times, which included animal data analysis. Statistical analysis and graphic design were calculated using GraphPad Prism 8.0 software (version 8.0, GraphPad Software, San Diego, CA). It was given a p-value of <0.05 for the definition of the level of statistical significance.

Part I - BIOLOGICAL CHARACTERIZATION OF NANOPARTICLES OVER OSTEOBLASTS AND OSTEOCLASTS

Results

We initially synthesize the nanoparticles in an attempt to reproduce the synthesis as previously described [28]. By following the same procedure, we synthesized apatite nanoparticles containing different strontium percentages. They were named accordingly to their calcium substitution percentage (0 % Sr named NanoSr 0%; 10% Sr named NanoSr 10%; and 90% Sr named NanoSr 90%). Then, we studied their morphology by SEM, as depicted in the **Figure 4.1**. The size distribution of the particles ranges from 20-40nm holding a spherical-shaped nanostructure. Likewise, they share similarities with bone apatite regarding the Ca/P molar ratio, crystallite size, and chemical structure [28]. Taking advantage of these characteristics, in the present study we tested the nanoparticles biological response on osteoblasts and osteoclast cultures *in vitro.*

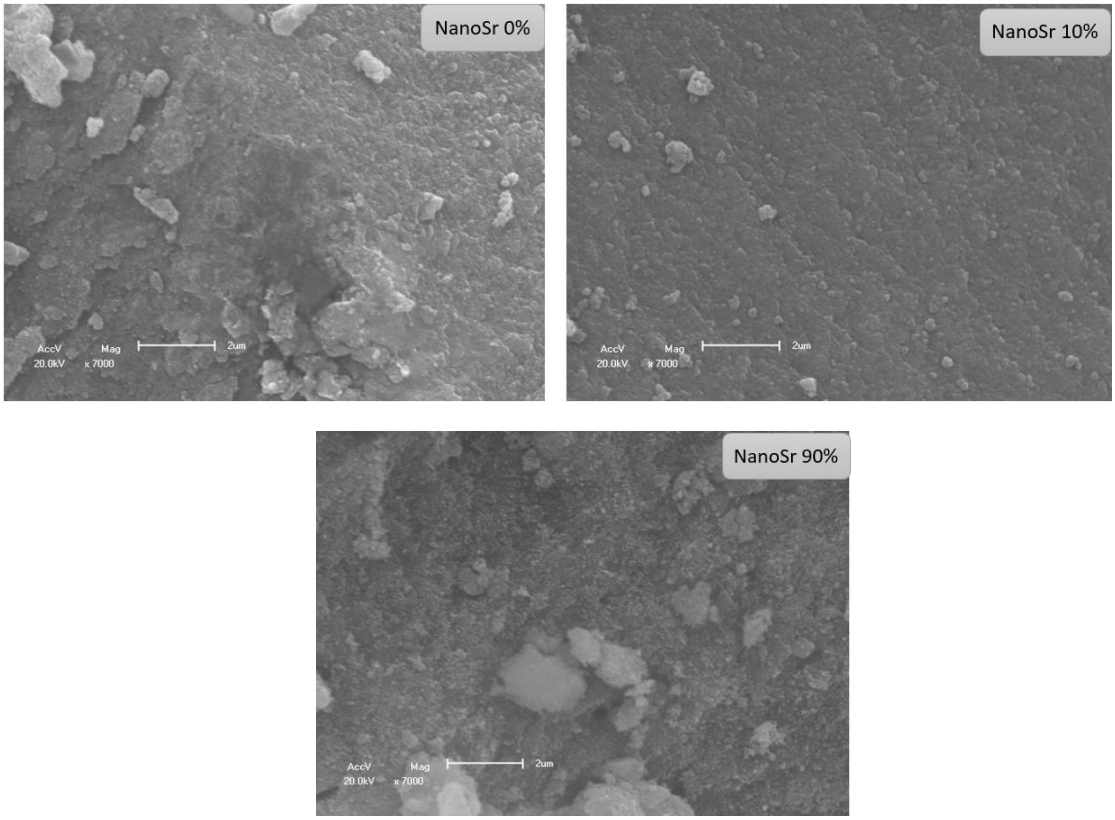

FIGURE 4. 1. SCANNING ELECTRON MICROSCOPY (SEM) IMAGES OF THE NANOPARTICLES STRUCTURE.

The nanoparticles containing the higher amount of Sr^{2+} (NanoSr 90%) were initially added to MC3T3-E1 pre-osteoblast cell line cultures at different concentrations (10 µg/mL, 100 µg/mL, and 1000 µg/mL) for 24, 48, and 72 hours in order to evaluate their cytotoxicity. Cell viability was not reduced in short-time exposure to NanoSr 90% **(Figure 4.2A),** what reinforces the safety already reported for other calcium phosphates [38–41]. However, we observed that particles in dispersions at concentrations higher than 10 µg/mL tend to aggregate, resulting in nanoparticle clusters that could interfere with further analysis. Hence, we opted to use the concentration of 10 µg/mL for further experiments with MC3T3-E1 cells at longer exposure periods (7 and 14 days). As shown in **Figure 4.2B**, cell viability measured through MTT assays was sustained in the presence of the nanoparticles when compared to the control (cells grown in the absence of the nanoparticles). In parallel, in order to compare the effects of the nanoparticles, we used strontium ranelate (previously used as an oral treatment for osteoporosis - i.e., PROTELOS®/Osseor®) as a second Sr^{2+}-delivery compound, at the same maximum final concentration of Sr^{2+} (0.3mM) released by the NanoSr 90% (**Figure 4.3**).

.

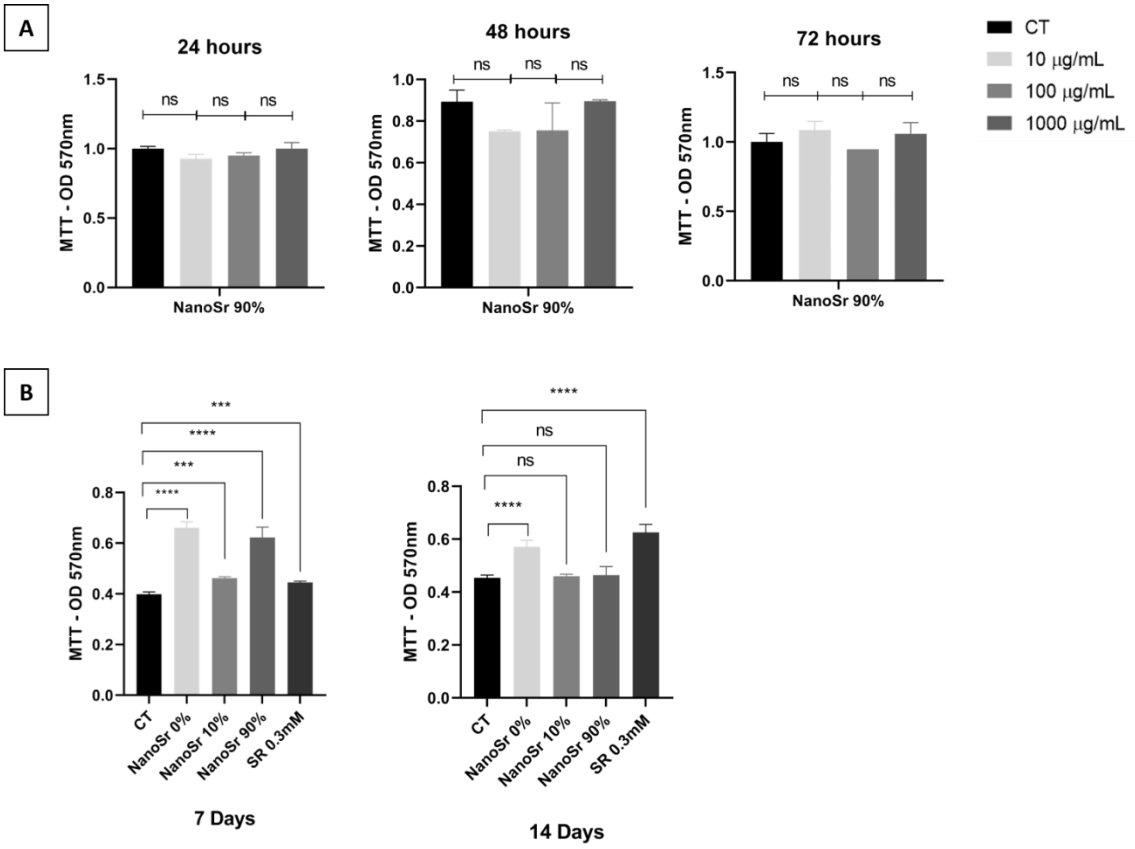

FIGURE 4. 2. *IN VITRO* RESPONSE OF MC3T3-E1 CELLS TO THE STRONTIUM NANOPARTICLES.

(A) Cell viability was measured through the MTT assay after 24 hours, 48 hours, and 72 hours in the presence of the nanoparticles. **(B)** Cells were treated with 10µg/mL of nanoparticle and 0.3 mM of strontium ranelate. Viability was measured by MTT assay and multiple statistical comparisons were performed by two-way ANOVA, P value for day 7, ***p= 0.0002, ****p<0.0001; for day 14, **p=0.0016 and ****p<0.0001. The results represent mean ± SD for triplicate determination for one experiment.

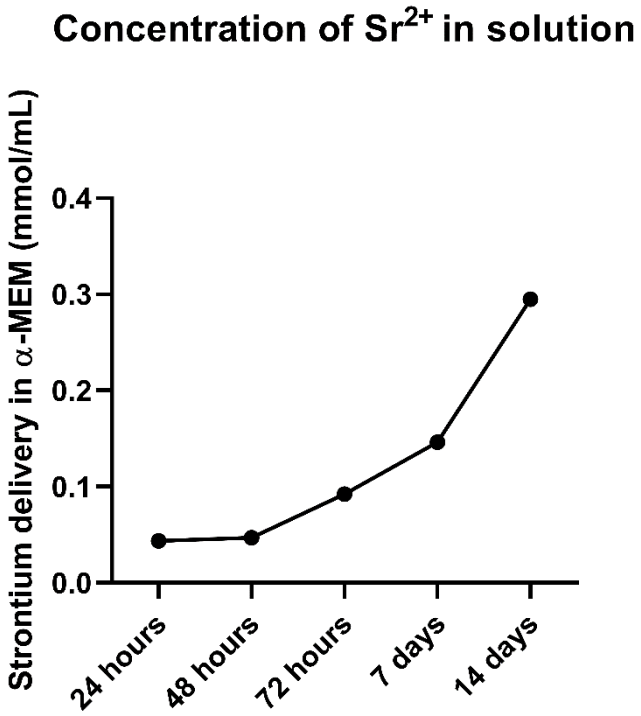

FIGURE 4. 3. THE CONCENTRATION OF FREE STRONTIUM ION IN A-MEM AFTER 14 DAYS OF INCUBATION WITH NANOSR 90% (REFERENCE NANOPARTICLE).

Additionally, we observed that the nanoparticles are able to deliver free Sr^{2+} ions in solution **(Figure 4.3)**, a process driven by the well-known dissolution/reprecipitation mechanism typical of calcium phosphates [30]. The concentration of Sr^{2+} in the culture medium (α-MEM) increased from 0.043 mmol/L after 24 hours of dispersion to 0.3 mmol/L after 14 days. Similar results have been reported for experiments with cells in the presence of Sr^{2+} in which activation of osteoblasts mineralization and reduction of resorption by osteoclasts were observed [42]. Therefore, we proceeded with the investigation regarding the nanoparticle's effects on the regulation of biomineralization markers.

TNAP is an isoform of alkaline phosphatase, which is strongly expressed in bone, liver, and kidney and plays a pivotal role in calcification and bone formation [43,44]. TNAP is attached to the outer surface cell membrane of osteoblasts, and it is primarily involved with the inorganic phosphate uptake by hydrolyzing pyrophosphate, a natural inhibitor of mineralization. In 2011, Whyte and coworkers demonstrated that the inactivation of the

TNAP gene was linked to reduced longitudinal growth, reduced body weight, the presence of hypo-mineralized areas in bones, and reduced survival in mice[45].

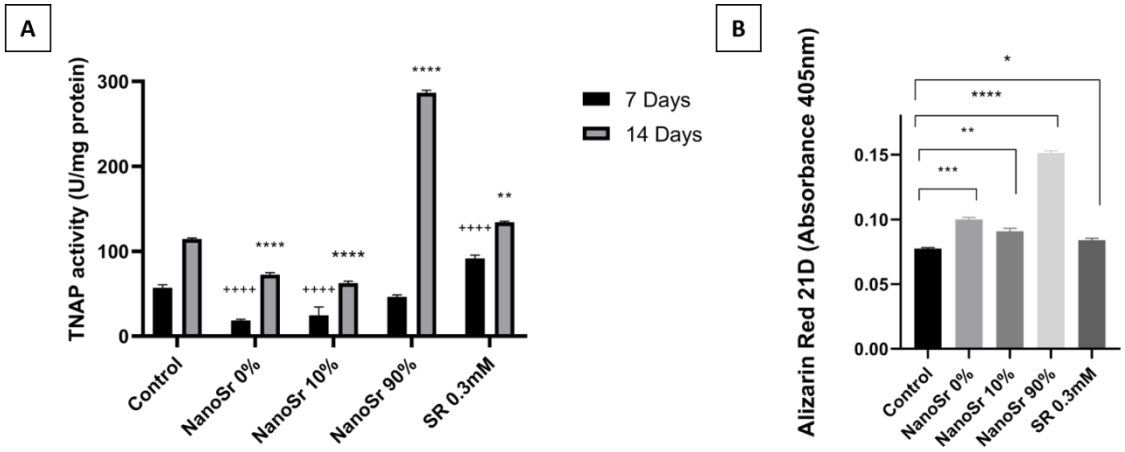

FIGURE 4. 4. EFFECT OF THE STRONTIUM NANOPARTICLES ON TNAP ENZYME ACTIVITY AND MATRIX MINERALIZATION.

(A) We measured TNAP activity after 7- and 14-day of cell culture in the presence of the nanoparticles. For TNAP activity, multiple statistical comparisons were performed by two-way ANOVA, $^{++++}$P< 0.0001, **p = 0.0018, ****p < 0.000. **(B)** The quantification of the matrix deposition was determined by Alizarin red staining after 21 days of culture in the presence of the nanoparticles and the strontium ranelate. Mineralized nodules were dissolved using acetic acid, then NH_4OH neutralization, and read at 405nm (absorbance) for quantification. Results represent the mean ± SD for triplicate determination for one experiment. Multiple statistical comparisons were performed by one-way ANOVA, *p= 0.014, **p= 0.0069, ***p= 0.0004, ****p< 0.0001. The results represent mean ± SD for triplicate determination for one experiment.

Herein, we show that NanoSr 90% significantly increased TNAP activity when compared to the nanoparticles containing a lower amount of Sr^{2+} and strontium ranelate **(Figure 4.4A)**. Increased TNAP activity after the addition of an Sr^{2+}- flavonoid complex to osteoblasts was also found by Cruz et al., (2018) [29]. However, in our experimental setting, increased TNAP activity was higher on the 14th day of culture compared to the 7th day. Of note, NanoSr 90% increased TNAP activity almost three-times compared to the control. High TNAP activity at this time point is pivotal to osteoblast mineralization since the hydrolysis and delivery of inorganic phosphate are required to prompt mineral growth. Alternatively, cells treated with strontium ranelate slightly increased TNAP activity when compared to the control pointing to an improved response of the formulated nanoparticle.

Matrix mineralization after treatment of MC3T3-E1 cells was also quantified through *alizarin red S staining,* followed by the of its absorbance measurement at 405nm **(Figure 4.4B)**. All the nanoparticles stimulated matrix mineralization *in vitro.* NanoSr 0%

is mainly composed of hydroxyapatite with a structure similar to bone apatite [42]. The stimulus of osteoblasts mineralization by calcium phosphates has been reported [46–50]. Based on this, hydroxyapatite may activate osteoblast turnover and matrix mineralization by providing the ionic precursors needed for the synthesis of new bone. In this line, the cells cultivated in the presence of NanoSr 90% exhibited the best mineralization performance, which corroborates the higher TNAP activity found for cells cultivated in the presence of these particles **(Figure 4.4B)**. Moreover, TNAP is a metalloenzyme, so the ionic substitution by divalent ions in the active site can increase the catalytic response in a dose-defendant mechanism, as reported by Ciancaglini et al., (2010)[51]. This find draws us to the following question: since TNAP is a metalo-protein, could Sr^{2+} replace Mg^{2+} at its active site? To answer this question, we dialyzed a purified sample of TNAP to remove all the Mg^{2+} remaining in the reactive media, the purification step is described elsewhere[52,53], and incubated it with Sr^{2+}, $Mg^{2+,}$ and Sr^{2+}: Mg^{2+} (molar ratio) at different concentrations **(Figure 4.5).**

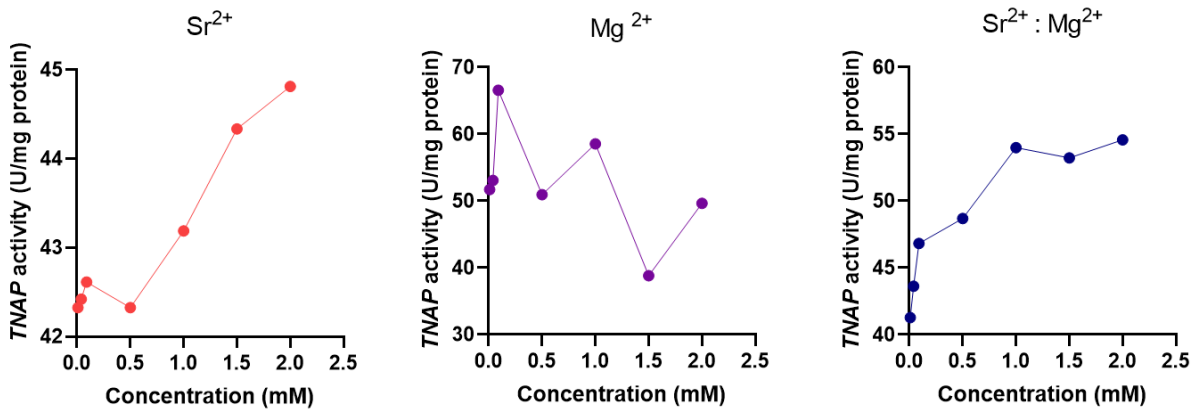

FIGURE 4. 5. THE EFFECT OF SR2+ ON TNAP ACTIVITY IS CONCENTRATION DEPENDENT.

We measured TNAP activity to check whether Sr^{2+} would replace magnesium at the enzyme active site. By means of comparison, we used strontium, magnesium (which is the natural metal of TNAP), and Sr^{2+}: Mg^{2+}.

Interestingly, as we can see in Fig 4.5, we found that Sr^{2+} can replace Mg^{2+} in the active site, since the activity of TNAP increases when Sr^{2+} concentration is increased. However, the efficiency in hydrolyzing para-nitrophenylphosphate (pNPP) showed to be lower in comparison to the Mg^{2+}, as revealed by the lower specific activity values. This finding is reasonable, since Mg^{2+} is a natural metal in the TNAP active site [43]. Moreover, the mixture of Sr^{2+}: Mg^{2+}, that would simulate normal physiological conditions, showed to be more efficient of pNPP hydrolysis in comparison to pure $Sr^{2+.}$

Further, we exploited the effect of the nanoparticles on the expression of osteogenesis-related genes by addressing the messenger RNA levels of two transcriptional factors widely reported in the literature, *Runx2* and *Sp7*, and two markers of osteoblastic differentiation, namely *Tnap* and *Ocn*. Based on previous studies related to the time course events related to the expression of these genes we decided to use 5 and 14 days of cell culture **(Figure 4.6)** [27,54–57]

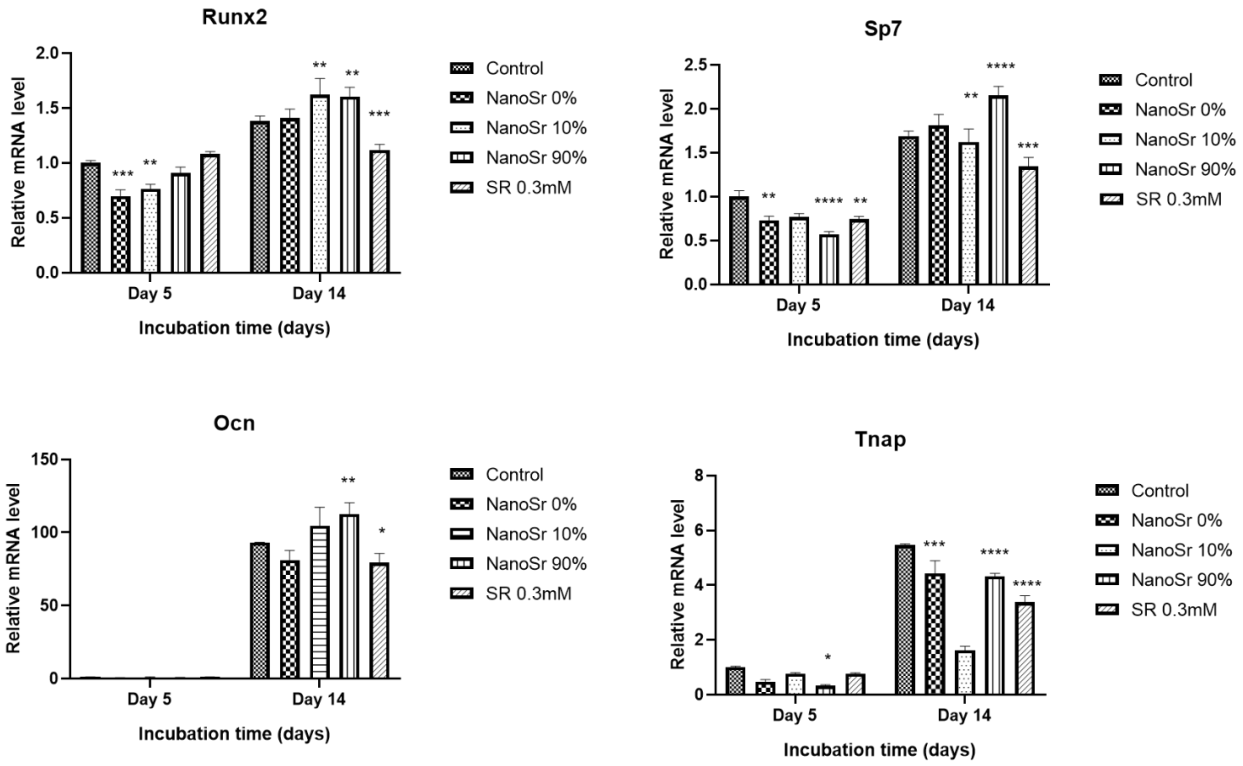

FIGURE 4. 6. TREATMENT WITH THE NANOPARTICLES INCREASES MRNA EXPRESSION OF RUNX2, SP7, AND OCN, AND PROTEIN LEVEL OF RUNX2 IN MC3T3-E1 CELLS AFTER 14 DAYS OF EXPOSURE.

Real-time PCR was performed to analyze the mRNA expression of Runx2, Ocn, Tnap, and Sp7. qRT-PCR data were normalized to Gapdh. Multiple statistical comparisons were performed by two-way ANOVA, *p< 0.05, **p< 0.05, ***p≤ 0.0002, ****p< 0.0001. The results represent mean ± SD for triplicate determination for one experiment.

As seen in **Figure 4.6**, the two transcriptional factors, *Runx2* and *Sp7* were upregulated by the NanoSr 90% after 14 days of culture, even though they did not affect the expression of both the genes in short-time culture (5 days). The data also revealed that the NanoSr 90% stimulated the maturation of the MC3T3 towards a mineralizing phenotype. Under similar conditions, strontium ranelate reduced the expression of *Runx2* and *Sp7.* The expression of the Ocn gene was increased after 14 days of culture in the presence of NanoSr 90%, albeit, NanoSr 0% and strontium ranelate reduced the

expression of this gene, compared to the control. Moreover, even though increased specific activity was found for TNAP, the expression of this gene was hindered by the presence of both the nanoparticles and strontium ranelate. Therefore, the apatite nanoparticles in which 90% of Ca^{2+} ions were replaced by Sr^{2+} upregulated the expression of genes important for osteogenesis. Since the concentration of Sr^{2+} released by NanoSr 90% and the concentration of strontium ranelate used in the cultures are similar, we can hypothesize that the carrier is an important factor.

Additionally western blotting analysis for RUNX2 and TNAP in the presence of the nanoparticles and strontium ranelate showed that after 5 days of treatment RUNX2 protein levels were only upregulated by strontium ranelate 0.3mM, whereas all the other treatments decreased the expression of this transcription factor **(Figure 4.7A)**.

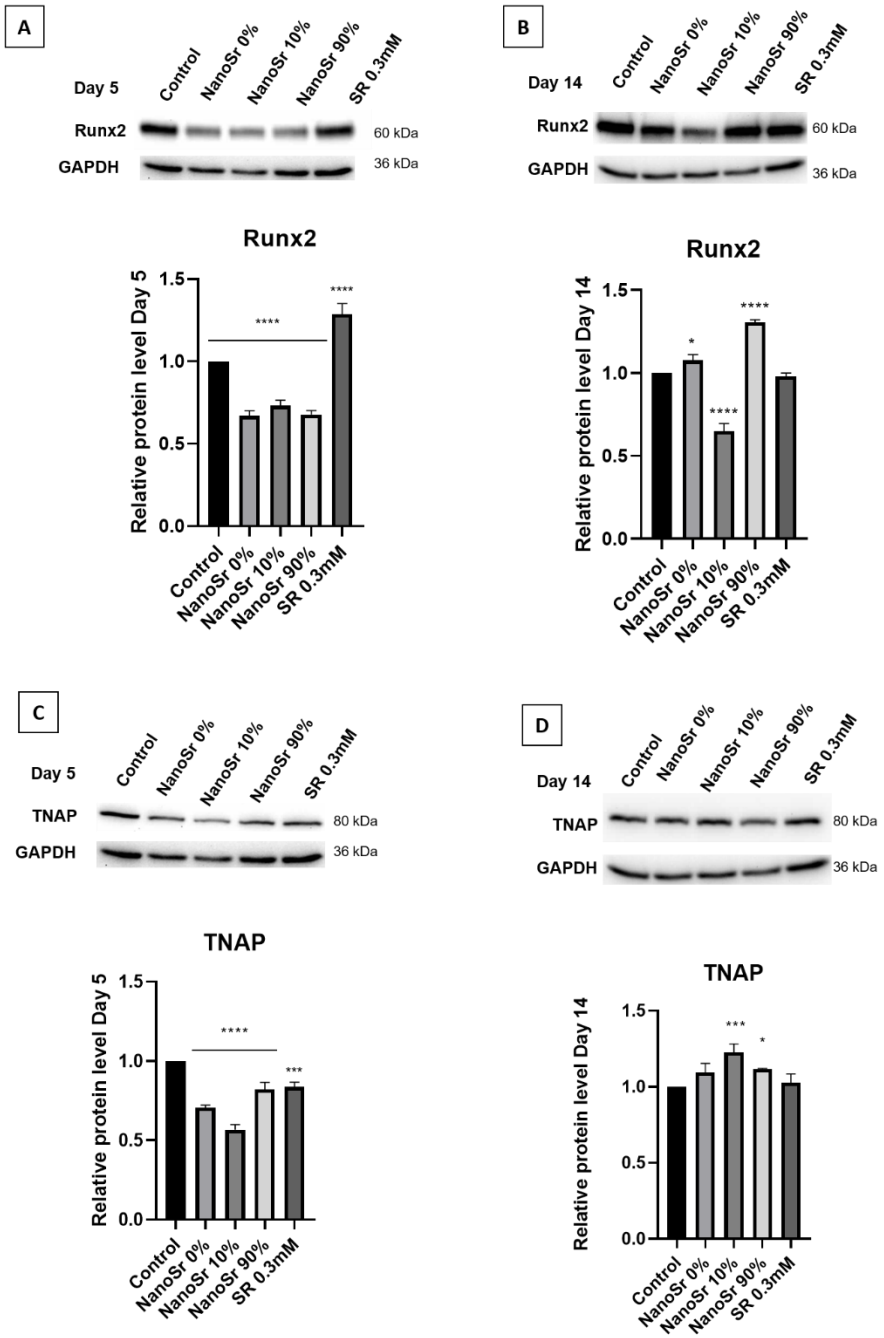

FIGURE 4. 7. WESTERN BLOTTING ANALYSIS OF RUNX2 AND TNAP EXPRESSION IN THE CELLS TREATED WITH STRONTIUM NANOPARTICLES AND STRONTIUM RANELATE

(A) Runx2 protein expression level on day 5; **(B)** Runx2 protein level on day 14; **(C)** TNAP protein expression level on day 5, **(D)** TNAP protein expression level on day 14. The nanoparticle treatments delay the Runx2 protein expression, whereas strontium ranelate stimulates this process. On day 14 NanoSr 0% and NanoSr 90% upregulated the Runx2 protein level. NanoSr 10% showed a negative effect on Runx2 protein level and strontium ranelate was similar to the control group. Multiple statistical comparisons were performed by one-way ANOVA, *p ≤0.03; ****p < 0.0001. For TNAP, all the treatments downregulated the expression of TNAP protein levels on day 5—on day 14 NanoSr 10% and NanoSr 90% upregulated TNAP protein level. Multiple statistical comparisons were performed by one-way ANOVA, *p ≤0.03; ***p= 0.0004; ****p < 0.0001. The results represent mean ± SD for triplicate determination for one experiment.

Alternatively, at higher incubation time (14 days), the synthesis of RUNX2 protein was significantly increased in the presence of NanoSr 90% **(Figure 4.7B)**, this difference may be related to the continuous delivery of Sr^{2+} into the media over time. RUNX2 is essential for osteoblast differentiation and chondrocyte maturation [58], and it regulates the transcription of Col1 and Ocn two markers of osteoblast differentiation and maturation. The presence of NanoSr 0% slightly increased the synthesis of RUNX2 as well, confirming the osteogenic potential of calcium phosphates [59–61]. We also investigated the effect of the nanoparticles on the synthesis of TNAP **(Figure 4.7C, D)**. The expression of this protein was slightly higher in the presence of NanoSr 10% and NanoSr 90% after 14 days of exposure **(Figure 4.7D)**, and none of the treatments enhanced its levels at short-term exposure (5 days) **(Figure 4.7C)**. Despite this, the influence of NanoSr 90% over TNAP protein expression may not be biologically significant, since the effects of Sr^{2+} on this marker obey a biochemistry/biophysical control by interfering with the TNAP enzyme active site pocket [51,62] rather than controlling its protein levels.

Many divalent ions can enhance the mineralization ability of osteoblasts [17,63,64]. Nevertheless, Sr^{2+} is a strong candidate in bone repair due to its dual effect on activating osteoblasts and strongly inhibiting osteoclasts [17,65]. The biochemical mechanism behind these effects is not completely understood, but it is already known that Sr^{2+} interferes in the $NF_{\kappa}B$ signaling cascade, a pathway involved with the transcription of RANKL (receptor activation of nuclear factor κ B-ligands)[15,66], that is necessary to osteoclast maturation. Moreover, many authors have related Sr^{2+} to anti-inflammatory response, since this ion modulates the TNF-α pathway, a potent $NF_{\kappa}B$ inducer [67–69]. Herein, we analyzed by MTT assay if the nanoparticle concentration previously used in the osteoblast culture (10 µg/mL) would be toxic to the osteoclast primary cells, since we want to promote an inhibitory effect rather than cytotoxicity **(Figure 4.8A)**.

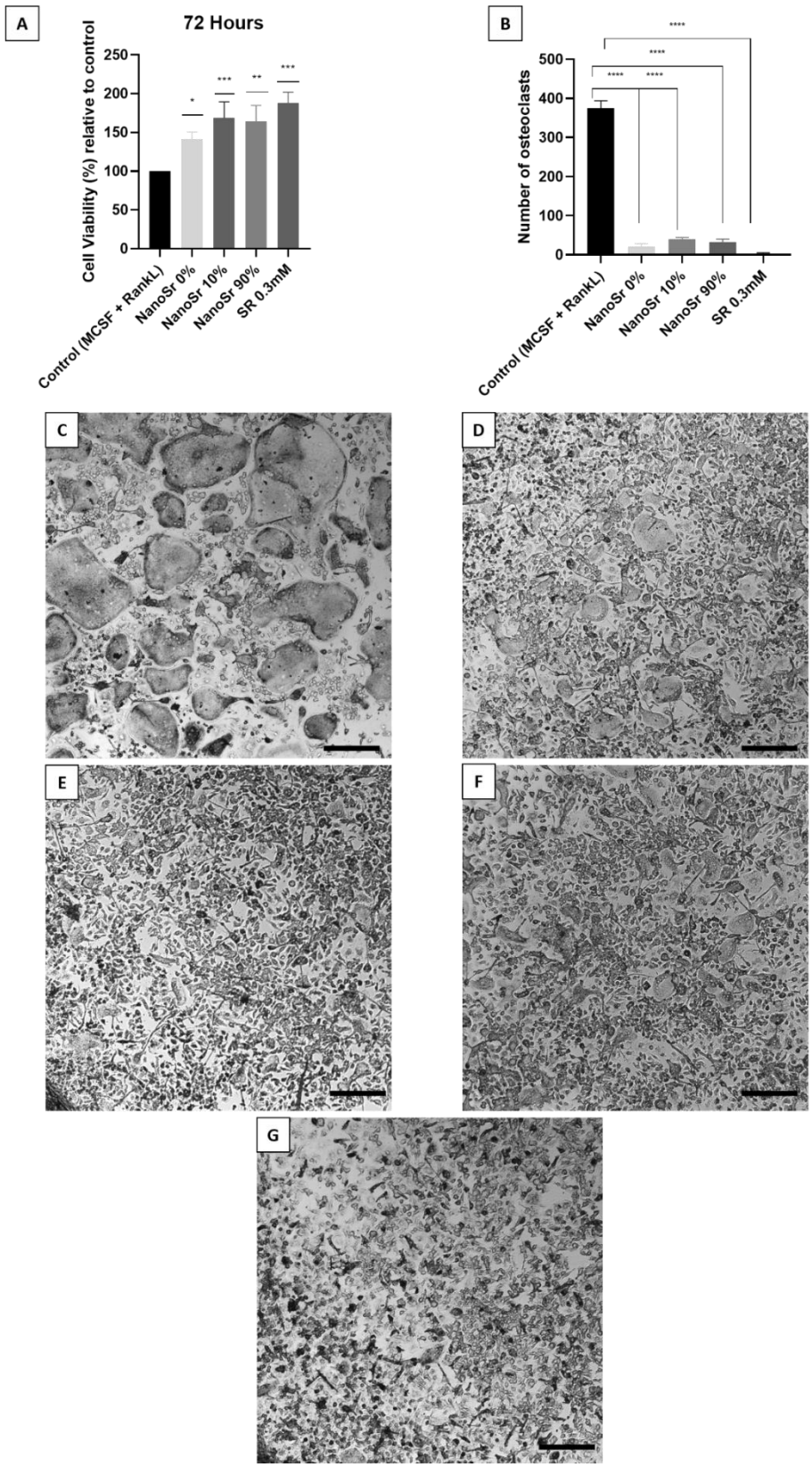

FIGURE 4. 8. NANOPARTICLES DID NOT AFFECT OSTEOCLAST VIABILITY BUT ABOLISHED OSTEOCLAST DIFFERENTIATION.

(A) Cell viability relative to control. Here, we kept the same nanoparticles and strontium ranelate concentrations used for the osteoblast analysis; **(B)** TRAP assay: mature osteoclasts (4 more conjugated

nuclei) were counted; **(C)** control, presence of multinucleated osteoclast cells; **(D)** cells were treated with NanoSr0%; **(E)** cells were treated with NanoSr 10%; **(F)** cells were treated with NanoSr 90%; **(G)** cells were treated with strontium ranelate. The statistical analysis was relative to the control (MCSF- RankL). P values for A) *p = 0.0219, ***p ≤ 0.0008. P values for B) ****p < 0.0001. The image scales correspond to 300nm.

Regarding cell viability **(Figure 4.8A)** neither of the compounds appear to be toxic to the osteoclasts after 72 hours of exposure. Then, we tested whether the nanoparticles and the strontium ranelate would affect the differentiation of cells using the Tartrate-resistant acid phosphatase (TRAP) activity **(Figure 4.8B)**, a histochemical marker expressed by mature osteoclasts, macrophages, dendritic cells, and many others[70]. The direct quantification of mature osteoclasts (multinucleated cells) depicted in Figure 4.8B and, images (C, D, E, F, G) clearly show that all the nanoparticles and strontium ranelate completely diminished osteoclast maturation, as no multinucleated cells were seen in either of the treatments (4.8B, D, E, F, and G), except in the control group (B, C).

Taking together, the *in vitro* outcome presented here confirmed that the presence of Sr^{2+} in the apatite structure stimulated osteoblast-associated events mainly regarding the biomineralization process. In addition, the nanoparticle completely hinders osteoclast maturation. Finally, in comparison to the already used and studied strontium ranelate, our nanoparticle takes advantage of gradual strontium ion delivery what renders higher efficiency in promoting mineralization and could avoid critical collateral effects associated with the chronic use of strontium ranelate.

The nanoparticles were first thought to be used as a carrier of strontium. So, the ion release and concentration should be time-dependent. However, driven by curiosity we asked whether the nanoparticles would be capable of being internalized by the cells. If so, would they have any sort of biological role? To answer this question, we treated the osteoblasts with the nanoparticles and performed transmission electron microscopy (TEM) **(Figure 4.9 A, B, C, D).** Additionally, we analyzed their superficial charge by zeta potential (ζ) **(Table 4.3).**

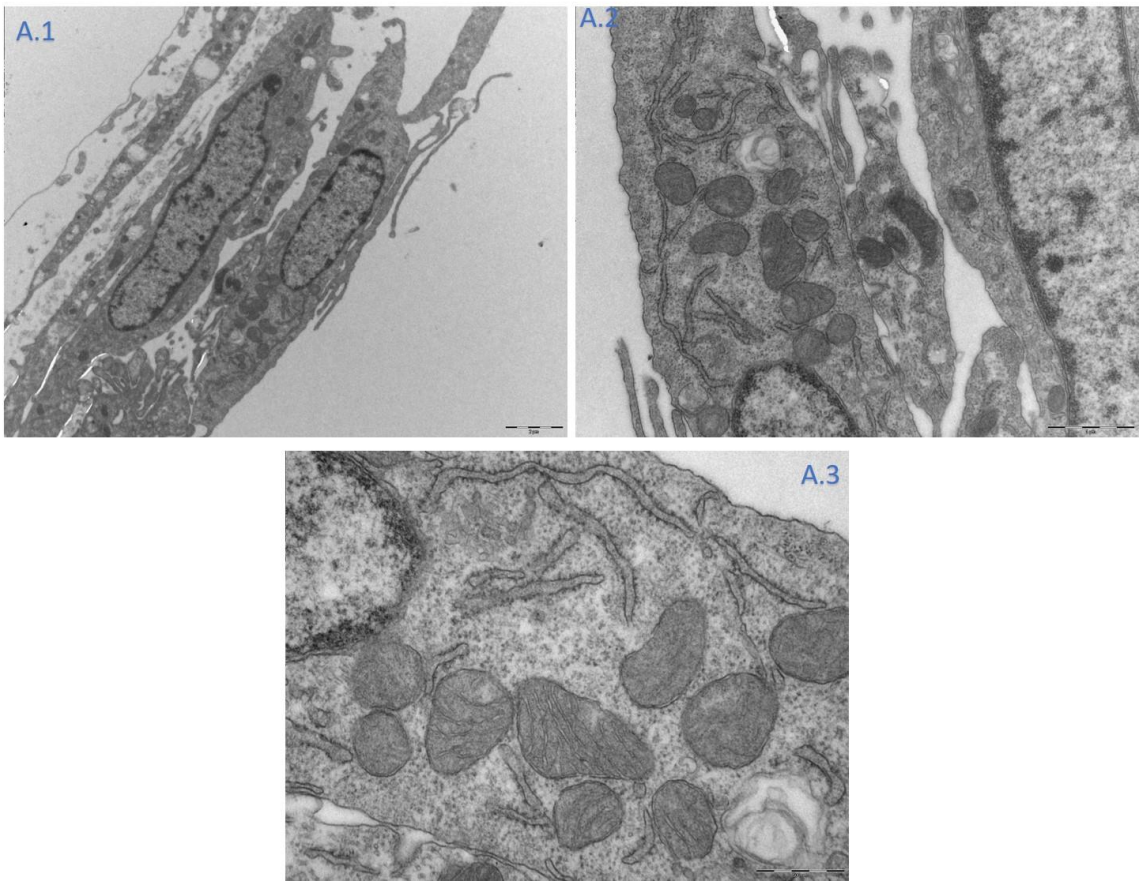

FIGURE 4. 9A. TRANSMISSION ELECTRON MICROSCOPY OF THE CONTROL GROUP.

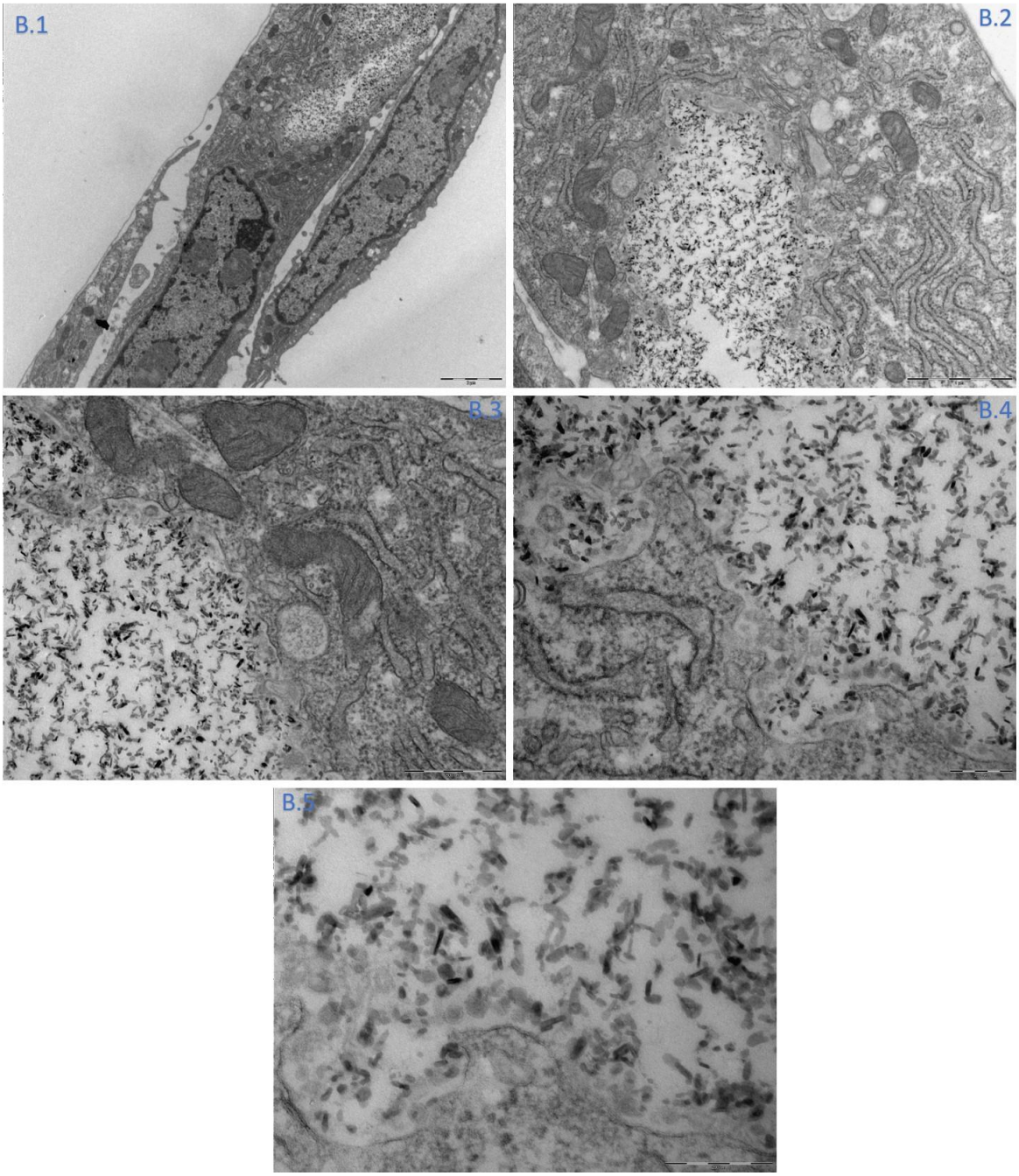

FIGURE 4. 9B. TRANSMISSION ELECTRON MICROSCOPY OF THE NANOSR 0%. NANOPARTICLES ARE SHOWN TO BE INTERNALIZED AND ISOLATED BY THE CELL

To confirm internalization, we analyzed at least three different cells.

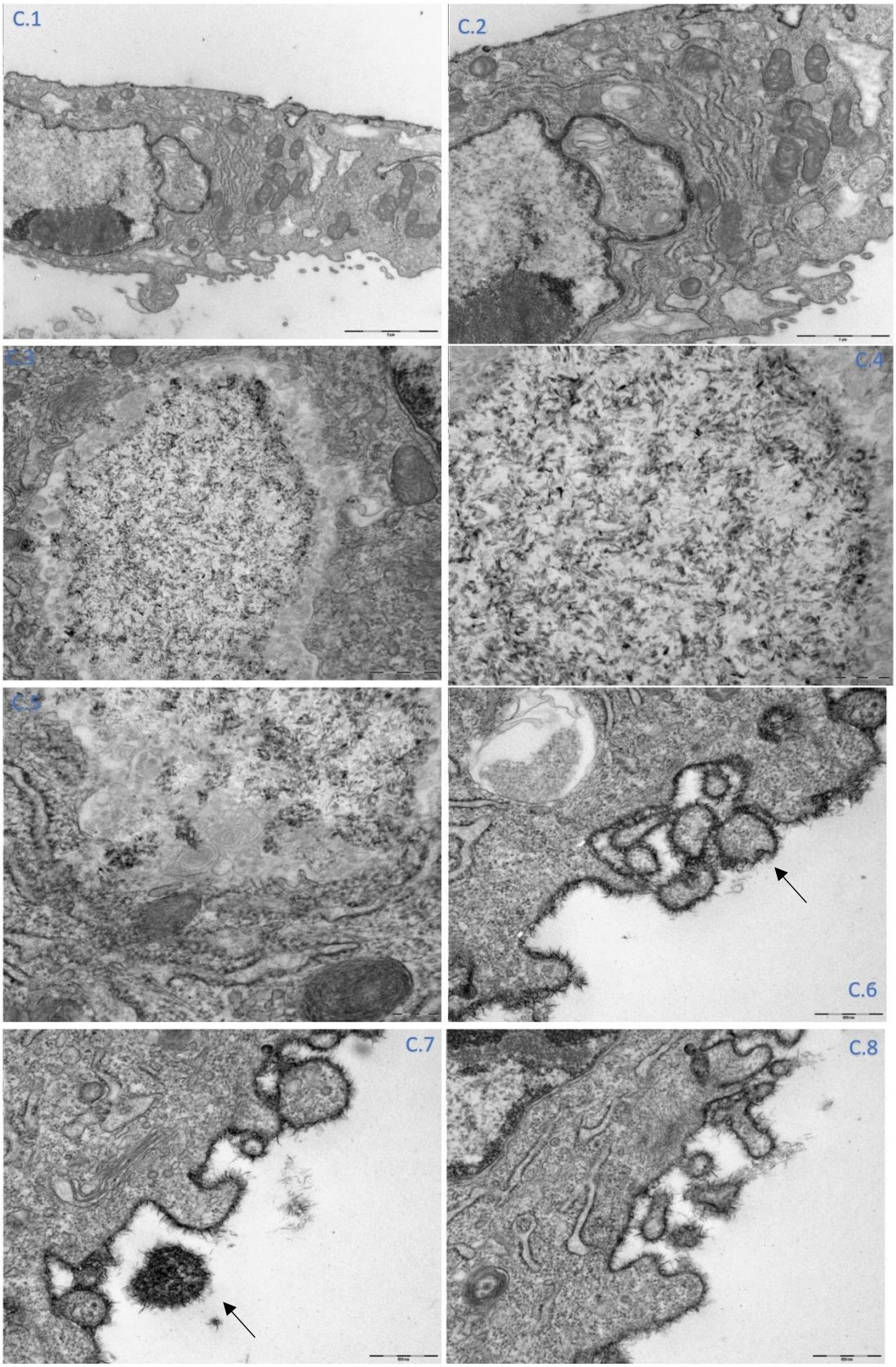

FIGURE 4. 9C. TRANSMISSION ELECTRON MICROSCOPY OF THE NANOSR 10%.

Nanoparticles are shown to be internalized and isolated by the cell. Due to its superficial charge, the accumulation of nanoparticles can also be seen throughout the cell membrane (black arrow). To confirm internalization, we analyzed at least three different cells.

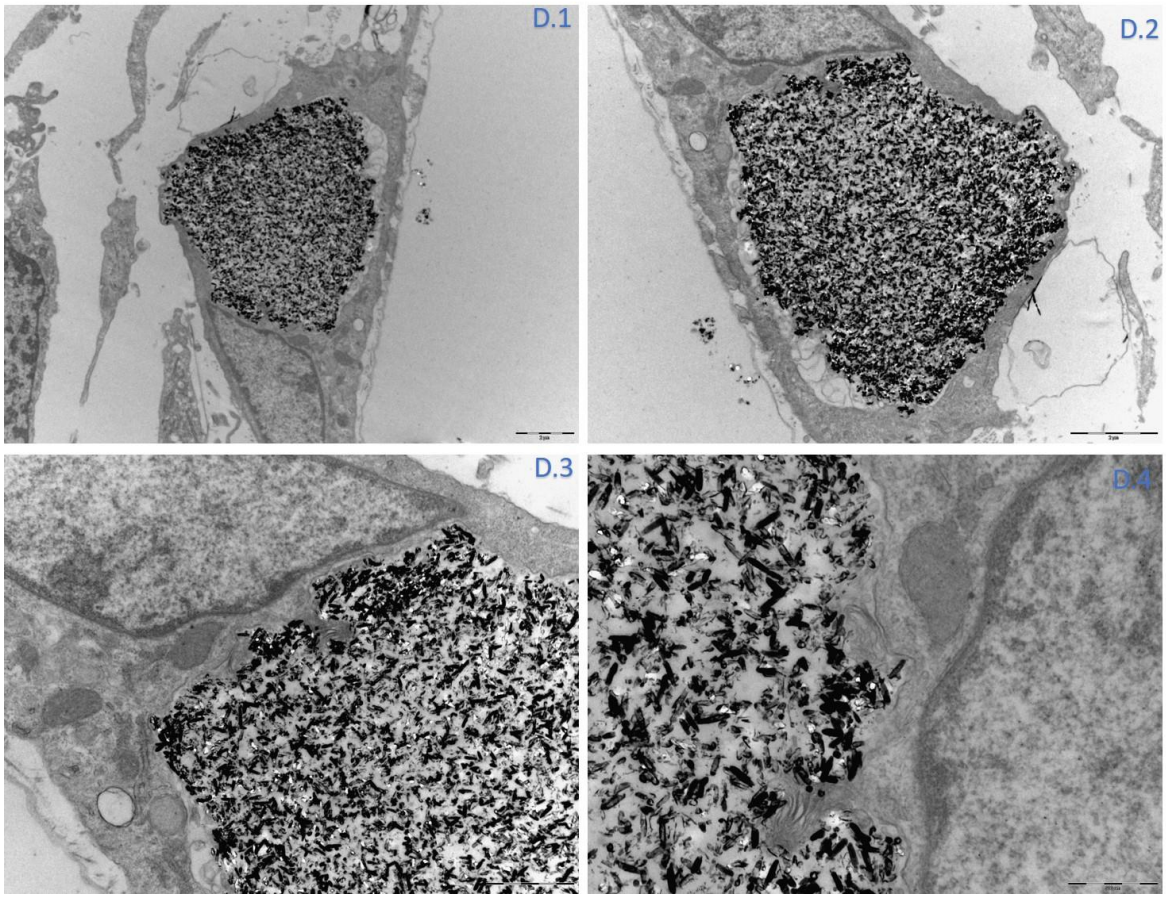

FIGURE 4. 9D. TRANSMISSION ELECTRON MICROSCOPY OF THE NANOSR 90%.

Nanoparticles are shown to be internalized and isolated by the cell. NanoSr 90% is darker due to its electronegativity. To confirm internalization, we analyzed at least three different cells.

TABLE 4. 3. SUPERFICIAL CHARGE MEASURED BY ZETA POTENTIAL (Z) OF THE NANOPARTICLES.

Nanoparticles	Zeta potential (ζ) (mV)
NanoSr 0%	-24,40 ± 0,93
NanoSr 10%	-22,43 ± 3,20
NanoSr 90%	-14,83 ± 2,28

As we can see in **Figure 4.9 (A-D)**, all the nanoparticles were internalized and compartmentalized by osteoblasts. Accordingly, to their superficial charge **(Table 4.3)**, NanoSr 90% shows the most electronegative nanoparticle, which means that their negative superficial charge is higher. Curiously, NanoSr 10% presented an accumulation

of nanoparticles throughout the superficial cell membrane (black arrow), which suggests that the nanoparticles superficial charge interferes with the nanoparticle's internalization.

Discussion

The use of bioactive nanoparticles aiming at bone healing can be more advantageous than the use conventional drugs as strontium ranelate in some respects. For example, nanoparticles have shown to be more efficient and less toxic to the organism [71]. However, it requires a deep investigation, not only at the biological level but also on how financially feasible they are to be implemented into the market, i.e., one has to measure the cost x benefit. For example, one milligram of gold nanoparticles costs about 80 USD and for a gram, it is around 80.000 USD. So, the high cost of nanomaterials limits their use in clinics. Despite this limitation, many nanoparticles have been approved by the Food and Drug Administration (FDA), that is the case of Abraxane and Doxil, used to treat breast and ovarian cancer, respectively[71–75].

Moreover, developing biomaterials aiming at bone healing is a frightfully hard task, for now, bone is a hard-to-reach organ, and not every biomaterial can mimic the tridimensional structure and the mechanical properties of the bone, nor induce a proper and sufficient response. Analogous bone graft has over 100 years of successful clinical use, however, many complications are significant, such as rejection and immunological complications[76]. For this reason, alternatives to the conventional replacement or filling of bone fractures are still necessary. Inspired by this, we proposed here a nanoparticle that resembles biological apatite in structure and mechanical properties, is easy to produce, and is financially feasible.

We started by evaluating their odds of negatively affecting the cells by means of cytotoxicity assay. We observed that on short-time (72h) exposure to higher concentrations (100 and 1000 µg/mL) of nanoparticles did not show any toxicity. However, it is known that physical loading can be sensed by mechanoreceptors presented in the cell membrane's outer surface, which is the main mechanism involved with osteoporosis derived from low gravity, i.e., no load bearing[77,78]. The pressure generated by the nanoparticles might result in cytoskeleton modulation and a change in gene expression profile, which can be harmful to cell health function[79]. Here, we did not evaluate the mechanical resistance generated by the nanoparticles upon the cell membrane and cytoplasm. So, to avoid such an effect, we opted to use the lowest

concentration (10 µg/mL) **(Figure 4.2.A-B)**. Moreover, we analyzed the Sr^{2+} concentration delivered into the culture media over several days. At the 14th day approximately 0.3 mM/mL of Sr^{2+} was detected **(Figure 4.3)**. Such concentration is enough to trigger fundamental biological pathways related to biomineralization[14,80].

Mineralization of the ECM requires a controlled sequence of events, from osteoblast proliferation to mineral deposition. Throughout this process, there are plenty of molecular checkpoints, which result in either a stimulatory or inhibitory effect upon biomineralization. One of these checkpoints involves the extracellular accumulation of PPi and Pi, both ATP bioproducts. TNAP is anchored at MV´s outer membrane and has a pivotal role in providing Pi from hydrolysis of ATP and PPi. The balance between Pi and PPi will dictate the transport and growth accumulation of Pi inside the MVs (along with Ca^{2+}), thus resulting in crystal growth. Based on this, we raised the following question: Is Sr^{2+} able to regulate TNAP activity, and would this effect contribute to a higher ECM mineralization?

Here, under the studied conditions we confirmed that the nanoparticles containing the higher Sr^{2+} concentration (NanoSr 90%) increased TNAP activity, which resulted in higher ECM mineralization, as revealed by alizarin red assay **(Figures 4.4.A-B)**. Also, strontium ranelate (a secondary source of Sr^{2+}) shown to be effective upon TNAP activity and mineral deposition. Finally, NanoSr 0%, strontium-free nanoparticle, also increased biomineralization, as attested by alizarin red staining, despite its low effect on TNAP activity. NanoSr 0% is a calcium-phosphate-based nanoparticle, and its ability to release Ca^{2+} was previously investigated[28]. Ca^{2+} is a major driver of osteoblast turnover and contributes to healthy mineralization[64,81–83]. Further, Mg^{2+} substitution by Sr^{2+} suggests that despite TNAP still keeping its function the efficiency is not as high as its natural metal (Mg^{2+}) (Figure 4.5). However, the mixture Sr^{2+}: Mg^{2+} seems to have a synergic effect on TNAP activity. In corroboration with this find, Hoiletts et al (2015) found that ionic substitution by divalent ions in the active site can increase the TNAP catalytic response[84].

The role of Sr^{2+} on molecular signaling and gene expression still needs investigation, which will be the next topic of this thesis. However, several studies show that Sr^{2+} is able to regulate osteogenesis at the molecular level by upregulating transcription factors and osteogenic-related genes[15,17,85,86]. At the genomic level, the nanoparticles prepared herein delay the expression of Runx2, ALP, and SP7 in the early stage (5 days) of osteoblast turnover, which is a common event (ref). In the late stage (14

days) NanoSr 90% upregulated the expression of Runx2, Sp7, and OCN, all markers of osteoblast turnover, which shows their ability as a bioactive biomaterial. Runx2 and Sp7 are two important transcription factors that are pivotal for osteoblast differentiation. Among other genes, Runx2 and Sp7 control the expression of Col1, OCN, and bone matrix proteins[49,58,87].

In addition, NanoSr 90% upregulated Runx2 at the protein level after 5 and 14 days. For TNAP neither the treatments increased protein expression level at day 5. At day 14 only NanoSr 90% affected protein expression, however, due to its low statistical significance we judged it as being biologically irrelevant. Together with the data from TNAP kinetics, we believe that Sr^{2+} modulates TNAP activity, rather than its expression at either genomic or protein level. We will support this idea later in this thesis when we describe in deep the Sr^{2+} effect at the molecular level.

Nowadays biomaterials aiming at bone regeneration of small fractures must be capable of controlling not only osteoblasts but also osteoclasts activity. Thus, we tested the nanoparticles potential in inhibiting osteoclast differentiation since Sr^{2+} is known to have an inhibitory effect over osteoclastogenesis[29,69,88,89]. Data from the MTT assay double-checked their safety (Figure 4.8) as well as attested their inhibitory effect over osteoclast maturation.

Finally, we observed that all the nanoparticles were internalized and compartmentalized inside the osteoblasts. Nanoparticles internalization varies according to their superficial charge as we can see in **Figure 4.9 (A-D)** and Table 4.3. The biological significance of this finding needs further investigation, and some questions have been raised. For example, can they interfere with any biological response? How does the cytoskeleton recognize the external body and collectively isolate the nanoparticles? Does it interfere with MV secretion and biomineralization? It was previously shown that negatively charged HA nanoparticles induced osteoblast proliferation *in vitro* and *in vivo* [90,91]. Yet, researchers have developed nanoparticles presenting switch-like behavior, where the superficial charge is tunned depending on the pH of the medium and the nanoparticles still effective[92,93]. Also, charged peptides and phospholipids (PEG shields) have been deposited on nanoparticles surface upon pH variation to allow translocation toward the cell cytosol[94,95]. More information on molecular and biophysical involved of nanoparticles engulfment can be found here[79].

PART II - *In vivo* response of PPMMA-containing nanoparticles

Specific background

In the previous section, we studied the nanoparticles' ability to induce pre-osteoblasts and inhibit osteoclasts turnover in vitro. Despite interesting outcomes drawn from each nanoparticle we selected NanoSr 90% to carry out further in vivo experiments since NanoSr 90% had the best biological performance on osteoblasts and was shown to be effective over osteoclasts.

The mechanical characterization of pPMMA cement and the in vitro biological response of pPMMA containing nanoparticles with different proportions of Sr^{2+} were previously addressed by our group[5,28]. In this thesis, we tested their ability to induce osteogenesis *in vivo* using female *New Zealand* rabbits. To this, we implanted the pPMMA associated with NanoSr 90% (from now named NanoSr 90%+pPMMA) into the rabbits' femur and tibia. We used pPMMA without the nanoparticles (we named, pPMMA) as a control.

The steps of the surgery procedure are depicted in the **Figure 4.10**. After 8 weeks following the biomaterial implantation, we sacrificed the animals, harvested the femur and tibia, and studied the osteoinductive capability of the pPMMA containing the nanoparticles by SEM, qRT-PCR, and histology. Then, we followed the osteointegration by mechanical tests (push-out), computerized microscopy, CT), micro-computerized microscopy, µCT) and characterized the deposited mineral structure by Raman.

FIGURE 4. 10. SCHEMATIC REPRESENTATION OF THE ANIMAL MODEL SURGERY.

From left to right: The animals were initially weighed followed by their sedation. We started by opening a 1mm hole to assess the bone cavity, and then we expanded it to 8mm. Then, we prepared the porous cement according to [28], containing and non-containing the nanoparticles. Eight weeks after surgery, we sacrificed all the animals and harvested the bone with the implants.

Results

The *in vitro* assay previously characterized by our group[28] have shown that the cement itself also favors osteoblast cell invasion and the formation of a bone-like mineral on its surface. The addition of the apatite nanoparticles to the cement resulted in increased surface roughness when compared to the unmodified porous cement [42]. Working with complex organisms where one cannot exclude the influence of the surrounding tissues, hormones, electrolytes, complex metabolites, and immune system, to cite a few, is a hard task. Whether Sr^{2+} affects other cell types and how indirectly it (other cell types) contributes to either bone formation or resorption will not be investigated here, however, this characterization is rather important in the upcoming future, more so if one thinks about the potential use of the nanoparticles in clinics. Here, we limited our study to understand whether the nanoparticles associated with a vehicle (here the scaffold of pPMMA cement) would attract osteoblast and induce its mineralization in the pPMMA cement, which is a sign of osteointegration. To accomplish that, first we isolated

the cement from the surgery area and studied osteogenic-related genes (*Runx2, Col1, Vegf, Alp, Sp7, Opn,Ocn* and Bmp2) by qRT-PCR **(Figure 4.11**M.

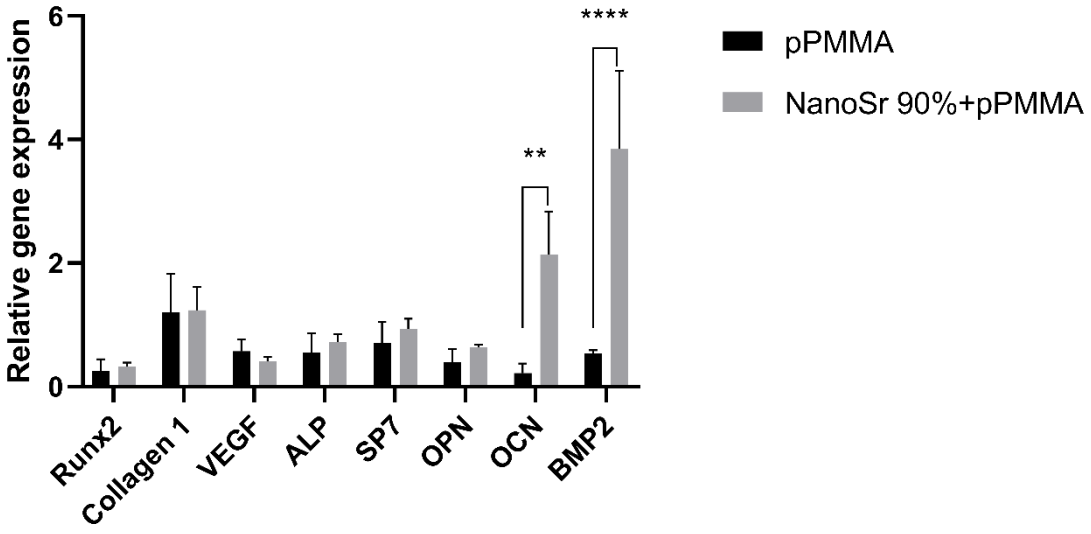

FIGURE 4. 11. RELATIVE GENE EXPRESSION OF OSTEOGENIC MARKERS INDUCED BY THE PPMMA CEMENT AND PPMMA CONTAINING NANOSR 90%.

Relative gene expression of osteogenic markers induced by the pPMMA cement and pPMMA containing NanoSr 90%. Results represent the mean ± SD for triplicate determination for one experiment. Multiple statistical analysis comparisons were performed by two-way ANOVA, where **p= 0.0036, ****p<0.0001.

The animals were exposed for 8 weeks based on recent studies where authors claim that in the first 5 weeks after surgery the major effect observed is inflammation, which delays the accumulation of local osteoblasts, hence interfering with the biomineralization process[8,96]. Following Fig 4.11, we observed that pPMMA+ NanoSr 90% upregulated the mRNA level of *Ocn* and *Bmp2. Ocn* is secreted by osteoblasts and is the most abundant non-collagenous protein found in bone. However it has been suggested that *Ocn* is not involved in the regulation of bone formation and bone quantity per se, but rather controls bone quality by aligning biological apatite and collagen fibrils[87].

Finally, *Bmp2*, a member of the transforming growth factor-β (TGF- β) and one of the main inducers of osteogenic differentiation [97], has shown to positively interfere with the expression of *Ocn* and collagen I. Due to this, many authors combine it with synthetic scaffolds to improve the reconstruction of bone defects[98–100]. Furthermore, *Runx2, Col1,*

Vegf, Alp, Sp7, and *Opn* mRNA levels did not respond to the treatment, which is reasonable since both genes are expressed in osteoblasts' early-stage (~10 days) development, and here we are studying an 8 weeks old implant.

Following our previous work[5], herein, the porous cement demonstrated to be highly osteointegrative, reinforcing its potential to be used in clinical trials. Indeed, histological evaluation (H&E staining) showed no sign of blood infiltration inward of the porous cement, while osteoblasts were found and the bone morphology was maintained in both the control and in the group containing the nanoparticles **(Figure 4.12A and B**, respectively). Newly formed bone was observed in both groups **(Figure 4.12A, B** indicated with *) which supports the integration of the implants.

The mineralization of extracellular matrix (ECM) has been described as a process driven by osteoblasts through the release of collagen and matrix vesicles[101,102]. Matrix vesicles bind to collagen fibrils controlling the local specific precipitation of apatite minerals to propagate mineralization[103,104]. H&E staining is not specific in detecting and marking collagen fibers, thus to investigate the migration of osteoblasts and the secretion of collagen inside the pores of the cements, we applied Masson's trichrome staining **(Figure 4.12 C and D)**, which is widely used to stain collagen[105]. As confirmed in Figure 4.12 (C, D) multiple sites all over the porous cement were covered by a collagen matrix **), as well as osteoblastic cells, however, no difference was observed comparing the groups.

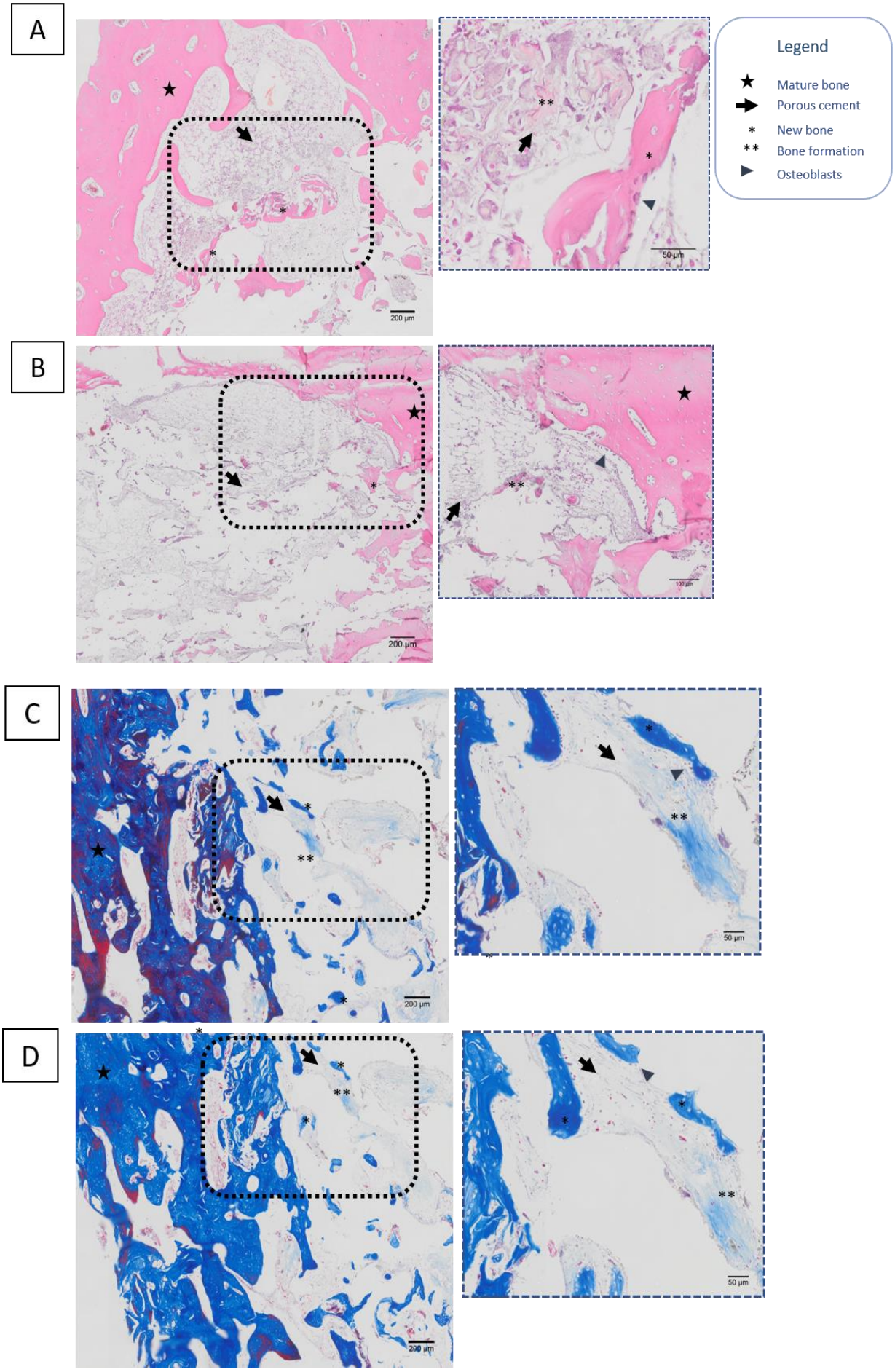

FIGURE 4. 12. REPRESENTATIVE H&E AND MASSON´S TRICHROME STAINING FOR ALL GROUPS.

The rabbits´ tibia were stained with H&E for both groups: porous cement without the nanoparticle, pPMMA, and with the strontium nanoparticle, NanoSr 90%+pPMMA (A and B, respectively); To conform collagen secretion upon the cement we applied Masson´s trichome stain for pPMMA and NanoSr 90%+pPMMA (C, and D respectively). No statistical difference was observed between the groups.

Histological staining is a good technique to analyze cell events at a microscopic level, however, results at a macroscopic level are poorly covered by the technique. Previous data using the cement in the absence of the nanoparticles support that 6 months is still not enough to visualize complete healing after the biomaterial implantation[106]. Here, we applied computerized tomography (CT) on the rabbits´ femur implanted site to check for osteointegration **(Figure 4.13)**. In addition, to measure the cement/bone interface bonding we applied the *push-out* mechanical test **(Table 4.4)**.

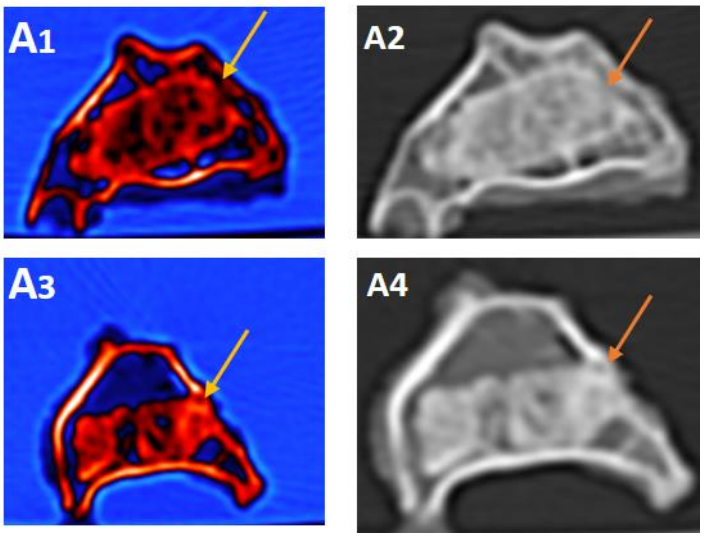

FIGURE 4. 13. COMPUTERIZED TOMOGRAPHY (CT) OF THE RABBITS´ FEMUR.

A1 and A2 = pPMMA; A3 and A4 = NanoSr 90%+pPMMA. A1 and A3 rainbow red highlights the cement, pores, and the osteointegration between cement and native bone (yellow arrow). Likewise, A2 and A4 x-rays colored with osteointegration nod (yellow arrow).

TABLE 4. 4. MECHANICAL TEST (PUSH-OUT) VALIDATION.

Groups	8 weeks pPMMA	8 weeks NanoSr 90%-pPMMA
@Maximum strength(N)	425.3 ± 126.9	433.2 ± 130
Maximum deformation (mm)	0.94 ± 0.31	0.95 ± 0.69

The rabbits were sacrificed after 8 weeks, and the femurs were collected. The mechanical test evaluates the strength needed to dislocate the external body (biomaterial) from the native bone, expressed in Newton´s (N).

Corroborating with the histology data, computerized tomography (Fig. 4.13) revealed no difference between groups, though they presented regions of osteointegration (yellow arrow), which are defined as non-visible boundaries between bone and cement. Finally, the mechanical test also indicated no statistical difference among the groups, though NanoSr 90%+pPMMA slightly presented a higher maximum strength (N) than the control group.

Finally, the mineral structure deposited over the pPMMA cement was studied by Raman spectroscopy (**Figure 4.14)**, which is an essential technique for determining the mineral crystal structure [107,108]. The RAMAN spectrum of the bone reveals the presence of characteristic bands at ~960 cm^{-1} (n_1 PO_4^{3-}) and ~1050 cm^{-1}, (n_3 PO_4^{3}) stretching of hydroxyapatite as described previously[107–110]. The RAMAN spectra of the minerals deposited on the cement after implantation share similarities with the spectrum of bone, revealing tissue deposition on the biomaterial.

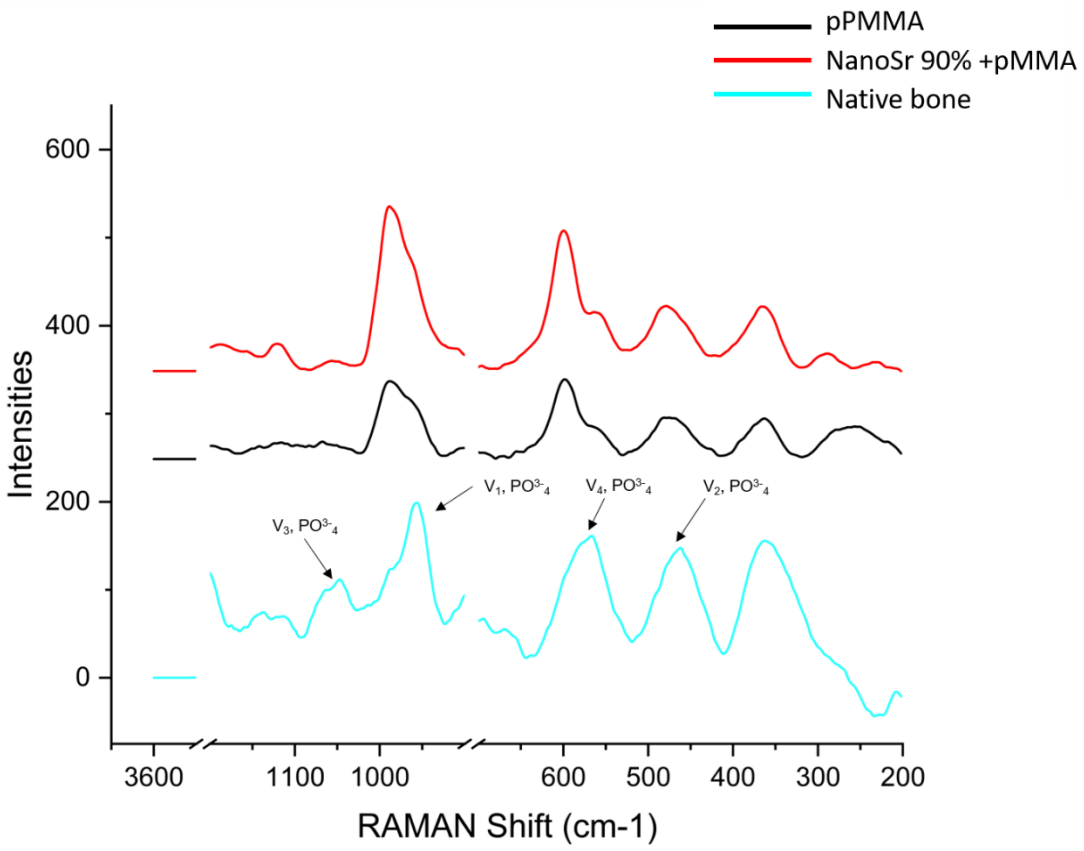

FIGURE 4. 14. MINERAL CHARACTERIZATION BY RAMAN SPECTROSCOPY.

Raman spectroscopy of calcium-phosphate-based minerals produced over the porous cement in both groups as indicated by the colors. Data are reported as the mean of triplicate measurement of three independent analyses.

Discussion

The addition of bioactive molecules aiming at tissue regeneration is part of the development of second-generation biomaterials. Bone regeneration is a hot topic in clinical research. Here we focus on the study of bioactive nanomaterial capable of inducing osteoblast differentiation and function, and osteoclast inhibition. The addition of this biomaterial to a well-characterized porous cement based on PMMA was shown to increase the cement´s mechanical properties as well as increase its bioactive in vitro[28]. Moreover, porous cement, rather than solid cement, facilitates the invasion of osteoblasts, allowing the constant flux of nutrients, cytokines, hormones, and growth factors, which helps in the regenerative process.

Throughout this work, we have shown scientific shreds of evidence that the NanoSr 90% is a powerful candidate to improve the pPMMA cement performance by increasing

its bioactivity. To confirm this, we used an in vivo model to check the real effect of the nanoparticles associated with the scaffold of pPMMA cement, since in vitro culture lacks plenty of components that may indirectly control bone regeneration. Hence, we started by studying by qRT -PCR the expression of genes involved in bone development. OCN and BMP2 expression were upregulated in the NanoSr 90%+pPMMA group. OCN is the most abundant non-collagenous protein found in bone secreted by osteoblasts. The role of OCN in biomineralization is still under discussion, however, scientists have shown that this protein regulates bone quality by aligning biological apatite throughout the collagen fiber[87]. In addition, BMP2 is a member of the transforming factor-β family (TGF- β), and their role involves the differentiation and function of osteoblasts, thus bone development [97]. Also, BMP2 controls the expression of type 1 collagen and OCN. Thus, BMP2 is a compelling candidate to be associated with synthetic biomaterials (scaffolds)[98,111–113] in order to improve the reconstruction of bone defects.

Osteoblasts' invasion through the pPMMA cement porous was observed in both the control and NanoSr90%+pPMMA groups **(Figures 4.12)**, as well as the secretion of collagen fiber, followed by the synthesis of a new bone (4.12 c,d). To analyze macroscopic changes (for example osteointegration) we applied computerized tomography **(Figure 4.13)**. We observed that both groups, with no statistical difference, displayed osteointegration areas as pointed out by the yellow arrows (Figure 4.13). Mechanical test data corroborated osteointegration of the materials (Table 4.3) without a statistical difference between the groups.

Several calcium phosphate structures have been identified as the earliest inorganic precursor to bone minerals. However, they are unstable and have not been identified in bone tissue[108]. Here, we have seen that the mineral structure deposited onward the pPMMA cement lacks the V_3 stretching (~1050nm), which could be indicative of a change in the mineral structure. Biological tissue characterization by RAMAN spectroscopy might be a difficult task, since many elements can interfere with the analysis, such as blood, cell debris, electrolytes, and so on.

As aforementioned, inflammation is a strong driver of osteoclastogenesis with its initial effect in the first month after surgery [8]. Curiously, Sr^{2+} showed to be a strong anti-inflammatory agent, involved with the inhibition of the TNFα signaling chain as well as the secretion of pro-inflammatory cytokines and interleukins[89,114–116]. However, here we did

not dive into the complex world of biomaterials and inflammation, which is a must-do study for further projects.

Formerly, our group has shown previously that there were still porous areas unfilled with bone 6 months after biomaterial implantation[5] which suggests that complete osteointegration can take longer than we thought. Here we opted to sacrifice the animals after 8 weeks to, (1) avoid a false-negative response occasioned by inflammation, and (2) utilize animal accommodation. Finally, throughout this first section, we described the potential effect that nanoparticles have on bone formation, however, unfilled cement areas can still be visualized, and no major differences between the groups were archived, although the NanoSr 90%+pPMMA group presented high levels of OCN and BMP2, which are two markers of bone formation. To achieve a better understating of the real in vivo nanoparticle's potential, we suggest either increasing the experimental time or increasing the amount of NanoSr 90% per area.

Conclusion

In the last 60 years, massive efforts have been applied toward the understanding and development of biomaterials that are capable of avoiding severe inflammation, and additionally have the potential to drive specific cellular responses at the molecular level. However, this task is not always easy, as many factors must be taken into consideration, for example, which cell type or tissue will the material induce, what are the side effects, how feasible financially this material is, whether it needs a carrier or not, and so forth. Due to this, the development of biomaterials has become a multi-area task, ranging from engineering to molecular biology and esthetics.

The healing of non-critical bone defects needs special attention since they are one of the major causes of severe rupture in bone. Thus, the development of biomaterials aiming at such a purpose is critical and would undoubtedly increase the life quality of the patients. We devoted the whole of Chapter 4 to the characterization and applicability of a strontium-based nanoparticle suitable for the padding of small fractures. Here, we investigated three different compositions of apatite-based nanoparticles, one purely composed of calcium-phosphate which we named NanoSr 0%, NanoSr 10% which at least 10% of all $Ca^{2+}$was substituted by Sr^{2+}, and finally NanoSr 90%, following the same logic than the former. We opted to use Sr^{2+} due to its similarities and the already known effect of Sr^{2+} on the function of osteocompetent cells. In this chapter, we demonstrated

the reliability of using NanoSr at 90%, once it is not toxic and displayed a high effect on osteoblast and biomineralization. In addition, these particles inhibit osteoclast maturation which is a desirable feature if one argues about bone regeneration. Moving forward, we tested this nanoparticle in vivo using porous PMMA cement, which holds a bone-like structure and is shown to present no toxicity to the host. However, due to its low bioactivity, we hypothesized that the nanoparticles would contribute to the migration of osteoblasts and induce the secretion of ECM followed by mineral deposition. Our results demonstrated no difference between the groups, despite all of them displaying osteointegration and osteoblast migration. Hence, we believe that for further experiments two variables should be taken into consideration in order to achieve a better host response, they are (1) time of exposure, which one should increase, and (2) nanoparticles concentration.

In the next chapter, we will focus our attention on the molecular aspect of Sr^{2+}-osteogenic cell modulation and MVs secretion. Additionally, we will deepen our knowledge and observations of how Sr^{2+} regulates MV secretion, function, composition, and how it is translated into ECM mineralization.

References

1. Rodan, G. A. Introduction to bone biology. *Bone* **13**, S3–S6 (1992).

2. Kawamura, N. *et al.* Akt1 in Osteoblasts and Osteoclasts Controls Bone Remodeling. *PLoS One* **2**, e1058 (2007).

3. Ross, M. H., & Pawlina, W. *Histology: A text and atlas: With correlated cell and molecular biology*. (2010).

4. Fromigué, O. *et al.* Calcium sensing receptor-dependent and receptor-independent activation of osteoblast replication and survival by strontium ranelate. *J. Cell. Mol. Med.* **13**, 2189–2199 (2009).

5. Cimatti, B. *et al.* Safety, osseointegration, and bone ingrowth analysis of <scp>PMMA</scp> -based porous cement on animal metaphyseal bone defect model. *J. Biomed. Mater. Res. Part B Appl. Biomater.* **106**, 649–658 (2018).

6. Lambers, F. M., Bouman, A. R., Rimnac, C. M. & Hernandez, C. J. Microdamage caused by fatigue loading in human cancellous bone: relationship to reductions in bone biomechanical performance. *PLoS One* **8**, e83662 (2013).

7. Lewis, G. Properties of acrylic bone cement: state of the art review. *J. Biomed. Mater. Res.* **38**, 155–82 (1997).

8. Anderson, J. M., Rodriguez, A. & Chang, D. T. Foreign body reaction to biomaterials. *Semin. Immunol.* **20**, 86–100 (2008).

9. Hench, L. L. & Polak, J. M. Third-generation biomedical materials. *Science* **295**, 1014–7 (2002).

10. Hench, L. L. & Thompson, I. Twenty-first century challenges for biomaterials. *J. R. Soc. Interface* **7 Suppl 4**, S379-91 (2010).

11. Qiao, Z. *et al.* Fracture Healing and the Underexposed Role of Extracellular Vesicle-Based Cross Talk. *Shock* **49**, 486–496 (2018).

12. Wu, H. *et al.* MIR145-3p promotes autophagy and enhances bortezomib sensitivity in multiple myeloma by targeting HDAC4. *Autophagy* **16**, 683–697 (2020).

13. Robin, M. *et al.* The Concentration of Bone-Related Organic Additives Drives the Pathway of Apatite Formation. *Cryst. Growth Des.* **21**, 3994–4004 (2021).

14. Bonnelye, E., Chabadel, A., Saltel, F. & Jurdic, P. Dual effect of strontium ranelate: Stimulation of osteoblast differentiation and inhibition of osteoclast formation and resorption in vitro. *Bone* **42**, 129–138 (2008).

15. Saidak, Z. & Marie, P. J. Strontium signaling: Molecular mechanisms and therapeutic implications in osteoporosis. *Pharmacol. Ther.* **136**, 216–226 (2012).

16. Marie, P. J. *et al.* An uncoupling agent containing strontium prevents bone loss by depressing bone resorption and maintaining bone formation in estrogen-deficient rats. *J. Bone Miner. Res.* **8**, 607–615 (2009).

17. Marx, D., Rahimnejad Yazdi, A., Papini, M. & Towler, M. A review of the latest insights into the mechanism of action of strontium in bone. *Bone reports* **12**, 100273 (2020).

18. SHORR, E. & CARTER, A. C. The usefulness of strontium as an adjuvant to calcium in the remineralization of the skeleton in man. *Bull. Hosp. Joint Dis.* **13**, 59–66 (1952).

19. DOW, E. C. & STANBURY, J. B. Strontium and calcium metabolism in metabolic bone diseases. *J. Clin. Invest.* **39**, 885–903 (1960).

20. Meunier, P. J. *et al.* The Effects of Strontium Ranelate on the Risk of Vertebral Fracture in Women with Postmenopausal Osteoporosis. *N. Engl. J. Med.* **350**, 459–468 (2004).

21. Riggs, B. L. & Parfitt, A. M. Drugs Used to Treat Osteoporosis: The Critical Need for a Uniform Nomenclature Based on Their Action on Bone Remodeling. *J. Bone Miner. Res.* **20**, 177–184 (2004).

22. Ducy, P., Zhang, R., Geoffroy, V., Ridall, A. L. & Karsenty, G. Osf2/Cbfa1: A Transcriptional Activator of Osteoblast Differentiation. *Cell* **89**, 747–754 (1997).

23. Kifor, O. *et al.* Regulation of MAP kinase by calcium-sensing receptor in bovine parathyroid and CaR-transfected HEK293 cells. *Am. J. Physiol. Physiol.* **280**, F291–F302 (2001).

24. Chau, J. F. L., Leong, W. F. & Li, B. Signaling pathways governing osteoblast proliferation, differentiation and function. *Histol. Histopathol.* **24**, 1593–606 (2009).

25. Surgery, M. A comparison of osteogenesis-related gene expression of mesenchymal stem cells during the osteoblastic differentiation induced by Type-I collagen and / or fibronectin Ryotaro Ozawa , 1 YoichiYamada , 2 Tetsuro Nagasaka , 3 and Minoru Ueda collagens (type. **1**, 139–146 (2003).

26. Takaoka, S., Yamaguchi, T., Yano, S., Yamauchi, M. & Sugimoto, T. The Calcium-sensing Receptor (CaR) is involved in strontium ranelate-induced osteoblast differentiation and mineralization. *Horm. Metab. Res.* **42**, 627–31 (2010).

27. Sila-asna, M. & Bunyaratvej, A. Osteoblast Differentiation and Bone Formation Gene Expression in Strontium-inducing Bone Marrow Mesenchymal Stem Cell. **53**, 25–35 (2007).

28. Tomazela, L. *et al.* Fabrication and characterization of a bioactive polymethylmethacrylate-based porous cement loaded with strontium/calcium apatite nanoparticles. *J. Biomed. Mater. Res. - Part A* **110**, 812–826 (2022).

29. Cruz, M. A. E. *et al.* Synthesis of Sr-morin complex and its: In vitro response: Decrease in osteoclast differentiation while sustaining osteoblast mineralization ability. *J. Mater. Chem. B* **7**, 823–829 (2019).

30. Tovani, C. B. *et al.* Strontium Calcium Phosphate Nanotubes as Bioinspired Building Blocks for Bone Regeneration. *ACS Appl. Mater. Interfaces* **12**, 43422–43434 (2020).

31. Zeng, J. *et al.* Osteoblastic and anti-osteoclastic activities of strontium-substituted silicocarnotite ceramics: In vitro and in vivo studies. *Bioact. Mater.* **5**, 435–446 (2020).

32. Molinuevo, M. S. *et al.* Advanced glycation end products and strontium ranelate promote osteogenic differentiation of vascular smooth muscle cells in vitro: Preventive role of vitamin D. *Mol. Cell. Endocrinol.* **450**, 94–104 (2017).

33. Brauer, A., Pohlemann, T. & Metzger, W. Osteogenic differentiation of immature osteoblasts: Interplay of cell culture media and supplements. *Biotech. Histochem.* **91**, 161–9 (2016).

34. de Faria, A. N., Zancanela, D. C., Ramos, A. P., Torqueti, M. R. & Ciancaglini, P. Estrogen and phenol red free medium for osteoblast culture: study of the

mineralization ability. *Cytotechnology* **68**, 1623–32 (2016).

35. Simão, A. M. S. *et al.* Culture of osteogenic cells from human alveolar bone: a useful source of alkaline phosphatase. *Cell Biol. Int.* **31**, 1405–13 (2007).

36. Hayman, A. R. Tartrate-resistant acid phosphatase (TRAP) and the osteoclast/immune cell dichotomy. *Autoimmunity* **41**, 218–23 (2008).

37. Livak, K. J. & Schmittgen, T. D. Analysis of Relative Gene Expression Data Using Real-Time Quantitative PCR and the 2−ΔΔCT Method. *Methods* **25**, 402–408 (2001).

38. Cruz, M. A. E. *et al.* Synthesis of Sr-morin complex and its in vitro response: decrease in osteoclast differentiation while sustaining osteoblast mineralization ability. *J. Mater. Chem. B* **7**, 823–829 (2019).

39. Cruz, M. A. E. *et al.* Phosphatidylserine controls calcium phosphate nucleation and growth on lipid monolayers: A physicochemical understanding of matrix vesicle-driven biomineralization. *J. Struct. Biol.* **212**, 107607 (2020).

40. Khalifehzadeh, R. & Arami, H. Biodegradable calcium phosphate nanoparticles for cancer therapy. *Adv. Colloid Interface Sci.* **279**, 102157 (2020).

41. Sokolova, V. & Epple, M. Biological and Medical Applications of Calcium Phosphate Nanoparticles. *Chemistry* **27**, 7471–7488 (2021).

42. Tomazela, L. *et al.* Fabrication and characterization of a bioactive polymethylmethacrylate-based porous cement loaded with strontium/calcium apatite nanoparticles. *J. Biomed. Mater. Res. A* **110**, 812–826 (2022).

43. Millán, J. L. Alkaline Phosphatases : Structure, substrate specificity and functional relatedness to other members of a large superfamily of enzymes. *Purinergic Signal.* **2**, 335–41 (2006).

44. Bolean, M. *et al.* Biophysical aspects of biomineralization. *Biophys. Rev.* **9**, 747–760 (2017).

45. Fedde, K. N. *et al.* Alkaline phosphatase knock-out mice recapitulate the metabolic and skeletal defects of infantile hypophosphatasia. *J. Bone Miner. Res.* **14**, 2015–26 (1999).

46. Hong, Y. J., Chun, J.-S. & Lee, W.-K. Association of collagen with calcium phosphate promoted osteogenic responses of osteoblast-like MG63 cells. *Colloids Surf. B. Biointerfaces* **83**, 245–53 (2011).

47. Liang, W., Ding, P., Li, G., Lu, E. & Zhao, Z. Hydroxyapatite Nanoparticles Facilitate Osteoblast Differentiation and Bone Formation Within Sagittal Suture During Expansion in Rats. *Drug Des. Devel. Ther.* **15**, 905–917 (2021).

48. Tien Lam, N., Minh Quan, V., Boonrungsiman, S. & Sukyai, P. Effectiveness of bio-dispersant in homogenizing hydroxyapatite for proliferation and differentiation of osteoblast. *J. Colloid Interface Sci.* **611**, 491–502 (2022).

49. Wang, R. *et al.* Nano-Hydroxyapatite Modulates Osteoblast Differentiation Through Autophagy Induction via mTOR Signaling Pathway. *J. Biomed. Nanotechnol.* **15**, 405–415 (2019).

50. Kapustin, A. N. *et al.* Calcium regulates key components of vascular smooth muscle cell-derived matrix vesicles to enhance mineralization. *Circ. Res.* **109**, e1-12 (2011).

51. Ciancaglini, P. *et al.* Kinetic analysis of substrate utilization by native and TNAP-, NPP1-, or PHOSPHO1-deficient matrix vesicles. *J. Bone Miner. Res.* **25**, 716–23 (2010).

52. Bolean, M. *et al.* Proteoliposomes with the ability to transport Ca(2+) into the vesicles and hydrolyze phosphosubstrates on their surface. *Arch. Biochem. Biophys.* **584**, 79–89 (2015).

53. Favarin, B. Z. *et al.* Effect of the presence of cholesterol in the interfacial microenvironment on the modulation of the alkaline phosphatase activity during in vitro mineralization. *Colloids Surf. B. Biointerfaces* **155**, 466–476 (2017).

54. Hasegawa, T. *et al.* Ultrastructural and biochemical aspects of matrix vesicle-mediated mineralization. *Jpn. Dent. Sci. Rev.* **53**, 34–45 (2017).

55. Kulterer, B. *et al.* Gene expression profiling of human mesenchymal stem cells derived from bone marrow during expansion and osteoblast differentiation. *BMC Genomics* **8**, 70 (2007).

56. Okamura, K., Inagaki, Y., Matsui, T. K. & Matsubayashi, M. OPEN RT - qPCR

analyses on the osteogenic differentiation from human iPS cells : an investigation of reference genes. *Sci. Rep.* 1–11 (2020) doi:10.1038/s41598-020-68752-2.

57. Koo, K. *et al.* Time-dependent expression of osteoblast marker genes in human primary cells cultured on microgrooved titanium substrata. **14**, 714–722 (2013).

58. Komori, T. *et al.* Targeted Disruption of Cbfa1 Results in a Complete Lack of Bone Formation owing to Maturational Arrest of Osteoblasts. *Cell* **89**, 755–764 (1997).

59. Guastaldi, F. P. S. *et al.* A new multiphase calcium phosphate graft material improves bone healing-An in vitro and in vivo analysis. *J. Biomed. Mater. Res. B. Appl. Biomater.* **110**, 2686–2704 (2022).

60. Tao, Z.-S. *et al.* Co-modification of calcium phosphate cement to achieve rapid bone regeneration in osteoporotic femoral condyle defect with lithium and aspirin. *Am. J. Transl. Res.* **13**, 952–966 (2021).

61. Gharibi, B. *et al.* Gene expression responses to mechanical stimulation of mesenchymal stem cells seeded on calcium phosphate cement. *Tissue Eng. Part A* **19**, 2426–38 (2013).

62. Bechkoff, G., Radisson, J., Bessueille, L., Bouchekioua-Bouzaghou, K. & Buchet, R. Distinct actions of strontium on mineral formation in matrix vesicles. *Biochem. Biophys. Res. Commun.* **373**, 378–81 (2008).

63. Zhao, Z. *et al.* Capturing Magnesium Ions via Microfluidic Hydrogel Microspheres for Promoting Cancellous Bone Regeneration. *ACS Nano* **15**, 13041–13054 (2021).

64. Zayzafoon, M. Calcium/calmodulin signaling controls osteoblast growth and differentiation. *J. Cell. Biochem.* **97**, 56–70 (2006).

65. Kołodziejska, B., Stępień, N. & Kolmas, J. The Influence of Strontium on Bone Tissue Metabolism and Its Application in Osteoporosis Treatment. *Int. J. Mol. Sci.* **22**, (2021).

66. Caudrillier, A. *et al.* Strontium ranelate decreases receptor activator of nuclear factor-KB ligand-induced osteoclastic differentiation in vitro: involvement of the calcium-sensing receptor. *Mol. Pharmacol.* **78**, 569–76 (2010).

67. Huang, C., Li, L., Yu, X., Gu, Z. & Zhang, X. The inhibitory effect of strontium-doped

calcium polyphosphate particles on cytokines from macrophages and osteoblasts leading to aseptic loosening in vitro. *Biomed. Mater.* **9**, (2014).

68. Zhu, S. *et al.* Strontium inhibits titanium particle-induced osteoclast activation and chronic inflammation via suppression of NF-κB pathway. *Sci. Rep.* **6**, 1–11 (2016).

69. Yamaguchi, M. & Neale Weitzmann, M. The intact strontium ranelate complex stimulates osteoblastogenesis and suppresses osteoclastogenesis by antagonizing NF-κB activation. *Mol. Cell. Biochem.* **359**, 399–407 (2012).

70. Blumer, M. J. F. *et al.* Role of tartrate-resistant acid phosphatase (TRAP) in long bone development. *Mech. Dev.* **129**, 162–76 (2012).

71. Cheng, Z., Al Zaki, A., Hui, J. Z., Muzykantov, V. R. & Tsourkas, A. Multifunctional nanoparticles: cost versus benefit of adding targeting and imaging capabilities. *Science* **338**, 903–10 (2012).

72. Yuan, H. *et al.* Albumin Nanoparticle of Paclitaxel (Abraxane) Decreases while Taxol Increases Breast Cancer Stem Cells in Treatment of Triple Negative Breast Cancer. *Mol. Pharm.* **17**, 2275–2286 (2020).

73. Hama, M. *et al.* Evidence for Delivery of Abraxane via a Denatured-Albumin Transport System. *ACS Appl. Mater. Interfaces* **13**, 19736–19744 (2021).

74. Porche, D. J. Liposomal doxorubicin (Doxil). *J. Assoc. Nurses AIDS Care* **7**, 55–9 (1996).

75. Rivankar, S. An overview of doxorubicin formulations in cancer therapy. *J. Cancer Res. Ther.* **10**, 853–8 (2014).

76. Schmidt, A. H. Autologous bone graft: Is it still the gold standard? *Injury* **52 Suppl 2**, S18–S22 (2021).

77. Herrmann, M. *et al.* Interactions between Muscle and Bone-Where Physics Meets Biology. *Biomolecules* **10**, (2020).

78. Smith, S. M. *et al.* Effects of artificial gravity during bed rest on bone metabolism in humans. *J. Appl. Physiol.* **107**, 47–53 (2009).

79. Zhang, S., Gao, H. & Bao, G. Physical Principles of Nanoparticle Cellular Endocytosis. *ACS Nano* **9**, 8655–71 (2015).

80. Barbara, A., Delannoy, P., Denis, B. . & Marie, P. . Normal matrix mineralization induced by strontium ranelate in MC3T3-E1 osteogenic cells. *Metabolism* **53**, 532–537 (2004).

81. Munns, C. F. *et al.* Global Consensus Recommendations on Prevention and Management of Nutritional Rickets. *J. Clin. Endocrinol. Metab.* **101**, 394–415 (2016).

82. Hasegawa, T. *et al.* Matrix Vesicle-Mediated Mineralization and Osteocytic Regulation of Bone Mineralization. *Int. J. Mol. Sci.* **23**, (2022).

83. Blair, H. C., Schlesinger, P. H., Huang, C. L. H. & Zaidi, M. Calcium signalling and calcium transport in bone disease. *Subcell. Biochem.* **45**, 539–62 (2007).

84. Hoylaerts, M. F. *et al.* Functional significance of calcium binding to tissue-nonspecific alkaline phosphatase. *PLoS One* **10**, e0119874 (2015).

85. Minamizaki, T. *et al.* The matrix vesicle cargo miR-125b accumulates in the bone matrix, inhibiting bone resorption in mice. *Commun. Biol.* **3**, 30 (2020).

86. Metab, J. B. M. *et al.* Effects of strontium ranelate treatment on osteoblasts cultivated onto scaffolds of trabeculae bovine bone. *J. Bone Miner. Metab.* (2017) doi:10.1007/s00774-017-0822-y.

87. Komori, T. What is the function of osteocalcin? *J. oral Biosci.* **62**, 223–227 (2020).

88. Li, D. *et al.* Osteoclast-derived exosomal miR-214-3p inhibits osteoblastic bone formation. *Nat. Commun.* **7**, 10872 (2016).

89. Huang, C., Li, L., Yu, X., Gu, Z. & Zhang, X. The inhibitory effect of strontium-doped calcium polyphosphate particles on cytokines from macrophages and osteoblasts leading to aseptic loosening in vitro. *Biomed. Mater.* **9**, 025010 (2014).

90. Ohgaki, M., Kizuki, T., Katsura, M. & Yamashita, K. Manipulation of selective cell adhesion and growth by surface charges of electrically polarized hydroxyapatite. *J. Biomed. Mater. Res.* **57**, 366–73 (2001).

91. Teng, N. C. *et al.* A new approach to enhancement of bone formation by electrically polarized hydroxyapatite. *J. Dent. Res.* **80**, 1925–9 (2001).

92. Crayton, S. H. & Tsourkas, A. pH-titratable superparamagnetic iron oxide for

improved nanoparticle accumulation in acidic tumor microenvironments. *ACS Nano* **5**, 9592–601 (2011).

93. Reshetnyak, Y. K., Andreev, O. A., Segala, M., Markin, V. S. & Engelman, D. M. Energetics of peptide (pHLIP) binding to and folding across a lipid bilayer membrane. *Proc. Natl. Acad. Sci. U. S. A.* **105**, 15340–5 (2008).

94. Davies, A., Lewis, D. J., Watson, S. P., Thomas, S. G. & Pikramenou, Z. pH-controlled delivery of luminescent europium coated nanoparticles into platelets. *Proc. Natl. Acad. Sci. U. S. A.* **109**, 1862–7 (2012).

95. Kale, A. A. & Torchilin, V. P. Environment-responsive multifunctional liposomes. *Methods Mol. Biol.* **605**, 213–42 (2010).

96. Pereira De Vasconcelos, D. Modulation of the Inflammatory Response to Biomaterials: Macrophages and NLRP3 Inflammasome DOUTORAMENTO BIOTECNOLOGIA MOLECULAR E CELULAR APLICADA ÀS CIÊNCIAS DA SAÚDE. (2019).

97. Zhou, N. *et al.* BMP2 induces chondrogenic differentiation, osteogenic differentiation and endochondral ossification in stem cells. *Cell Tissue Res.* **366**, 101–11 (2016).

98. Ki, M.-R. *et al.* BMP2-Mediated Silica Deposition: An Effective Strategy for Bone Mineralization. *ACS Biomater. Sci. Eng.* **9**, 1823–1833 (2023).

99. Bayat, H. *et al.* Osteogenic differentiation of follicular stem cells on nano-Saghez scaffold containing BMP2. *J. Orthop. Surg. Res.* **14**, 442 (2019).

100. Kuttappan, S. *et al.* Bioinspired nanocomposite fibrous scaffold mediated delivery of ONO-1301 and BMP2 enhance bone regeneration in critical sized defect. *Mater. Sci. Eng. C. Mater. Biol. Appl.* **110**, 110591 (2020).

101. Murshed, M. Mechanism of Bone Mineralization. *Cold Spring Harb. Perspect. Med.* **8**, (2018).

102. Bottini, M. *et al.* Matrix vesicles from chondrocytes and osteoblasts: Their biogenesis, properties, functions and biomimetic models. *Biochim. Biophys. Acta - Gen. Subj.* **1862**, 532–546 (2018).

103. Landis, W. J. & Jacquet, R. Association of calcium and phosphate ions with collagen in the mineralization of vertebrate tissues. *Calcif. Tissue Int.* **93**, 329–37 (2013).

104. Xu, Y. F. *et al.* Intermolecular channels direct crystal orientation in mineralized collagen. *Nat. Commun.* **11**, 5068 (2020).

105. Rieppo, L. *et al.* Histochemical quantification of collagen content in articular cartilage. *PLoS One* **14**, e0224839 (2019).

106. Cimatti, B. *et al.* Safety, osseointegration, and bone ingrowth analysis of PMMA-based porous cement on animal metaphyseal bone defect model. *J. Biomed. Mater. Res. B. Appl. Biomater.* **106**, 649–658 (2018).

107. Stammeier, J. A., Purgstaller, B., Hippler, D., Mavromatis, V. & Dietzel, M. In-situ Raman spectroscopy of amorphous calcium phosphate to crystalline hydroxyapatite transformation. *MethodsX* **5**, 1241–1250 (2018).

108. Crane, N. J., Popescu, V., Morris, M. D., Steenhuis, P. & Ignelzi, M. A. Raman spectroscopic evidence for octacalcium phosphate and other transient mineral species deposited during intramembranous mineralization. *Bone* **39**, 434–42 (2006).

109. Pinheiro, A. L. B. *et al.* Laser/LED phototherapy on the repair of tibial fracture treated with wire osteosynthesis evaluated by Raman spectroscopy. *Lasers Med. Sci.* **33**, 1657–1666 (2018).

110. Marques, M. P. M. *et al.* Heat-induced Bone Diagenesis Probed by Vibrational Spectroscopy. *Sci. Rep.* **8**, 15935 (2018).

111. Smeets, R. *et al.* Impact of rhBMP-2 on regeneration of buccal alveolar defects during the osseointegration of transgingival inserted implants. *Oral Surg. Oral Med. Oral Pathol. Oral Radiol. Endod.* **108**, e3–e12 (2009).

112. Lu, S. X. *et al.* Evaluation of a compression resistant matrix for recombinant human bone morphogenetic protein-2. *J. Clin. Periodontol.* **40**, 688–97 (2013).

113. Wan, Z. *et al.* A dual-responsive polydopamine-modified hydroxybutyl chitosan hydrogel for sequential regulation of bone regeneration. *Carbohydr. Polym.* **297**, 120027 (2022).

114. Alves, S. M. *et al.* Anti-inflammatory and anti-nociceptive effects of strontium ranelate on the zymosan-induced temporomandibular joint inflammatory hypernociception in rats depend on TNF-α inhibition. *Pharmacol. Reports* **69**, 764–772 (2017).

115. Berksoy Hayta, S. *et al.* The reduction in inflammation and impairment in wound healing by using strontium chloride hexahydrate. *Cutan. Ocul. Toxicol.* **37**, 24–28 (2018).

116. Topal, F. *et al.* Strontium chloride: Can it be a new treatment option for ulcerative colitis. *Biomed Res. Int.* **2014**, (2014).

Chapter V

Strontium regulates biomineralization at the molecular level

1. Introduction

The proper cellular function and physiological homeostasis depend on a series of metabolites, which include Ca^{2+} and Pi. Ca^{2+} is the fifth most abundant divalent cation found in higher concentrations in the extracellular milieu and is stocked inside specialized organelles, like the endoplasmic reticulum[1,2]. Ca^{2+} acts as either a primary signal inducer or as a secondary messenger generated by other signaling pathways. Moreover, the cells require Ca^{2+} for basic cellular processes, including the mineralization of skeletal and dental tissues, nerve impulse transmission, blood clotting, muscle contraction, fertilization, cell death, and hormone release[3]. Ca^{2+} signaling is fast and efficient due to its distribution and storage between the extracellular and intracellular space. Also, the concentration gradient is conserved between intracellular organelles and the cytosol, thus facilitating a variety of Ca^{2+}-driven pathways[1]. Additionally, Ca^{2+} participates in the cytoskeleton organization and release of extracellular vesicles[4,5].

Nonetheless, Pi regulates a plethora of physiological functions. In soft tissues and cells, Pi is mainly associated with ester compounds, which are essential for fundamental processes such as energy storage and release (ATP, GTP, CTP), genetic information storage and propagation (DNA and RNA molecules), and structure and function of biological membranes (as phospholipids). As a free ion (PO_4^{3-}), Pi serves as a molecular signaling effector and messenger transmitter. The posttranslational protein modifications through the addition and/or removal of Pi (phosphorylation and dephosphorylation, respectively) are the two major and well-described processes involved in signal transmission (cascades).

Ca^{2+} and Pi directly contribute to biomineralization development and maintenance in two ways, (1) through the modulation of osteocompetent cells, and (2) the deposition on extracellular matrix, as described in Chapter 1. Physiological mineralization is pivotal for the formation and maintenance of skeletal and dental tissues. The maintenance of Ca^{2+} and Pi levels dictates a healthy physiological state, and their deficiency or excess leads to a variety of diseases. For example, limited availability of either Ca^{2+} and Pi during development contributes to the malformation of bone, which compromises its mechanical properties, while above-physiological levels of both ions result in pathological mineralization of soft tissues [6,7,8,9,10,11]. Nutritional deficiency of Ca^{2+} is linked to impaired

bone growth during development and contributes to the development of osteoporosis in adulthood, however, excess of Ca^{2+} or intake above certain levels do not result in hypermineralization[12,13,14]. Increased Pi levels (hyperphosphatemia) were previously linked to uncontrolled growth of bone (hyperostosis) and hypermineralization of dental tissues and pulp stones[15,16,17]. On the other hand, low levels of Pi (hypophosphatasia) caused by low intake and/or mutations in genes involved in the regulation of systemic Pi levels, result in skeletal abnormalities (rickets and osteomalacia)[18,19,20,21], and dental tissue malformation[22,23,8]. Interestingly, impairment of biomineralization, manifested as rickets, osteomalacia, and defective dentoalveolar complex, is characterized by deficiency of tissue-nonspecific alkaline phosphatase (TNAP)[24,25,26]. As described in the Chapter 1, TNAP is a crucial enzyme for the generation of Pi within the extracellular milieu, thus its deficiency is linked to the low availability of Pi [27]. Recently, it was proposed that Pi availability to osteogenic cells is a rate-limiting step in physiological mineralization[28].

Furthermore, analysis of ion homeostasis and mineralization disorders in humans [29,30,31,32] and knock-out mice[33], provide compelling evidence that Pi and Ca^{2+} have an active role in the production and release of matrix vesicles (MVs)[34]. Though the molecular mechanism that regulates this process is still under investigation, it is well accepted that the ions participate by affecting two different, but not isolated, events: (1) supporting the osteo/chondrogenic differentiation of progenitor cells into a mature form, and (2) stimulating the release and function of MVs. Pi and Ca2+-dependent signaling is thought to control the expression of osteogenic-related genes in chondrocytes, osteoblasts, vascular smooth muscle cells (VSMC), and human dental pulp stem cells, which favors the release of MVs. After cell commitment, these ions impact MVs release and function by either accumulating into the lumen or stimulating their release [35,36,37].

In Chapter 4, we have described the results of our studies on the role of Sr^{2+} released by NPs on osteoblast and osteoclast function, testing their potential to be used as a bioactive biomaterial. However, we did not analyze how Sr^{2+} affects the release and function of MVs. Moreover, how Sr^{2+} impacts signaling pathways related to osteogenic commitment and function is still unclear, but it is believed that this ion uses the same pathway of Ca^{2+}, due to their similarities. For comparison purposes, we also investigated the influence of Pi and Ca^{2+} over mineralization, since their mechanism of cellular induction is well described. To understand how Sr^{2+} contributes to biomineralization, we

studied molecular pathways related to the regulation of osteogenic-related genes, and the potential role of Sr^{2+} over the release and function of MVs. Part of the present chapter was developed in collaboration with Prof. Dr. Dobrawa Napierala, associated with the University of Pittsburgh, Department of Oral Biology, United States, during an internship using Print-USP financial resources.

2. Material and methods

2.1 Cell culture conditions and treatment

Mouse odontoblast-derived 17IlA11 was cultured in standard Dulbecco´s modified Eagle´s medium (DMEM, Gibco; Thermo Fisher Scientific, Logan, UT) supplemented with 5 vol.% FBS and 1 vol.% penicillin/streptomycin, at 37 ºC in a humidified atmosphere of 95% air and 5% CO_2. For osteogenic differentiation, 2 x 10^6 cells were plated into a 10 cm-dish and grown until confluence. To reach osteogenic differentiation we supplemented the growth media with 5 mM Na-Pi buffer (pH 7.4) and 50 µg/ml ascorbic acid.

2.2 Cell viability analysis by MTT assay

Cell viability was assessed by MTT assay after 24 h, 4, and 6 days of culture as described by Mosmann[38]. Briefly, after treatment, a fresh medium with MTT solution was added to the cells and incubated for 4 h. Formazan bioproduct was solubilized in DMSO, and optical densities were measured at 570 nm using a plate reader.

2.3 Alizarin red staining assay

Cells were initially plated 1 x 10^6 per well in a 12-well plate, following the treatment with 5 mM Pi, strontium ranelate (SR) (0.1-1.0 mM), and $CaCl_2$ (0.1- 1.0 mM) for 4 and 6 days. Then, cells were fixed in 4% paraformaldehyde and stained with 40 mM alizarin red-S (Sigma) for 10 min. Excess dye was removed by washing with deionized water.

2.4 Von Kossa staining assay

Cell cultures were washed twice with PBS, fixed in paraformaldehyde for 10 min, and washed twice with deionized water. The water was removed, and 2% silver nitrate solution was added, then the plate was exposed to sunlight for 20 minutes after which the

plate was rinsed with water. Sodium thiosulfate (5%) was added for 5 min, followed by washing with deionized water.

2.5 Quantitative RT-PCR

Total RNA was extracted using the Trizol protocol (Invitrogen) and purified using the GenElute Mammalian Total RNA miniprep kit (Sigma). Total RNA (1 µg) was initially treated with DNase I (Invitrogen) and then was converted into cDNA with SuperScript III reverse transcriptase kit (Invitrogen). Gene expression analysis was carried out using AB Biosystems 7500 fast real-time PCR system and Fast SYBR Green reaction mix (Roche Applied Science). Primer sequences are as follows: Osx F, GGGCGTTCTACCTGCGACTG, and R, ATCGGGGCGGCTGATTG; Runx2 F, TGGCCGGGAATGATGAGAAAC, and R, TGAAACTCTTGCCTCGTCCG; Phospho1 F, CCTGGGAAACAGCCGCCGATGTG, and R, CCCGGAGGAGCATAGCAAAGCGAAG; Gapdh F, GCAAGAGAGGCCCTATCCCAA and R, CTCCCTAGGCCCCTCCTGTTATT; Col1a1 F, GCAACAGTCGCTTCACCTACA, and R, CAATGTCCAAGGGAGCCACAT; Alpl F, CAGTGGGAGTGAGCGCAGCC, and R, GCACTGGGTGTGGCGTGGTT, Smpd3 F, ACATCGATTCTCCCACCAACACCT, and R, AATTCGCACAATGCAGCTGTCCTC.

2.6 Western Blotting Analysis

For the western blotting assay, cells were plated at 5 x 10^5 per well of a 6 well-plate. Following 24 h, the growth media were replaced with the following treatment: growth media containing 5mM of Na-Pi, osteogenic media supplemented with strontium ranelate (0.1-1.0 mM), and $CaCl_2$ (0.1-1.0 mM). Whole protein extracts were prepared by cell lysis in RIPA buffer supplemented with phosphatases and protease inhibitors: 1 mM NaF, 2 mM Na_2VO_4, 2 mM leupeptin, 2 mM pepstatin, 2 mM PMSF, and 10 µM MG132. Protein concentration was determined by a micro-BCA protein assay kit (Thermo Scientific, Rockford, lL). Subsequently, the protein concentration was determined by the method of BRADFORD (1976), using a solution of bovine serum albumin (BSA, 0.1 mg/mL) as a standard. Protein (15 µg) was subjected to electrophoresis on 4-12% precast BisTris gels (Invitrogen) and transferred onto a nitrocellulose membrane. Specific proteins were detected by fluorescence (Li-Cor Odyssey Infrared Imaging System, LI-COR Biosciences, Lincoln, NE). Primary antibodies against phospho-Erk1/2 (1:2000; Cell Signaling), Erk1/2 (1:1000, Cell Signaling), phospho-CREB (1:2000; Cell Signaling), Creb (1:1000, Cell Signaling), tissue-nonspecific alkaline phosphatase (1:1000, R&D

Systems), annexin V (1:2000, Abcam), α-tubulin (1:10.000, Sigma) and Lamp2a (1:1000, Abcam) were used. All fluorescent secondary antibodies (LI-COR Bioscience; Lincoln; NE) were used at 1:20.000 dilution.

2.7 Isolation and purification of vesicles

MVs were isolated and purified from the extracellular matrix (ECM) using a differential ultracentrifugation method described elsewhere [39,40]. Briefly, cells were washed with PBS and MVs were released from the ECM by enzymatic digestion with 2.5 mg/ml of collagenase IA (Sigma, St. Louis, MO), and 2 mM of $CaCl_2$ for 4 h at 37 ºC and 8 % CO_2. After digestion, the whole digestion mix containing shred ECM, vesicles, and cells was collected and centrifuged at 2000 rpm for 20 min to pellet the cells. The supernatant was then transferred to a new tube and centrifuged at 10,000 rpm for 30 min to remove cell debris, and then at 100,000 rpm for 70 min to obtain the MV pellet. MV pellets were resuspended in TBS and centrifuged at 100,000 rpm for 70 min. Finally, the pellet was resuspended in 150 µL TBS and stored at -80 ºC.

2.8 Nanoparticle Tracking Analysis

The size and concentration of purified MVs were determined by Nanoparticle Tracking Analysis (NTA) using NanoSight NS300 (Malvern Instruments Ltd., Worcestershire, UK). Data acquisition and analysis were performed using NTA 2.3 Analytical Software. The parameters were as follows: five video files of 60 s (each) at camera level 10 from each sample were recorded. The detection threshold limit was settled to 10 to analyze the size and concentration of the MVs. Matrix vesicle secreted per cell was obtained by dividing the total MV concentration by the number of cells, as previously described here [34].

2.9 Transmission electron microscopy

Morphology and size of the MVs were examined by JEOL JEM-100 CXII transmission electron microscopy, by drying a drop of the MV colloidal dispersion on a copper grid covered with a conductive polymer. Then, the sample was treated with phosphotungstic acid (PTA, 1%) for 15 min and then analyzed.

2.10 Atomic force microscopy

MVs were filtered using 0.22 µm pore size Millipore® membranes to avoid MV aggregates and ECM debris. Then, to prevent vesicle deformation and disruption, the samples were stabilized with 1.4% glutaraldehyde (v/v). The mixtures were homogenized and heated at 37 ºC for 5 min. Then, 15 µL of each sample was dropped onto a freshly cleaved mica substrate, dried at room temperature, and imaged using Shimadzu SPM-9600 Scanning probe.

2.11 Mineral analysis by ATR-FTIR

The mineral formation and composition were measured by means of ATR-FTIR spectroscopy (IRPrestige-21, Shimadzu Co., Tokyo, Japan). Precipitated minerals in the presence of MVs were placed at the surface of an attenuated total reflectance (ATR) accessory made of a ZnSe crystal to assess the chemical groups. We calculated the ratio of areas of the band corresponding to the asymmetrical stretching of the PO_4^{3-} group at 1032 cm^{-1} and the band assigned to the carbonyl (C = O) at 1680 cm^{-1} to quantify mineral formation, as described by [41,42].

2.12 Alkaline phosphatase activity

To determine TNAP activity, we harvested MV fraction in triplicate according to Simão (2007). ALP activity was accomplished by the degradation of p-nitrophenylphosphate (pNPP) and its subproduct was analyzed. ALP activity was expressed as U mg^{-1} of total protein content and one unit of enzyme is defined as the amount of enzyme capable of hydrolyzing 1.0 nmol of substrate per mg of protein at 37 ºC.

2.13 Matrix vesicle in vitro mineralization- turbidimetry

The assay was performed in accordance with [41,43,44]. Succinctly, the MVs were incubated in synthetic cartilage lymph (SCL) buffer containing 2 mM Ca^{2+}, 104.5 mM Na^{+}, 133.5 mM Cl^{-}, 63.5 mM sucrose, 16.5 mM Tris, 12.7 mM K^{+}, 5.55 mM glucose, 1.83 mM HCO^{3-}, 0.57 mM SO_4^{2-}, and 2 mM Mg^{2+} at pH 7.5. As a source of Pi, we used 2 mM of ATP. Mineral precipitation and propagation were measured by turbidimetry at 340 nm using a multi-well microplate reader (SpectraMax® M3, Molecular Devices LLC, San

Jose, CA). We normalized the results by discounting the absorbance value obtained from the first measurement for each sample.

2.14 Statistical analysis

All experiments were conducted on at least three replicates. Data are presented as the mean ± S.D. Probability values were calculated using the Student´s t-test. For only one variable (for example treatment) the One-way ANOVA test was used to determine the statistical difference among the groups, while for at least two variables (treatment and time) we used two-way ANOVA to determine the statistical difference among the groups. P values vary according to each experiment and their value will be displayed separately.

2.15 Lipidomic analysis

Sample preparation

The extraction protocol was developed as previously described[45]. Shortly, 250 µL of each sample was distributed into an Eppendorf tube, 40 µL of internal standard solution (IS) was added, and the solvent proportions were normalized to 1) MTBE/Methanol/H_2O (10:3:2.5 v/v/v). Then, the mixture was incubated for 1 hour at RT under agitation, and then incubated for 10 min in the ice bath. After that, the mixture was centrifuged at 12,000 rpm for 10min at 4 ºC. After centrifugation, three phases can be seen. The upper phase (organic) was collected and subsequently dried under a vacuum atmosphere at 45 ºC.

After extraction, the samples were reconstituted in 40 µL of isopropanol: acetonitrile: H2O (2:1:1) mixture. Then, the samples were centrifuged for 10 minutes at 5,000 rpm at 4 ºC. Finally, the supernatant was transferred to the LC-MS/MS injection vials system.

LC-MS/MS conditions

For the analysis, an Acquity UPLC CSH C18 column (100 × 2.1 mm; 1.7 µm) was used, the composite mobile phase consisted of 10 mM ammonium formate and 1.0 % (v/v) acid acetic in A) 60:40 acetonitrile: water (v/v) and B) 90:10 (v/v) isopropanol: acetonitrile. The elution mode was: 0.0 min, 40% B; 0-2 min, 43% B; 2-2.1 min, 50% B; 2.1-12.0 min, 70% B; 12-14.0 min, 99% B; 14.0-14.10 min, 40% B; 14.1-17.0 min, 40% B. The flow rate was maintained at 0.4 mL.min $^{-1}$ and the column temperature at 55 °C. 5 µL of each sample were injected in positive and negative ionization mode, respectively.

MS operating conditions: capillary voltage, 5500 V in positive mode or 4500 V in negative mode, mass range, 50-1250 m/z; nebulizer gas pressure, 55 psi; drying gas pressure, 50 psi; gas temperature, 550 °C, curtain gas, 35 (arbitrary units), declustering potential, 80 V. Automatic equipment calibration was performed every five injections by the self-calibration system (CDS) using commercial calibration solutions from Sciex (Concord, CA).

Data processing and statistical analysis

Here we used the untargeted mode to profile the matrix vesicle lipid content. Data acquisition and processing were performed using PeakViewTM software (Sciex, Foster, CA, USA) and MS DIAL 5.12304229 software (RIKEN PRIMe, Japan). For the statistical analysis, we used MetaboAnalyst 5.0 online platform (25897128), to carry out principal component analysis (PCA), VIP score, and heat map.

Results

To evaluate the role of Ca^{2+}, Pi, and Sr^{2+} in biomineralization we started by exploring the maximum concentration capable of inducing a cellular response, but not being toxic to the cells (**Figure 5.1, A-F).** We studied the effect of the ions using two different mediums: (i) growth media, so one can exploit the isolate action of the ions without any other stimulator, and (ii) osteogenic medium, which represents a more reliable physiologic condition, so one can attest the effect of the ion in association to osteogenic inductors (i.e., ascorbic acid and NaPi, named AA+Pi).

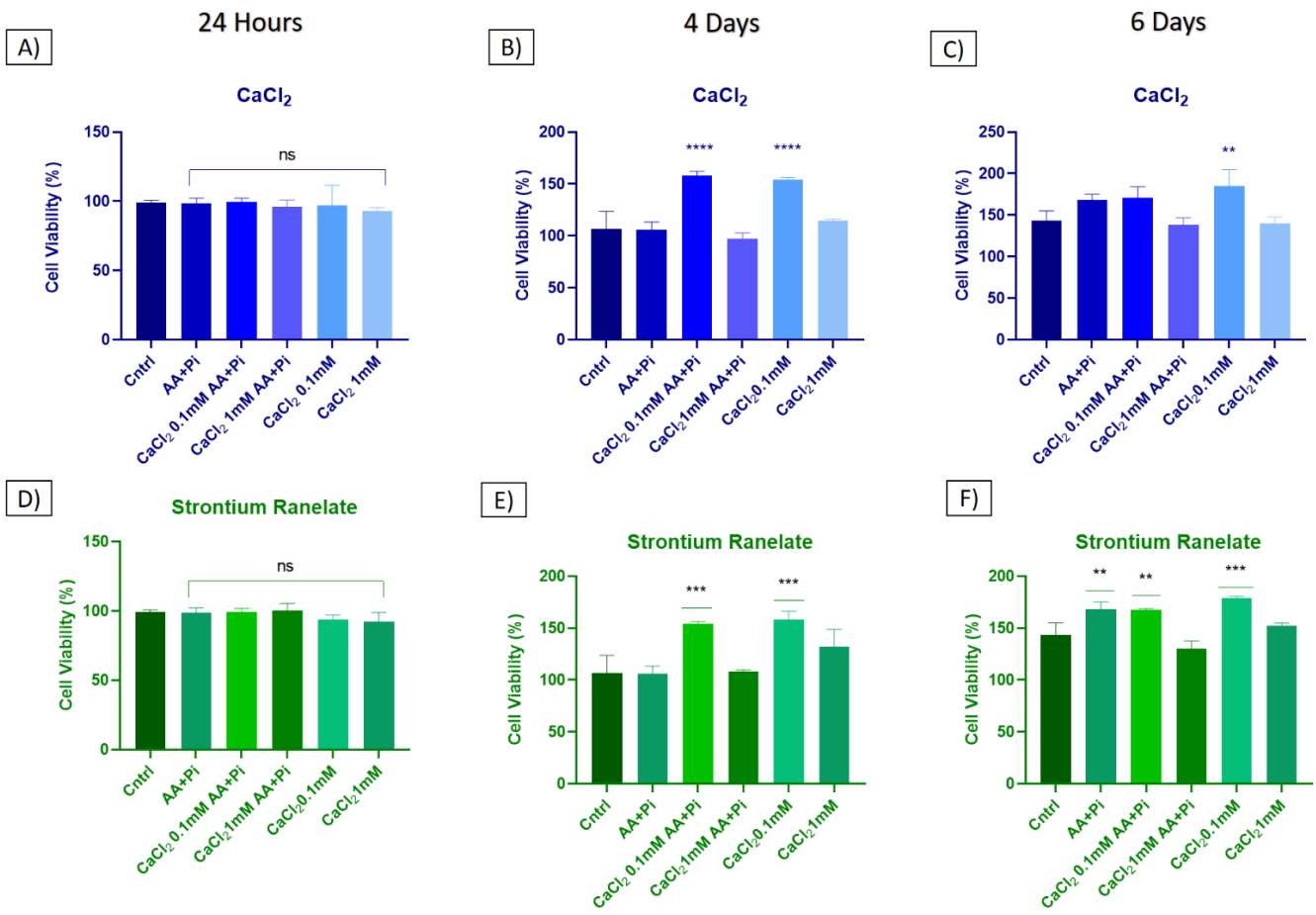

FIGURE 5. 1. CELLS TREATED WITH CACL2, AND SR FOR UP TO 6 DAYS AT DIFFERENT CONCENTRATIONS.

Viability was measured by MTT assay and multiple statistical comparisons were performed by two-way ANOVA, P values for $CaCl_2$ treatment **p< 0.0047, ****p< 0.0001, and for SR **p< 0.0028, ***p< 0.0001. The results represent mean ± SD for triplicate determination for one experiment.

As displayed in **Figure 5.1 (A-F)** we used 0.1 mM and 1.0 mM of $CaCl_2$ and SR and cultured the cells for 24h, 4 as 6 days. Additionally, for this study, we used an odontoblast-derived cell (17IIA11) that showed to be a reliable model for biomineralization (25128529, 26883946, 36519511, 35082271). This cell line expresses high levels of Sp7 and Runx2, so they are already committed to a mineralization profile, and in ~8 days they completely mineralize the ECM. Finally, SR was chosen to be the primary source of Sr^{2+} due to its already-proven effect on osteocompetent cells.

Figure 5.1 shows that no cytotoxic effect was observed in the concentration range studied, rather in some particular cases (B, C, E, and F) they stimulate cell proliferation. We also tested 2 mM (data not shown), but it decreased the cell population significantly.

For Pi, we use a fixed concentration of 5 mM, which was previously described to promote mineralization [34,46].

The formation of mineralized nodules in the different conditions was analyzed by Alizarin Red S and Von Kossa staining for 4 and 6 days, in growth media **(Figure 5.2, a-b)** and osteogenic conditions **(Figure 5.2, c-d)**.

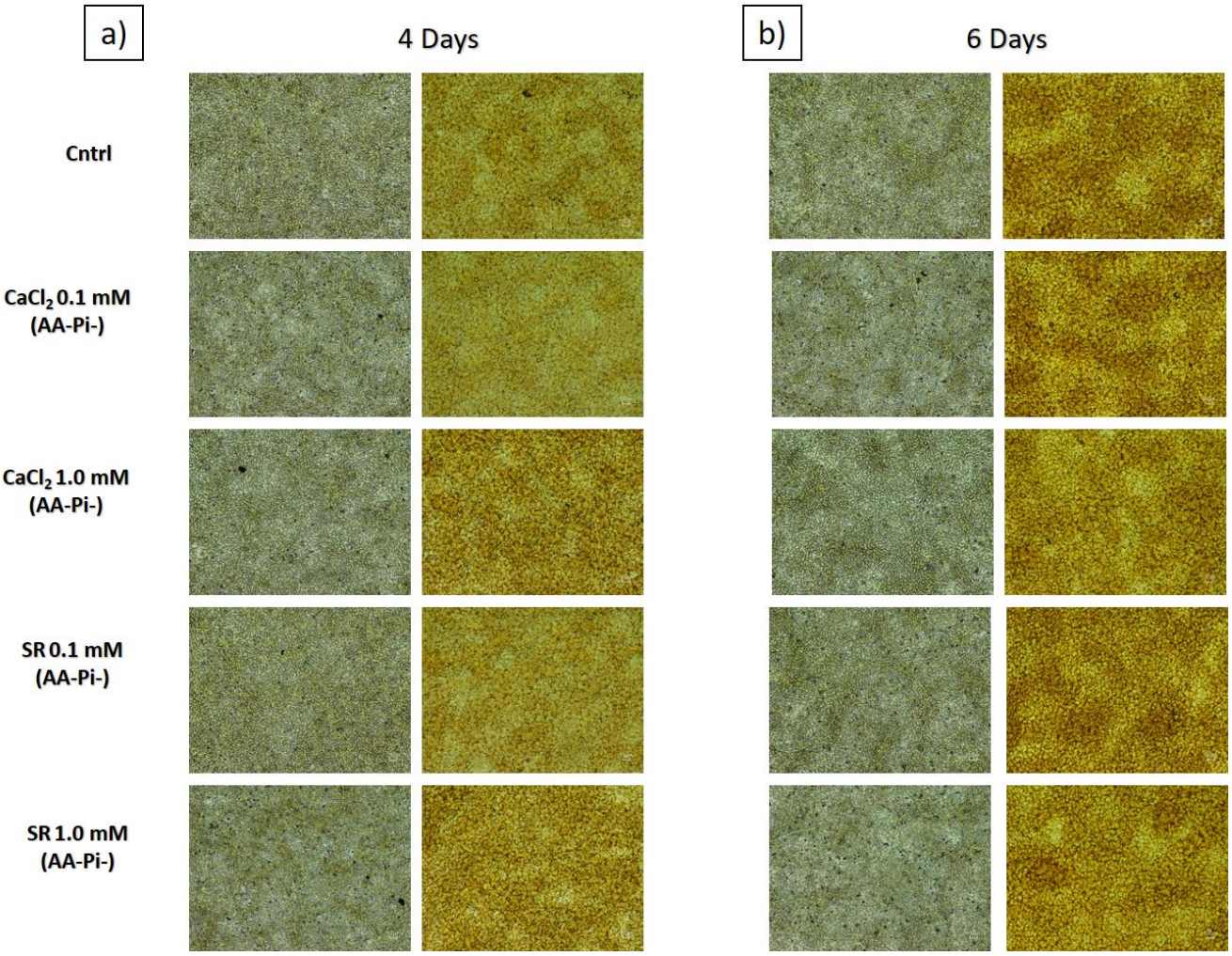

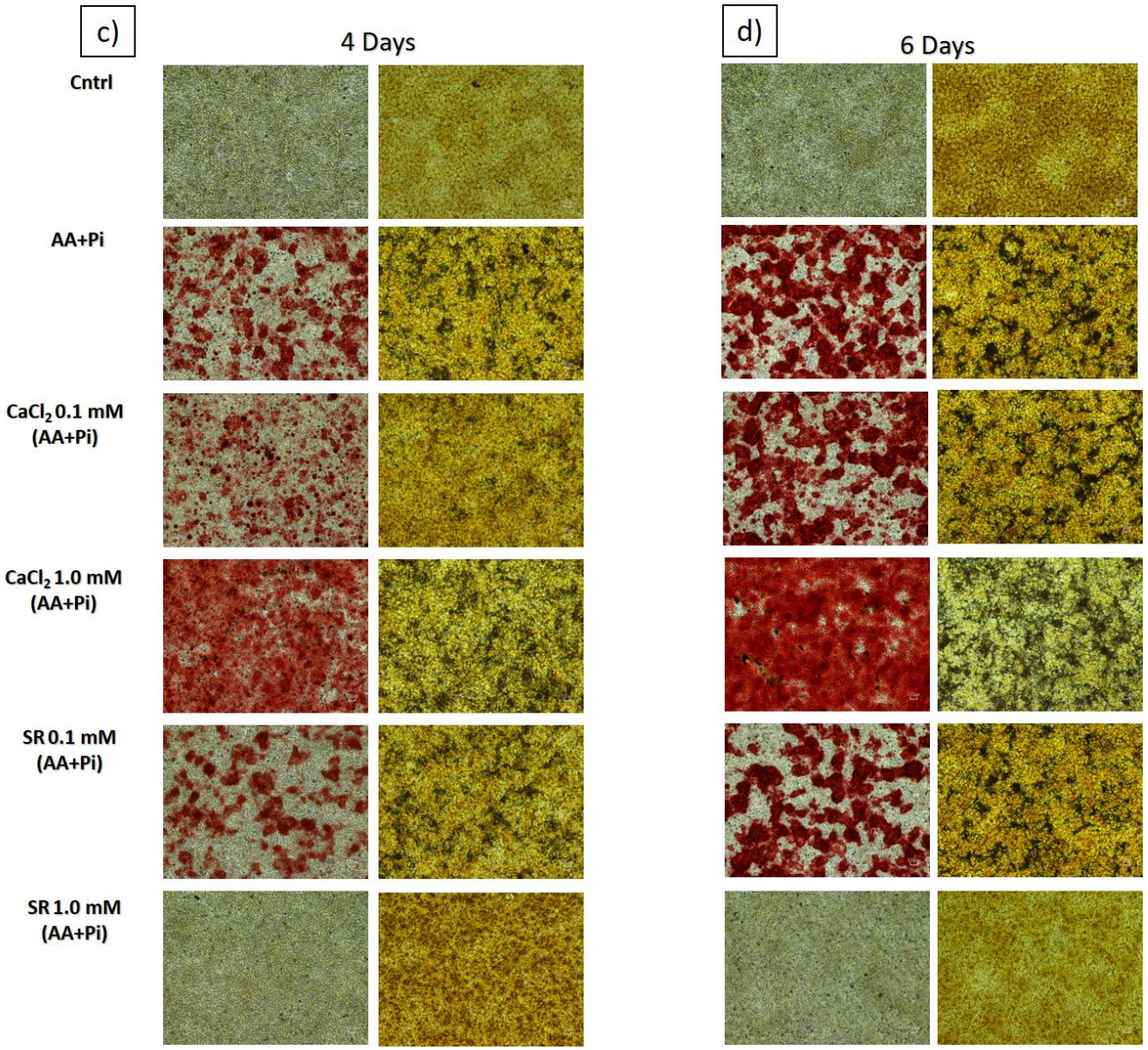

.

FIGURE 5. 2. THE MINERAL DEPOSITION WAS INVESTIGATED BY ALIZARIN RED S AND VON KOSSA STAINING, AFTER TREATMENT FOR 4 AND 6 DAYS.

(A-B) represents the $CaCl_2$ and SR in growth media (AA-Pi-), and C-B in osteogenic media (AA+Pi). In every representation, the left column represents the Alizarin Red S, and the right panel Von Kossa staining

As displayed **in Figure 5.2 (a-b)** no ion was capable of inducing in vitro mineralization in a growth medium, which is reasonable since ascorbic acid participates in the collagen synthesis cascade, and Pi is required for apatite synthesis and deposition. On the other hand, under osteogenic conditions **Figure 5.2 (c-d)** all the treatments induced mineralization of the ECM, however high doses of SR (1.0 mM) inhibit mineralization, which contradicts previous reports [47,48]. Whether mineralization

impairment is dose-dependent or whether it depends on the cell line[48] remains to be investigated, since in osteoblasts high doses of Sr^{2+} stimulate mineralizing [49,50]. Since alizarin red stains Ca^{2+}-rich mineral nodules and we used Ca^{2+} as one of the treatments, to avoid false positives and double-check biomineralization, we performed Von Kossa staining, which is a more precise histological technique to study mineral deposition[51]. The Von Kossa assay confirmed the impairment of mineralization by higher Sr^{2+} concentration.

Additionally, the mineralization of ECM is a coordinated event that responds to several stimuli, which include cell-to-cell communication, cytokines, interleukins, ions, mechanical stress, and extracellular vesicle-cell interactions, among other processes. Under stimulation, a complex net of intertwined signaling pathways transmits the external stimuli downstream to the membrane. The response varies according to the stimulus, however, for simplicity here we will summarize the outcomes in a matter of genomic response through the modulation of osteogenic-related genes, and further biomineralization. The main pathways responsive to Ca^{2+} concentration is the CREB, and to Pi is the Erk1/Erk2. Both pathways were previously described to influence matrix mineralization[50,52]. Here we investigated whether Sr^{2+} is capable of stimulating CREB and Erk1/2 **(Figure 5.3a-f)** signaling pathways, by analyzing their phosphorylation state (pCREB and pErk1/2). Also, we stimulated the cells for 15 and 30 minutes, to verify early and late responses, respectively. Since no mineralization was observed in the growth media conditions, we decided to exclude them from further analysis.

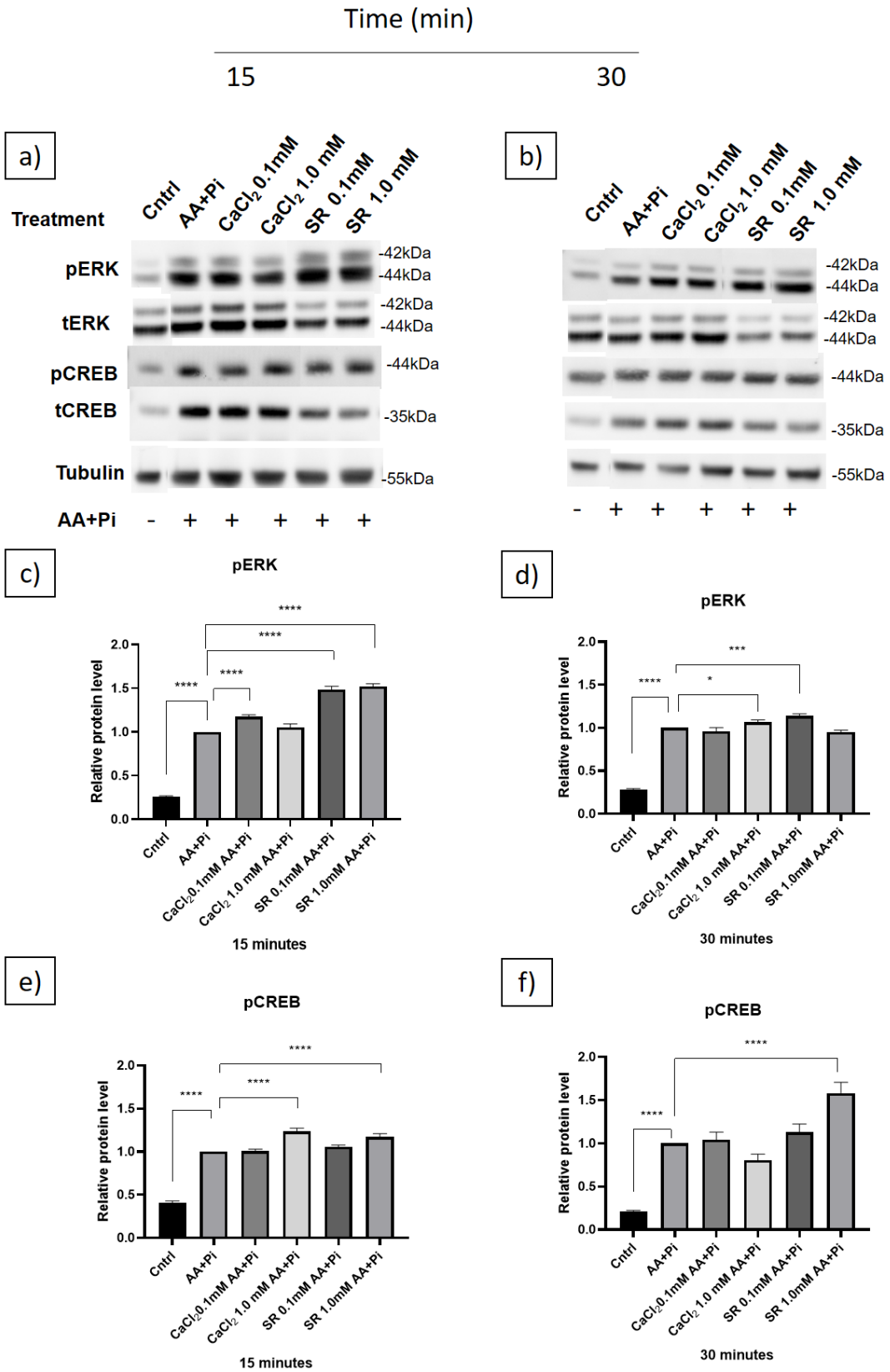

FIGURE 5. 3. WESTERN BLOTTING ANALYSIS OF PERK1/2 AND PCREB.

We analyzed the activity of Erk1/2 and CREB pathways by means of phosphorylation of those proteins when stimulated by $CaCl_2$ and SR at different concentrations for 15 and 30 minutes. Multiple statistical

comparisons were performed by one-way ANOVA, P values for pERK 15 min: ****p<0.0001, and 30min: *p< 0.0239, ****p<0.0001; for pCREB 15min: ****p<0.0001, and 30min: ****p<0.0001. The results represent mean ± SD for triplicate determination for one experiment.

Western blotting analysis revealed that Erk1/2 and CREB activation are dependent on stimulation time and ion concentration. Erk1/2 activation is constitutive and cyclic with waves of activation and inactivation in response to select stimuli[53]. It was previously observed that Erk1/2 activation normally happens in two stages, called the first wave (~15min) and the second wave after approximately 8 hours, however, this time varies according to the type of cell[53–55]. Here, we studied this pathway in the first wave (15 min, Fig 5.3a, c,e) and late response, after 30 min (Fig.5.3b,d,f). Moreover, all the treatments were compared to the osteogenic media (AA+Pi). Short-time (first wave) exposure revealed that $CaCl_2$ 0.1 mM, SR 0.1 mM, and SR 1.0 mM increased the phosphorylation state of Erk1/2, and since all the treatments were carried out in osteogenic media, one can consider the synergistic effect of the ions with ascorbic acid and Pi upon the activation of this pathway. The late response of pErk1/2 was also affected by SR 0.1 mM, with an increase in the phosphorylation of Erk1/2. These results demonstrate that Sr^{2+} can sensibilize the Erk1/2 pathway, while $CaCl_2$ did not interfere with the pathway in late response.

Under physiological circumstances, the transcription factor cyclic AMP response-binding protein (CREB) is expressed in all the nucleated cells and participates in many stages of cell development and maintenance. Phosphorylation of CREB occurs in response to growth factors, steroids, cytokines, calcium, and many other stimulators[56]. Despite an ever-growing number of studies linking dysregulation of CREB to cancer[56–60], CREB signaling was also associated with bone development and maintenance[61,62]. We have shown here that only a high concentration of SR and $CaCl_2$ (1.0mM) were able to stimulate the phosphorylation of CREB in either early or late response, and in the case of $CaCl_2$ only in early response (Figure 5.3). Interestingly, CREB and Erk1/2 activation was previously described to be modulated by CaSR[63–66], which is also responsive to Ca^{2+} and Sr^{2+} [47].

Additionally, the activation of Erk1/2 and CREB signaling was previously described to regulate the mRNA of osteogenic genes[47,50,67–69]. Based on this, we checked if the activation of both pathways influences the expression of Runx2, Sp7, and Collagen 1, and the phosphatases, ALP, Smpd3, and PHOSPHO1 **(Figure 5.4).**

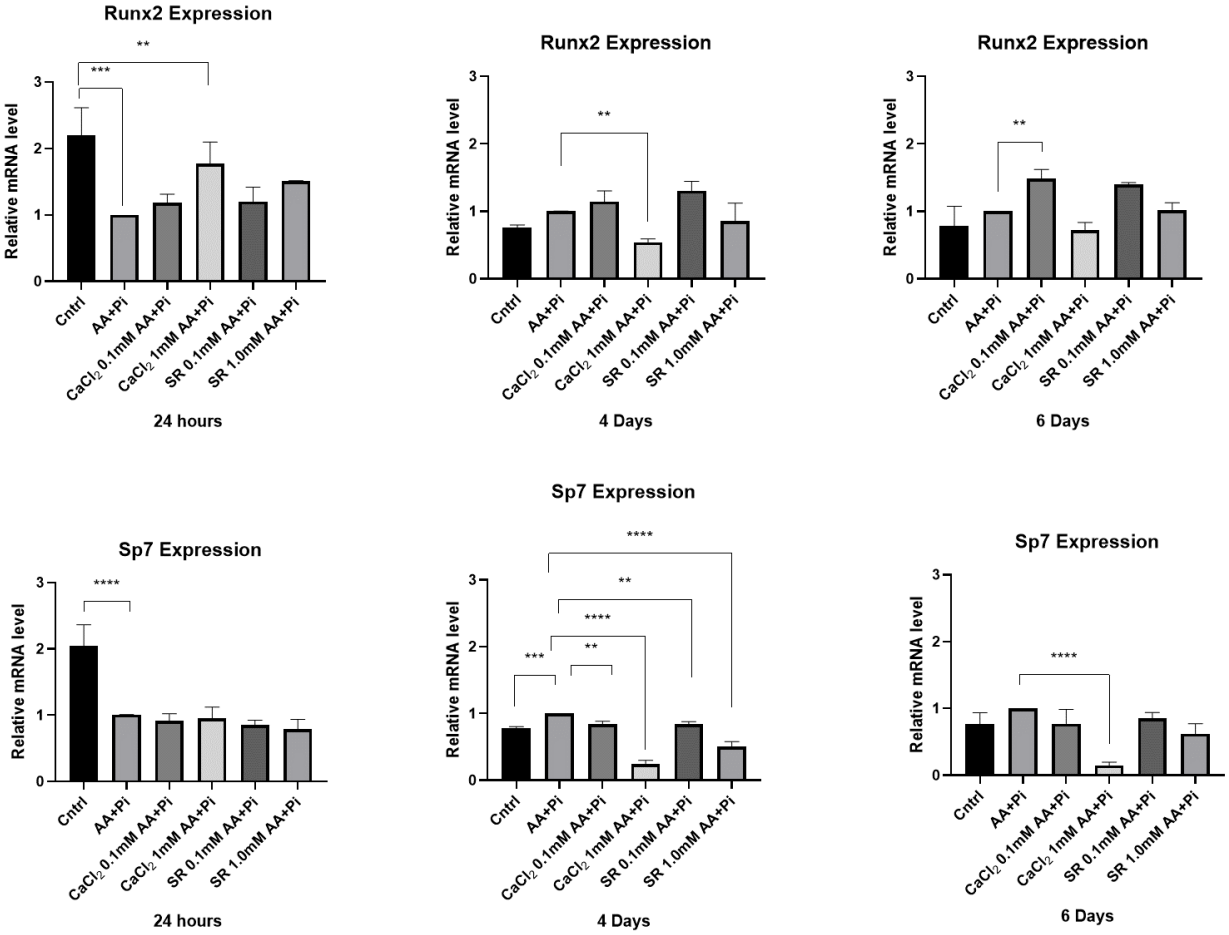

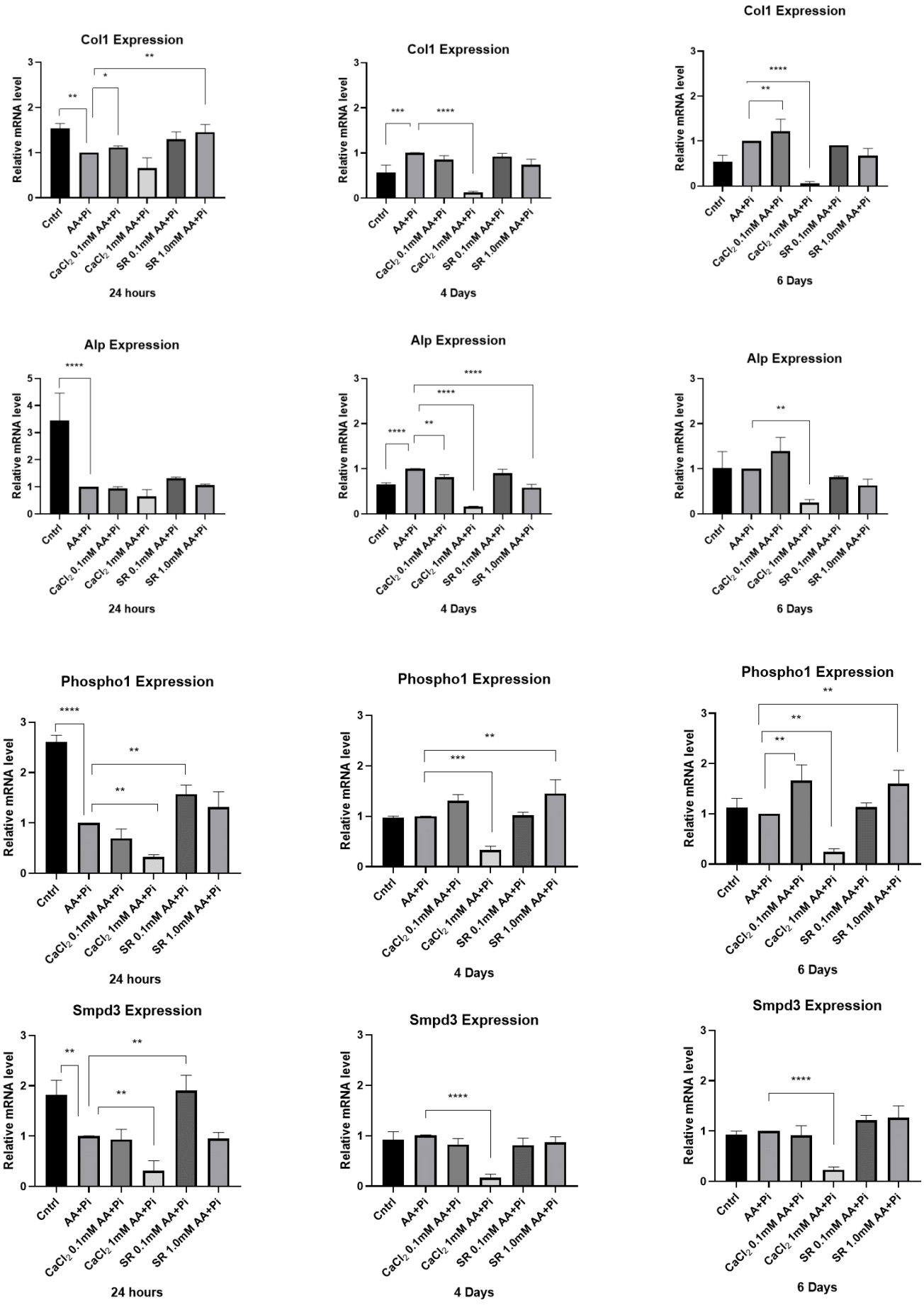

FIGURE 5. 4. OSTEOGENIC GENE EXPRESSION LEVEL MEASURED BY QUANTITATIVE PCR (QRT-PCR).

We studied the effect of $CaCl_2$ and SR at different concentrations over the expression of osteogenic genes for 24 hours, 4, and 6 days. Multiple statistical comparisons were performed by one-way ANOVA, P values for Runx2: *p=0.0235,**p=0.0079, ***p= 0.0002; for Sp7: *p=0.0204,**p=0.0045, ***p=0.0004,****p<0.0001; for Col1: *p=0.0421, **p=0.0025, ***p= 0.0006, ****p<0.0001; for ALP: **p=0.0049, ****p<0.0001; for PHOSPHO1: *p=0.0479, **p=0.0017, ***p=0.0002, ****p<0.0001; for Smpd3: **p=0.0024, ****p<0.0001.

The analysis of osteogenic gene expression by quantitative PCR demonstrated a low-to-minimum influence of both $CaCl_2$ and SR over time. The analysis of the transcription factors, Runx2 and Sp7 after 24 hours, 4 days, and 6 days of culture revealed differences after 4 days, in which $CaCl_2$ and SR decreased the expression level of Runx2 ($CaCl_2$ 1 mM), and Sp7 (all the treatments). At day 6, Runx2 expression was upregulated by $CaCl_2$ 0.1 mM, and Sp7 expression level was downregulated by $CaCl_2$ 1.0 mM. Similarly, the expression of Col1 was downregulated by $CalCl_2$ 1.0 mM at day 4,6, however lower concentration of the ion upregulated the expression at day 6. SR did not affect the expression of Col1 on days 4 and 6, but at 24-hour SR 1.0 mM slightly increased the Col1 expression level.

The expression of three phosphatases, ALP, PHOSPHO1, and Smpd3 was also studied. mRNA ALP level significantly decreased on day 4 upon treatment with $CaCl_2$ (0.1-1.0 mM) and SR (1.0 mM), nonetheless $CaCl_2$ (1.0 mM) also negatively affected ALP at day 6, with no statistic difference for the other treatments at the same time. Moreover, the higher concentration of $CaCl_2$ (1.0 mM) downregulated the expression of PHOSPHO1 at days 4 and 6, albeit the lower concentration (0.1 mM) upregulated the mRNA of PHOSPHO1 at day 6. SR (1.0mM) also upregulated the expression of PHOSPHO1 (mRNA) on days 4 and 6, while the lower concentration did not affect the phosphatase. Smpd3 was also downregulated by $CaCl_2$ 1.0 mM at 24 hours, day 4, and day 6. Curiously, SR 0.1 mM upregulated the level of Smpd3 at 24 hours.

Additionally, Chaudhary et al (2016)[34] demonstrated the importance of Pi in stimulating mineralizing competent cells to release MVs and mineralization. At the molecular level, they have described that Pi mediates MV release through the activation of Erk1/2 signaling, which was accompanied by the re-organization of actin fibers. Also, the protein composition of the MVs changes when compared to the classic osteogenic factors, namely ascorbic acid and Pi.

Thus, we studied how $CaCl_2$ and SR affect the release and function of MVs as well as their protein content. Our study differs from that carried out by René (ref) since we treat the cells instead of incubating MVs with the ions. Also, we included one more treatment (5 mM Pi) by means of comparison. First, we analyzed the release of MVs and then their function. We exploited the MVs size and concentration by quantitative nanoparticle tracking analysis (NTA), **Figure 5.5.** In order to facilitate the analysis, we separated the MVs according to their size and concentration, as indicated in the **Figure 5.6.**

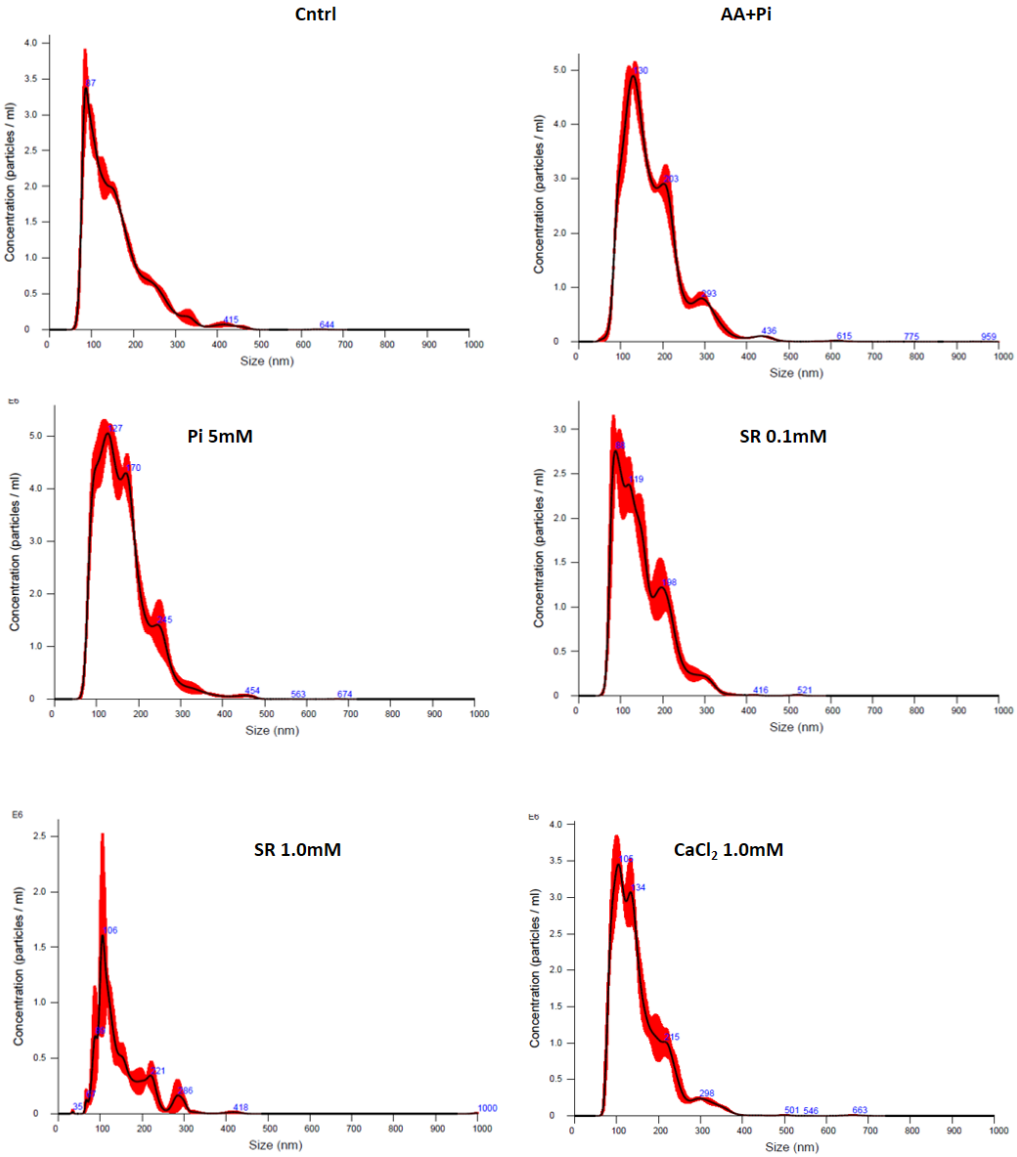

FIGURE 5. 5. THE NUMBER OF VESICLES AND SIZE DISTRIBUTION WERE MEASURED USING NANOPARTICLE TRACKING ANALYSIS (NTA).

Secretion of vesicles was stimulated by the growth media, osteogenic media (AA+Pi), 5mM Pi, 1.0 mM $CaCl_2$, and (0.1-1.0 mM) SR in the presence of osteogenic media for 24 hours. The vesicles were harvested according to multi-step ultracentrifugation as described elsewhere [70–72].

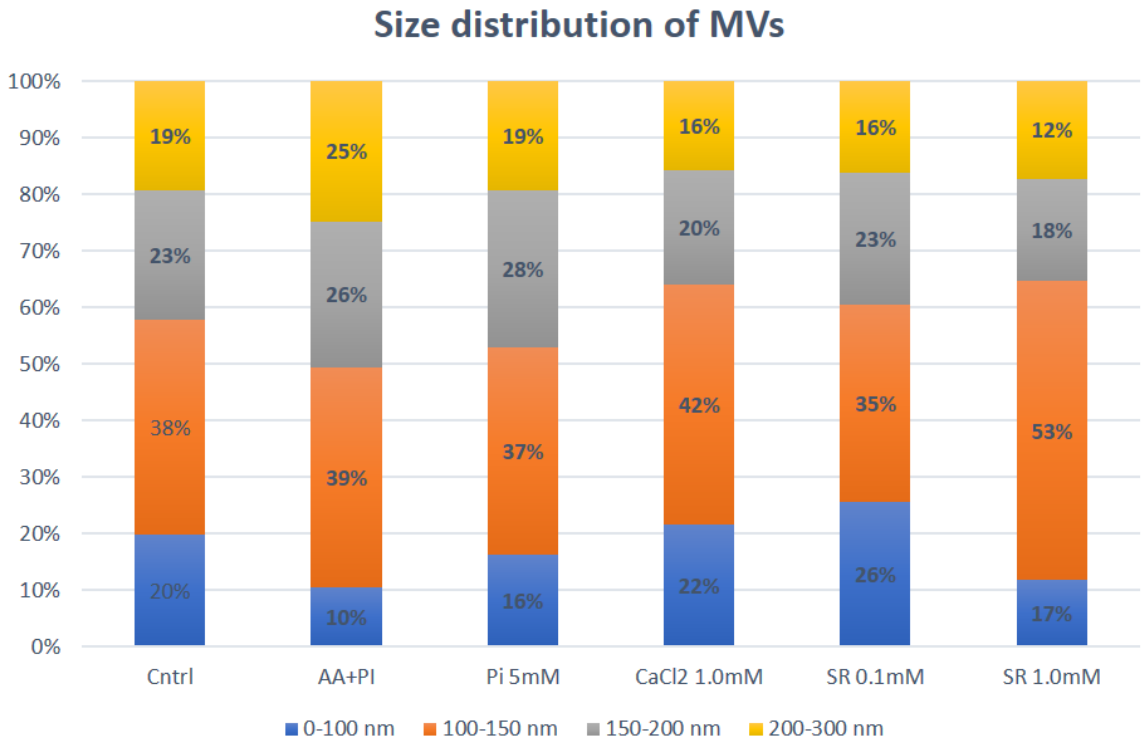

FIGURE 5. 6. SIZE DISTRIBUTION OF MATRIX VESICLES FOR EACH TREATMENT AND THE UNTREATED GROUP (CONTROL).

The size distribution of MVs was similar compared to the different treatments. The mean diameters were found in the 100-150 nm range, followed by 150-200nm, which is characteristic of MVs (ref). We also observed that SR 1.0 mM and $CaCl_2$ 1.0 mM increased the percentage of MVs with diameters ranging from 100 to 150 nm (Figures 5.5 and 5.6). After that, we quantified the amount of MV released per cell **(Figure 5.7).**

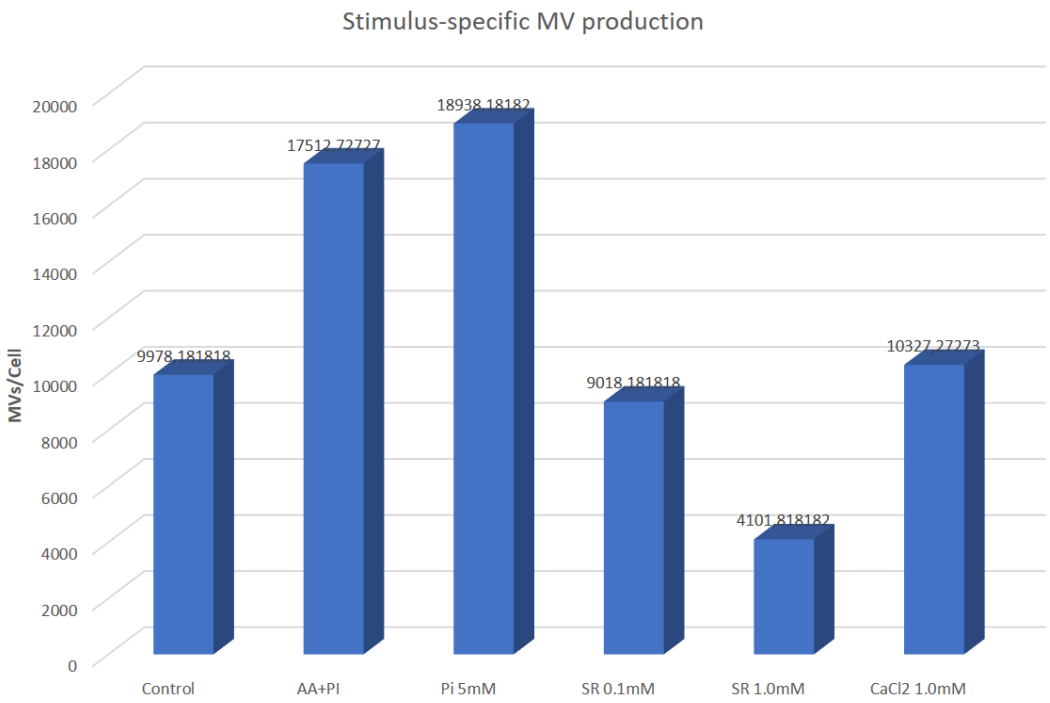

FIGURE 5. 7. THE NUMBER OF MATRIX VESICLES IN THE EXTRACELLULAR MATRIX (ECM) NORMALIZED TO THE NUMBER OF CELLS.

Pi is a strong driver of MV release as evidenced in Figure 5.7. This result corroborates previous studies by Chaudhary et al (2016). It also supports the involvement of Erk1/2 as previously suggested[34]. Additionally, SR (0.1 and 1.0 mM) and $CaCl_2$ 1.0 mM decreased the amount of MV released by the cells. It is worth noting that cells exposed to the growth media presented an intermediate level of MV release. We also studied by western blot three proteins found in competent MVs, lysosomal membrane glycoprotein (Lamp1), AnxV, and TNAP **(Figure 5.8).**

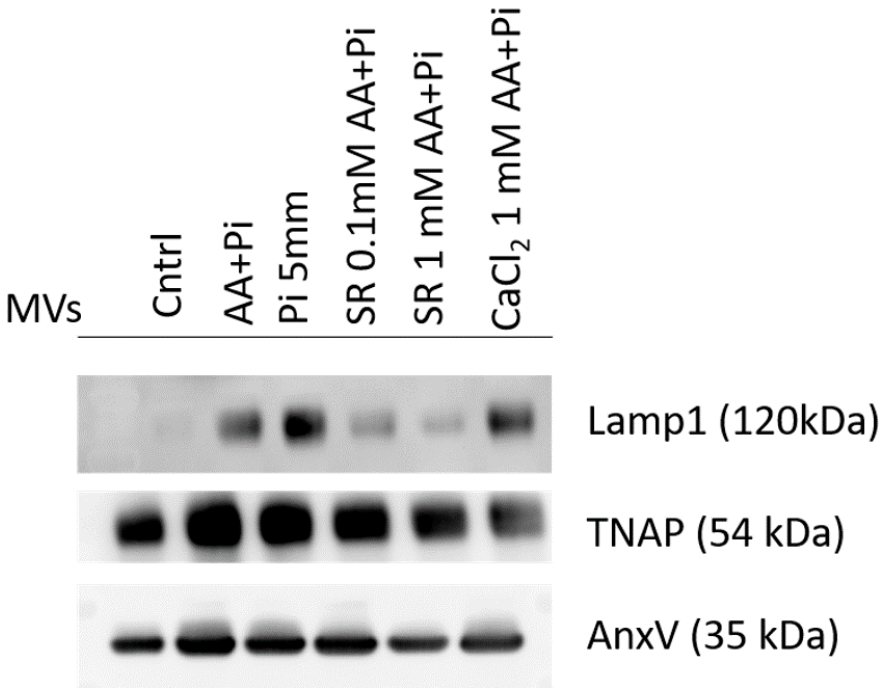

FIGURE 5. 8. WESTERN BLOTTING ANALYSIS OF LAMP1, TNAP, AND ANXV. 17IIA11.

Cell line was exposed to standard growth media, standard osteogenic media, Pi 5mM, $CaCl_2$ 1.0mM, and SR (0.1 and 1.0 mM) in osteogenic media for 24 hours.

TNAP is involved in the production of PI and AnxV in the of Ca^{2+}, and their role in biomineralization has also been studied (ref). Of note, their expression was found in the growth media. Here, we detected only one isoform of TNAP, however, MVs isolated from 17IIA11 cell lines treated with osteogenic media were previously described as pursuing at least three TNAP isoforms (26883946). Additionally, we analyzed the expression of Lamp1, which is a common protein found in MVs originating from 17IIA11. In contrast, MV derived from the growth media and SR (0.1 and 1.0mM) poorly expressed Lamp1. The role of Lamp1 in biomineralization still needs a deeper explanation, however, it was pointed out that they participate in the regulation of pH [73] inside the lysosomes. Since the pH affects the synthesis and deposition of hydroxyapatite[74], one could hypothesize that Lamp1 may indirectly affect the biomineralization process.

The amount of MV released by cells is not always directly related to their function. In other words, the functionality of MVs is directly related to their protein and lipid composition, not to the number of vesicles. We initially investigated the function of Mvs

released from cells treated in different conditions by measuring the TNAP activity. Then, the vesicles were incubated in SCL containing ATP and the mineral propagation was followed by turbidimetry (340nm), as previously described[42,44] **(Figure 5.9a-b).**

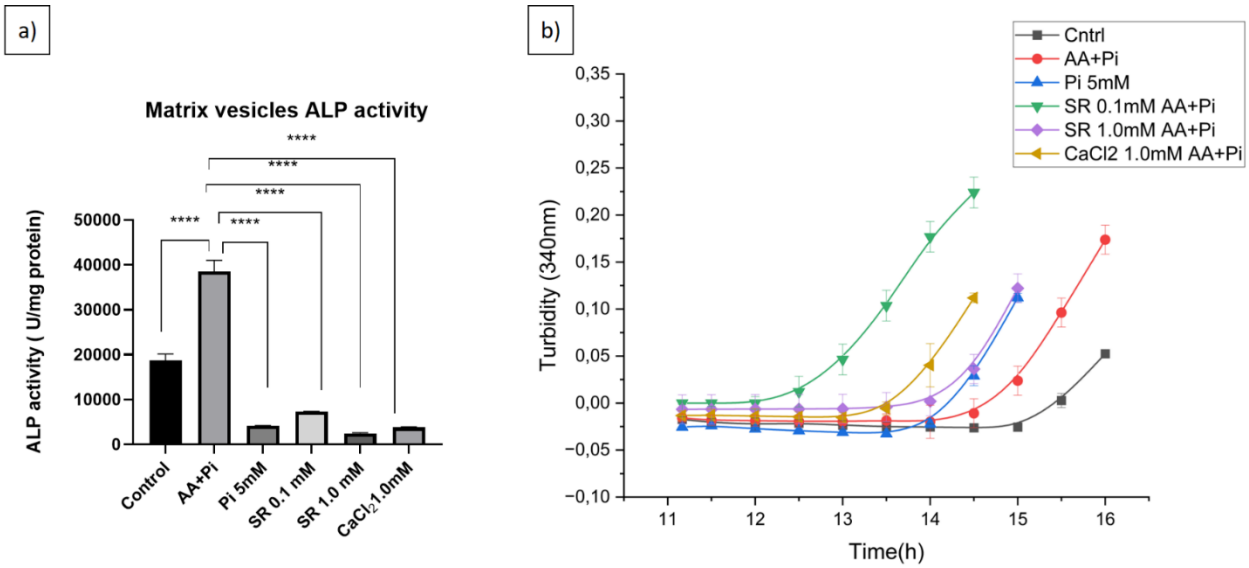

FIGURE 5. 9. ANALYSIS OF THE MVS´ ABILITY TO PROMOTE IN VITRO MINERALIZATION.

(A) TNAP activity, **(B)** mineral propagation after incubation of MVs in SCL containing ATP, measured by turbidity (340nm). Multiple statistical comparisons were performed by one-way ANOVA, P values for TNAP activity, ****p<0.0001.

In comparison to the osteogenic media (AA+Pi), all the treatments and the untreated group (control) depicted a significant decrease in TNAP activity (Figure 5.9a). Surprisingly, mineral deposition/propagation (Figure 5.9b) showed that among all the treatments, SR 0.1 mM was the most efficient (shorter time and high turbidimetry) in producing minerals despite their lower TNAP activity and lower MV release, which endorses the assumption that MV number and TNAP activity are not always related to a higher mineralization profile. On the contrary, a lower mineral propagation efficiency was observed in the control and osteogenic media groups, though they displayed a high TNAP activity as well as an increase in MV release. Additionally, SR 1.0 mM, CaCl2 1.0mM, and Pi 5 mM also presented an efficient response in comparison to the osteogenic media and the control. Then, we analyzed the mineral structure by ATR-FTIR spectroscopy **(Figure 5.10).**

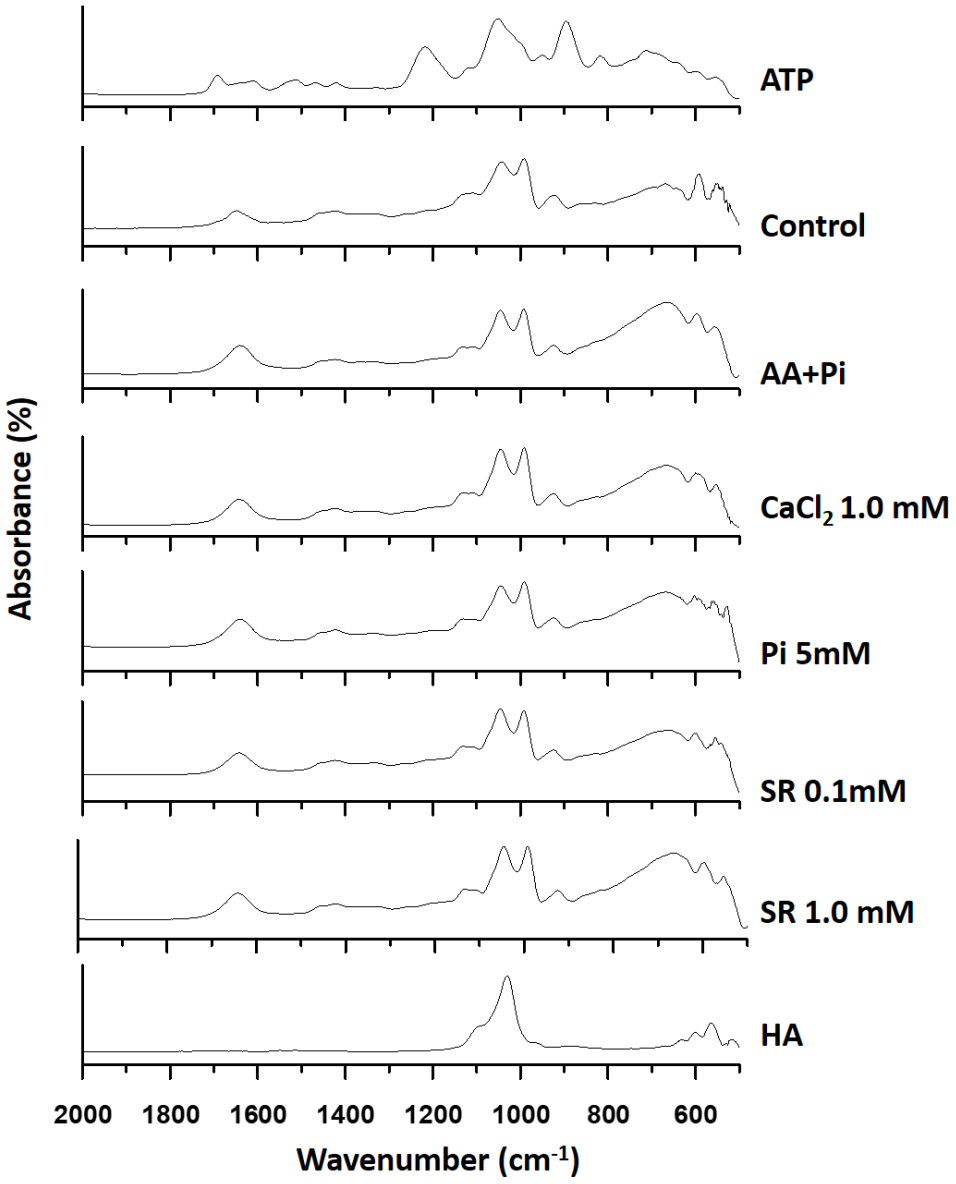

FIGURE 5. 10. MINERAL CHARACTERIZATION BY ATR-FTIR SPECTROSCOPY.

Spectra of minerals produced by MVs isolated from cell treatment under different conditions as indicated by the colors. For comparison reasons, we compared the ATP and HA spectra. Data are reported as the mean of triplicate measurement of three independent analyses.

The analysis of ATR-FTIR spectra revealed MVs isolated from cells in all the conditions presented characteristic bands of HA[75]. The intense bands at 1040 are related to the asymmetric stretching of the PO_4^{3-} group and 940 cm^{-1} is related to HPO_4^{2-}, a precursor of apatite. It is clear from the comparison with the spectra of ATP that all the subtract was consumed since no bands related to it were identified in the spectra of minerals isolated from MVs.

Atomic force microscopy (AFM) is a powerful technique that can generate high-resolution images at the nanometer scale[76]. It is possible by using AFM to qualitatively distinguish differences in the fluidity of the membrane (a property called viscoelasticity), which in turn indicates a series of parameters, such as roughness, medium diameter, medium height, presence or absence of protrusions. AFM has been previously used for MV characterization[77–80]. We characterized the MVs by AFM and TEM **(Figure 5.11 and Table 5.1)** and analyzed their superficial charge by zeta potential **(Table 5.1).**

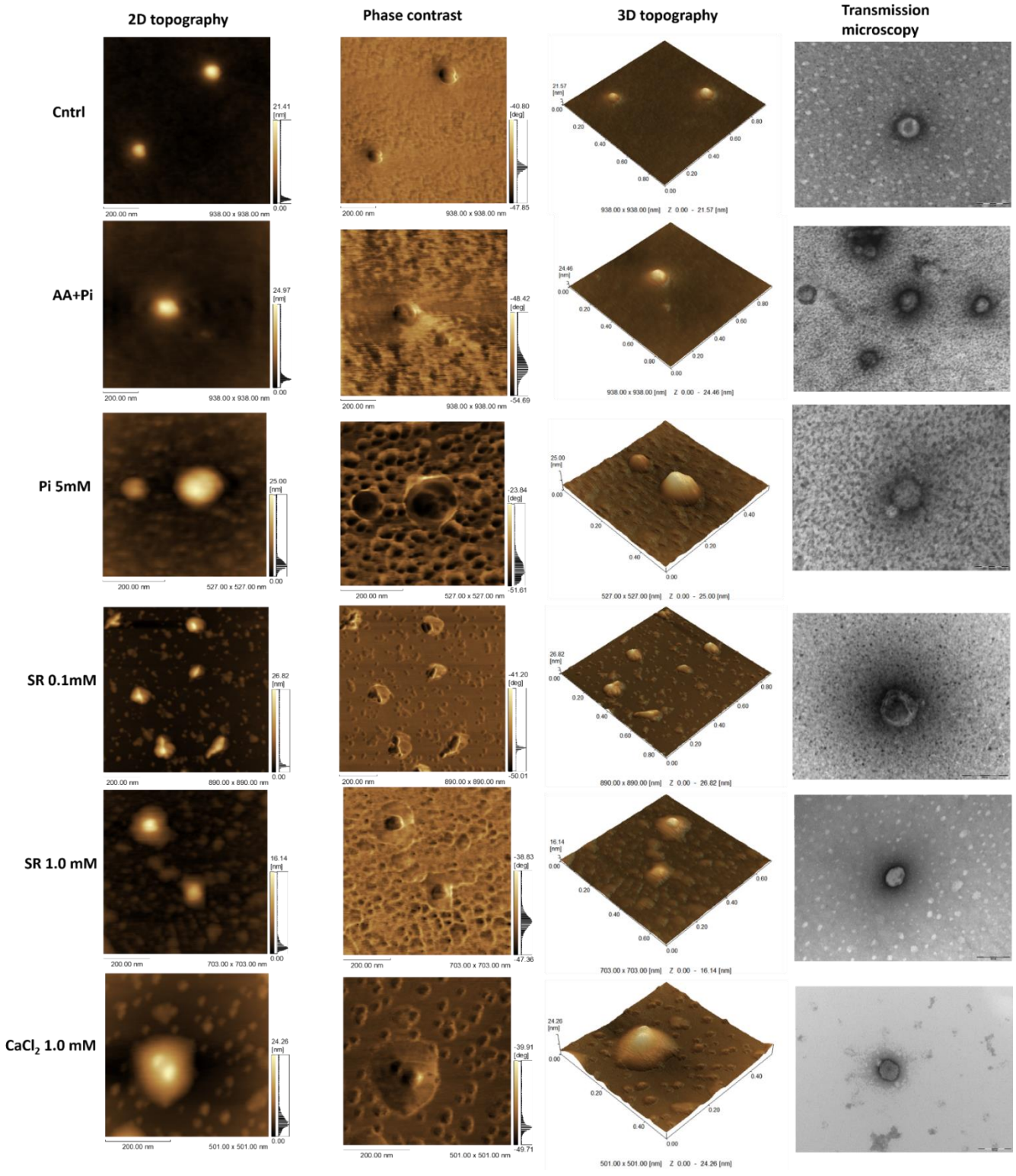

.

FIGURE 5. 11. AFM AND TEM IMAGES OF MATRIX VESICLES ISOLATED FROM CELLS GROWN IN DIFFERENT CONDITIONS FOR 24 HOURS.

Fom left to right: 2D topography, phase contrast, 3D topography, and transmission electron microscopy

TABLE 5. 1. PARAMETERS DERIVED FROM AFM ANALYSIS, MEDIUM DIAMETER, MEDIUM HEIGHT, PRESENCE OF PROTRUSION, AND RATIO ROUGHNESS.

We also analyzed the matrix vesicle surface charge measured with zeta potential (mV). *Protrusion size corresponds to the maximum peak reached by the protuberance.

Vesicles	Medium diameter AFM (nm)	Medium height AFM (nm)	Protrusion (nm)*	Mean roughness	Zeta potential (mV)
Control	101.1 ± 0.05	8.380	-	0.839 ± 0.2	-25.6 ± 3.0
AA+Pi	164.27 ± 0.08	8.617	-	0.889 ± 0.2	-22.2 ± 1.6
P_i 5mM	144.10 ± 0.12	10.36	2.14	0.722 ± 0.3	-18.7 ± 1.4
SR 0.1 mM	175.0 ± 0.07	22.71	14.91	1.13 ± 0.3	-23.5 ± 1.2
SR 1.0 mM	130.10 ± 0.05	3.548	7.30	0.645 ± 0.4	-21.9 ± 1.0
$CaCl_2$ 1.0 mM	158.40 ± 0.05	6.500	5.88	0.68 ± 0.30	-20.4 ± 0.5

Figure 5.11 demonstrates that the MV surface derived from the cells exposed to Pi 5 mM, SR (0.1 and 1.0 mM) and $CaCl_2$ 1.0mM presented structural differences in their outer membrane, as indicated by the presence of protrusions (darker area found on the MV top) with distinct differences in viscoelastic properties (phase contrast images). Also, such protrusions were barely identified in the MV exposed to the control and osteogenic media. In addition, from AFM data we calculated a series of parameters as described in Table 5.1. The overall diameter of the MVs is around 100-200nm, supporting the data found in the NTA analysis **(Figures 5.5 and 5.6).** The medium height variable differs between each condition. MVs isolated after treatment with SR 0.1 mM preset the higher medium height and the higher protrusion (14.91nm). Furthermore, membrane roughness also varied between the groups, where SR 0.1mM presents the highest roughness, which might be indicative of a change in the lipid and protein composition throughout the MV membrane[79].

The lipid composition was previously described as a modulator of the catalytic activity of enzymes incorporated at the MV bilayer, thus directly affecting the biomineralization ability[42]. Since the AFM data pointed to a change in the viscoelastic property of the MVs´ membrane, and we also noticed a change in the MVs´ mineralization profile **(Figure 5.9a-b),** here we applied a lipidomic approach to screening the overall lipid content of the MVs (**Figure 5.12**).

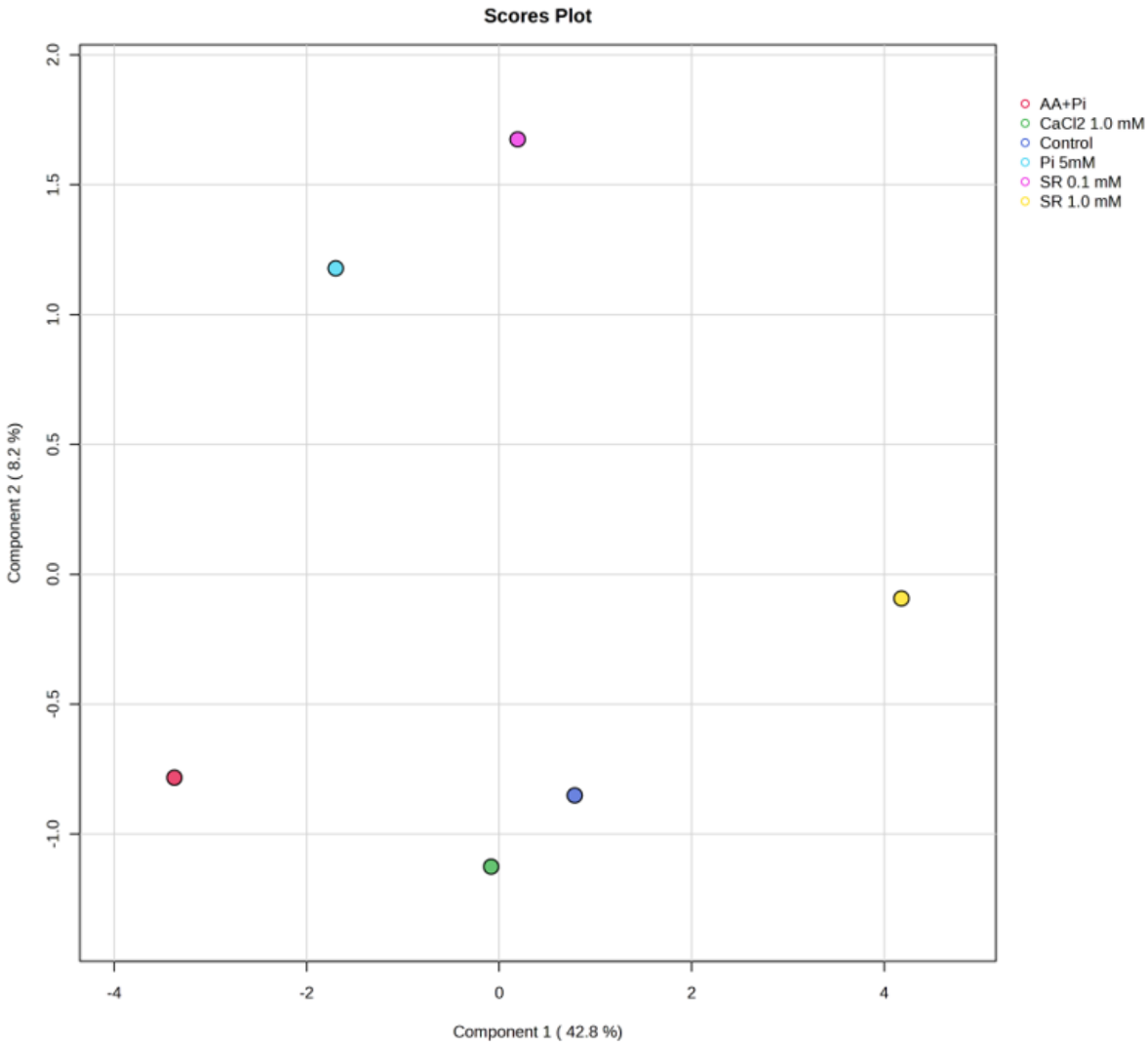

FIGURE 5. 12. PRINCIPAL COMPONENT ANALYSIS SCORE PLOT OF LIPID PROFILES OBTAINED FROM MVS .

17IIA11 cell line treated with growth media (control), osteogenic media (AA+Pi), Pi 5 mM, $CaCl_2$ 1.0mM and SR (0.1 and 1.0mM) in osteogenic media.

The principal component analysis (PCA) plot **(Figure 5.12)** demonstrates the heterogeneity among the groups. The analysis described 51% of the total variance, which includes 42.8% of principal component 1, and 8.2% of principal component 2, whereby component 1 was the major component of discrimination.

After that, we represented the overall lipid content extracted from the MVs as described by the following heat map **(Figure 5.13)**, and the 30 top lipids that were differently regulated by the treatments **(Figure 5.14).**

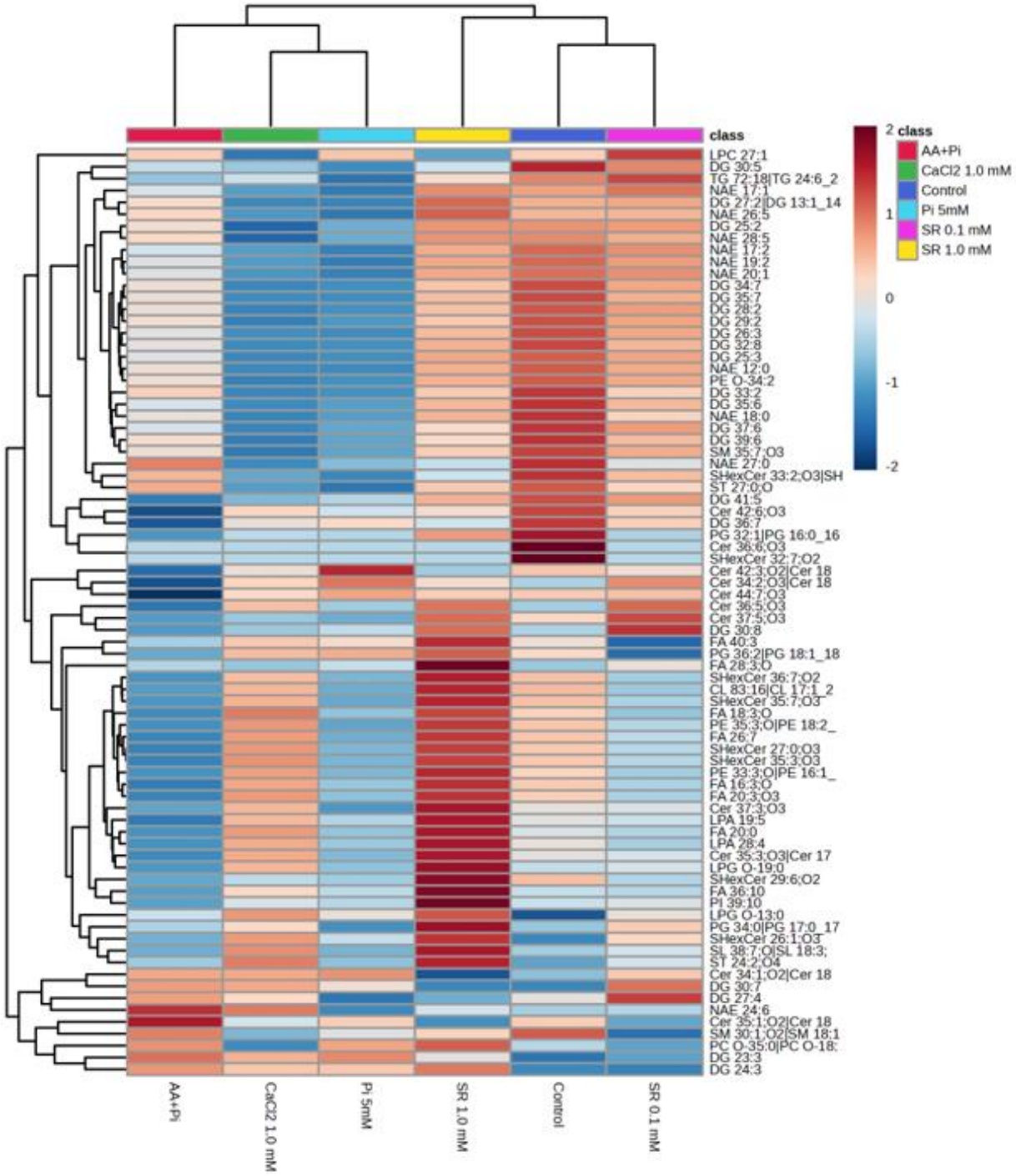

FIGURE 5. 13. HEAT MAP REPRESENTATION OF 81 LIPIDS FOUND IN THE MV FROM THE SIX CONDITIONS.

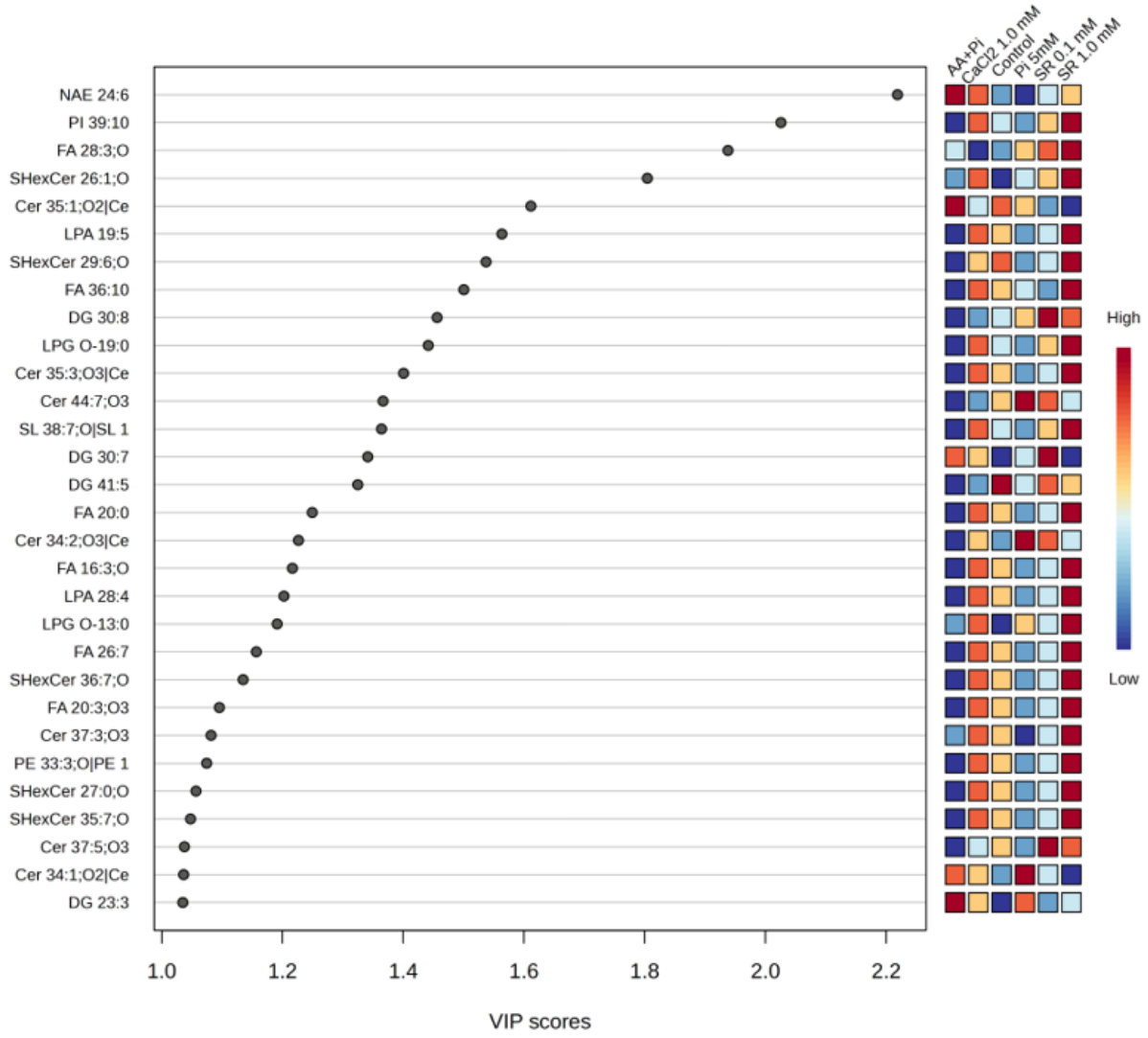

FIGURE 5. 14. VARIABLE IMPORTANCE IN PROJECTION (VIP SCORE) PLOT OF THE 30 LIPIDS THAT WERE DIFFERENTIALLY REGULATED AMONG THE SIX CONDITIONS.

A total of 81 lipids were found in the matrix vesicle composition **(Figure 5.13).** The lipid classes varied significantly depending on the treatment. MVs isolated from cells treated with SR 0.1mM are enriched in ceramide (Cer), diacylglycerol (DG), sphingomyelin (SM), and a plethora of fatty acids. For MVs isolated from cells treated with SR 1.0mM, lipid composition resembles the profile observed for SR 0.1mM but with a higher content of LPG, PI, PE, and LPA, among others. A similar lipid profile was observed in the control group. For the cells treated with Pi (5 mM), the MVs presented a high content of Cer, and phosphatidylcholine (PC), and a similar profile was observed in

the osteogenic media group with a higher Cer and SM content. Finally, $CaCl_2$ 1.0mM was enriched in N-acyl ethanolamine (NAE) and others.

Next, we selected the 30 most differently regulated lipids among the six groups, as represented in the variable importance in the projection (VIP) plot, **Figure 5.14**. The individual lipids NAE, PI, FA, Cer, LPA, SHexcer, DG, and LPG were altered according to the treatment. Further, bar plots were constructed to represent the lipids change depending on the treatment, we grouped them into classes, like neutral lipids (TG, DG), fatty acids (FA, NAE) sterol lipids (ST), phospholipids (PC, PE, LPC, CL, PI, SL, LPA, PG, LPG), and finally sphingolipids (SM, Cer, and SHexCer) **(Figure 5.15).**

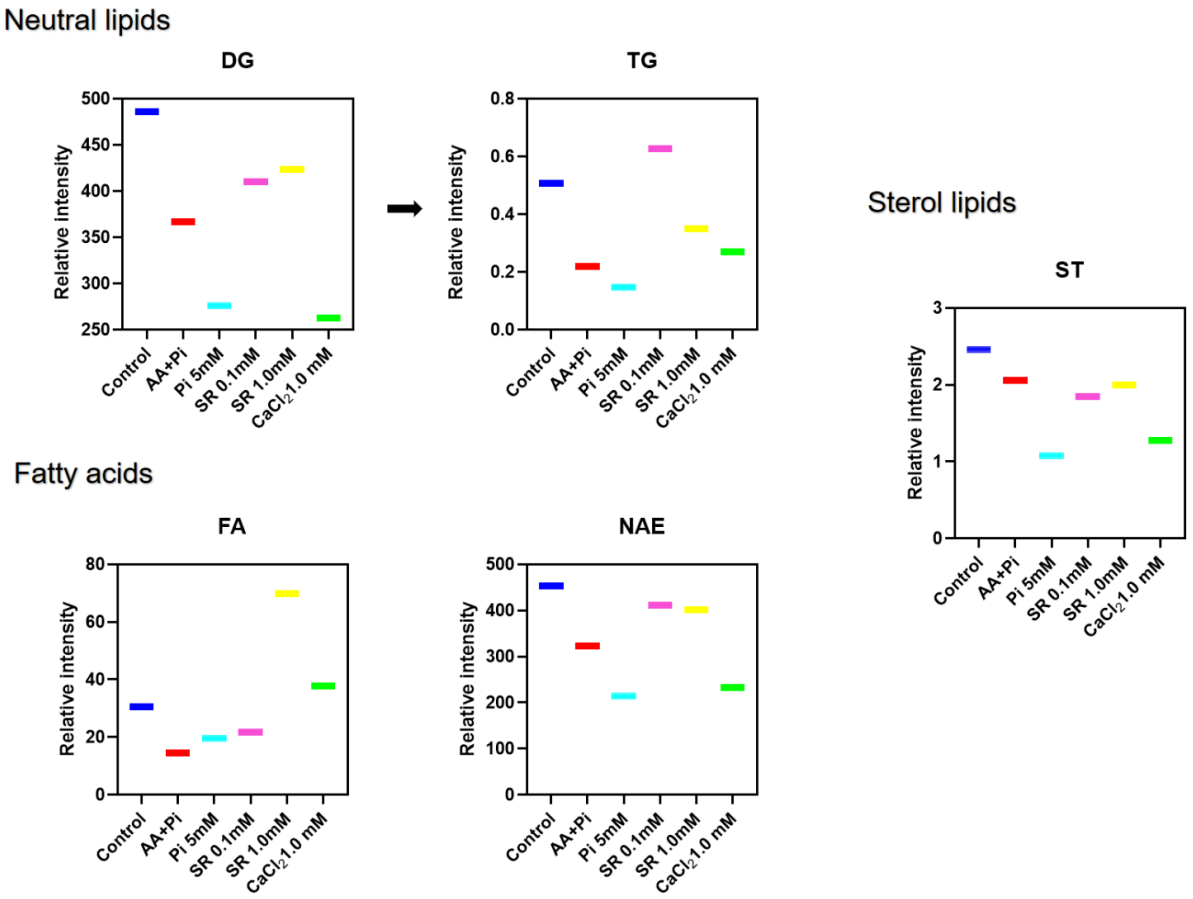

Phospholipids

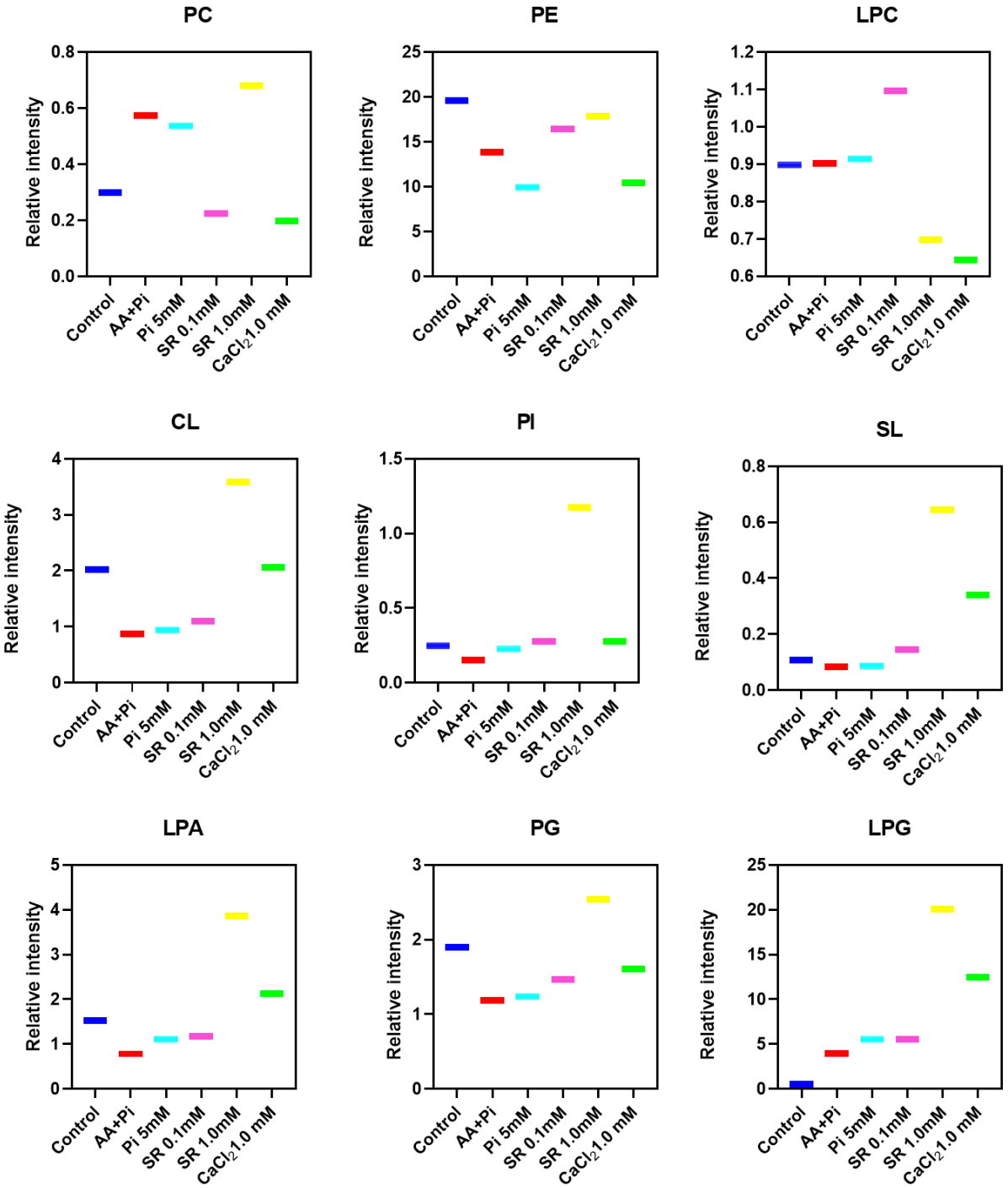

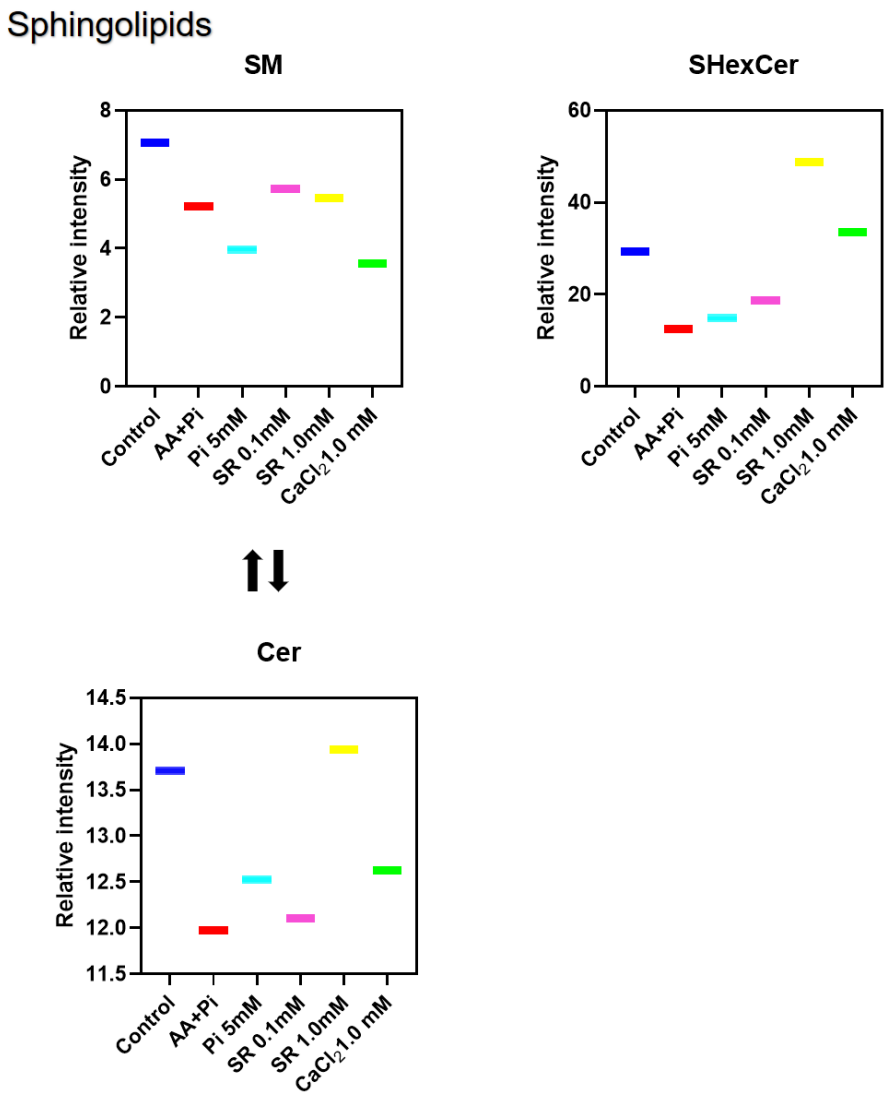

FIGURE 5. 15. BAR PLOTS DEPICTING LIPID CHANGES BASED ON TREATMENT

Bar plot representation of neutral lipids (DG and TG), sterol lipids (ST), fatty acids (FA and NAE), phospholipids (PC, PE, LPC, CL, PI, SL, LPA, PG, LPG), and sphingolipids (SM, Cer and SHexCer) content, isolated from MVs obtained from 17IIA11 stimulated with standard growth media, osteogenic media (AA+Pi), Pi 5 mM, SR 0.1 and 1.0mM and $CaCl_2$ 1.0mM.

Due to its importance in bole physiology, here we will focus our attention on the sphingolipids class (SM, Cer, and SHexCer). The conversion of SM into Cer is played by the neutral sphingomyelin phosphodiesterase3 (Smpd3). Here we observed that SR 0.1 mM bears a higher amount of SM and SR 1.0 mM a higher amount of Cer. $CaCl_2$ and Pi group was enriched in Cer. Finally, SHexCer is a ceramide associated with a sugar radical, which can be reduced to ceramide. A high level of SHexCer was observed in the SR 1.0 mM and $CaCl_2$ groups.

Discussion

The role of ions in life spans from homeostasis control to serving as signaling regulators. Ca^{2+} and Pi are the two most abundant ions involved in the regulation of bone homeostasis. Ca^{2+} participates in a plethora of physiological processes, such as muscle contraction, apoptosis, and cell proliferation[81]. It also acts as a signal transducer and second messenger [82–84]. Aiming at bone tissue, fluctuation of extracellular Ca^{2+} concentration plays a critical role in regulating osteoblast function through the modulation of osteogenic-associated genes[85]. It was previously reported that Ca^{2+} regulates osteoblast activity through the activation of a G-protein coupled receptor, CaSR [47]. The same receptor is involved with Ca^{2+} homeostasis, through the regulation of parathyroid hormone (PTH) secretion by the parathyroid glands and regulates levels of Ca^{2+} excretion by the kidney[86]. Many pathways are responsive to Ca^{2+} stimulation, for example, Erk1/2[47,50,87] and CREB[64,88]. Either pathway is also involved in the regulation of cell proliferation and transcription of osteogenic genes[89]. However, a high concentration of Ca^{2+} was seen to suppress osteogenic differentiation in human periodontal ligaments[90].

Furthermore, Pi participates in the maintenance of bone tissue as well as affects the mineralization steps in many ways. First, Pi is a structural component of the inorganic phase of the mineralized ECM, thus its availability will affect mineral formation. Second, Pi is a strong signaling molecule involved in many biological processes, so its addition or removal regulates the function of many proteins, for example, activation by phosphorylation[34,91]. Third, Pi regulates the expression of multiple osteogenic-related genes involved with osteoblast proliferation, maturation, and function[22,92,93].

The function of Sr^{2+} on biomineralization had been previously reported, however, its mechanism of action has not yet been fully comprehended. Due to their chemical similarity, it has been hypothesized that Sr^{2} participates and modulates many pathways as Ca^{2+} does. Takaoka et al., (2010) demonstrate that SR activates CaSR leading to the activation of the Erk1/2 signaling cascade, which culminates in the regulation of osteogenic genes[47,94]. SR was also observed to activate Wnt/NFATc receptor[95,96], and others[97].

Initiation of mineralization is supported by the secretion of mineral competent MVs. However, the action of Sr^{2+} in such process is not fully understood, though it has been previously investigated[98]. Here we tried to add knowledge regarding the mechanism of

action of Sr^{2+} on osteocompetentes cells. We started by choosing the proper ion concentrations by addressing the MTT assay. We used SR and $CaCl_2$ at low and high concentrations (0.1 and 1.0mM), since no cytotoxic effect was observed, on the contrary, the ion compounds stimulated cell proliferation at days 4 and day 6. We also used 5mM Pi, as previously described[34], and standard growth and osteogenic media.

The effect of SR and $CaCl_2$ on biomineralization was assessed by alizarin red s and Von Kossa staining. In accordance with previous studies[99], low concentration of SR (0.1mM) dispersed in osteogenic media (AA+Pi) promoted mineralization, whereas higher concentrations of SR impaired it. The association of Ca^{2+} and osteogenic media is a potent driver of biomineralization, which is reasonable since Ca^{2+} is involved with the formation of apatite. Interestingly, but not surprisingly, no mineralization was observed when either ion (Sr^{2+} and Ca^{2+}) was solubilized in standard growth media. Ascorbic acid and Pi, both components of the osteogenic media, participate in the biosynthesis of type I collagen, support the formation of HAp, regulate intrinsic cellular responses, and stimulate the expression of osteogenic genes. So, the depletion of both components hampers the formation of a mineralized tissue.

We demonstrated here that SR activates Erk1/2 and CREB signaling by inducing phosphorylation. A similar effect was observed for $CaCl_2$ (1.0 mM). Activation of Erk1/2 and CREB was previously described to play a role in the regulation of osteogenic genes [100–104]. Nonetheless, here we observed a minimum effect of $CaCl_2$ and SR on the gene expression of Runx2, Sp7, Col1, TNAP, PHOSPHO1, and Smpd3. The odontoblast-derived cell line 17IIA11 constitutionally encompasses a high level of osteogenic genes, which means that in physiological conditions this cell line is already committed to a mineralizing phenotype so that no differentiation induction is needed. A great number of articles that correlate the effect of Sr^{2+} on osteocompetent cells with higher expression of osteogenic gene levels, generally use the pre-osteoblast cell line MC3T3-E1. This cell line still needs to differentiate into mature osteoblasts through the activation and transcription of osteogenic-related genes. Due to this, the effect of Sr^{2+} on the regulation of gene expression can be easily studied. Thus, we believe that due to the high expression of osteogenic genes in the cell line 17IIA11, the effect of $CaCl_2$ and SR over them was not evident.

Moreover, we noticed that Sr^{2+}, Ca^{2+}, and Pi have the ability to regulate the release and function of MVs. Our results demonstrated that a lower and higher concentration of

SR and $CaCl_2$ downregulates the release of MVs and decreases the TNAP activity. However, in the case of SR, the MVs were more efficient in synthesizing minerals. In accordance with Chaudhary et al., (2016), here we show that Pi can by itself trigger the release of competent MVs. Competent MVs derived from 17IIA11 are enriched in proteins associated with the regulation of Ca^{2+} and Pi but lack the expression of exosome markers. The protein composition of these MVs have been studied[34]. We observed that the MVs derived from cells treated with SR 0.1 and 1.0 mM poorly expressed Lamp1. The role of Lamp1 on MVs is still unknown, but in lysosomes, it is believed that this protein is involved with the regulation and maintenance of an acid environment[73]. Hap nucleation and propagation are extremely sensible and respond to variations in the environment pH[105,106], so we can hypothesize that Lamp1 presented in the MVs somehow participates in the regulation of the surrounding pH. Yet, protein levels of TNAP and AnxV were higher in MVs isolated from cells treated with Pi, $CaCl_2$, and SR.

In addition, it was previously demonstrated that highly disordered precursor mineral is part of the mineralization pathway[107]. Such mineral precursors can be stored, dissolved, and manipulated, thus allowing the formation of a more ordered and functional mineral. The presence of the band at 940 cm^{-1} supports the mineral formation through an HPO_4^{2-} precursor for all the samples, while be band at 1040 cm^{-1} attests to the ability of MVs to promote apatite formation.

The analysis of parameters calculated from AFM and TEM revealed a change in the membrane viscoelastic features from the MVs, which is indicative of a change in the lipids and protein content. Pi, $CaCl_2$, and SR induced the formation of surface protrusions (dark surface displayed in the MVs phase contrast images) at the MVs membrane. AFM images from proteoliposomes harboring TNAP also demonstrated the presence of protrusions[108]. Lipid content also controls the membrane fluidity, thus giving rise to the protrusions. However, it is not possible to attest that the protrusions are located outside or inside the vesicles, which could be indicative of mineral formation in the lumen. The surface charge investigated by zeta potential measurements did not vary among the samples.

As aforementioned, the change in the MVs membrane constituents was first indicated by phase contrast images acquired by AFM. Then, we tracked the changes through the analysis of the MV´s lipid content. PCA analysis demonstrated significative differences in the lipid composition among the groups, which was later confirmed by lipid

class heat map and VIP score. First, the VIP score of the 30 lipids that were differently regulated among the groups, presented the following species, NAE, PI, FA, SHexCer, Cer, LPA, LPG, DG, and SL. To facilitate the analysis, we divided the lipids into three groups, they are neutral (DG and TG), fatty acid (FA and NAE), sterol (ST), phospholipids (PC, PE, LPC, CL, PI, SL, LPA, PG and LPG), and sphingolipids (SM, Cer and SHexCer), and their content in all the groups was indicated by the bar plots (Figure 14). In accordance, it was previously described that the MV´s membrane is enriched in phospholipids, SM, and cholesterol[109]. Here we found a variety of lipids, for example present in all cell membranes, including lysophosphatidylcholine (LPC), phosphatidylethanolamine (PE), phosphocholine (PA), phosphatidylinositol (PI), phosphatidylserine (PS), sphingomyelin (SM), ceramide (Cer), hexosylceramide (HexCer) and free cholesterol (FC; sterol). Also, we observed the presence of cardiolipin (CL), which is a lipid predominantly located in inner mitochondrial membranes. Finally, we observed the presence of storage lipids, including sterol (ST), diacylglycerol (DG), and triacylglycerol (TC).

Apart from structural and storage roles, the sphingolipids class serves as bioactive signaling molecules and they are involved in many biological regulations, like inflammation, cell death, and proliferation[110]. In the context of MVs and bone physiology, this class together with cholesterol and PS is extremely important, since they are involved with the anchoring and regulation of key proteins, for example, TNAP, organization of lipid bilayer, and creation of lipid microdomains (lipid rafts). A better understanding of how sphingolipids and cholesterol regulate MVs proteins and help to coordinate the lipids throughout the vesicle membrane can be exploited here [111–117].

In this context, SM and Cer are highly found in healthy bone tissue and are required for normal mineralization, so their presence in the lipidome of mineral-competent MVs is not a surprise[118]. It was previously observed that osteoporotic mice present lower levels of SM and Cer in their femur[119], thus attesting to their role in healthy bone homeostasis. Cer is a potent signaling molecule, and it was previously reported to be pro-apoptotic[120]. Hydrolysis of Cer into sphingosine by Smpd3, accompanied by their phosphorylation into ceramide-1-phosphate and sphingosine-1-phosphate, are important bioactive molecules that modulate many biological processes, such as proliferation, apoptosis, cell migration, and adhesion[110]. Moreover, in situ SM catabolism is needed for bone and dentin mineralization, hence in vitro mineralization of MVs was associated with a rapid

degradation of SM [121]. Additionally, mature osteoblasts were seen to have higher expression of Smpd3, a key enzyme involved with the hydrolysis of SM into PC and Cer[122,123]. A similar effect was observed in odontoblasts[124]. Despite their role in bone physiology, the role of SM and Cer on MVs is not fully understood and requires further investigation. It has been hypothesized that the hydrolysis of SM into phosphocholine and ceramide would increase the free PO_4^{3-} in the vicinity of the MVs, thus favoring the initiation of mineralization[118]. Finally, the MVs isolated from cells treated with SR 0.1 and 1.0 mM and $CaCl_2$ 1.0 mM displayed higher mineralizing efficiency (Figure 5.9b) and presented higher SM and Cer content (Figure 5.15).

Taken together, our results demonstrate that SR and $CaCl_2$ actively participate in the promotion of biomineralization through the modulation of Erk1/2 and CREB signaling pathways, and by regulating the release and activity of matrix vesicles. SR action on osteocompetent cells and competent MVs is dependent on concentration. Finally, we described here that MVs´ lipid content varies according to different stimuli, and these changes directly impact the MV function, hence their ability to mineralize the ECM.

Conclusion

Can life happen without ions? We doubt so, at least not on this planet. Ions participate in many biological mechanisms, as cofactors, as signaling molecules, as secondary messengers, a so on. They are needed in all instances of life, and yet only two of them are the most abundant in the human body, namely calcium and phosphate. These two ions coordinate a broad series of events in our body, from hormone control to bone development, from muscle contraction to genetic regulation, to cite a few. However, there are certain ions classified as trace elements that also play a crucial role in life, including strontium (Sr), selenium (Se), copper (Cu), chromium (Cr), and molybdenum (Mo), among others. They are involved with the normal growth and development of tissues, they serve as cofactors for many enzymatic cascades, they regulate the circadian cycle, and so forth. So, to think about using trace elements as key regulators aiming at the healing medicine field is not trivial.

The use of strontium as medicine dates back to 1870. However, only a few years later (1960) it was reported the first use of strontium lactate to treat osteoporotic patients. In the last couple of years, strontium was used in the form of Strontium Ranelate, which

received its approval in Europe. The biochemical and biophysical mechanisms of strontium action on cells have been widely investigated. Strontium has a peculiar mechanism, where it activates osteoblasts, thus is anabolic for bone development, and inhibits osteoclasts, which diminish bone resorption. Due to its chemical similarity to calcium, one can hypothesize that strontium is involved in the same mechanisms as calcium does. However, the strontium mechanisms on osteocompetent cells still need further clarification.

In this chapter, we dedicated our efforts to studying and understanding the role of strontium on an osteocompetent cell, namely 17IIA11. Since this cell line is already committed to an osteogenic profile, we did not evaluate the ability of strontium to induce cell differentiation, which was done in Chapter IV with the pre-osteoblast MC3T3E1. Thus, here we investigated how strontium stimulates the release and function of matrix vesicles. As a matter of comparison and to guide the analysis, we also studied $CaCl_2$ and Pi.

Here we demonstrated that SR facilitates biomineralization by modulating MVs´ surface lipids and then its viscoelastic properties, which we found to be enriched in SM and Cer, and thus its function. Though a similar effect was observed in $CaCl_2$, the MV effectiveness was lower in comparison to either SR concentration. Pi was able to induce the release of MVs, but their role in the genomic expression control and Erk1/2 and CREB signaling was not contemplated here. At the genomic level, we did not notice any significant control of SR over osteogenic genes, that might be attributed to the 17IIA11 constitutional expression of osteogenic markers. Nonetheless, due to intrinsic cellular control mechanisms, the stimulation of such genes through regulation of Erk1/2 and CREB cascade was not pronounced. From a molecular biology point of view, it demonstrates the caviar of genomic control, despite continued stimulation.

Finally, we brought here pieces of evidence on how strontium affects biomineralization. Also, we added more knowledge on the importance of lipids to MVs function, and how some types of ions, especially strontium, change the MVs´ lipids constituents. Nevertheless, there are still unanswered questions that urge a deeper investigation, for example, is the action of strontium on Erk1/2 and CREB signaling pathways mediated by an activation of membrane receptors? And how specifically do the lipids, especially SM and Cer, control mineralization? To cite a few.

Reference

1. Carreras-Sureda, A., Pihán, P. & Hetz, C. Calcium signaling at the endoplasmic reticulum: fine-tuning stress responses. *Cell Calcium* **70**, 24–31 (2018).

2. He, H., Lam, M., McCormick, T. S. & Distelhorst, C. W. Maintenance of calcium homeostasis in the endoplasmic reticulum by Bcl-2. *J. Cell Biol.* **138**, 1219–28 (1997).

3. Berridge, M. J., Lipp, P. & Bootman, M. D. The versatility and universality of calcium signalling. *Nat. Rev. Mol. Cell Biol.* **1**, 11–21 (2000).

4. Yang, W. *et al.* Extracellular vesicles in vascular calcification. *Clin. Chim. Acta.* **499**, 118–122 (2019).

5. Bennett, J. & Weeds, A. Calcium and the cytoskeleton. *Br. Med. Bull.* **42**, 385–90 (1986).

6. Stokes, V. J., Nielsen, M. F., Hannan, F. M. & Thakker, R. V. Hypercalcemic Disorders in Children. *J. Bone Miner. Res.* **32**, 2157–2170 (2017).

7. Kinder, B. K. & Stewart, A. F. Hypercalcemia. *Curr. Probl. Surg.* **39**, 349–448 (2002).

8. Kapustin, A. N. *et al.* Vascular smooth muscle cell calcification is mediated by regulated exosome secretion. *Circ. Res.* **116**, 1312–23 (2015).

9. Rajamannan, N. M. *et al.* Calcific aortic valve disease: not simply a degenerative process: A review and agenda for research from the National Heart and Lung and Blood Institute Aortic Stenosis Working Group. Executive summary: Calcific aortic valve disease-2011 update. *Circulation* **124**, 1783–91 (2011).

10. Anderson, H. C. *et al.* Sustained osteomalacia of long bones despite major improvement in other hypophosphatasia-related mineral deficits in tissue nonspecific alkaline phosphatase/nucleotide pyrophosphatase phosphodiesterase 1 double-deficient mice. *Am. J. Pathol.* **166**, 1711–20 (2005).

11. Kirsch, T. *et al.* Annexin V-mediated calcium flux across membranes is dependent on the lipid composition: Implications for cartilage mineralization. *Biochemistry* **36**, 3359–3367 (1997).

12. Matkovic, V. & Heaney, R. P. Calcium balance during human growth: evidence for threshold behavior. *Am. J. Clin. Nutr.* **55**, 992–6 (1992).

13. Jackman, L. A. *et al.* Calcium retention in relation to calcium intake and postmenarcheal age in adolescent females. *Am. J. Clin. Nutr.* **66**, 327–333 (1997).

14. Winzenberg, T. M., Shaw, K., Fryer, J. & Jones, G. Calcium supplementation for improving bone mineral density in children. *Cochrane database Syst. Rev.* **2006**, CD005119 (2006).

15. Reynolds, J. L. *et al.* Human vascular smooth muscle cells undergo vesicle-mediated calcification in response to changes in extracellular calcium and phosphate concentrations: a potential mechanism for accelerated vascular calcification in ESRD. *J. Am. Soc. Nephrol.* **15**, 2857–67 (2004).

16. Bobryshev, Y. V, Orekhov, A. N., Sobenin, I. & Chistiakov, D. A. Role of bone-type tissue-nonspecific alkaline phosphatase and PHOSPO1 in vascular calcification. *Curr. Pharm. Des.* **20**, 5821–8 (2014).

17. Villa-Bellosta, R., Millan, A. & Sorribas, V. Role of calcium-phosphate deposition in vascular smooth muscle cell calcification. *Am. J. Physiol. Cell Physiol.* **300**, C210-20 (2011).

18. Giachelli, C. M., Speer, M. Y., Li, X., Rajachar, R. M. & Yang, H. Regulation of vascular calcification: roles of phosphate and osteopontin. *Circ. Res.* **96**, 717–22 (2005).

19. Jono, S. *et al.* Phosphate regulation of vascular smooth muscle cell calcification. *Circ. Res.* **87**, E10-7 (2000).

20. Palmer, S. C. *et al.* Serum levels of phosphorus, parathyroid hormone, and calcium and risks of death and cardiovascular disease in individuals with chronic kidney disease: a systematic review and meta-analysis. *JAMA* **305**, 1119–27 (2011).

21. Camalier, C. E. *et al.* An integrated understanding of the physiological response to elevated extracellular phosphate. *J. Cell. Physiol.* **228**, 1536–50 (2013).

22. Khoshniat, S. *et al.* The emergence of phosphate as a specific signaling molecule in bone and other cell types in mammals. *Cell. Mol. Life Sci.* **68**, 205–18 (2011).

23. Beck, G. R. Inorganic phosphate as a signaling molecule in osteoblast differentiation. *J. Cell. Biochem.* **90**, 234–43 (2003).

24. Laudenbach, P., Boudière, J. P. & Heubès, J. [Disturbances in development of the maxilla following interstitial radium therapy for a facial rhabdomyosarcoma at the age of 3 years (author's transl)]. *Rev. Stomatol. Chir. Maxillofac.* **80**, 174–7 (1979).

25. Shanahan, C. M. *et al.* Medial localization of mineralization-regulating proteins in association with Mönckeberg's sclerosis: evidence for smooth muscle cell-mediated vascular calcification. *Circulation* **100**, 2168–76 (1999).

26. Shalhoub, V. *et al.* Chondro/osteoblastic and cardiovascular gene modulation in human artery smooth muscle cells that calcify in the presence of phosphate and calcitriol or paricalcitol. *J. Cell. Biochem.* **111**, 911–21 (2010).

27. Alves, R. D. A. M., Eijken, M., van de Peppel, J. & van Leeuwen, J. P. T. M. Calcifying vascular smooth muscle cells and osteoblasts: independent cell types exhibiting extracellular matrix and biomineralization-related mimicries. *BMC Genomics* **15**, 965 (2014).

28. New, S. E. P. & Aikawa, E. Role of extracellular vesicles in de novo mineralization: an additional novel mechanism of cardiovascular calcification. *Arterioscler. Thromb. Vasc. Biol.* **33**, 1753–8 (2013).

29. Orimo, H. The mechanism of mineralization and the role of alkaline phosphatase in health and disease. *J. Nippon Med. Sch.* **77**, 4–12 (2010).

30. Bielesz, B., Klaushofer, K. & Oberbauer, R. Renal phosphate loss in hereditary and acquired disorders of bone mineralization. *Bone* **35**, 1229–39 (2004).

31. Marini, F., Giusti, F., Iantomasi, T. & Brandi, M. L. Congenital Metabolic Bone Disorders as a Cause of Bone Fragility. *Int. J. Mol. Sci.* **22**, (2021).

32. Reznikov, N. *et al.* Biological stenciling of mineralization in the skeleton: Local enzymatic removal of inhibitors in the extracellular matrix. *Bone* **138**, 115447 (2020).

33. Socorro, M. *et al.* Deficiency of Mineralization-Regulating Transcription Factor Trps1 Compromises Quality of Dental Tissues and Increases Susceptibility to Dental Caries. *Front. Dent. Med.* **3**, (2022).

34. Chaudhary, S. C. *et al.* Phosphate induces formation of matrix vesicles during odontoblast-initiated mineralization in vitro. *Matrix Biol.* **52–54**, 284–300 (2016).

35. Wu, L. N. *et al.* Morphological and biochemical characterization of mineralizing primary cultures of avian growth plate chondrocytes: evidence for cellular processing of Ca2+ and Pi prior to matrix mineralization. *J. Cell. Biochem.* **57**, 218–37 (1995).

36. Hasegawa, T. *et al.* Ultrastructural and biochemical aspects of matrix vesicle-mediated

mineralization. *Jpn. Dent. Sci. Rev.* **53**, 34–45 (2017).

37. Strzelecka-Kiliszek, A., Bozycki, L., Mebarek, S., Buchet, R. & Pikula, S. Characteristics of minerals in vesicles produced by human osteoblasts hFOB 1.19 and osteosarcoma Saos-2 cells stimulated for mineralization. *J. Inorg. Biochem.* **171**, 100–107 (2017).

38. Mosmann, T. Rapid colorimetric assay for cellular growth and survival: application to proliferation and cytotoxicity assays. *J. Immunol. Methods* **65**, 55–63 (1983).

39. Kirsch, T., Nah, H. D., Shapiro, I. M. & Pacifici, M. Regulated production of mineralization-competent matrix vesicles in hypertrophic chondrocytes. *J. Cell Biol.* **137**, 1149–60 (1997).

40. Balcerzak, M. *et al.* A comparative analysis of strategies for isolation of matrix vesicles. *Anal. Biochem.* **361**, 176–82 (2007).

41. Simão, A. M. S. *et al.* Lipid microenvironment affects the ability of proteoliposomes harboring TNAP to induce mineralization without nucleators. *J. Bone Miner. Metab.* **37**, 607–613 (2019).

42. Favarin, B. Z. *et al.* Lipid composition modulates ATP hydrolysis and calcium phosphate mineral propagation by TNAP-harboring proteoliposomes. *Arch. Biochem. Biophys.* **691**, 108482 (2020).

43. Genge, B. R., Wu, L. N. Y. & Wuthier, R. E. Kinetic analysis of mineral formation during in vitro modeling of matrix vesicle mineralization: effect of annexin A5, phosphatidylserine, and type II collagen. *Anal. Biochem.* **367**, 159–66 (2007).

44. Andrilli, L. H. S. *et al.* NPP1 and TNAP hydrolyze ATP synergistically during biomineralization. *Purinergic Signal.* (2022) doi:10.1007/s11302-022-09882-2.

45. Matyash, V., Liebisch, G., Kurzchalia, T. V, Shevchenko, A. & Schwudke, D. Lipid extraction by methyl-tert-butyl ether for high-throughput lipidomics. *J. Lipid Res.* **49**, 1137–46 (2008).

46. Kuzynski, M. *et al.* Dual role of the Trps1 transcription factor in dentin mineralization. *J. Biol. Chem.* **289**, 27481–93 (2014).

47. Takaoka, S., Yamaguchi, T., Yano, S., Yamauchi, M. & Sugimoto, T. The Calcium-sensing Receptor (CaR) is involved in strontium ranelate-induced osteoblast differentiation and mineralization. *Horm. Metab. Res.* **42**, 627–31 (2010).

48. Canalis, E., Hott, M., Deloffre, P., Tsouderos, Y. & Marie, P. J. The divalent strontium salt S12911 enhances bone cell replication and bone formation in vitro. *Bone* **18**, 517–523 (1996).

49. Barbara, A., Delannoy, P., Denis, B. G. & Marie, P. J. Normal matrix mineralization induced by strontium ranelate in MC3T3-E1 osteogenic cells. *Metabolism.* **53**, 532–7 (2004).

50. Mizumachi, H. *et al.* Calcium-sensing receptor-ERK signaling promotes odontoblastic differentiation of human dental pulp cells. *Bone* **101**, 191–201 (2017).

51. Schneider, M. R. Von Kossa and his staining technique. *Histochem. Cell Biol.* **156**, 523–526 (2021).

52. Park, H., Jo, S., Jang, M.-A., Choi, S. H. & Kim, T.-H. Dikkopf-1 promotes matrix mineralization of osteoblasts by regulating Ca+-CAMK2A- CREB1 pathway. *BMB Rep.* **55**, 627–632 (2022).

53. Bowers, S. L. K., Borg, T. K. & Baudino, T. A. The dynamics of fibroblast-myocyte-capillary interactions in the heart. *Ann. N. Y. Acad. Sci.* **1188**, 143–52 (2010).

54. Hadi, T. *et al.* Biphasic Erk1/2 activation sequentially involving Gs and Gi signaling is required in beta3-adrenergic receptor-induced primary smooth muscle cell proliferation. *Biochim. Biophys. Acta* **1833**, 1041–51 (2013).

55. Matsubayashi, Y., Ebisuya, M., Honjoh, S. & Nishida, E. ERK activation propagates in epithelial cell

sheets and regulates their migration during wound healing. *Curr. Biol.* **14**, 731–5 (2004).

56. Steven, A. *et al.* What turns CREB on? And off? And why does it matter? *Cell. Mol. Life Sci.* **77**, 4049–4067 (2020).

57. Sapio, L. *et al.* Targeting CREB in Cancer Therapy: A Key Candidate or One of Many? An Update. *Cancers (Basel).* **12**, (2020).

58. Zhang, H., Yang, S., Wang, J. & Jiang, Y. Blockade of AMPK-Mediated cAMP-PKA-CREB/ATF1 Signaling Synergizes with Aspirin to Inhibit Hepatocellular Carcinoma. *Cancers (Basel).* **13**, (2021).

59. Mantamadiotis, T., Papalexis, N. & Dworkin, S. CREB signalling in neural stem/progenitor cells: recent developments and the implications for brain tumour biology. *Bioessays* **34**, 293–300 (2012).

60. Kinjo, K., Sandoval, S., Sakamoto, K. M. & Shankar, D. B. The role of CREB as a proto-oncogene in hematopoiesis. *Cell Cycle* **4**, 1134–5 (2005).

61. Sun, P. *et al.* Regulation of body length and bone mass by Gpr126/Adgrg6. *Sci. Adv.* **6**, eaaz0368 (2020).

62. Matsumoto, T., Kuriwaka-Kido, R., Kondo, T., Endo, I. & Kido, S. Regulation of osteoblast differentiation by interleukin-11 via AP-1 and Smad signaling. *Endocr. J.* **59**, 91–101 (2012).

63. Huang, S. *et al.* Transcription factor CREB is involved in CaSR-mediated cytoskeleton gene expression. *Anat. Rec. (Hoboken).* **298**, 501–12 (2015).

64. Avlani, V. A. *et al.* Calcium-sensing receptor-dependent activation of CREB phosphorylation in HEK293 cells and human parathyroid cells. *Am. J. Physiol. Endocrinol. Metab.* **304**, E1097-104 (2013).

65. McNeil, S. E., Hobson, S. A., Nipper, V. & Rodland, K. D. Functional calcium-sensing receptors in rat fibroblasts are required for activation of SRC kinase and mitogen-activated protein kinase in response to extracellular calcium. *J. Biol. Chem.* **273**, 1114–20 (1998).

66. Kifor, O. *et al.* Regulation of MAP kinase by calcium-sensing receptor in bovine parathyroid and CaR-transfected HEK293 cells. *Am. J. Physiol. Renal Physiol.* **280**, F291-302 (2001).

67. Li, L. *et al.* Knockdown of FOXA1 enhances the osteogenic differentiation of human bone marrow mesenchymal stem cells partly via activation of the ERK1/2 signalling pathway. *Stem Cell Res. Ther.* **13**, 456 (2022).

68. Jiang, Y. *et al.* αCGRP Regulates Osteogenic Differentiation of Bone Marrow Mesenchymal Stem Cells Through ERK1/2 and p38 MAPK Signaling Pathways. *Cell Transplant.* **31**, 9636897221107636 (2022).

69. Su, S., Zhu, Y., Li, S., Liang, Y. & Zhang, J. The transcription factor cyclic adenosine 3',5'-monophosphate response element-binding protein enhances the odonto/osteogenic differentiation of stem cells from the apical papilla. *Int. Endod. J.* **50**, 885–894 (2017).

70. Bobrie, A., Colombo, M., Krumeich, S., Raposo, G. & Théry, C. Diverse subpopulations of vesicles secreted by different intracellular mechanisms are present in exosome preparations obtained by differential ultracentrifugation. *J. Extracell. vesicles* **1**, (2012).

71. Ali, S. Y., Sajdera, S. W. & Anderson, H. C. Isolation and characterization of calcifying matrix vesicles from epiphyseal cartilage. *Proc. Natl. Acad. Sci. U. S. A.* **67**, 1513–1520 (1970).

72. Balcerzak, M. *et al.* Proteome analysis of matrix vesicles isolated from femurs of chicken embryo. *Proteomics* **8**, 192–205 (2008).

73. Zhang, J. *et al.* Lysosomal LAMP proteins regulate lysosomal pH by direct inhibition of the

TMEM175 channel. *Mol. Cell* **83**, 2524-2539.e7 (2023).

74. Blair, H. C. *et al.* Support of bone mineral deposition by regulation of pH. *Am. J. Physiol. Cell Physiol.* **315**, C587–C597 (2018).

75. Wuthier, R. E. *et al.* Isolation and characterization of calcium-accumulating matrix vesicles from chondrocytes of chicken epiphyseal growth plate cartilage in primary culture. *J. Biol. Chem.* **260**, 15972–9 (1985).

76. Rousso, I. & Deshpande, A. Applications of Atomic Force Microscopy in HIV-1 Research. *Viruses* **14**, (2022).

77. Sebinelli, H. G. *et al.* Shedding Light on the Role of Na,K-ATPase as a Phosphatase during Matrix-Vesicle-Mediated Mineralization. *Int. J. Mol. Sci.* **23**, (2022).

78. Plaut, J. S. *et al.* Quantitative atomic force microscopy provides new insight into matrix vesicle mineralization. *Arch. Biochem. Biophys.* **667**, 14–21 (2019).

79. Bolean, M. *et al.* Topographic analysis by atomic force microscopy of proteoliposomes matrix vesicle mimetics harboring TNAP and AnxA5. *Biochim. Biophys. acta. Biomembr.* **1859**, 1911–1920 (2017).

80. Sebinelli, H. G., Borin, I. A., Ciancaglini, P. & Bolean, M. Topographical and mechanical properties of liposome surfaces harboring Na,K-ATPase by means of atomic force microscopy. *Soft Matter* **15**, 2737–2745 (2019).

81. Resende, R. R. *et al.* Nucleoplasmic calcium signaling and cell proliferation: calcium signaling in the nucleus. *Cell Commun. Signal.* **11**, 14 (2013).

82. Baird, G. S. Ionized calcium. *Clin. Chim. Acta.* **412**, 696–701 (2011).

83. Fairley, J. A. Calcium: a second messenger. *Adv. Dermatol.* **4**, 95–110; discussion 111 (1989).

84. Hardingham, G. E. & Bading, H. Calcium as a versatile second messenger in the control of gene expression. *Microsc. Res. Tech.* **46**, 348–55 (1999).

85. Gabusi, E. *et al.* Extracellular calcium chronically induced human osteoblasts effects: specific modulation of osteocalcin and collagen type XV. *J. Cell. Physiol.* **227**, 3151–61 (2012).

86. Brown, E. M. & MacLeod, R. J. Extracellular calcium sensing and extracellular calcium signaling. *Physiol. Rev.* **81**, 239–297 (2001).

87. Xu, Z. *et al.* Effect of the calcium sensing receptor on rat bone marrow-derived mesenchymal stem cell proliferation through the ERK1/2 pathway. *Mol. Biol. Rep.* **39**, 7271–9 (2012).

88. Swarthout, J. T., D'Alonzo, R. C., Selvamurugan, N. & Partridge, N. C. Parathyroid hormone-dependent signaling pathways regulating genes in bone cells. *Gene* **282**, 1–17 (2002).

89. Viti, F. *et al.* Osteogenic Differentiation of MSC through Calcium Signaling Activation: Transcriptomics and Functional Analysis. *PLoS One* **11**, e0148173 (2016).

90. Han, Y. High concentrations of calcium suppress osteogenic differentiation of human periodontal ligament stem cells in vitro. *J. Dent. Sci.* **16**, 817–824 (2021).

91. Takashi, Y. & Fukumoto, S. Phosphate-Sensing. *Adv. Exp. Med. Biol.* **1362**, 27–35 (2022).

92. Foster, B. L. *et al.* Regulation of cementoblast gene expression by inorganic phosphate in vitro. *Calcif. Tissue Int.* **78**, 103–12 (2006).

93. Julien, M. *et al.* Phosphate stimulates matrix Gla protein expression in chondrocytes through the extracellular signal regulated kinase signaling pathway. *Endocrinology* **148**, 530–7 (2007).

94. Coulombe, J., Faure, H., Robin, B. & Ruat, M. In vitro effects of strontium ranelate on the extracellular calcium-sensing receptor. *Biochem. Biophys. Res. Commun.* **323**, 1184–90 (2004).

95. Saidak, Z. & Marie, P. J. Strontium signaling: Molecular mechanisms and therapeutic implications in osteoporosis. *Pharmacol. Ther.* **136**, 216–226 (2012).

96. Rybchyn, M. S., Slater, M., Conigrave, A. D. & Mason, R. S. An Akt-dependent increase in canonical Wnt signaling and a decrease in sclerostin protein levels are involved in strontium ranelate-induced osteogenic effects in human osteoblasts. *J. Biol. Chem.* **286**, 23771–9 (2011).

97. Diepenhorst, N. *et al.* G protein-coupled receptors as anabolic drug targets in osteoporosis. *Pharmacol. Ther.* **184**, 1–12 (2018).

98. Bechkoff, G., Radisson, J., Bessueille, L., Bouchekioua-Bouzaghou, K. & Buchet, R. Distinct actions of strontium on mineral formation in matrix vesicles. *Biochem. Biophys. Res. Commun.* **373**, 378–81 (2008).

99. Almeida, M. M. *et al.* Strontium ranelate increases osteoblast activity. *Tissue Cell* **48**, 183–8 (2016).

100. Wei, K. *et al.* ERK1/2 signaling mediated naringin-induced osteogenic differentiation of immortalized human periodontal ligament stem cells. *Biochem. Biophys. Res. Commun.* **489**, 319–325 (2017).

101. Liu, L. *et al.* The interaction between β1 integrins and ERK1/2 in osteogenic differentiation of human mesenchymal stem cells under fluid shear stress modelled by a perfusion system. *J. Tissue Eng. Regen. Med.* **8**, 85–96 (2014).

102. Yuh, D.-Y. *et al.* The secreted protein DEL-1 activates a β3 integrin-FAK-ERK1/2-RUNX2 pathway and promotes osteogenic differentiation and bone regeneration. *J. Biol. Chem.* **295**, 7261–7273 (2020).

103. Ghosh-Choudhury, N. *et al.* Concerted action of Smad and CREB-binding protein regulates bone morphogenetic protein-2-stimulated osteoblastic colony-stimulating factor-1 expression. *J. Biol. Chem.* **281**, 20160–70 (2006).

104. Xing, J. *et al.* AGS3 is involved in TNF-α medicated osteogenic differentiation of human dental pulp stem cells. *Differentiation.* **89**, 128–36 (2015).

105. Handley-Sidhu, S. *et al.* Influence of pH, competing ions, and salinity on the sorption of strontium and cobalt onto biogenic hydroxyapatite. *Sci. Rep.* **6**, 23361 (2016).

106. Landis, W. J. & Jacquet, R. Association of calcium and phosphate ions with collagen in the mineralization of vertebrate tissues. *Calcif. Tissue Int.* **93**, 329–37 (2013).

107. Akiva, A. *et al.* Mineral Formation in the Larval Zebrafish Tail Bone Occurs via an Acidic Disordered Calcium Phosphate Phase. *J. Am. Chem. Soc.* **138**, 14481–14487 (2016).

108. Bolean, M. *et al.* Biophysical aspects of biomineralization. *Biophys. Rev.* **9**, 747–760 (2017).

109. Lingwood, D. & Simons, K. Lipid rafts as a membrane-organizing principle. *Science* **327**, 46–50 (2010).

110. Airola, M. V & Hannun, Y. A. Sphingolipid metabolism and neutral sphingomyelinases. *Handb. Exp. Pharmacol.* 57–76 (2013) doi:10.1007/978-3-7091-1368-4_3.

111. Ermonval, M., Baychelier, F. & Fonta, C. TNAP, an Essential Player in Membrane Lipid Rafts of Neuronal Cells. *Subcell. Biochem.* **76**, 167–83 (2015).

112. Garcia, A. F. *et al.* Effects of GPI-anchored TNAP on the dynamic structure of model membranes. *Phys. Chem. Chem. Phys.* **17**, 26295–301 (2015).

113. Ciancaglini, P. *et al.* Kinetic analysis of substrate utilization by native and TNAP-, NPP1-, or PHOSPHO1-deficient matrix vesicles. *J. Bone Miner. Res.* **25**, 716–723 (2010).

114. Bolean, M., Simão, A. M. S., Favarin, B. Z., Millán, J. L. & Ciancaglini, P. The effect of cholesterol on the reconstitution of alkaline phosphatase into liposomes. *Biophys. Chem.* **152**, 74–9 (2010).

115. Almeida, P. F., Carter, F. E., Kilgour, K. M., Raymonda, M. H. & Tejada, E. Heat Capacity of DPPC/Cholesterol Mixtures: Comparison of Single Bilayers with Multibilayers and Simulations. *Langmuir* **34**, 9798–9809 (2018).

116. Barenholz, Y. Cholesterol and other membrane active sterols: from membrane evolution to 'rafts'. *Prog. Lipid Res.* **41**, 1–5 (2002).

117. Simons, K. & Ikonen, E. Functional rafts in cell membranes. *Nature* **387**, 569–72 (1997).

118. During, A., Penel, G. & Hardouin, P. Understanding the local actions of lipids in bone physiology. *Prog. Lipid Res.* **59**, 126–46 (2015).

119. During, A., Coutel, X., Bertheaume, N., Penel, G. & Olejnik, C. Long Term Ovariectomy-Induced Osteoporosis is Associated with High Stearoyl-CoA Desaturase Indexes in Rat Femur. *Calcif. Tissue Int.* **106**, 315–324 (2020).

120. Ogretmen, B. Sphingolipid metabolism in cancer signalling and therapy. *Nat. Rev. Cancer* **18**, 33–50 (2018).

121. Wu, L. N. Y., Genge, B. R., Kang, M. W., Arsenault, A. L. & Wuthier, R. E. Changes in phospholipid extractability and composition accompany mineralization of chicken growth plate cartilage matrix vesicles. *J. Biol. Chem.* **277**, 5126–33 (2002).

122. Aubin, I. *et al.* A deletion in the gene encoding sphingomyelin phosphodiesterase 3 (Smpd3) results in osteogenesis and dentinogenesis imperfecta in the mouse. *Nat. Genet.* **37**, 803–5 (2005).

123. Goldberg, M. *et al.* Sphingomyelin degradation is a key factor in dentin and bone mineralization: lessons from the fro/fro mouse. The chemistry and histochemistry of dentin lipids. *J. Dent. Res.* **87**, 9–13 (2008).

124. Khavandgar, Z. *et al.* Local regulation of tooth mineralization by sphingomyelin phosphodiesterase 3. *J. Dent. Res.* **92**, 358–64 (2013).

Chapter VI

General Discussion & Final Conclusions

General discussion and conclusions

Our group has long worked with the development of bioactive biomaterials aimed at the bone healing field[1–6]. So, the synthesis of hydroxyapatite-based nanoparticles was one of our major interests, mainly due to the following features. First, they resemble the natural structure found in bone apatite. Second, it has been suggested that hydroxyapatite (HA) by its nature is a potent inducer of osteoblasts turnover[7–10], and third they are cheap to synthesize. Regarding the last advantage, if one is looking for the production of biomaterials the price cannot be overlooked since it is a major cause of concern for the patient's long-term treatment. The use of strontium for osteoporotic patients is nothing new, however, its applicability as well as the drug administration have changed in the last few years. The foremost feature that makes strontium an attractive ion for the bone regenerative field is that it has the ability to stimulate bone-forming cells (osteoblasts), whereas inhibits the proliferation and activity of bone-resorptive cells (osteoclasts). Based on this, our group synthesized a new class of HAp nanoparticles with a replacement of calcium by strontium. The local and gradual delivery of strontium into the cellular microenvironment overcomes some of the problems associated with the systemic administration of strontium, for example, the use of strontium ranelate is a major cause of concern due to its ability to induce ectopic mineralization[11], since its mechanism of action is also capable of inducing vascular smooth muscle cells to mineralize.

Further, the use of porous polymethylmethacrylate (pPMMA) cement has been previously characterized and proved to be a suitable biomaterial aimed toward the filling of bone fractures and dentistry[12]. Despite its promising properties as a bone substitute, there are still bottlenecks that need to be addressed. Among them, pPMMA cement is not a bioactive material (i.e., it does not induce a specific cellular response), though the influx of osteoblasts toward the cement vicinity was previously reported[5,13]. Second, microcomputerized tomography (µCT) analysis, revealed that the tridimensional structure and pore size of the pPMMA cement facilitates osteointegration, therefore avoiding implant loosening, which is a common drawback in orthopedics[14]. However, this process can take as long as six months until total osteointegration is accomplished.

To address these restrictions, the first interest of this thesis was to characterize the NPs-containing strontium and evaluate their ability to not only promote biomineralization but also speed up the process. The next step was to analyze the NP's

effect on promoting osteointegration in vivo. As the NPs are in the form of powder their application straight in the bone failure is unfeasible. Based on this, we opted to use the pPMMA cement as a scaffold and the nanoparticle carrier, as previously described [5].

Throughout the NP´s characterization in vivo and later in vitro, many questions arose regarding its molecular mechanism of action. It inspired us to dig further. Based on the NP´s characterization results we hypothesized that strontium would likely affect osteocompent cells in two ways, though we recognized that other routes could be stimulated/inhibited by strontium, they are: (1) by affecting intrinsic signaling pathways that regard osteogenic cell commitment profile, and (2) through the stimulation of matrix vesicle´s release and function. First, we exploited the first hypothesis through the study of Erk1/2 and CREB signaling pathways, and after we investigated the influence of strontium and $CaCl_2$ over the expression level of osteogenic genes. Second, we analyzed the influence of strontium on the release and function of matrix vesicles. We also applied lipidomic characterization analysis to understand the influence of strontium on the overall lipid content of matrix vesicles.

In **Chapter IV** we showed that the presence of Sr^{2+} in osteoblasts culture administrated from NPs modulates the activity of TNAP in vitro, thus leading to increased formation of mineral nodules. Moreover, the nanoparticles impaired the osteoclasts' differentiation. Then we asked if the nanoparticles would be as efficient *in vivo*. Surprisingly, we found that NanoSr 90% increased BMP2 and OCN gene levels. A mechanical test (push-out) revealed that porous cement loaded with the nanoparticles and unloaded increased the interface bone/cement de-bonding maximum strength. Histological assays revealed the influx of osteoblasts, secretion of collagen type I on cement, and new-bone synthesis, in both groups. Finally, Computerized tomography displayed areas of osteointegration with no difference between the groups.

In vivo models of bone tissue repair, are the next step of every in vitro study that aims at tissue healing [15–17]. Nonetheless, sometimes the in vitro results, or their tendencies, are not observed (extrapolated) when one implants the biomaterial to an in vivo model[17], due to different reasons. First, in vivo, many cells are activating as well as inhibiting the formation of bone. Second, the nanoparticles could be diluted since a constant influx of blood is flowing through the injured site, so the standardization of the nanoparticle´s concentration must be precise. Third, one cannot overlook the influence of the immune system, especially in the first month of the biomaterial implantation, whereby

an inhibitory effect on osteoblasts is observed, rather than its stimulation[18]. Fourth, time plays a crucial role in bone regeneration. We have previously observed that 6 months is not enough to accomplish total bone osteointegration[12].

Taken together, our results attest to the nanoparticle potential as a bioactive agent that could be aimed at bone regeneration. Regarding in vivo experimentation, to observe a more pronounced difference between pPMMA and pMMA cement loaded with NanoSr 90%, one shall increase the nanoparticle concentration to above 1% of the cement's total mass, and additionally increase the animal time-exposure to the cement.

Afterward, in **Chapter V** we explored thoroughly how strontium would affect important molecular signaling cascades related to the induction of osteogenic genes. Here, we opted to study Erk1/2 and CREB signaling pathways; the genes Runx2, Sp7, Collagen type I, and the phosphatases Smpd3, Phospho1, and Alp. As chemically strontium resembles calcium, we opted to also analyze calcium. Later, we investigated how strontium participates in the release and function of matrix vesicles, and how the lipid content shapes itself under the influence of different stimulators.

The outcomes demonstrated that strontium and calcium activate Erk1/2 and CREB signaling pathways in a dose-dependent and time-dependent manner. Activation of Erk1/2 and CREB signaling poorly affected osteogenic genes, however, we attributed this aftermath due to the nature of the cell line 17IIA11. As previously discussed, 17IIA11 constitutionally holds a higher expression of osteogenic genes, due to its commitment to the osteogenic profile, which takes about 7 days to archive complete extracellular matrix mineralization. Based on this, the 17IIA11 overstimulation through the addition of osteo inductors ($CaCl_2$ and SR) will not be translated in the increase of the gene expression level. After that, we observed that SR and $CaCl_2$ inhibit the release of MVs as well as their TNAP activity function. Curiously, SR lower concentration (0.1mM) had the higher efficiency, followed by calcium at 1.0mM. Then, by AFM and TEM analysis, we observed a change in the MVs membrane viscoelastic properties, which is likely associated with a change in lipid composition[19,20]. Later, we confirmed that the lipid profile changes upon different stimulations. Strontium-treated and calcium-treated cells demonstrate MVs with a higher content of SM and Cer, two sphingolipids likely associated with bone development[21,22]. Hence, we concluded that strontium likely stimulates the mineralization of ECM through the activation of competent matrix vesicles.

References

1. Cruz, M. A. E. *et al.* Interface-driven Sr-morin complexation at Langmuir monolayers for bioactive coating design. *Colloids Surf. B. Biointerfaces* **181**, 856–863 (2019).

2. Cruz, M. A. E., Zanatta, M. B. T., da Veiga, M. A. M. S., Ciancaglini, P. & Ramos, A. P. Lipid-mediated growth of SrCO3/CaCO3 hybrid films as bioactive coatings for Ti surfaces. *Mater. Sci. Eng. C. Mater. Biol. Appl.* **99**, 762–769 (2019).

3. Cruz, M. A. E. *et al.* Synthesis of Sr-morin complex and its: In vitro response: Decrease in osteoclast differentiation while sustaining osteoblast mineralization ability. *J. Mater. Chem. B* **7**, 823–829 (2019).

4. Tovani, C. B. *et al.* Strontium Calcium Phosphate Nanotubes as Bioinspired Building Blocks for Bone Regeneration. *ACS Appl. Mater. Interfaces* **12**, 43422–43434 (2020).

5. Tomazela, L. *et al.* Fabrication and characterization of a bioactive polymethylmethacrylate-based porous cement loaded with strontium/calcium apatite nanoparticles. *J. Biomed. Mater. Res. A* **110**, 812–826 (2022).

6. Nogueira, L. F. B. *et al.* Three-dimensional cell-laden collagen scaffolds: From biochemistry to bone bioengineering. *J. Biomed. Mater. Res. - Part B Appl. Biomater.* **110**, 967–983 (2022).

7. Liang, W., Ding, P., Li, G., Lu, E. & Zhao, Z. Hydroxyapatite Nanoparticles Facilitate Osteoblast Differentiation and Bone Formation Within Sagittal Suture During Expansion in Rats. *Drug Des. Devel. Ther.* **15**, 905–917 (2021).

8. Tien Lam, N., Minh Quan, V., Boonrungsiman, S. & Sukyai, P. Effectiveness of bio-dispersant in homogenizing hydroxyapatite for proliferation and differentiation of osteoblast. *J. Colloid Interface Sci.* **611**, 491–502 (2022).

9. Wang, R. *et al.* Nano-Hydroxyapatite Modulates Osteoblast Differentiation Through Autophagy Induction via mTOR Signaling Pathway. *J. Biomed. Nanotechnol.* **15**, 405–415 (2019).

10. Hao, J. *et al.* Enhanced osteoblast and osteoclast responses to a thin film sputtered hydroxyapatite coating. *J. Mater. Sci. Mater. Med.* **22**, 1489–99 (2011).

11. Golub, E. E. Biomineralization and matrix vesicles in biology and pathology. *Semin. Immunopathol.* **33**, 409–17 (2011).

12. Cimatti, B. *et al.* Safety, osseointegration, and bone ingrowth analysis of PMMA-based porous cement on animal metaphyseal bone defect model. *J. Biomed. Mater. Res. B. Appl. Biomater.* **106**, 649–658 (2018).

13. Moursi, A. M., Winnard, A. V, Winnard, P. L., Lannutti, J. J. & Seghi, R. R. Enhanced osteoblast

response to a polymethylmethacrylate-hydroxyapatite composite. *Biomaterials* **23**, 133–44 (2002).

14. Ries, M. D. *et al.* In vivo behavior of acrylic bone cement in total hip arthroplasty. *Biomaterials* **27**, 256–61 (2006).

15. Saeidnia, S., Manayi, A. & Abdollahi, M. From in vitro Experiments to in vivo and Clinical Studies; Pros and Cons. *Curr. Drug Discov. Technol.* **12**, 218–24 (2015).

16. Abdullahi, A., Amini-Nik, S. & Jeschke, M. G. Animal models in burn research. *Cell. Mol. Life Sci.* **71**, 3241–55 (2014).

17. Dunn, L. *et al.* Murine model of wound healing. *J. Vis. Exp.* e50265 (2013) doi:10.3791/50265.

18. Anderson, J. M., Rodriguez, A. & Chang, D. T. Foreign body reaction to biomaterials. *Semin. Immunol.* **20**, 86–100 (2008).

19. Bolean, M. *et al.* Biophysical aspects of biomineralization. *Biophys. Rev.* **9**, 747–760 (2017).

20. Favarin, B. Z. *et al.* Lipid composition modulates ATP hydrolysis and calcium phosphate mineral propagation by TNAP-harboring proteoliposomes. *Arch. Biochem. Biophys.* **691**, 108482 (2020).

21. During, A., Penel, G. & Hardouin, P. Understanding the local actions of lipids in bone physiology. *Prog. Lipid Res.* **59**, 126–46 (2015).

22. Khavandgar, Z. & Murshed, M. Sphingolipid metabolism and its role in the skeletal tissues. *Cell. Mol. Life Sci.* **72**, 959–69 (2015).